Fachbereich Chemie der Universität Dortmund

Chemistry of Metallacalix[n]arenes Derived from Square-Planar Metal Centers, *cis*-$M^{II}a_2$ (M = Pt, Pd and a_2 = 2,2'-bpy, en, tmeda), with Pyrimidine Nucleobases (Uracil, Cytosine): Self-Assembling, Characterization and Interconversion Mechanisms of Species

Elisa Gil Bardají

Dem Fachbereich Chemie der Universität Dortmund
zur Erlangung des akademischen Grades eines
Doktors der Naturwisenschaften
genehmigte Dissertation.

Referent:	Prof. Dr. Bernhard Lippert
Korreferent:	Prof. Dr. Jorge A. R. Navarro
Tag der mündlichen Prüfung:	20.12.2006

In the time from June 2003 till December 2006 this work came into being at the Lehrstuhl für Anorganische Chemie III des Fachbereichs Chemie der Universität Dortmund.

My special thanks go to my Ph. D. Supervisor

Prof. Dr. Bernhard Lippert

for the opportunity to carry out research in his group, for the interesting topic, for taking care of my scientific advance, for the academic and human engagement and for all his help.

I thank Prof. Dr. Jorge A. R. Navarro for taking over the part of the second examiner.

I would also like to thank:

- Dr. Jens Müller and Dr. Fabian-Alexander (Polonski) Polonius for carefully reading my thesis, correcting my English and the very good suggestions that they made,

- my colleagues of the working group, Dominik Böhme, Nicole Düpre, Oliver Gebersmann, Dr. Deepali Gupta, Lars Holland, Dr. Patrick Lax, Dominik Megger, Marta Morell, Dr. Clodagh Mulcahy, Barbara Müller, Dr. Fabian-Alexander Polonius, Dr. Michael Roitzsch, Dr. Pablo Sanz, Thea Welzel, Tushar van der Wijst and especially Pilar Brandi, Dr. Marta Garijo and Weizheng Shen for the good atmosphere in the office and the great time we spent together,

- Michaela Markert, Birgit Thormann and Dr. Gabriele Trötscher-Kaus for their help and funny conversations,

- Dr. Andrea Erxleben, Marta Morell, Dr. Thorsten Oldag, Dr. Pablo Sanz, Dr. Markus Schürmann and Dr. Uwe Zachwieja for their help with the X-ray crystal structures and especially Dr. Eva Freisinger for her help and collaboration to solve the crystal structures and the rapid answer to all my questions about crystallography.

- Prof. Dr. Burkhard Costisella, Annette Danzmann and Christa Nettelbeck for the NMR experiments that they carried out and for the good atmosphere,

- Markus Hüffner for carrying out the elemental analyses,

- Christine Klimek, Alex Klauke, Christian Nowak and Thorsten Grund,

- the Niemeyer group and especially Dr. Bülent Ceyhan for his friendship and the nice times and moments we spent together. Don´t worry next time I let you win ("Ich lasse dich platzen!"),

- Prof. Dr. Luis Oro for giving me the possibility to come to Dortmund,

- Inés, Joaquín, Marta, Miguel, Pilar and Pili for their friendship, their help in the hard moments and for being my "family" in Germany,

- all my Spanish friends, who have been and are still waiting for me, although I sometimes forgot their birthdays,

- Gudrun Polonius-Neubert and Prof. Dr. med. M. J. A. R. Polonius for their help and the encouragement that they always gave me, as well as the lovely and delicious sunday morning breakfasts,

- Fabian and my family, Joaquín, Asunción, Rafael, Orosia, Cristina, Alfonso, Marisa, Diego and Nicolás for their continuous support, patience, help and love. Thanks for always being there for me when I needed you.

A mis padres

Table of Contents

Chapter II:
Bis-Uracil Complexes

Abbreviations

AMP	adenosine monophosphate
2,2’-bpy	2,2’-bipyridine
C	cytosine dianion
CH	cytosine monoanion
CH_2	cytosine
ca.	approximately
COSY	Correlated Spectroscopy
d	days
d (NMR)	doublet
δ	chemical shift
en	ethylenediamine
ESI-MS	Electro Spray Ionisation Mass Spectrometry
equiv.	equivalents
et al.	and co-workers
h	hours
HMBC	Heteronuclear Multiple–Bond Correlation
HSQC	Heteronuclear Multiple–Quantum Correlation
IR	infrared
M	molar mass
m (NMR)	multiplet
9-MeGH	9-Methylguanine
min	minutes
M^{n+}	M = metal and n = charge of the metal
NMR	Nuclear Magnetic Resonance
NOESY	Nuclear Overhauser Enhancement Spectroscopy
pD	negative logarithms of the deuterium ion concentration
pH	negative logarithms of the hydrogen ion concentration
pK_a	negative logarithms of the acidity constant
ppm	parts per millon
RT	room temperature
s (NMR)	singulet
t (NMR)	triplet

TMA	tetramethylammonium tetrafluoroborate
tmeda	tetramethylethylenedimine
TOCSY	Total Correlated Spectroscopy
TSP	sodium-3-(trimethylsilyl)-propanesulfonate
U	uracil dianion
UH	uracil monoanion
UH_2	uracil

A INTRODUCTION

Cisplatin (*cis*-diamminedichloroplatinum(II)) was discovered in 1965 while Rosenberg et al. were studying the effect of an electric current on *E. coli.*[1,2] It was eventually found that cell division was inhibited by the production of platinum(II) derivates, from the platinum electrodes and the cell culture medium. Further studies on the drug indicated that it possessed antitumor activity. The National Cancer Institute introduced *Cisplatin* into clinical trials in 1972.[3] It has a major role in the treatment of several human tumors, especially in case of testicular and ovarian cancer.[4] The efficency of *Cisplatin* is based on its strong binding to DNA nucleobases,[5,6] which is a kinetically rather than thermodynamically controlled process.[7]

Since the discovery of *Cisplatin* by Rosenberg, thousand of platinum compounds have been synthesized and their antitumor activities investigated.[8] They belong to the most promising drugs in chemotherapy.[9] Despite significant efforts to design new antitumor agents based on platinum[10,11] in an effort to overcome *Cisplatin* resistence[12,13] or improve its antitumor activity,[14] there are only a few examples of Pt-based drugs, namely carboplatin (diammine[1,1-cyclobutane-dicarboxylato(2–)]-*O,O'*-platinum(II)),[15,16] oxaliplatin (*trans*-L-Diaminocyclo-hexane)oxalatoplatinum(II)),[17,18] and nedaplatin (*cis*-Diammine–glycoloato-*O,O'*-platinum(II)),[19] that are of immediate clinical relevance today. Carboplatin has received worldwide approval and achieved routine clinical use.[20] Extensive research has been undertaken to generate new transition-metal complexes as potential chemotherapy agents with increased efficiency. Many of these complexes were designed to interact with DNA by different binding strategies (such as electrostatic binding, hydrophobic binding to the minor groove, or intercalation) or to react with DNA directly (via oxidative strand cleavage, hydrolytic strand cleavage, or oxidative reactions with the DNA bases).[21]

In the early 1970's , a class of antitumor agents derived from *Cisplatin* and pyrimidine nucleobases was found that had very characteristic features, which was called "Platinum Pyrimidine Blues" (see below). These compounds have been investigated in the last three decades (e.g. Lippert,[22] Flynn et al.,[23] and Chu et al.[24]) but they still provide fascination due to their not fully understood behavior.

1 History of antitumor active "Platinum Blues"

The original report of "Platinblau" was made in 1908 by Hoffmann and Bugge,[25] which dealt with blue compounds derived from aqueous solutions of platinum(II) with amides.

The great interest in these complexes sparked when in 1972 the Rosenberg group discovered that aquated products of the antitumor drug cis-dichlorodiammineplatinum(II) underwent a slow reaction with pyrimidine nucleobase derivatives to form blue complexes. The unexpected activity of these compounds against the Ascites S-180 tumor system and also the low toxicity made these "blues" promising second generation Pt drugs at that time.[26,27]

It was observed that "platinum pyrimidine blues" could interact with DNA. The first published study was made once again by Rosenberg and co-workers,[28] which unequivocally proved an interaction between "Pt uracil blue" and DNA. The "blues" were and in fact still are useful as stains for electron microscopy of fine structural studies of cells. It had been shown that these compound penetrate cell membranes and stain nuclear components, while normally not reacting with proteins.[29] However, problems with the characterization of the products and a reproducible synthesis soon became evident.

In 1977 the Lippard group[30] published the formation and X-ray structure of a "Pt blue" derived from *cis*-$[(NH_3)_2Pt(H_2O)_2]^{2+}$ and α-pyridone (Figure 1). The characterized structure of the complex showed two *cis*-diammineplatinum units bridged by two *head-head* oriented α-pyridonate ligands. In addition, two α-pyridonate ligands bridged dimers are held together by H-bonds between NH_3 ligands and exocyclic O atoms of the α-pyridonate ligands. The formal oxidation state of platinum in the "zigzag" tetranuclear chain is 2.25.

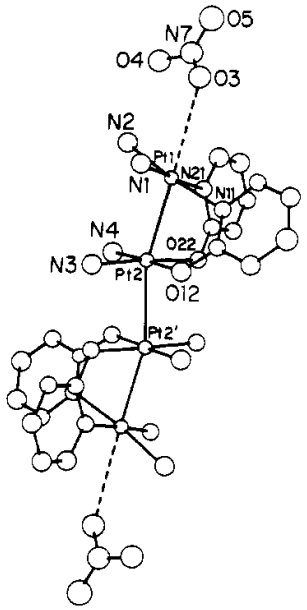

Figure 1: Crystal structure of $[Pt_2(NH_3)_4(C_5H_4ON)_2]_2(NO_3)_5$. Non-coordinated nitrate ions omitted.[30]

The phenomenon of the color in these kind of compounds is due to intervalence charge transfer (CT) transitions, hence, due to the presence of Pt in different oxidation states.[9]

A few years later the existence of dinuclear *N,O*-bridged Pt^{II} complexes proved that the "blues" can also be derived from 1-substituted pyrimidine nucleobases such as 1-methyluracil[31] and 1-methylthymine[32,33] as well as imides.[34] Then an anologue of the "α-pyridone blue" was found for 1-methyluracil.[35,36]

Unsubstituted pyrimidine nucleobases like uracil and cytosine, can also give rise to the formation of "blues". In this case, there are many possible combinations of two or more binding sites, making them very versatile ligands (Scheme 1). Hence, one still has a long way to go to fully understand of the nature of these "blues".[9]

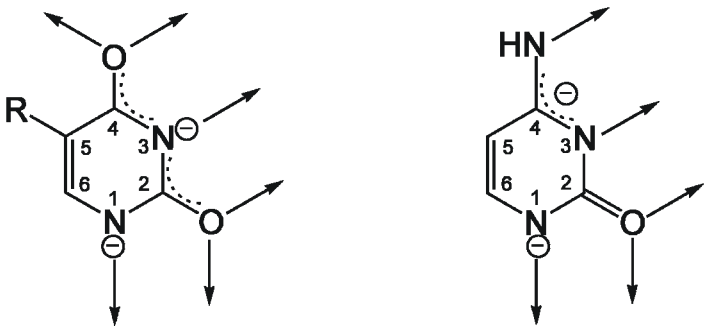

Scheme 1: Possible metal binding sites in unsubstituted uracil (R=H) or thymine (R=CH_3) (left) and cytosine (right).

A series of these binding patterns could already be determined for unsubstituted uracil by X-ray crystallography[37-40] and by spectroscopic studies,[41,42] and also for unsubstituted cytosine.[43-45]

In the mid 1980's the existence of heteronuclear species consisting of Pt metal fragments with other transition metal ions like Ag^+ [46,47] or Pd,[48,49] which had a formal oxidation state of 3, was found (Scheme 2). These heteronuclear species provided a rationale for the formation of the partially oxidized species.

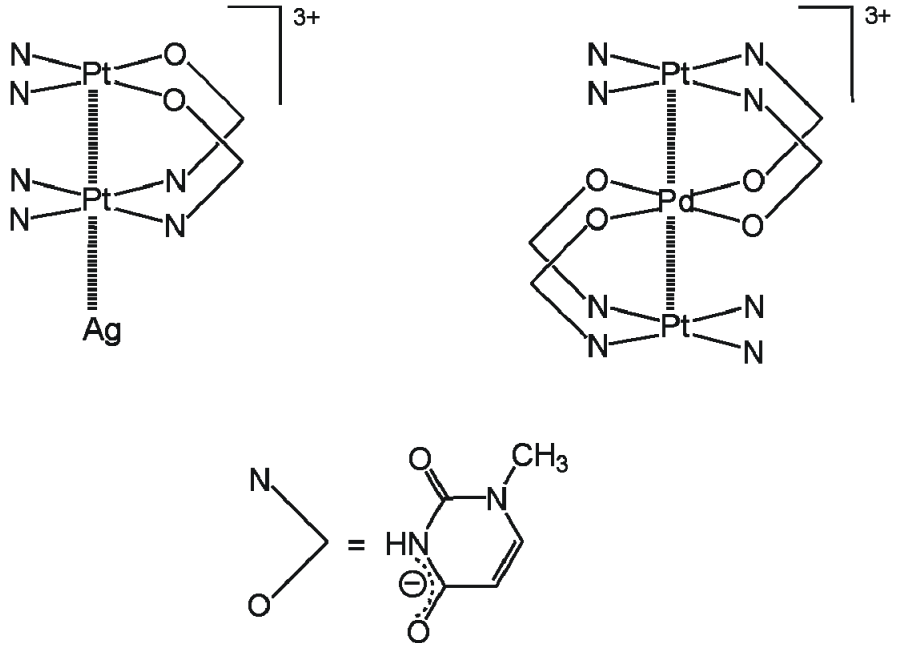

Scheme 2: Schematic representation of the cations $[\{(NH_3)_2Pt(1\text{-}MeU)\}_2Ag]^{3+}$,[47](left) and *cis*-$[(NH_3)_2Pt(1\text{-}MeU)_2Pd(1\text{-}MeU)_2Pt(NH_3)_2]^{3+}$,[48] (right) with (1-MeU = 1-Methyluracil).

It was always supposed that a linear arrangement of Pt centers connected via d_z^2 orbitals was present. An alternative suggestion was made by B. Lippert in 1981,[41] who proposed that the "Pt blues" can also be cyclic oligomers. Eleven years later, cyclic platinum complexes with pyrimidine ligands as tetra- and octanuclear boxes were indeed reported.[38-40] A schematic diagram of these compounds is given in Scheme 3.

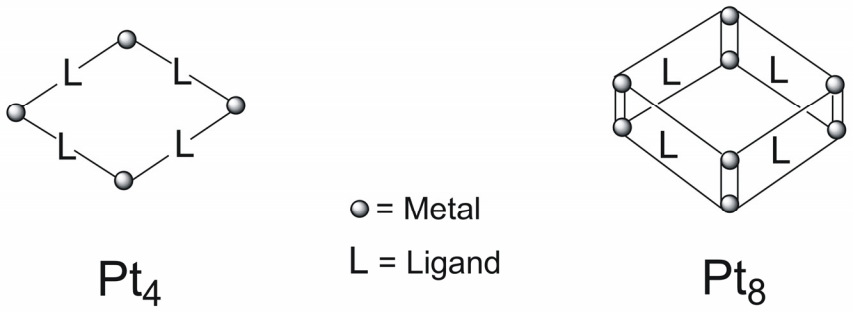

Scheme 3: Schematic diagrams of the tetra- and octanuclear cations $[(en)Pt(UH\text{-}N1,N3)]_4^{4+}$ (left),[38,39] and $[\{(en)Pt(U\text{-}N1,N3,O2,O4)Pt(NH_3)_2\}_4]^{8+}$ (right).[40]

The cyclic "Pt blues" oligomers with nucleobases[38-40] can also be considered as metal derivatives of the classical calixarenes. These coordination compounds showed structural similarities with the organic calixarenes. In addition, the

positive overall charge of these cycles leads to new properties of the metallacalix[n]arenes in comparison with the organic calix[n]arenes, making them very versatile compounds with numerous potential applications.

2 Analogy between Calix[n]arenes and Metallacalix[n]arenes

Calixarenes, cyclic compounds with a well-structured cavity, are presently the subject of considerable attention due to their versatility as host for inclusion complexation.[50-52] In addition, calixarenes can also act as efficient ligands for metal ions, through their basic oxo surface[53-58] and likewise through the arene π-electrons.[59-61] More recently, this approach has also been extended to systems containing metal fragments and organic ligands (see below). These metalla-analogues show a close similarity to the purely organic host systems like calix[n]arenes. However, the metal entities introduce a wide range of novel applications. To explain those, one has to look at the metallacalix[n]arene structures.

The strategy of forming metallacalix[n]arenes is the combination of metal fragments with 90° bond angles and organic ligands, which provide 120° bond angles. This situation is present in d^8 square planar metal entities like L_2M^{II} with M^{II} = Pt^{II} or Pd^{II} and L = *cis*-diammine. On the other hand, pyrimidine nucleobases like uracil, thymine and cytosine, provide the necessary 120° bond angles.[62,63]

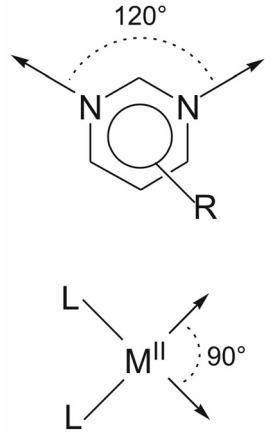

This strategy of formation is related to the formation of organic macrocycles. The metal entities replace the methylene groups and likewise the pyrimidine nucleobases replace the phenol moieties of the classical calixarenes.[64] These similarities are sketched in Scheme 4.

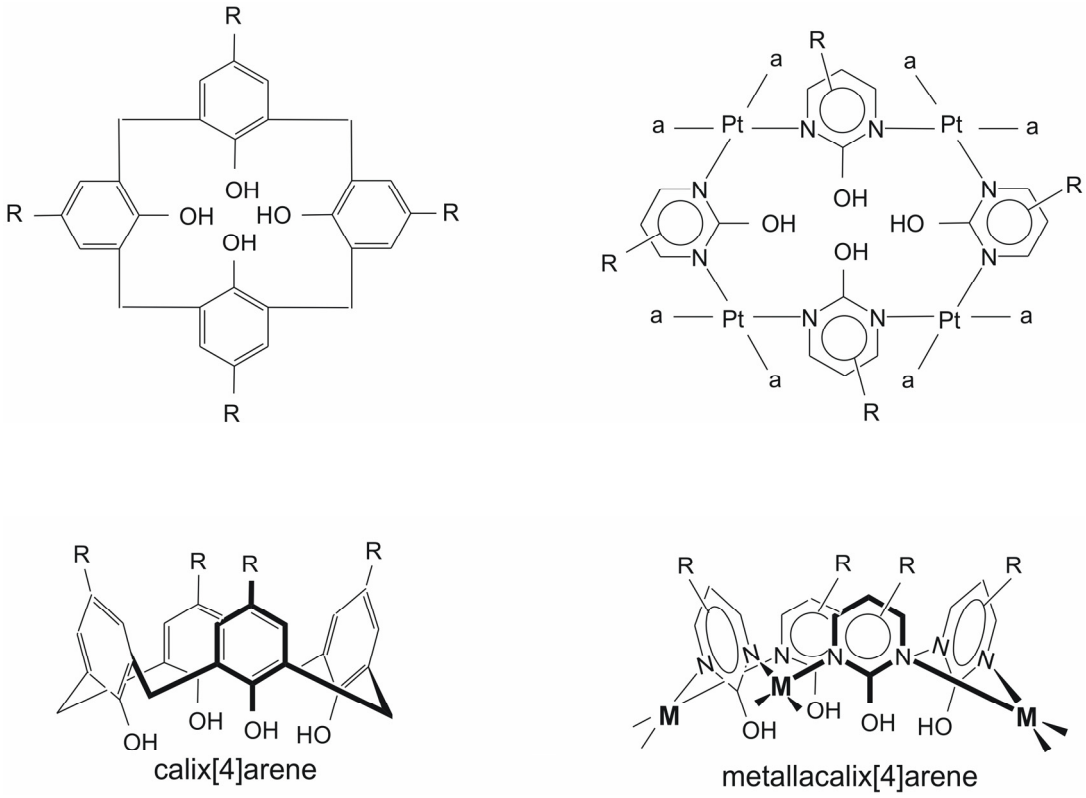

Scheme 4: Analogy between calix[4]arenes and metallacalix[4]arenes.

It was shown that this strategy allows to engineer the desired size (n = 3,[65] 4,[38,39,62,66-70] 6[64]) and functionalisation of the metallacalix[n]arenes through the appropriate choice of N-heterocycles and metal fragment.

Few years ago, H. Rauter et al.[38,39] showed the formation of a metallacalix[4] arene consisting of four Pt^{II}(en) entities cross-linked by four uracilate dianions, which later was proven to be able to act as an efficient ligand for additional metal ions.[40]

More recently, K. Yamanari et al.[71] described the formation of a cyclic hexamer. The complex consists of six Rh metal ions, six pentamethyl-cyclopentadienyl units and six 6-purinethione ribosido ligands, forming a cubic cavity.

In 2003, S.-Y. Yu et al.[72] proved that the self-assembly of six planar modules, three metal-coordination-complex ions, and three rigid aromatic ligand (4,7-pheneanthroline) lead to formation of metallacalix[3]arenes. The metal-

coordination complexes are cis-protected metal centers such as Pd^{II}(en), Pt^{II}(en), Pd^{II}(2,2'-bpy), Pt^{II}(2,2'-bpy), Pd^{II}(phen), and Pt^{II}(phen).

E. Barea et al.[64] reported the formation of a metallacalix[4]arene and a metallacalix[6]arene achieved by a self-assembly process, which involved *cis*-$[Pda_2(H_2O)_2]^{2+}$ (a_2 = (*R,R*)-1,2-diaminocyclohexane (*R,R*-dach), (*S,S)*-1,2-diaminocyclohexane (*S,S*-dach)), metal entities and hydroxypyrimidine derivatives.

Then M. A. Galindo et al.[73] showed a multicomponent reaction consisting of Pd^{II}(en) metal fragments, 2-pyrimidinol derivates and 4,7-phenanthroline, which led to the formation of three different metallacalix[n]arenes, in which n = 3, 4, 6 (Figure 2). After observing the large variety of possible products obtained by the self-assembly of metal entities and N-heterocycles, a the great versatility of these compounds is not unexpected.

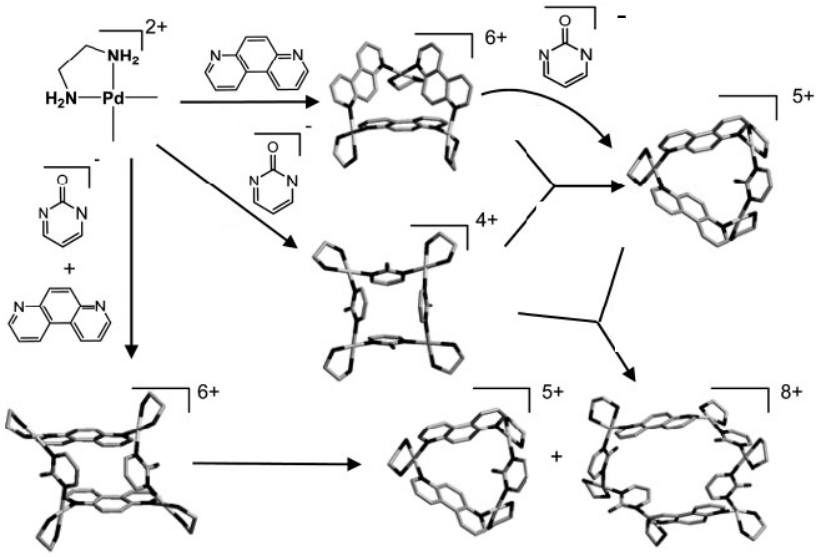

Figure 2: Summary of the cyclic species that can be obtained from ethylenediaminepalladium(II), 4,7-phen and 2-pymo derivatives.[73]

The metal entities introduce a wide range of novel applications in the host-guest chemistry. These metal fragments can act as efficient ligands for metal ions employing the exocyclic O-donor groups (pyrimidine derivatives) for binding, as do the organic calixarenes. For example, Navarro et al.[68] showed the coordination of some transition metals (Cu^{2+}, Co^{2+}, Ni^{2+} and Zn^{2+}) to [Pt(U-

N1,N3)(en)]$_4^{4+}$, where the heterometals are directly bonded to the oxygen atoms of the metallacalix[4]arene. Moreover, this kind of compounds can also include guest molecules through H-bonding interactions. The metallacalix[4]arene [Pt(pymo)(en)]$_4^{4+}$ (Hpymo = 2-hydroxypyrimidine) shows these receptor properties.[67] A [Cu(H$_2$O)$_6$]$^{2+}$ cation is sandwiched between the oxo surface of two [Pt(pymo)(en)]$_4^{4+}$ cations and interacts strongly through H bonding interactions between the water molecules coordinated to the copper center and the oxo surface of the metallacalix[4]arene (Figure 3).

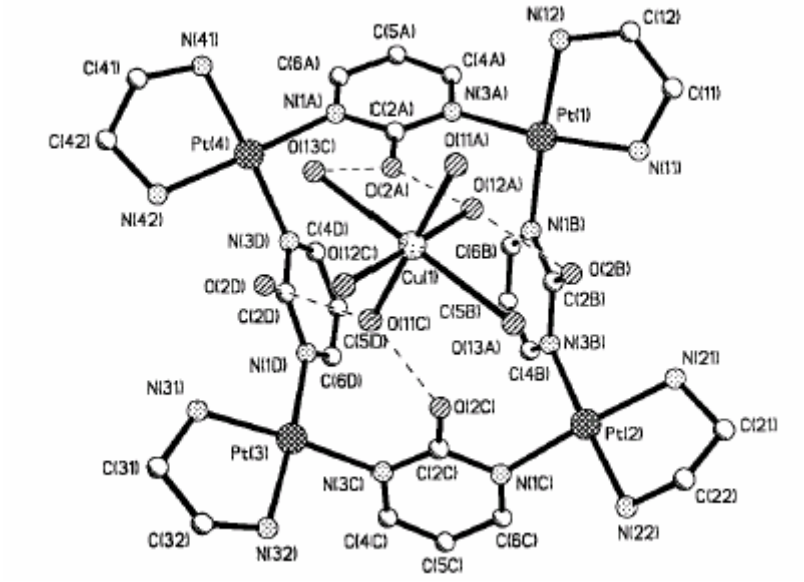

Figure 3: View of the interaction between [Cu(H$_2$O)$_6$]$^{2+}$ and a tetranuclear [Pt(pymo-N^1,N^3)(en)]$_4^{4+}$ cation.[67]

However, the metallacalix[n]arenes can also selectively encapsulate organic anions[63,66,74] due to the combination of the positive charge in the complex and the presence of an apolar cavity.

The formation of mixed–metal (Pt,Pd) metallacalix[n]arenes is reversible (Pd-N or Pd-O bonds are labile) and proceeds under thermodynamic control. Consequently, they might be adequately discussed in terms of Dynamic Combinatorial Chemistry (DCC). Some examples of Dynamic Combinatorial Libraries containing metal ions have been reported in the last years by Lehn,[75] Stulz et al.,[76] Gauthier et al.,[77] Saur et al.,[78] Brasey et al.[79] and Kubota et al.,[80] among others.

B AIM

The aim of this work is the preparation of cyclic complexes of unsubstituted uracil and unsubstituted cytosine with different Pt^{II} and Pd^{II} entities and the determination of their solid state structures. The unsubstituted nucleobases are considered very versatile ligands due to the large number of association patterns. There is not only the possibility of these ligands to bind to metal ions via N(1), N(3) or C(5) (only for uracil,[81]). Many possible combinations of two or more binding sites are feasible, as can be seen from Scheme 5.

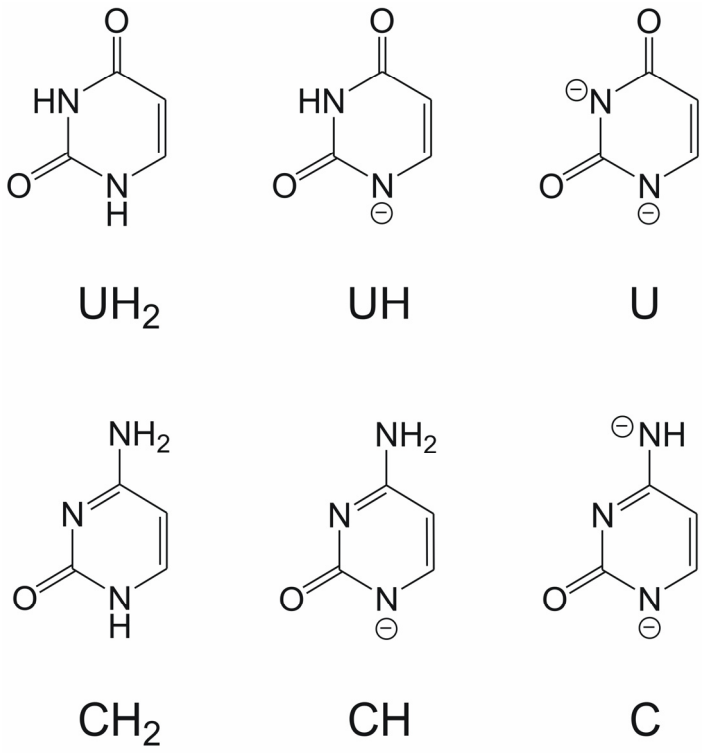

Scheme 5: Structures and abbreviations used for uracil and cytosine ligands. For UH, only the N(1) deprotonated tautomer is shown, and other appropriate mesomeric structures are ignored.

On the other hand, the use of the unsubstituted pyrimidine nucleobases with platinum metal fragments can lead to the formation of the so-called "platinum blues", which have not completely been understood until now. Therefore another aim of this work includes the clarification of the reactivity patterns of these "platinum pyrimidine blues". One characteristic property of these compounds is their intense color due to the charge transfer (CT) between the mixed-valence Pt centers.

The goals of this thesis therefore are:

- To synthesize a series of metallacalix[n]arenes, derived from square planar metal fragments and unsubstituted pyrimidine nucleobases (uracil and/or cytosine). Herefore, different bulky ligands bonded to the metal ions (Pt^{II} and Pd^{II}) shall be used, such as *cis*-diammine, ethylenediamine, 2,2'-bipyridine or *N,N,N',N'*-tetramethylethylenediamine. These can be expected to influence the size of the macrocycles that are synthesised.

- To understand the reactivity patterns of these systems, for example in the case of the removal of the metal entities bonded to the oxygen atoms or the interconversion mechanism of these species.

- To use these complexes as versatile hosts for different guest molecules such as anions and cations, where the size of the complex cavities as well as the conformation adopted for the nucleobaes will play an important role.

- To help to clarify the mystery of the "platinum pyrimidine blues" by substituting slowly reacting *cis*-$Pt^{II}(NH_3)_2$ entities by faster reacting *cis*-$Pd^{II}a_2$ analogues, which at the same time prevent the Pt redox chemistry.

In the following, several X-ray structural characterized compounds (indicated with numbers in bold), some isolated compounds by ^{1}H NMR spectroscopy (with a letter) and a multitude of postulated compounds that could not be isolated nor detected in the reaction mixtures by ^{1}H NMR spectroscopy (with number) will be discussed. In the schemes of the interconversion mechanisms of these species, the X-ray structurally characterized complexes are marked by a red box. Finally, it should be noted that compounds derived from the Pd^{II}(2,2'-bpy) entity are indicated without prime, compounds derived from Pd^{II}(en) are indicated with a prime and compounds derived from Pd^{II}(tmeda) are indicated with a double prime.

C RESULTS AND DISCUSSION

Chapter I:
Mixed-Nucleobase (Uracil and Cytosine) Complexes

1 Introduction

Supramolecular chemistry and self-assembly are at the frontiers of the molecular sciences, as evidenced by the intense interest and the great growth of publications in this area in the last years.[82] Particularly, metal-coordination-driven self-assembly has been successfully used for the construction of two- and three dimensional supramolecular units with diverse structures and properties.[83] Their sizes and shapes can be conveniently controlled by modification of the ligand and by the selection of metal fragments with appropriate geometries. It is noteworthy to mention that intramolecular forces, such as hydrogen bonds, also play an important role in the "molecular architecture".[63]

This work specifically deals with the combination of transition-metal units with 90° bond angles (*cis*-$M^{II}a_2$; M = Pt or Pd) and unsubstituted pyrimidine nucleobases (uracil and cytosine) providing 120° bond angles via the N(1) and N(3) sites.

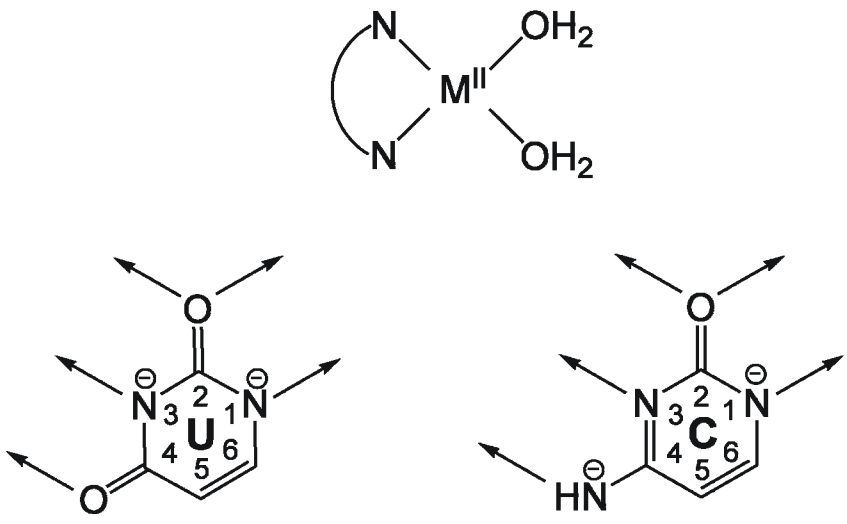

Scheme 6: Schematic representation of the square planar metal geometry and the pyrimidine nucleobase binding patterns (uracil and cytosine dianions), respectively.

This combination can lead to a large number of possible geometries. One possibility is the formation of open boxes or molecular squares. Some of these patterns are depicted in Scheme 7.

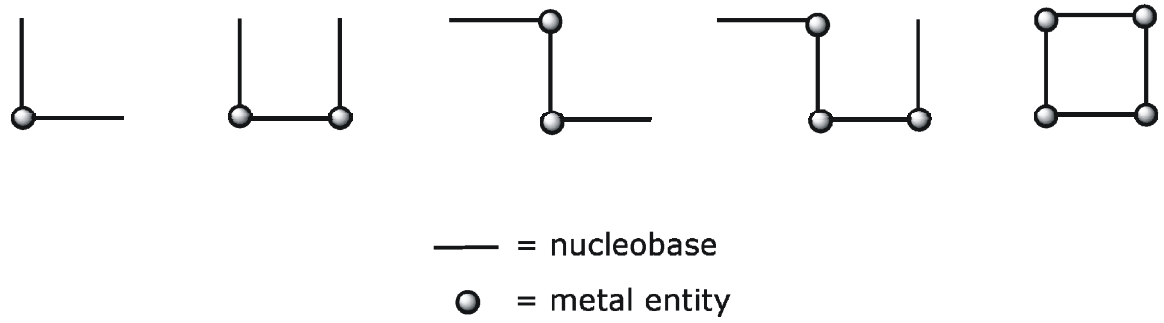

Scheme 7: Schematic representation of fragments leading to a molecular square/box.

Here, one has to quote the cyclic, tetranuclear Pt(II)-uracil-complex synthetized by H.Rauter et al.[38-40] It is a metal-containing analogue of the classical calixarenes. The combination of the 90° angle of the Pt^{II}(en) entity with the 120° angle between the vectors of the N(1) and the N(3) sites of the uracil nucleobase led to the spontaneous self-assembly to the $[Pt(UH\text{-}N1,N3)(en)]_4(NO_3)_4$ molecular box (Figure 4), which consists of four Pt^{II}(en) entities forming the corners and four uracil dianions comprising the sides of this square. Because the heterocyclic nucleobases are essentially perpendicular to the Pt coordination planes, the expression "open box" seems to be appropriate.

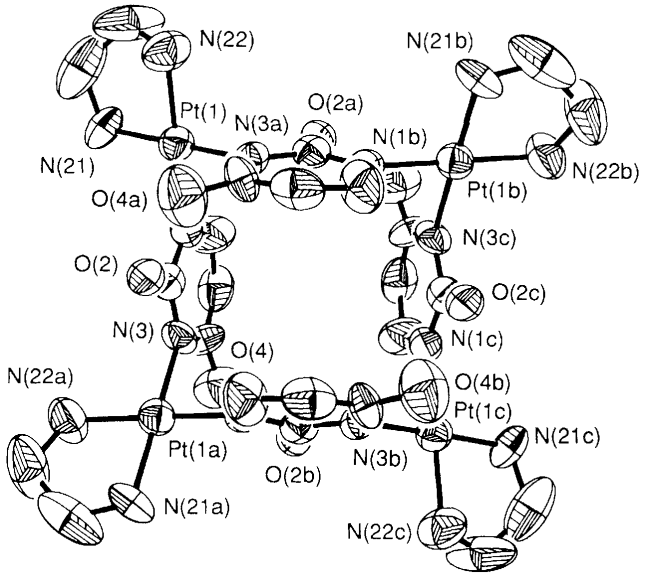

Figure 4: Crystal structure of the cation $[Pt(UH\text{-}N1,N3)(en)]_4^{4+}$.[38]

As in the classical calix[4]arenes, in which the phenol groups can adopt four conformations, in the metallacalix[4]arenes the orientation of the nucleobases can lead to the formation of different conformers. The four possible calix[4]arene conformers are shown in Scheme 8.

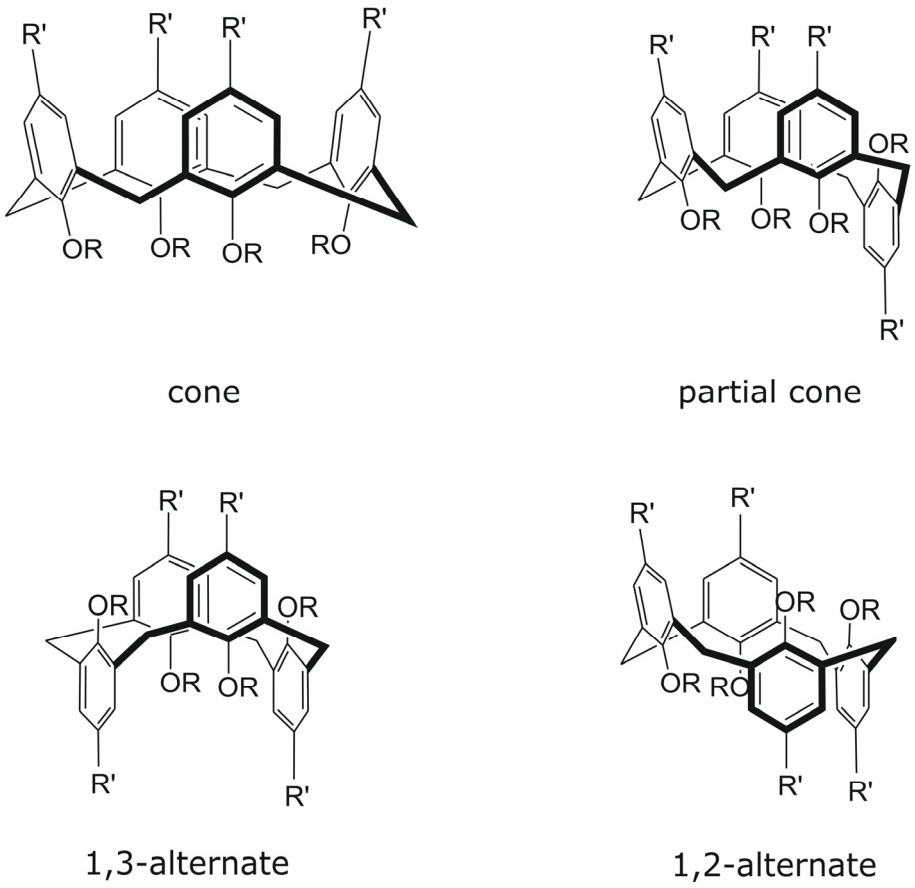

Scheme 8: Schematic representation of the four conformations of the classical calix[4]arenes.

On the other hand, due to the presence of exocyclic O(2) and O(4) sites of the uracil, and O(2) and N(4) sites of the cytosine (see Scheme 6), additional coordination of (more) metal entities to these sites is possible. The result is the formation of "extended" molecular boxes. A schematic diagram of the addition of more metal units to the parent compound is given in Scheme 9.

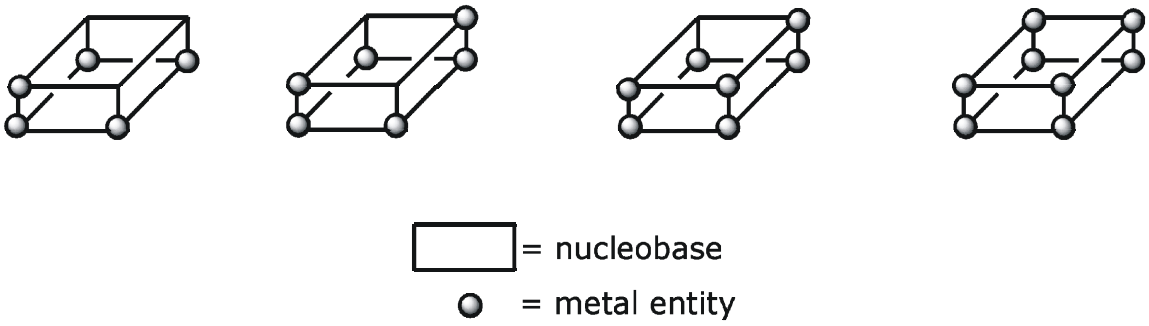

Scheme 9: Schematic representation of "extended" molecular boxes.

Several of these complexes can also be found in the literature. For example, addition of *cis*-$Pt^{II}(NH_3)$ moieties to the O(2) and O(4) exocyclic positions of the uracil in the $[Pt(UH\text{-}N1,N3)(en)]_4^{4+}$ metallacalix[4]arene (Figure 4) led to the octanuclear complex $[\{(en)Pt(U\text{-}N1,N3,O2,O4)Pt(NH_3)_2\}_4]^{8+}$ (Figure 5).[40] In the same way, reactions of the *1,3*-alternate conformer of the tetranuclear complex with other divalent ions like Cu^{2+}, Co^{2+}, Ni^{2+} or Zn^{2+}, result in the formation of octanuclear compounds with general formula $[\{(en)Pt(U\text{-}N1,N3,O2,O4)M\}_4]^{8+}$.[68]

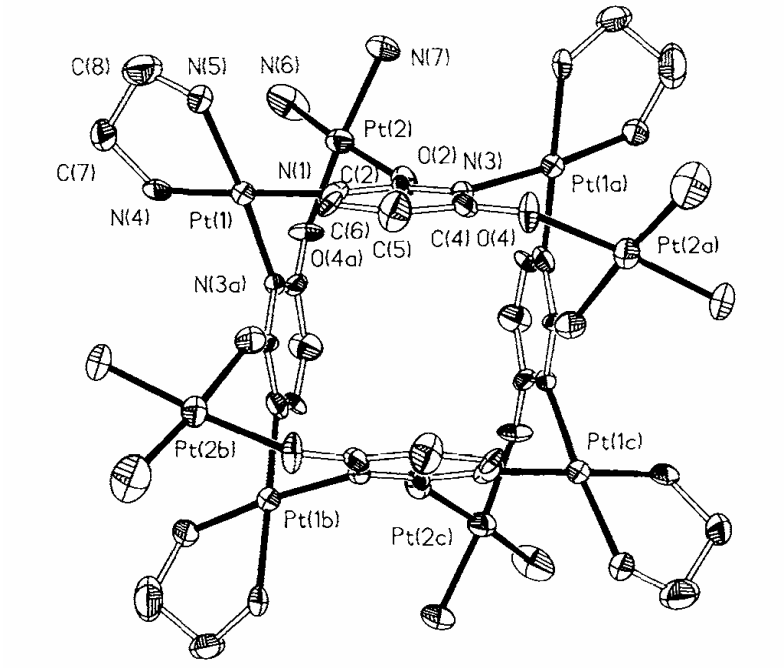

Figure 5: Crystal structure of the cation $[\{(en)Pt(U\text{-}N1,N3,O2,O4)Pt(NH_3)_2\}_4]^{8+}$.[40]

Theoretically, the 90° angle metal fragments and the pyrimidine nucleobases can also lead to the formation of larger, strongly folded structures that are different from the metallacalix[n]arenes discussed so far.

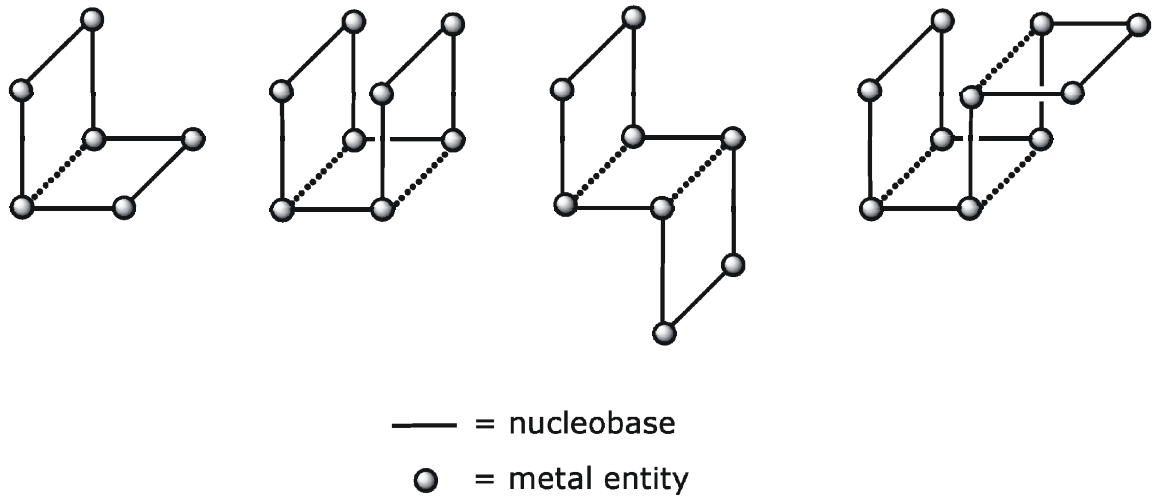

Scheme 10: Schematic representation of "extended" molecular boxes.

In this chapter, the formation of different molecular boxes derived from the reaction of a mixed-nucleobase compound of Pt with different *cis*-$M^{II}a_2$ metal entities will be discussed.

2 Starting Compound: [Pt(UH-*N1*)(CH_2-*N3*)(en)]X•nH_2O (1)

The mixed 2:1 complexes with the nucleobases uracil and cytosine were obtained by addition of the 1:1 complex PtCl(UH-*N1*)(en)•H_2O[41] to unsubstituted cytosine (CH_2) in aqueous solution and abstraction of Cl^- by Ag^+.

$$\text{PtCl(UH-}N1\text{)(en)}\bullet H_2O \xrightarrow[\text{- AgCl}]{\text{1. } CH_2 \text{ 2. AgX}} \text{[Pt(UH-}N1\text{)(}CH_2\text{-}N3\text{)(en)]X}\bullet nH_2O$$

X = ClO_4, n = 3 (**1a**)
X = NO_3, n = 3.5 (**1b**)

Compound **1a**, which was used as starting material in most of the reactions, was synthesized and characterized by X-ray crystallography previously in our group.[84] The IR spectrum of **1b** is similar to **1a** with regard to the bands of the nucleobases. However, in **1b** an intense band at ca. 1380 cm^{-1} is observed, which is assigned to a nitrate ion in comparison to the bands of the perchlorate ion present in **1a** (1052, 1090 and 1120 cm^{-1}).

X-Ray Crystallography

The structure of **1b** was also determined by X-ray crystallography. Compound **1b** crystallizes in the triclinic space group P-1 with two different cations (I and II) forming the asymmetric unit. The structures of the two cations of **1b** are depicted in Figure 6 and the distances and angles of the structure are given in Table 1.

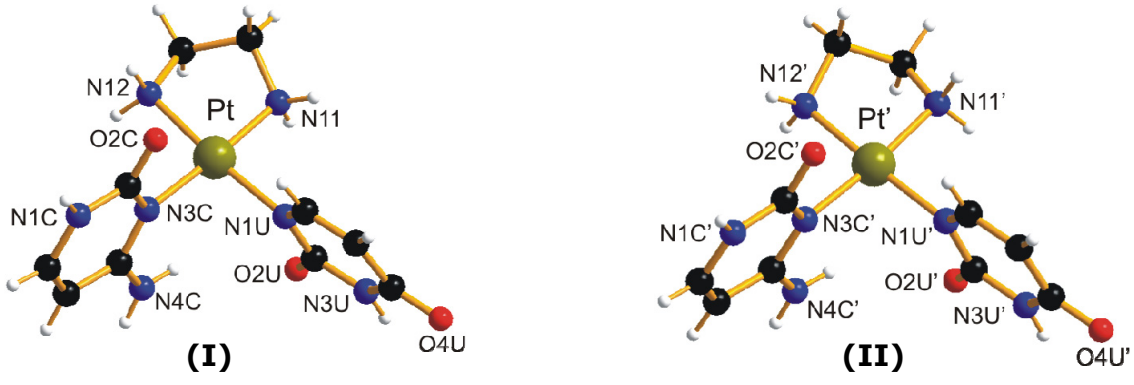

Figure 6: View of the two crystallographic independent cations of [Pt(UH-*N1*)(CH_2-*N3*)(en)](NO_3)•3.5H_2O (**1b**).

Table 1: Selected interatomic distances (Å) and angles (°) of the two different cations of [Pt(UH-*N1*)(CH_2-*N3*)(en)](NO_3)•3.5H_2O (**1b**).

Pt-N(1)U	2.030(9)	N(11)-Pt-N(12)	83.6(3)
Pt-N(3)C	2.019(7)	N(1)U-Pt-N(3)C	90.8(3)
Pt-N(11)	2.001(7)	N(11)-Pt-N(1)U	92.1(3)
Pt-N(12)	2.036(8)	N(12)-Pt-N(3)C	93.6(3)
Pt'-N(1)U'	2.025(8)	N(11)'-Pt'-N(12)'	83.0(3)
Pt'-N(3)C'	2.014(7)	N(1)U'-Pt'-N(3)C'	90.1(3)
Pt'-N(11)'	2.017(7)	N(11)'-Pt'-N(1)U'	94.2(3)
Pt'-N(12)'	2.030(9)	N(12)'-Pt'-N(3)C'	92.8(3)

A square planar coordination geometry for the platinum is observed in both cations. Distances and angles about the Pt and within the nucleobases are in the usual range. For example, the Pt-N distances are between 2.001(7) and 2.036(8) Å. As expected, cytosine is coordinated via the N(3) position while uracil is coordinated via the N(1) position to platinum. If the O(2) groups of the two nucleobases are used as a reference, the two bases are oriented *head-tail* in both cations, with O(2) of the uracilato ligand and O(2) of the cytosine at different sides of the Pt coordination plane, as could also be observed for the perchlorate salt **1a**. The two cations in **1b** differ with respect to angles between the nucleobases and PtN_4 planes (I, II), respectively. Dihedral angles between the PtN_4 coordination plane and the nucleobase planes are 79.4(3)° (CH_2) and 75.2(2)° (UH) in (I) and 87.8(2)° (CH_2) and 80.7(2)° (UH) in (II). The angle between the two bases is 77.8(2)° in (I) and 78.1(2)° in (II). In addition, the puckers of en ligands differ in (I) and (II) (Figure 6). The differences between coordinated and free ligands (CH_2[85], UH_2[86]) follow expectations previously discussed in detail for related coordination patterns.[37,38,87-89]

Both cations **1a** and cations (I) of **1b** form centrosymmetric dimers hydrogen-bonded through N(3)H and O(4) sites of uracilato ligands (2.85(1) in **1a**, and 2.813(10) Å in **1b**). Similar self-pairing schemes have been observed in other metal complexes containing N(1) bonded pyrimidine nucleobases.[90,91] These hydrogen bonds are represented in Figure 7 for **1b**.

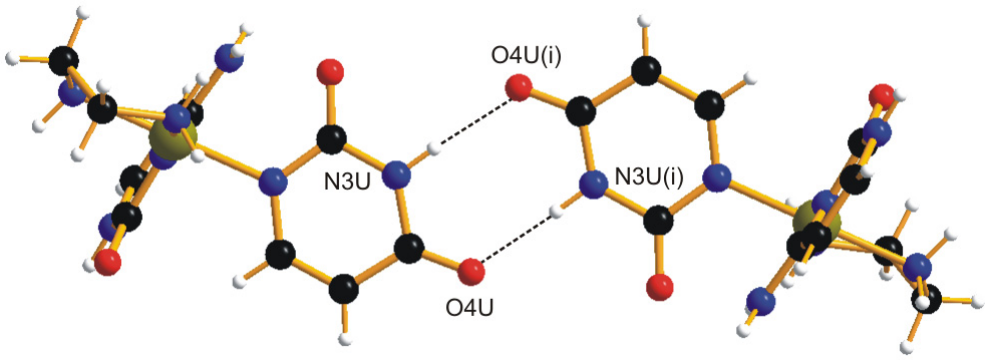

Figure 7: Detail of hydrogen bonding pattern between cations (I) in **1b** involving the uracilate ligands.

On the other hand, the cytosine ligands of cations (II) of **1b** likewise form centrosymmetric pairs, through N(1)H and O(2), with hydrogen bond lengths of 2.813(9) Å (Figure 8).

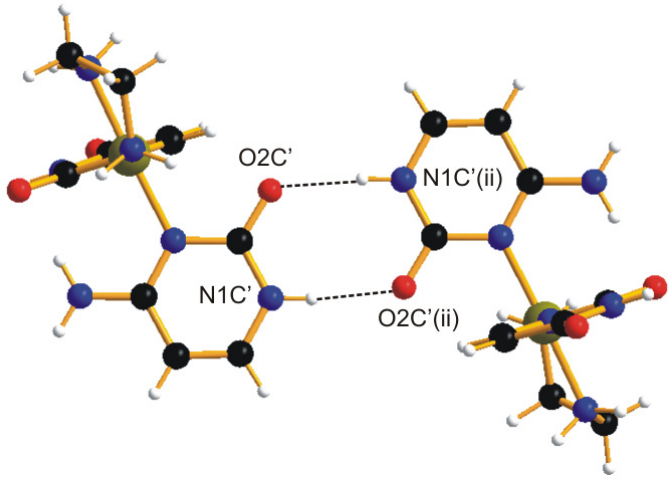

Figure 8: Detail of hydrogen bonding pattern between cations (II) in **1b** involving the cytosine ligands.

All atoms of the cation as well as all atoms of the nitrate ions and water molecules were refined anisotropically with the exception of two water molecules (O6W and O7W), which are each disordered over two positions (with occupancies of 50%).

The water molecules and the anions are involved in numerous H-bonding interactions, too. Feasible hydrogen bond lenghts are given in Table 2.

Table 2: Distances (Å) of the possible hydrogen bonds in [Pt(UH-*N1*)(CH_2-*N3*)(en)](NO_3)•3.5H_2O (**1b**).

N(3)U···O(4)U$^{(i)}$	2.813(10)	O(11)···O3w	2.787(9)
N(1)C′···O(2)C′$^{(ii)}$	2.813(9)	O(12)···-O1w	3.091(9)
N(3)U′-O1w	2.862(9)	O(21)···O3w	3.246(9)
O(4)U′-O7w	2.74(1)	O(22)···O1w	2.96(1)
O(2)U′-O6w	2.77(1)	O(31)···O5w	3.00(1)
O(2)C′···O5w	2.98(1)	O2w···O3w	2.68(1)
N(12)···O21	2.90(1)	O2w···O4w	2.76(1)

Symmetry codes: (i) –x,-y,-z-1; (ii) –x, 1-y, -z.

NMR Spectroscopy

The ^{1}H NMR spectrum of **1** consists of discrete doublets ($^3J \approx 7.3$ Hz for both nucleobases) for the H(5) and the H(6) resonances. Chemical shifts are given in Table 10 (see Chapter I: Summary) and the spectrum at pD = 5.45 is shown in Figure 9.

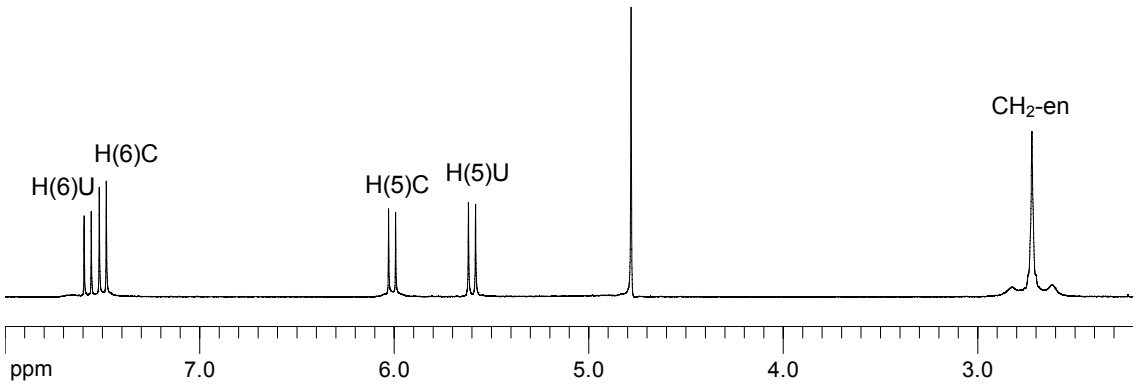

Figure 9: ^{1}H NMR spectrum of [Pt(UH-*N1*)(CH_2-*N3*)(en)](NO_3)•3.5H_2O (**1b**) in D_2O, pD = 5.45.

Only single sets of proton signals of the individual bases are observed, suggesting either rapid rotation of the nucleobases on the NMR time scale or hindered rotation (see Scheme 11). As expected there are no differences in the chemical shift of the signals of products **1a** and **1b** in the ^{1}H NMR spectra. As mentioned before, the starting compound **1a** was synthesized and characterized previously in our group, in which the assignment of the resonances to the

individual bases was accomplished using a ^{195}Pt edited spectrum. According to it, the cytosine displays ^{4}J coupling between ^{195}Pt and H(5) (17.5 Hz), whereas there is no ^{5}J coupling with H(6). The coupling constant for H(5) is in the expected range.[89] On the other hand, H(6) of the uracilato ligand is recognized by its considerably larger ^{3}J (^{195}Pt-^{1}H) coupling constant of 34 Hz, which is a consequence of the close proximity of Pt at N(1) and H(6). ^{4}J coupling with H(5) of UH is not observed.

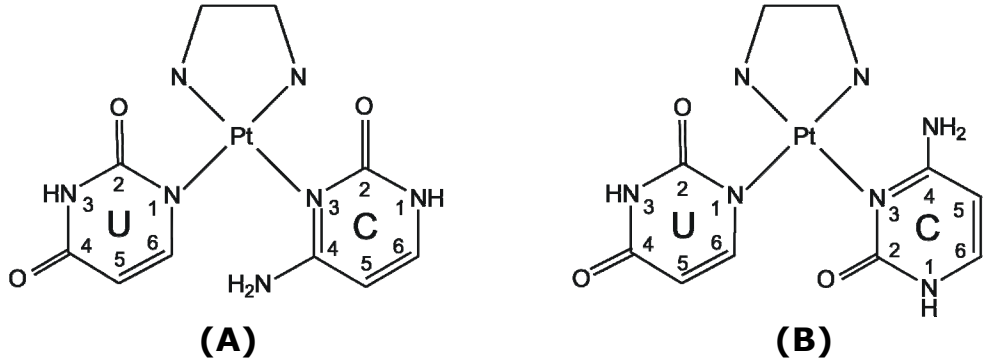

Scheme 11: Schematic diagram of the two possible rotation isomers of **1**.

Resonances of **1** in D_2O are constant over a wide range of pH* (1.5 - 8.5).[84] In more strongly alkaline solution deprotonation of the cytosine-N(1)H position takes place (pK_{a1} ~ 9.9), and eventually also deprotonation of the uracilato ligand at N(3)H sets on (pK_{a2} ~ 11.4). While H(5)- and H(6)-uracil as well as H(5)-cytosine are shifted upfield as a consequence of deprotonation, H(6)-cytosine undergoes a downfield shift. The effect of the acidification of the two nucleobases as a consequence of Pt^{II} binding is significant. The pK_a value of cytosine changes from 12.15[92] to 9.9 (2.25 log units), and for uracil in a similar magnitude, namely from 13.5-14.2 (pK_{a2} of uracil)[93-95] to 11.4.

With time a gradual isotopic exchange of the H(5) proton of the uracilate ligand by deuterium is observed.

Reactions of **1** with *cis*-$Pt^{II}a_2$ derivatives, such as Pt^{II}(en), were carried out and were studied by ^{1}H NMR spectroscopy previously in our group.[84] Several changes could be detected in the solutions, but these observations could not be interpreted in any straightforward way. Due to the failure to characterize any of the products formed from **1** and Pt^{II}(en), it was resorted to experiments

described in this thesis, in which **1** was allowed to react with *cis*-$Pd^{II}a_2$ analogues, where a_2 = (2,2'-bpy), (en) or (tmeda).

The major difference of the mixed-metal system in comparison to the system containing exclusively Pt^{II}(en) entity was the sharpness of the resonances observed in the ^{1}H NMR spectra in the mixed-metal systems. In the following chapters, these kinds of systems will be analysed and discussed.

3 Complexes with $[Pd(2,2'\text{-bpy})(H_2O)_2]^{2+}$

The first $Pd^{II}a_2$ entity that was reacted with $[Pt(UH\text{-}N1)(CH_2\text{-}N3)(en)]^+$ (**1**) was $Pd^{II}(2,2'\text{-bpy})$. The 2,2'-bipyridine (2,2'-bpy) is a planar bidentade ligand able to react with metal ions through the nitrogen atoms at N(1) and N(1') positions. In $PdCl_2(2,2'\text{-bpy})$, palladium adopts a square planar geometry. In aqueous solution, the chloride ions can be removed by addition of silver salts to give the aqua species $[Pd(2,2'\text{-bpy})(H_2O)_2]^{2+}$, which can, in our case, react with other molecules, such as nucleobases.

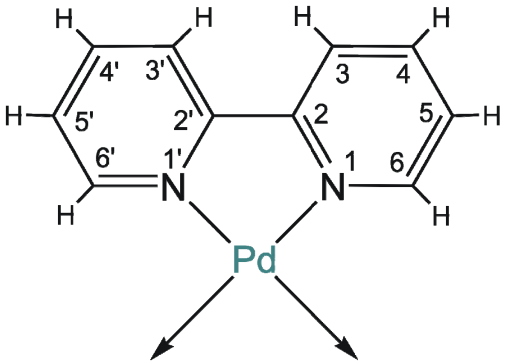

Several examples of this chelating ligand forming compounds of different size, depending on the cross-linked ligands, have been reported. Some of these examples that are related to this work are described below.

Fifteen years ago Lippert et al.[96-98] used the 2,2'-bipyridine ligand to substitute the ammine ligands of the *cis*-$Pt^{II}(NH_3)_2$ entities and to study the steric effects in the formation of the complexes with nucleobases. Drastical changes in the basic structural patterns were not observed.

More recently M. Quirós et al.[99] synthesized a dinuclear complex containing two $Pd^{II}(2,2'\text{-bpy})$ entities bonded at the N(3) and the N(4) positions of two anionic forms of the ligand 4,7-dihydro-7-oxo-[*1,2,4*]-triazolo[1,5-*a*]pyrimidine.

Cyclic tetra-, hexa-, and octanuclear complexes derived from $Pd^{II}(2,2'\text{-bpy})$ entities with linear ligands have been published by S-Y. Yu et al.[100] in 2005. Here, the Pd moieties occupy the corners of the molecular squares. Two $Pd^{II}(2,2'\text{-bpy})$ entities stacked in each corner can also be found in some of these compounds due to the ability of this ligand to build out π-stacking interactions.

3.1 Synthesis, Characterization and Reactivity

The reactions of $[Pd(2,2'\text{-bpy})(D_2O)_2]^{2+}$ added to solutions of $[Pt(UH\text{-}\textit{N1})(CH_2\text{-}\textit{N3})(en)](ClO_4)\bullet 3H_2O$ (**1a**) at different ratios in D_2O at room temperature were followed by ^1H NMR spectroscopy. Within minutes after the start marked changes took place, which included a rapid drop in pD (from ca. 5 to ca. 2) and the development of an intensive yellow color. The pD was adjusted to roughly 7.5 using NaOD (1M).

In Figure 10 representative ^1H NMR spectra of the reaction of **1a** with a $Pd^{II}(2,2'\text{-bpy})$ entity are shown. Several of the products (**2a**, **4** and **7**) were isolated and characterized by X-ray crystallography. The resonances observed in the ^1H NMR study are assigned from comparison with the ^1H NMR spectra of the crystals in solution. The three major species present in the mixture of **1** and $Pd^{II}(2,2'\text{-bpy})$ are the trinuclear complex $[(2,2'\text{-bpy})Pd\{(\textit{N1}\text{-CH-}\textit{N3})(en)Pt(UH\text{-}\textit{N1})\}_2]^{2+}$ "Pt_2Pd" (**2a**), the pentanuclear complex $[\{(2,2'\text{-bpy})Pd\}_3\{(en)Pt(\textit{N1}\text{-U-}\textit{N3,O4})(\textit{N3}\text{-CH-}\textit{N1})\}_2]^{4+}$ "Pt_2Pd_3" (**4**) and the hexanuclear complex $[\{(2,2'\text{-bpy})Pd\}_4\{(en)Pt(\textit{N1}\text{-U-}\textit{N3,O4})(\textit{N3}\text{-HC-}\textit{N1,O2})\}_2]^{6+}$ "Pt_2Pd_4" (**7**). Compound X could not be isolated in the solid state, but its formation was observed in other reactions, hence, its resonances could also be assigned in the ^1H NMR study (Figure 10).

There are two general points to be noted. First, some of the spectra display a large number of doublets of the H(5) and H(6) nucleobase resonances, representing a multitude of species formed simultaneously. Second, frequently gradual isotopic exchange of the H(5) protons of the uracil (and also of the cytosine) resonances is observed, resulting in "pseudo-triplet" patterns of H(6) resonances (see, e.g. resonance at 6.8 ppm Figure 10c) or eventually in H(6) singlets.

Severe overlap of bipyridine resonances occurs, which also affects the H(6) nucleobase resonances. With a few exceptions, these resonances were not analyzed for this reason.

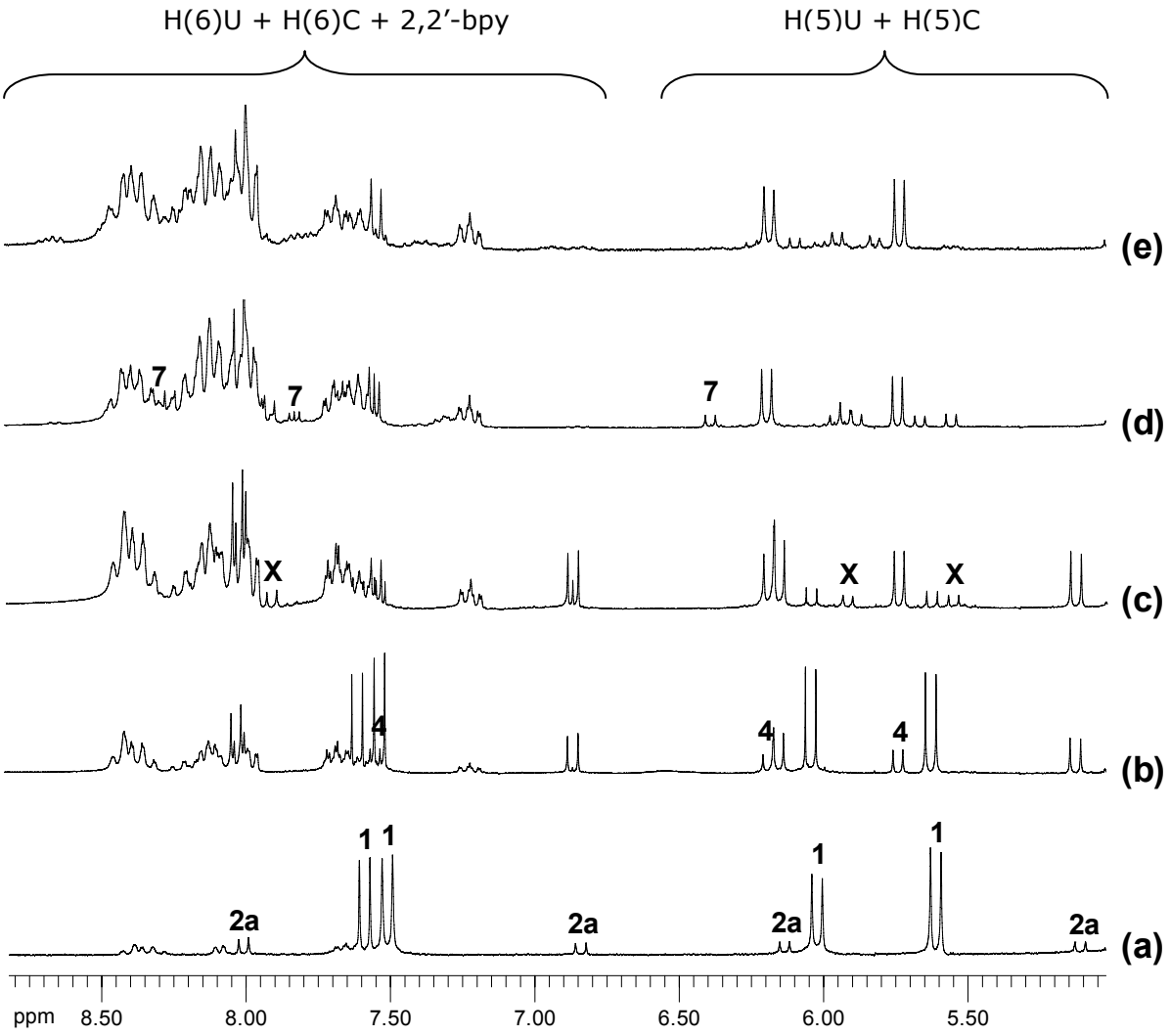

Figure 10: Low field section of the ^{1}H NMR spectra of the reaction of [Pt(UH-*N1*)(CH_2-*N3*)(en)](ClO_4)•3H_2O (**1a**) with [(Pd(2,2'-bpy)(D_2O)$_2$]$^{2+}$ in D_2O where r = Pt:Pd is:
(a) r = 1:0.1, pD = 7.35;
(b) r = 1:0.5, pD = 7.15;
(c) r = 1:1, pD = 7.15;
(d) r = 1:2, pD= 7.55;
(e) r = 1:3, pD = 7.02.

After the ^{1}H NMR study of Pd^{II}(2,2'-bpy) with **1a** in aqueous solution at different ratios (r), the aim was to isolate each of the compounds observed to understand the reactivity patterns of the system. Preparations at different ratios were carried out and also in some cases the pH of the solutions was changed. In the following, the synthesis and characterization of all of the compounds isolated are reported. Based on these established structures, possible ways of their formation can be discussed, including species which have not explicity been detected by ^{1}H NMR spectroscopy.

3.1.1 Pt_2Pd : $[(2,2'\text{-bpy})Pd\{(N1\text{-CH-}N3)Pt(UH\text{-}N1)\}_2](ClO_4)(NO_3)\cdot 4.9(H_2O)$ (2a) (Connectivity = cytosine-uracil-uracil-cytosine)

Addition of $[Pd(2,2'\text{-bpy})(H_2O)_2]^{2+}$ to an aqueous solution of **1a** at r = 0.5 leads to new resonances of a species **2a**, which was characterized as Pt_2Pd complex $[(2,2'\text{-bpy})Pd\{(N1\text{-CH-}N3)(en)Pt(UH\text{-}N1)\}_2]^{2+}$ (**2a**). In this case, $AgClO_4$ was used to obtain the aqua species of $PdCl_2(2,2'\text{-bpy})$, with subsequent filtration of AgCl. The yellow solution was stirred for one day (pH = 2.1). Afterwards, the pH was adjusted to 10 by addition of NaOH (1M) and a small amount of $NaNO_3$ was added to improve crystallization. After three days light yellow crystals of the title compound as its mixed ClO_4^- NO_3^- salt were obtained from the solution at room temperature, as well as colorless crystals of the starting compound **1a**.

X-Ray Crystallography

The composition and structure of **2a** were determined by X-ray crystallography. The trinuclear Pt_2Pd compound consists of two ethylenediamine platinum entities, one bipyridine palladium entity and four nucleobases. A view of the cation is given in Figure 11. Selected bond distances and angles of the cation are compiled in Table 3. Compound **2a** crystallizes in the triclinic space group P-1 with two cations of the trinuclear complex (I) and (II) forming the asymmetric unit. Formation of **2a** is the result of two cations of **1** being cross-linked by a $Pd^{II}(2,2'\text{-bpy})$ entity via each of the N(1) positions of the two cytosine ligands, following deprotonation of these sites. Preferential binding of Pd^{II} to N(1) of cytosine as opposed to N(3) of uracilate may be considered as expected, given the lower pK_a of N(1)H of cytosine as compared to N(3)H of uracilate. However, considering the binding patterns seen in the other structurally characterized compounds containing Pd-uracil-*N3* bonds, this argument should not be overemphasized. After all, the reactive Pd "aqua" species is present largely as a hydroxo complex capable of abstracting weakly acidic protons from nucleobases.

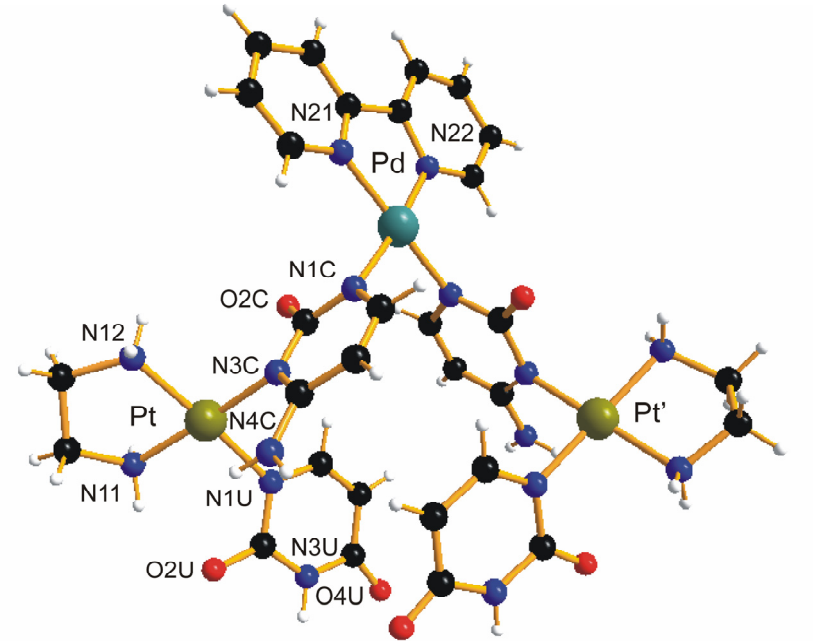

Figure 11: Crystal structure of the cation (I) of [(2,2'-bpy)Pd{(*N1*-CH-*N3*)(en)Pt(UH-*N1*)}$_2$](NO$_3$)(ClO$_4$)•4.9H$_2$O (**2a**).

Table 3: Selected interatomic distances (Å) and angles (°) in **2a**.

Pt-N(1)U	2.009(14) - 2.026(13)	N(11)-Pt-N(12)	82.2(5) - 85.8(8)
Pt-N(3)C	1.994(11) - 2.035(13)	N(1)U-Pt-N(3)C	87.8(5) - 91.3(5)
Pt-N(11)	2.019(12) - 2.045(14)	N(11)-Pt-N(1)U	92.7(6) - 94.6(6)
Pt-N(12)	1.930(14) - 2.050(13)	N(12)-Pt-N(3)C	90.2(5) - 96.4(5)
Pd-N(1)C	1.989(13) - 2.024(13)	N(21)-Pd-N(22)	80.4(6) - 81.4(6)
Pd-N(1)C'	1.990(12) - 2.033(12)	N(1)C-Pd-N(1)C'	88.3(5) - 89.0(5)
Pd-N(21)	2.000(13) - 2.004(14)	N(21)-Pd-N(1)C	95.1(6) - 95.8(5)
Pd-N(22)	2.020(14) - 2.024(14)	N(22)-Pd-N(1)C'	94.6(5) -95.4(5)

The asymmetric unit of **2a** is composed of the two crystallographically independent cation (I) and cation (II), as well as two nitrate and two perchlorate counterions. 9.8 crystal water molecules are also found in the structure. The oxygen atoms that belong to one of the perchlorate counterions are disordered over multiple positions with 50% occupancy each.

The two crystallographic independent cations of compound **2a** (I) and (II) differ from each other in the distances and angles of the metals with the nucleobases as well as in the puckers of the ethylenediamine ligands. The intermetallic Pt···Pd distances range from 5.847(2) Å to 5.908(2) Å in (I) and from 5.824(2) Å to 5.924(2) Å in (II).

In Scheme 12 a simplified version of the crystal structure of cation (I) of **2a** is shown, together with a schematic representation of the nucleobase connectivities (with Pt = Pt^{II}(en) and Pd = Pd^{II}(2,2'-bpy)).

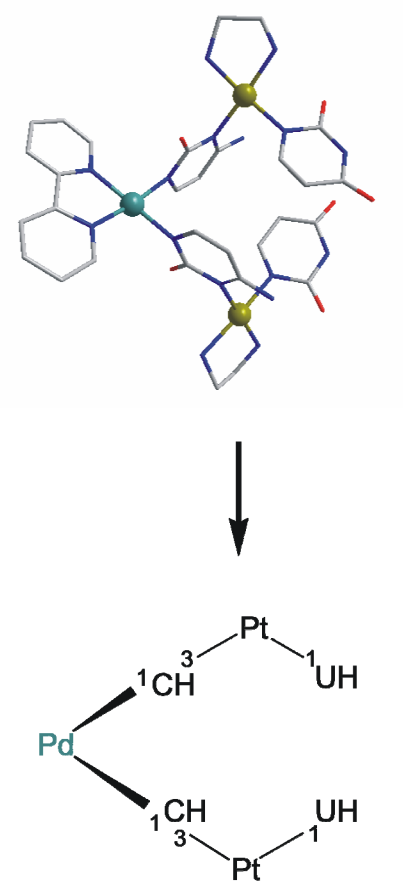

Scheme 12: Schematic view of the cation (I) of compound **2a** with nucleobase connectivities indicated.

As a consequence of this cross-linking pattern, the sequence of nucleobases in the tetrakis(nucleobase) complex is (UH-*N1*)Pt(*N3*-CH-*N1*)Pd(*N1*-CH-*N3*)Pt(*N1*-UH) (see Scheme 12, clockwise), hence the two inner cytosine nucleobases are adjacent to each other. The orientation of the nucleobases is *head-tail*, causing the two Pt atoms to be at opposite sites of the PtN_4 coordination plane. As can be seen from Figure 12, the two terminal uracilate ligands are stacked (4.0-4.6 Å).

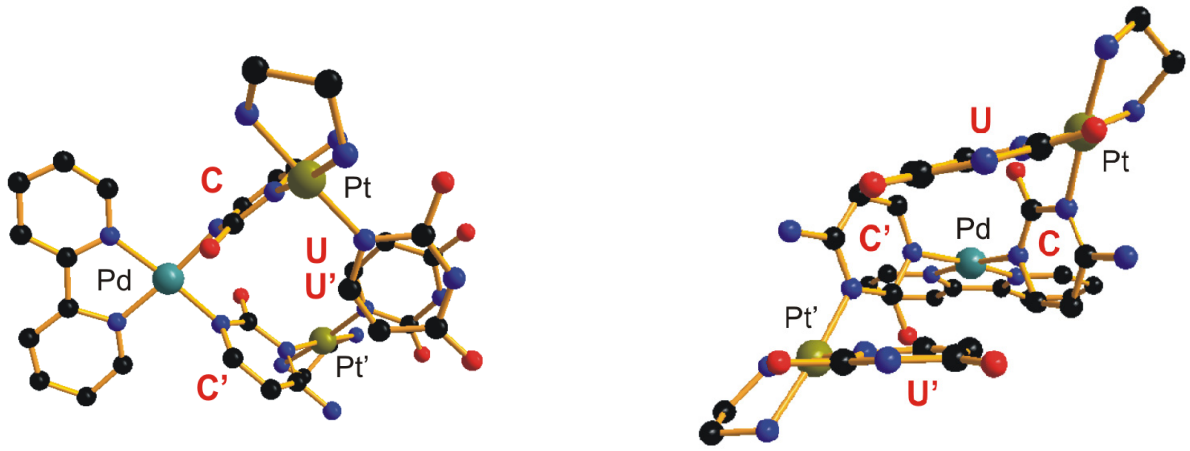

Figure 12: Two different views of the cation (I) of [(2,2'-bpy)Pd{(*N1*-CH-*N3*)(en)Pt(UH-*N1*)}$_2$](NO$_3$)(ClO$_4$)•4.9H$_2$O (**2a**).

NMR Spectroscopy

The ^{1}H NMR spectrum of **2a** in D_2O consists of discrete doublets ($^{3}J_{H\text{-}H} \approx 6.8$ Hz for cytosine and $^{3}J_{H\text{-}H} \approx 7.3$ Hz for uracil) for the H(6) and H(5) resonances. The signals corresponding to the bipyridine group and a broad signal that belongs to the ethylenediamine groups are also found. A part of the spectrum is shown in Figure 13 and the chemical shifts of all resonances are given in Table 10 (see Chapter I: Summary).

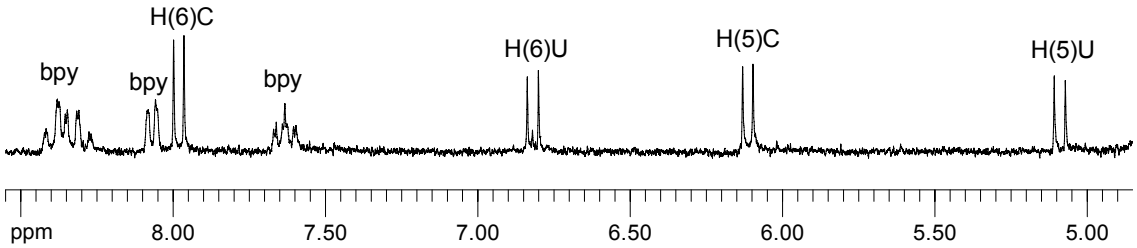

Figure 13: Low field section of the ^{1}H NMR spectrum of [(2,2'-bpy)Pd{(*N1*-CH-*N3*)(en)Pt(UH-*N1*)}$_2$](NO$_3$)(ClO$_4$)•4.9H$_2$O (**2a**) in D_2O, pD = 8.55.

An interesting detail of the ^{1}H NMR spectrum of **2a** in D_2O is the remarkable upfield shift of the H(6)-uracil resonance at 6.82 ppm as well as the H(5)-uracil at 5.16 ppm as compared to **1**. This effect seems to be due to the stacking of the terminal uracilate ligands, which thus appears to be also maintained in aqueous solution.

The bpy resonances are defined by four resonances, because the 2,2'-bpy ring is symmetrically bonded to Pd and *trans* to the N(1)-cytosine sites. They are localized at 7.63 ppm (t), 8.06 ppm (d), and 8.26-8.42 ppm (d, t).

Further addition of Pd^{II}(2,2'-bpy) to a solution of **2a** in D_2O showed a fast reaction to give immediatelly new signals. The signals corresponding to **2a** disappeared and a new product (**4**) remained stable in solution.

3.1.2 Pt_2Pd_3 : [{(2,2'-bpy)Pd}$_3${(en)Pt(U-*N1,N3,O4*)(CH-*N1,N3*)}$_2$](NO$_3$)$_4$•5H$_2$O (4) (Connectivity = cytosine-uracil-uracil-cytosine)

In the ^{1}H NMR study of reactions of Pd^{II}(2,2'-bpy) (see Figure 10) with **1a** in aqueous solution several species are observed. The first, Pt_2Pd (**2a**), is detected at the beginning, when the starting compound reacts with 0.1 eq of Pd^{II}(2,2'-bpy). When more Pd^{II}(2,2'-bpy) is added to the solution, one can observe a second group of signals, which, from comparison with the isolated and X-ray characterized complex, is attributed to the Pt_2Pd_3 species [{(2,2'-bpy)Pd}$_3$ {(en)Pt(U-*N1,N3,O4*)(CH-*N1,N3*)}$_2$]$^{4+}$ (**4**). This complex was crystallized as its NO_3^- salt.

To isolate this new compound, $AgNO_3$ was used to abstract the two chloro ligands of the $PdCl_2$(2,2'-bpy), followed by the filtration of AgCl. Afterwards, [Pd(2,2'-bpy)(H$_2$O)$_2$]$^{2+}$ was added to a solution of **1a** (r = 2) and the yellow solution (pH = 2.0) was stirred for two days. Then the pH was adjusted to 7.5 by addition of NaOH (1M) and the solution was kept at 4°C. After approximately two weeks the solution was evaporated and a mixture of orange blocks (**4**) and a yellow precipitate was recovered. The orange crystals were separated by hand under a microscope and the yellow precipitate was recrystallized to produce a new species (**7**).

X-Ray Crystallography

Complex **4** is a pentanuclear box consisting of two ethylenediamine platinum entities and three bipyridine palladium entities, with two of them being stacked (3.4-4.0 Å). The cation is cyclic, derived from **2a** by addition of two Pd^{II}(2,2'-bpy) moieties and linked via the two uracil rings. Therefore, the sequence of nucleobases in the cycle is also cytosine-uracil-uracil-cytosine. The cycle adopts a *1,3*-alternate configuration with the reference atoms being the exocyclic O(2) groups (see Figure 14). As in compound **2a**, a Pd^{II}(2,2'-bpy) entity is bonded via the N(1) positions of each of the two cytosine ligands. The two Pd ions are bonded in *head-tail* fashion through N(3) and O(4) of each of the uracil dianions with distances ranging from 1.998(10)Å to 2.043(10) Å and from

2.003(9) Å to 2.036(8) Å, respectively. Selected structural details are listed in Table 4.

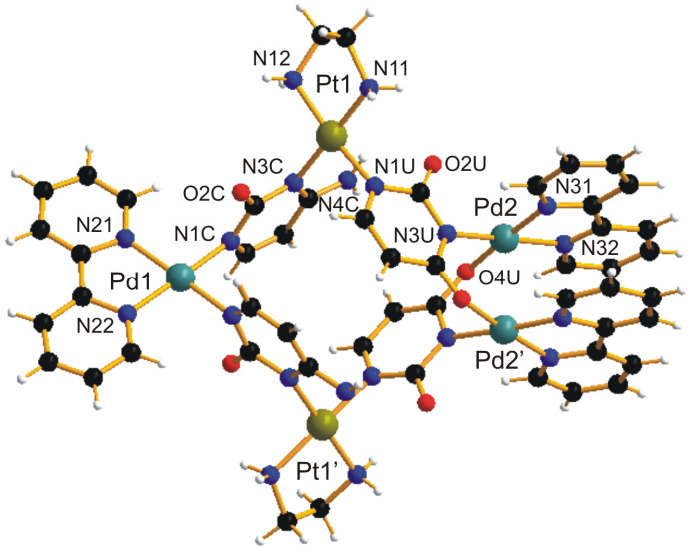

Figure 14: Crystal structure of the cation of $[\{(2,2'\text{-bpy})Pd\}_3\{(en)Pt(U\text{-}\textit{N1,N3,O4})(CH\text{-}\textit{N1,N3})\}_2](NO_3)_4 \cdot 5H_2O$ (**4**).

Table 4: Selected interatomic distances (Å) and angles (°) in **4**.

Pt(1)-N(1)U	1.999(12)	N(11)-Pt(1)-N(12)	83.1(4)
Pt(1)-N(3)C	2.050(11)	N(1)U-Pt(1)-N(3)C	89.3(4)
Pt(1)-N(11)	2.025(12)	N(11)-Pt(1)-N(1)U	92.2(4)
Pt(1)-N(12)	2.046(11)	N(12)-Pt(1)-N(3)C	96.1(4)
Pd(1)-N(1)C	2.004(11)	N(21)-Pd(1)-N(22)	81.0(5)
Pd(1)-N(1)C'	2.011(11)	N(1)C-Pd(1)-N(1)C'	88.1(5)
Pd(1)-N(21)	2.016(11)	N(21)-Pd(1)-N(1)C	95.6(5)
Pd(1)-N(22)	2.014(12)	N(22)-Pd(1)-N(1)C'	95.5(5)
Pd(2)-N(3)U	1.998(10)	N(31)-Pd(2)-N(32)	80.6(4)
Pd(2)-O(4)U'	2.036(8)	N(3)U-Pd(2)-O(4)U'	88.0(4)
Pd(2)-N(31)	1.993(10)	N(31)-Pd(2)-N(3)U	96.6(4)
Pd(2)-N(32)	1.989(11)	N(32)-Pd(2)-O(4)U'	94.8(4)
Pd(2)···Pd(2')	2.8190(18)		

Compound **4** can be described as an extended metallacalix[4]arene with an additional metal added to one of the four corners. The corner with the two adjacent uracil rings has been opened and has been replaced by a two-metal unit (Pd(2), Pd(2')). As a consequence of this change of the basic metallacalix[4]arene structure, the mixed-metal distances are very different, depending on the coordination of the metals to the nucleobases. The Pt···Pd distances, which involve the endocyclic sites of the nucleobases, are about 5.755(2) Å – 5.898(2) Å long. The Pt···Pd distances defined by the coordination of Pd to the exocyclic O(4) of each of the uracilate ligands have a length of 7.354(3) Å and 7.384(3) Å, respectively. Hence, these distances are longer than the typical 5.8-5.9 Å seen in metallacalix[4]arenes. The diagonal intermetallic Pt···Pt distance is 8.242(2) Å. In Scheme 13 a simplified version of the crystal structure of the cation of **4** is shown, together with a schematic representation of the nucleobase connectivities (with Pt = Pt^{II}(en) and Pd = Pd^{II}(2,2'-bpy)).

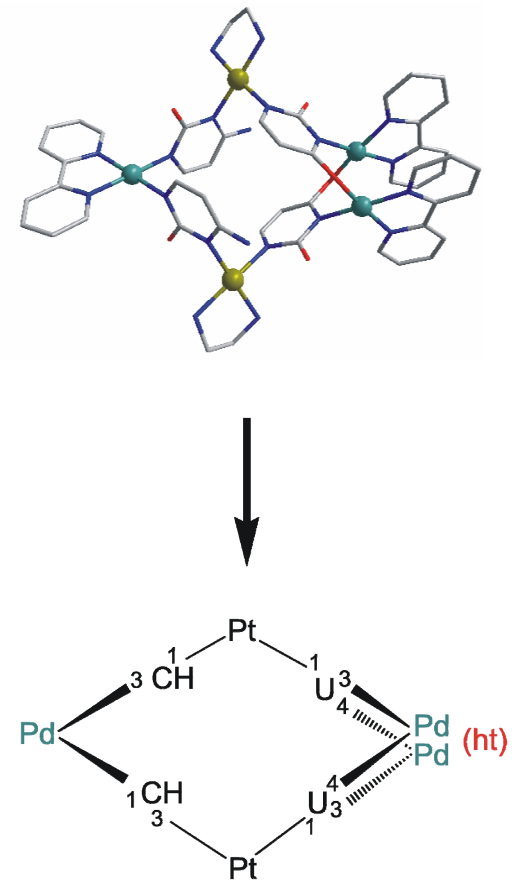

Scheme 13 : Schematic view of the cation of **4** with nucleobase connectivities indicated.

The Pd^{II}(2,2-bpy) entity bonded to the N(1) position of the cytosines is perpendicular to the other two Pd^{II}(2,2-bpy) entities, which are stacked on each other. The Pd(2)···Pd(2') distance of 2.817(2) Å within the dimer entity of **4** is closely similar to that observed in a related complexes, such as a dinuclear Pd^{II}(2,2'-bpy) complex with two bridging (*head-tail*) 1-methylthyminato ligands and N(3), O(4) coordination[97] and a dinuclear $Pd^{II}(NH_3)_2$ compound with two bridging (*head-tail*) 1-methylcytosinato nucleobases coordinated via N(3), N(4) sites.[101] In Figure 15 the orientation adopted for the bipyridine ligands can be easily visualized.

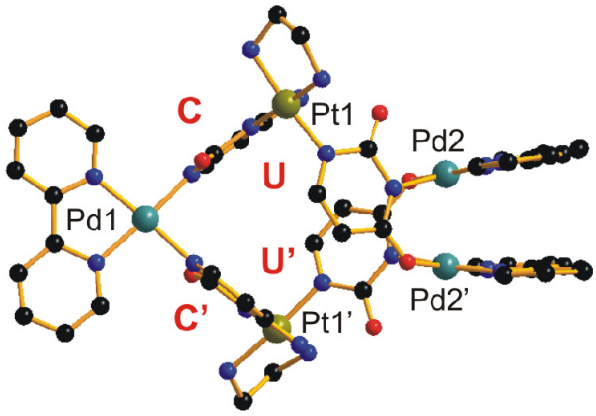

Figure 15: Another view of the cation of [{(2,2'-bpy)Pd}$_3${(en)Pt(U-*N1,N3,O4*)(CH-*N1,N3*)}$_2$](NO$_3$)$_4$•5H$_2$O (**4**).

Formation of **4** conceivably takes place from the "open" complex **2a** upon addition of two Pd^{II}(2,2'-bpy) entities. Comparison of the structure of the cations of **2a** and **4** reveals the relatively minor structural changes necessary to accomplish "addition" of two Pd^{II}(2,2'-bpy) moieties to the uracil ligands making them no longer coplanar. Hence, the major structural change is the loss of the uracil stacking, as can be seen in Figure 16 .

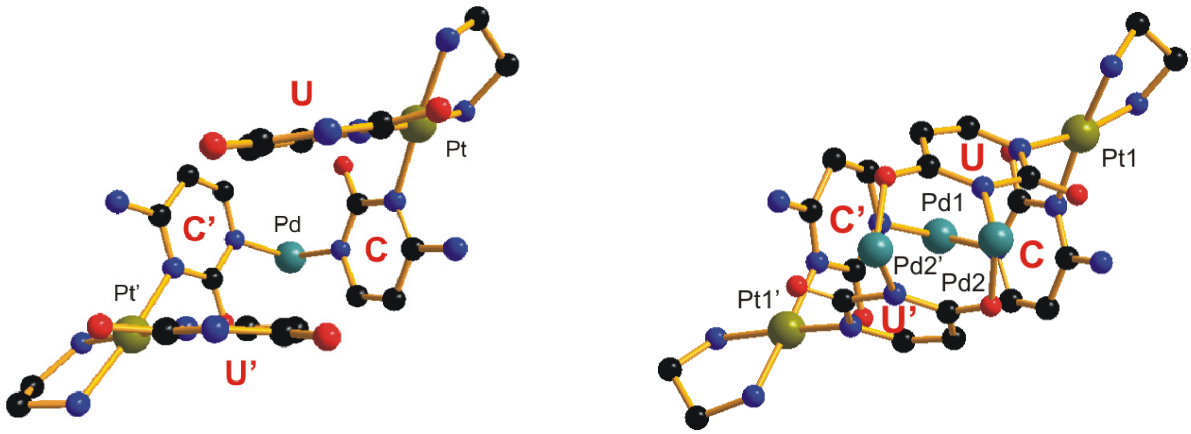

Figure 16: Crystal structure of the cations of **2a** (left) and **4** (right) with the 2,2'-bpy ligands omitted for clarity.

ESI-Mass Spectrometry

Electrospray ionization Fourier-transform ion-cyclotron-resonance (ESI-FTICR) mass spectrometric experiments of **4** were carried out by Prof. Dr. C. A. Schalley (Berlin). Three intensive signals corresponding to [**4** – 2 NO$_3$]$^{2+}$, [**4** – NO$_3$]$^{3+}$ and

[**4**]$^{4+}$ are detected at m/z 931.07, 600.04 and 434.53, respectively. Aditionally, the loss of the HNO_3 can be observed from the +2 and +3 charge states (with two and one nitrate ions, respectively), indicating a deprotonation of the en ligands at the Pt centers as has been observed for other similar coordination compounds.[102] Two low-intensity signals appear for the monocation [(en)Pt(CH)$_2$(bpy)Pd]$^+$ (m/z 736) and for a triply charged dimer (m/z 931), as has been observed for other metallo-supramolecular complexes.[103,104] Thus, this analysis is fully consistent with the structure assignment made for **4**.

NMR Spectroscopy

The ^{1}H NMR spectrum in D_2O of **4** consists of discrete doublets ($^3J_{H\text{-}H} \approx 6.8$ Hz for both nucleobases) for the H(6) and the H(5) resonances, as well as signals corresponding to the bipyridine groups and to the ethylenediamine groups. The spectrum is shown in Figure 17 and chemical shifts are given in Table 10 (see Chapter I: Summary). Unlike in the precursor **2a**, no upfield shift for the uracil resonances is observed.

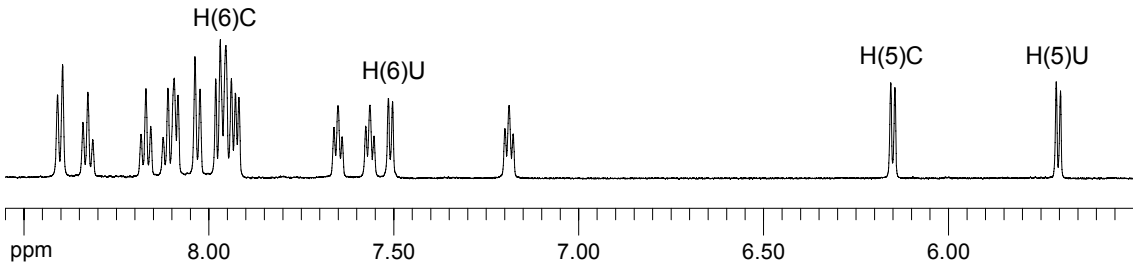

Figure 17: Low field section of the ^{1}H NMR spectrum of [{(2,2'-bpy)Pd}$_3${(en)Pt(U-*N1,N3,O4*)(CH-*N1,N3*)}$_2$](NO$_3$)$_4$•5H$_2$O (**4**) in D_2O, pD = 9.23.

To distinguish the uracil and cytosine resonances, two-dimensional NMR experiments were performed. In the first stage, a 2D ^{1}H,^{1}H NOESY experiment was carried out for complex **4** (Figure 18). The signal of the proton H5 at 5.70 ppm gives intense cross-peaks with the signal of the H6 proton located at 7.50 ppm. Furthermore, intensive cross-peaks between the H5 at 6.16 ppm and the H6 signal at 7.97 ppm, respectively are observed. It should be noted that TSP was not used as internal standard to adjust the chemical shifts of the signals in

the 2D $^{1}H,^{1}H$ NOESY experiment and therefore the shifts derived from Figure 18 do not accurately match those given above.

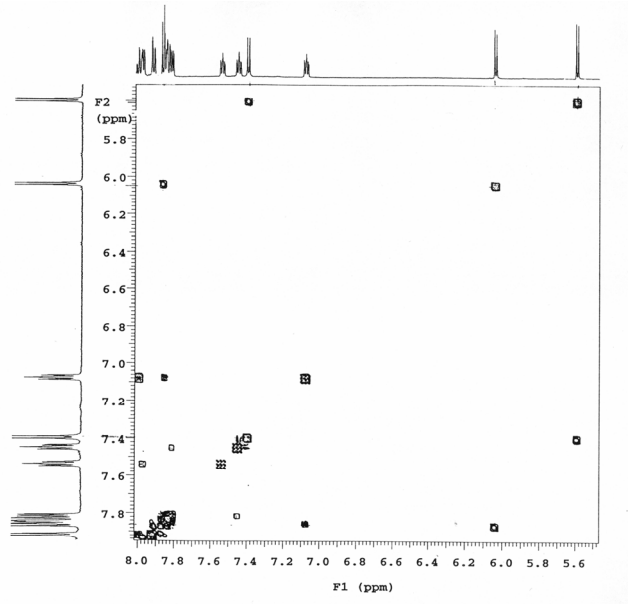

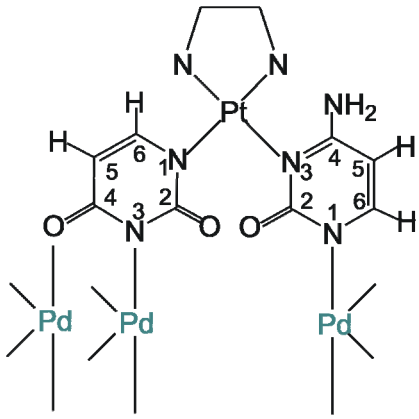

Figure 18: 2D ^{1}H, ^{1}H NOESY spectrumof compound **4** in D_2O.

Then a 2D ^{1}H, ^{13}C COSY experiment was carried out with the help of direct (HSQC) and long range ^{1}H, ^{13}C coupling (HMBC) (Figure 19). In the case of uracil, the signal of the H5 proton gives cross-peaks to the C5 and C6 signals. The H6 resonances of uracil shows cross-peaks to the C2, C4, C5 and C6 signals, which were assigned according to Pretsch et al.[105] Analogously, cytosine cross-peaks between the signal of H5 and the C4, C5 and C6 signals, as well as cross-peaks between the H6 resonance of cytosine and the C2,C4, C5 and C6 signals are observed (see Table 5). The results of this analysis clearly showed that the upfield shift of the uracil resonances as observed in **2a** and attributed to the stacking of the uracil ligands is absent in **4**, consistent with the X-ray structural data.

Table 5: ^{1}H NMR chemical shifts of aromatic nucleobase protons and ^{13}C NMR resenonances of carbon atoms of **4** (δ, D_2O).

	^{1}H NMR (ppm)	^{13}C NMR (ppm)
Uracil	5.70(H5) 7.50(H6)	162.5(C2), 178.5(C4), 102.3(C5), 158.5(C6)
Cytosine	6.16(H5) 7.97(H6)	161.1(C2), 165.6(C4), 95.4(C5), 157.0(C6)

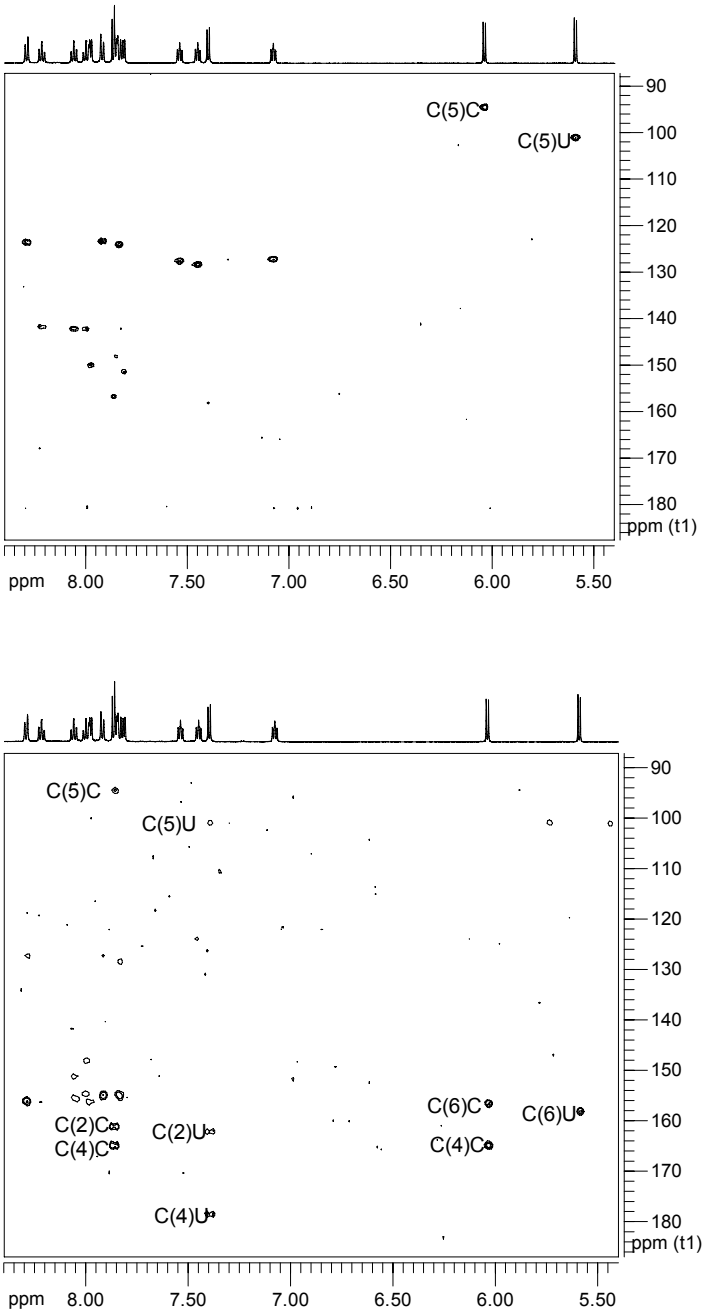

Figure 19: 2D ^{1}H, ^{13}C COSY spectra of compound **4** in D_2O, HSQC (top) and HMBC (bottom).

An interesting point of the ^{1}H NMR spectum of **4** in D_2O is the remarkable upfield shift of one of the 2,2'-bpy resonances (the triplet at 7.19 ppm). To analyze the 2,2'-bpy resonances of this compound in more detail 1D TOCSY experiments were carried out, since TOCSY spectra can be used to obtain information on all protons within a ring system. The spectra (irradiated signals indicated) are shown in Figure 20.

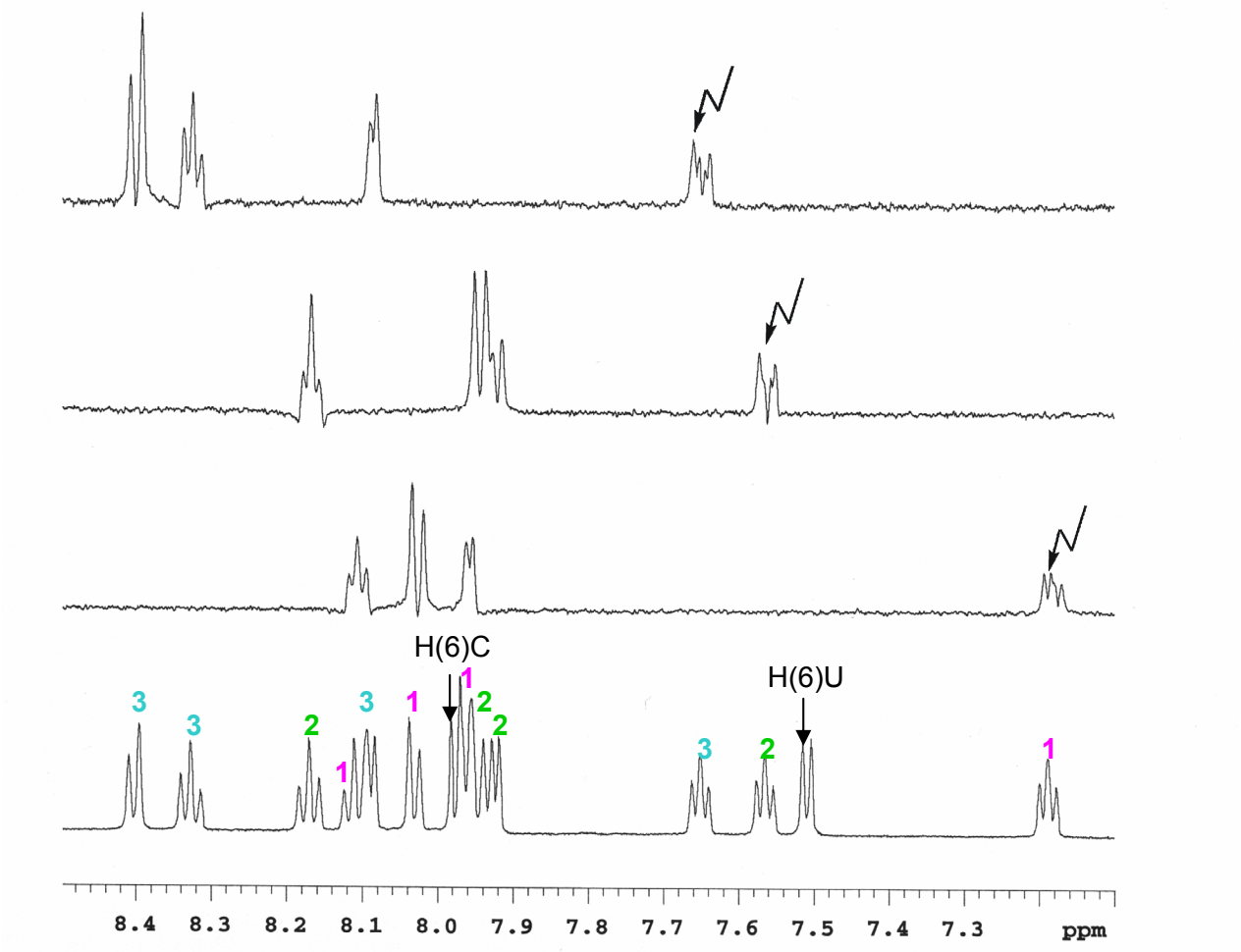

Figure 20: Low field section of the ^{1}H NMR spectrum of **4** (bottom) and 1D TOCSY experiments (top) applied to separate the bipyridine resonances.

As expected, three sets of the bpy resonances can be observed. Four resonances corresponding to the 2,2'-bpy ring symmetrically bonded to Pd(1) and *trans* to N(1)-cytosine sites and two times four resonances of the two stacked bpy rings due to the non-equivalence of the two pyridine "halves" as a consequence of different *trans*-positioned Pd(2) donor atoms (N(3), O(4)), can be differentiated this way. The set of resonances of the 2,2-bpy ligand bonded to Pd(1) (indicated with blue color in Figure 21) has chemical shifts of δ [ppm] = 7.65 (t), 8.09 (d), 8.33 (t), and 8.40 (d). These chemical shifts correspond well with those of the bpy ligand in **2a**, as expected. The two other sets of four 2,2'-bpy resonances, represent the stacked bpy entities at Pd(2) and Pd(2'), are grouped at δ [ppm] = 7.19 (t), 7.96 (d), 8.03 (d), and 8.11 (t) (indicated with pink color in Figure 21); as well as 7.57 (t), 7.92 (d), 7.94 (d), and 8.17 (t) (green color in Figure 21). As pointed out, the 7.19 ppm signal exhibits the highest upfield shift of all 12 bpy

resonances, clearly reflecting bpy stacking. In Figure 21 a view along the Pd(2)…Pd(2') vector in **4** is shown, which suggests that this resonance should be assigned to the H5 protons of the bipyridine rings *trans* to the N(3) positions of the uracil ligands. These protons are located above/below the π-electron system of the pyridine half of 2,2'-bpy trans to the O(4) positions and which therefore is expected to experience the ring current effect most.

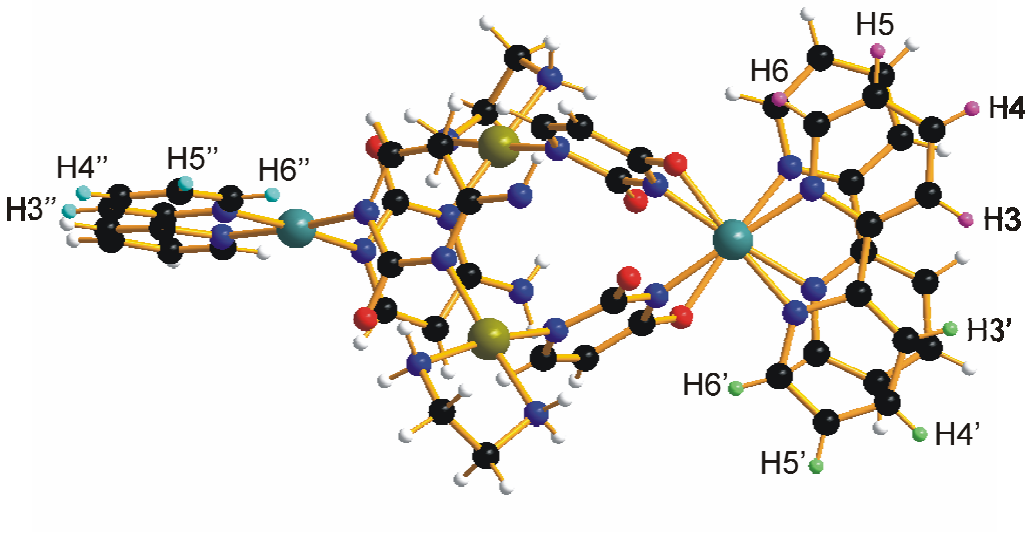

Figure 21: View of the cation of **4** along the Pd(2)···Pd(2') vector.

Compound **4** is very stable in D_2O. The ^1H NMR spectrum does not change with time. Only a isotopic exchange of the H(5) protons by deuterium is detected after more than one week. Several reactions, which were followed by ^1H NMR spectroscopy, were carried out to understand the solution behavior of this complex.

At first, the pD was raised up to 11.8. No changes in the spectrum were observed. Only under more basic conditions decomposition of **4** and the appearance of new signals, which can not be assigned to any isolated product, were detected.

Secondly, a solution of **4** in D_2O was heated to 70°C for two days. Only an accelerated exchange of the H5 protons of uracil and cytosine by deuterium could be observed in the spectrum. Finally, even in the presence of an excess of NaCl (more than 100 eq) compound **4** remains stable in solution.

On the other hand, if the pH is decreased by addition of DCl (pD < 1), decomposition to the starting compound **1** takes place, again accompanied by isotopic exchange of uracil-H5 and cytosine-H5. In the presence of four equivalents of a good ligand such as 9-methylguanine (9-MeGH) only minor decomposition of **4** to **1** (10%) is observed. After one day compound **2a** also seems to have reformed (10%).

As has been seen in the structure of compound **4**, the four nucleobases of the cation enclose a cavity, but no guest molecules can be localized inside the cavity in the solid state. The cation has free coordination sites (O(2) exocyclic atoms of uracil and cytosine, as well as N(4) position of the cytosine). Therefore this cation could conceivably act as guest for other cations, as was observed for other metallacalix[4]arenes.[67,68] Reactions of a solution of **4** in D_2O with two or four equivalents of *cis*-$Pt^{II}(NH_3)_2$ were also carried out, but in these cases no reaction were observed. On the other hand, this cycle could also be capable of including in its cavity inorganic anions or anionic organic ligands (e.g. TSP[66] or AMP[74]) due to its high positive charge. It should be noted, however, that only the cone conformers of metallacalix[4]arenes are, in principle, capable of incorporating guest species.

Host-guest chemistry reactions with cations and anions were carried out for compound **4** and followed by ^{1}H NMR spectroscopy. In the first case, solutions of **4** were mixed with Li^+, Na^+, or K^+, as well as with Cu^{2+} or Ni^{2+}, but neither changes in color nor in the ^{1}H NMR spectra (when applicable) were detected. Reactions with anions such as NO_3^-, ClO_4^-, CO_3^{2-}, F^-, I^- or CH_3COO^- also show no sign of interaction. Finally, reactions with the organic ligands TSP and AMP were carried out. Again, no reaction took place, apparently because the size of the cavity of the cation is too small for these molecules.

3.1.3 Pt_2Pd_4 : $[\{(en)Pt\}_2(\mathit{N1}\text{-U-}\mathit{N3,O4})_2(\mathit{N3}\text{-HC-}\mathit{N1,O2})_2\{(2,2'\text{-bpy})Pd\}_4](NO_3)_6$ (7) (Connectivity = cytosine-uracil-cytosine-uracil)

If the ratio of **1a** to Pd^{II}(2,2'-bpy) is increased up to 1:2, a new set of resonances is detected in the ^1H NMR spectra (Figure 10d), which from comparison with the isolated and X-ray structurally characterized complex **7**, is attributed to the Pt_2Pd_4 species.

A mixture of **4** and a yellow precipitate was obtained from a solution of $[Pd(2,2'\text{-bpy})(H_2O)_2]^{2+}$ and **1a** (r = 2, pH = 7.5). The orange crystals of **4** were separated by hand under a microscope and analyzed. Crystals of the title compound **7** were obtained upon recrystalization of the yellow precipitate in the presence of additional nitrate in the form of KNO_3 at pH = 9.5.

X-Ray Crystallography

Composition and structure of **7** were determined by X-ray chrystallograpy. The compound crystallizes in the triclinic space group P-1. Complex **7** is a hexanuclear box consisting of two ethylenediamine platinum entities and four bipyridine palladium entities. The cation of $[\{(en)Pt\}_2(\mathit{N1}\text{-U-}\mathit{N3,O4})_2(\mathit{N3}\text{-HC-}\mathit{N1,O2})_2\{(2,2'\text{-bpy})Pd\}_4]^{6+}$ (**7**) is composed of a tetranuclear, cyclic Pt_2Pd_2 core unit, in which the sequence of nucleobases is (*N1*-HC-*N3*)Pt(*N1*-U-*N3*)Pd(*N1*-HC-*N3*)Pt(*N1*-U-*N3*)Pd. This is different from the cases discussed so far. Unlike in compound **4**, which displays a *head-tail* arrangement of the nucleobases, in compound **7** the two Pd^{II}(2,2'-bpy) units (bonded pairwise through O(2) of the cytosine monoanion and O(4) of the uracil dianion) are added on top of the two other (2,2'-bpy)Pd^{II} entities, thus leading to *head-head* arrangements and short Pd···Pd contacts of 2.815(1) Å, (Pd(1)-Pd(2)) and 2.844(1) Å, (Pd(1')-Pd(2')). These distances are closely similar to that observed in a related dinuclear Pd^{II}(2,2'-bpy) complex with two bridging (*head-head*) 1-methylthyminato ligands N(3), O(4) coordination[97].

The cation of compound **7** is depicted in Figure 22 and selected structural features are compiled in Table 6.

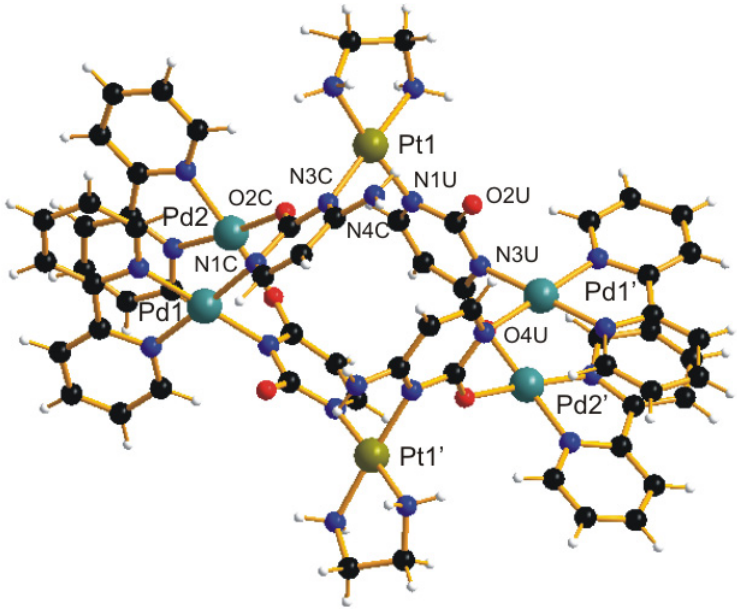

Figure 22: Crystal structure of the cation of $[\{(en)Pt\}_2(\mathit{N1}\text{-U-}\mathit{N3,O4})_2(\mathit{N3}\text{-HC-}\mathit{N1,O2})_2\{(2,2'\text{-bpy})Pd\}_4](NO_3)_6$ (**7**)

Table 6: Selected interatomic distances (Å) and angles (°) in **7**.

Pt(1)-N(1)U	2.017(6)	N(11)-Pt(1)-N(12)	83.0(3)
Pt(1)-N(3)C	2.055(7)	N(1)U-Pt(1)-N(3)C	89.2(3)
Pt(1)-N(11)	2.022(7)	N(11)-Pt(1)-N(1)U	94.4(3)
Pt(1)-N(12)	2.039(6)	N(12)-Pt(1)-N(3)C	93.5(3)
Pd(1)-N(3)U'	2.025(7)	N(11)-Pd(1)-N(12)	80.7(3)
Pd(1)-N(1)C	2.024(7)	N(3)U'-Pd(1)-N(1)C	85.9(3)
Pd(1)-N(11)	2.022(7)	N(11)-Pd(1)-N(3)U'	96.9(3)
Pd(1)-N(12)	1.998(7)	N(12)-Pd(1)-N(1)C	96.5(3)
Pd(2)-O(4)U'	2.021(6)	N(11)-Pd(2)-N(12)	81.4(3)
Pd(2)-O(2)C	2.026(7)	O(4)U'-Pd(2)-O(2)C	92.5(3)
Pd(2)-N(11)	1.984(7)	N(11)-Pd(2)-O(4)U'	93.2(3)
Pd(2)-N(12)	1.982(7)	N(12)-Pd(2)-O(2)C	93.1(3)
Pd(1)···Pd(2)	2.844(1)		
Pd(1')···Pd(2')	2.815(1)		

Uracilate and cytosine nucleobases adopt an *1,3*-alternate conformation as far as their substituents are concerned, e.g. O(2)-uracil and O(2)-cytosine. On the other hand, the Pd^{II}(2,2-bpy) entitities, which are pairwise stacked, are perpendicular to each other. In Figure 23 the orientation adopted for the bipyridine ligans can be readily observed.

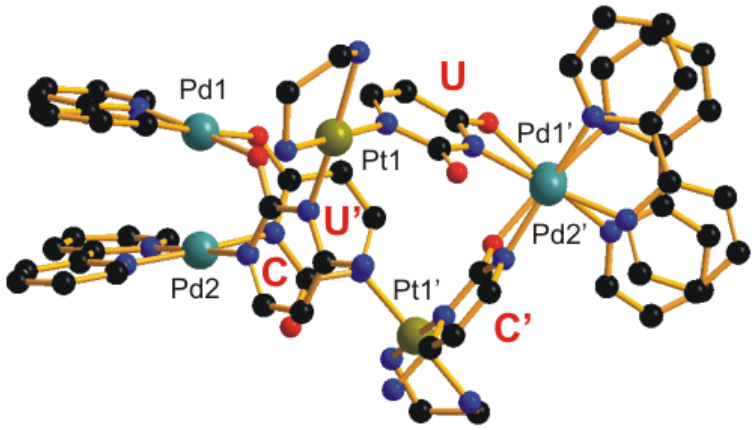

Figure 23: Another view of the cation of $[\{(en)Pt\}_2(N1\text{-U-}N3,O4)_2(N3\text{-HC-}N1,O2)_2\{(2,2'\text{-bpy})Pd\}_4](NO_3)_6$ (**7**).

Compound **7** can be described as an extended metallacalix[4]arene with two additional metals added to two of the four corners. The Pt···Pd distances, which involve the endocyclic sites of the nucleobases, are in the normal range (5.743(2) – 5.917(2) Å). The Pt···Pd distances defined by the coordination of Pd to the exocyclic O(4) of each of the uracilate ligands are about 7.375 Å - 7.399(3) Å long, which is close to the related distances for compound **4**. However, Pt···Pd distances involving the exocyclic O(2) of each of the cytosine ligands are much shorter, ranging from 4.822(1)(2) Å to 4.887(1)(3) Å

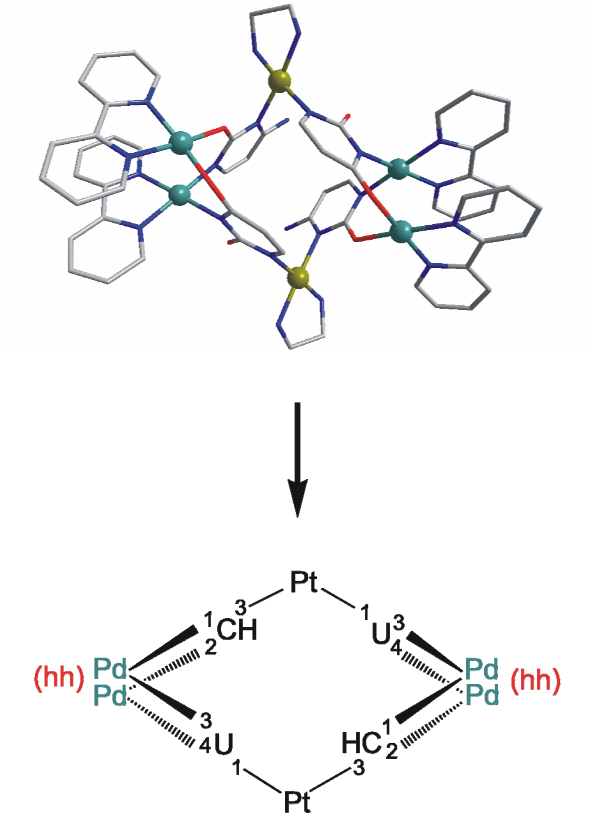

Scheme 14 : Schematic view of the cation of compound **7** with nucleobase connectivities indicated.

The geometry of the Pt_2Pd_2 core unit closely resembles that of $[\{(en)Pt(UH)\}_4]^{4+}$ [38,39] as far as intermetallic distances and overall arrangement of the pyrimidine bases (*1,3*-alternate, see Figure 24) are concerned. In Figure 24 two views of the cation of **7** are depicted. Bpy and en ligands have been omitted for clarity.

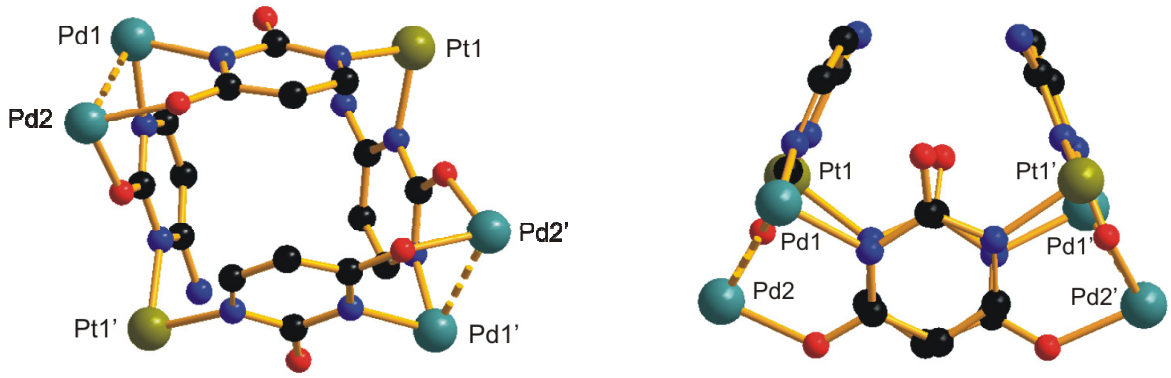

Figure 24: Two different views of the cation of **7** with bipyridine and ethylenediamine groups omitted for clarity.

The four central metal ions cross-linking the endocyclic *N*(1) and N(3) sites of the four nucleobases (Pt(1), Pt(1'), Pd(1), Pd(1')) form a distorted square. These metal atoms are not in a plane, but rather they adopt a flat butterfly structure. Two metals are slightly above the best mean plane, with deviations of 0.2525(3) Å (Pt(1)) and 0.2580(3) Å (Pt(1')) and the other two metals are slightly below this plane , -0.2550(3) Å (Pd(1) and -0.2555(3) Å (Pd(1')) (Figure 25). The sides of the square range from 5.743(2) Å to 5.917(2) Å (see above). The length of the diagonal intermetallic distances are 7.873(2) Å for Pt···Pt and 8.531(2) Å for Pd···Pd.

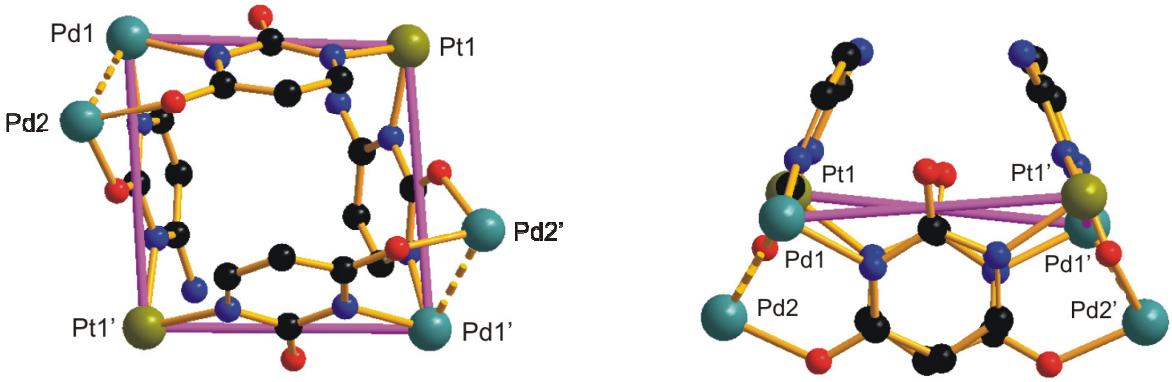

Figure 25: Two different views of the cation of **7** with bipyridine and ethylenediamine groups omitted for clarity. The Pt_2Pd_2 core unit (defined by the endocyclic coordination at the nucleobases) is indicated.

The oxygen atoms of anions, as well as some nitrogen atoms of some anions are disordered over multiple positions. To model the structure, the reflection contributions from the anions and feasible water molecules were removed using the program PLATON, function SQUEEZE[106], which determined that there were 367 electrons removed from a volume of 1519.2 Å^3. These electrons were assigned to twelve NO_3^- of the asymmetric unit (z =2). In agreement with this, the IR spectrum showed only bands corresponding to the nitrate groups. Due to the low number of electrons, which were found, it was supposed that there are not any crystal water molecules in the structure. It should be noted that the crystals of compound **7** were obtained when the solution was completely dry.

All atoms of the cation were refined anisotropically with the exception of two carbon atoms and one nitrogen atom of the en ligand, which are disordered over two positions each, all with occupancies of 50%.

NMR Spectroscopy

The ^{1}H NMR spectra of **7** in D_2O shows only one doublet for each of the uracil and cytosine protons ($^3J_{H-H}$ = 6.8 Hz). A group of signals corresponding to the bipyridine resonances and also a broad signal corresponding to the ethylenediamine group are observed in the spectra. However, the title compound is not stable in solution. The ^{1}H NMR study of **7** in D_2O shows rapid spectroscopic changes. A series of low intensity nucleobase doublets (range 5.6-6.5 ppm) appears soon, before within one day signals due to compound **4** dominate. If NaCl is added to a freshly prepared solution of **7** in D_2O, there is a inmediate precipitation of $PdCl_2$(2,2'-bpy) and formation of a new set of resonances assigned to an unknown species X (Figure 26). According to the intensities of the bpy and nucleobase resonances in the ^{1}H NMR spectra of **7** (Figure 26a), the Pt/Pd ratio is 1:2, while in the ^{1}H NMR spectra of X (Figure 26b) the Pt/Pd ratio is 1:1. Therefore, two Pd^{II}(2,2'-bpy) entities are displaced from the cation of **7** and precipitate as $PdCl_2$(2,2'-bpy). Chemical shifts are given in Table 10 (see Chapter I: Summary).

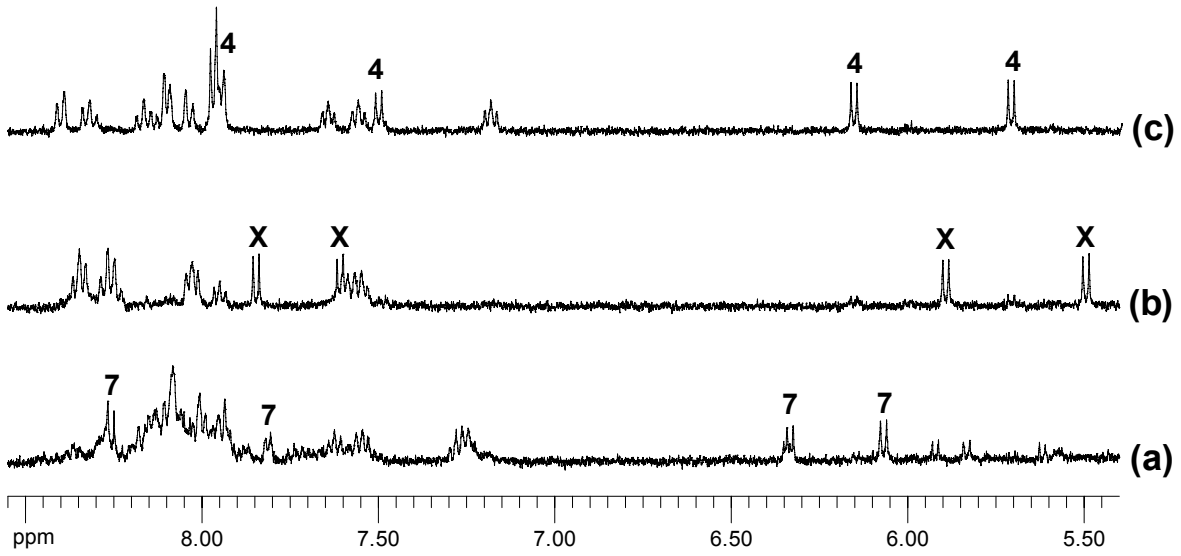

Figure 26: Lowfield shift sections of ^{1}H NMR spectra of compound **7** when redissolved in D_2O and after addition of NaCl: (a) Inmediatelly after sample preparation, pD = 7.23; (b) after two hours; (c) after one day.

It is assumed that the loss of the O-bonded Pd^{II}(2,2'-bpy) entities of the cation gives, at first, a Pt_2Pd_2 cycle (resonances marked with X in Figure 26), in fact corresponding to the metallacalix[4]arene with the sequence of nucleobases cytosine-uracil-cytosine-uracil (compound X) and eventually **4**. The loss of the bpy resonances of **7** at 7.3 ppm, believed to be characteristic for stacked 2,2'-bpy entitites, during the conversion of **7** to X is consistent with this assumption.

The mechanism of conversion of the tetranuclear species Pt_2Pd_2 (X) to **4**, which involves a change in the sequence of nucleobases (this is possible only, if fragmentation of X and a rearrangement process take place), will be discussed in the following. In Scheme 15 a schematic diagram of this process is shown.

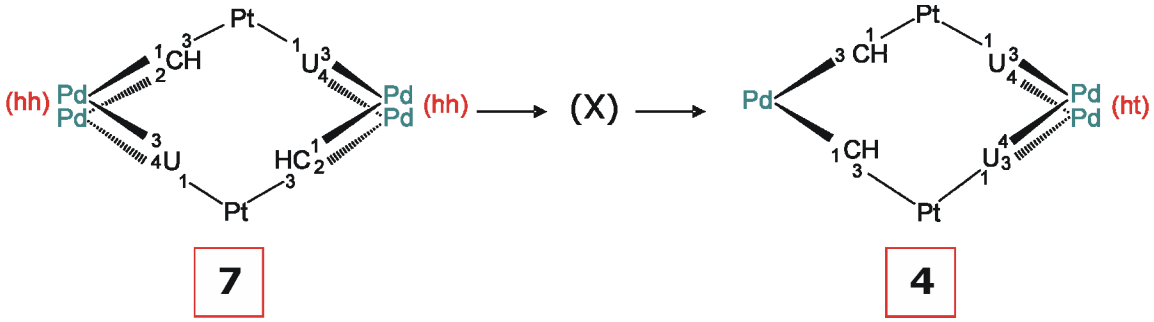

Scheme 15 : Proposed conversion process of **7** to **4**.

3.1.4 Pt_4Pd_4 : $[\{(en)Pt(N1\text{-}U\text{-}N3)(N3\text{-}HC\text{-}N1)\}_4\{(2,2'\text{-bpy})Pd\}_4](NO_3)_3(ClO_4)\cdot 56.1H_2O$ (9a) (Connectivity = cytosine-uracil-cytosine-uracil)

The title compound was not detected in the ^1H NMR study of the system **1**/Pd^{II}(2,2'-bpy) (Figure 10). However, it was isolated in the solid state.

The compound $[\{(en)Pt(N1\text{-}U\text{-}N3)(N3\text{-}HC\text{-}N1)\}_4\{2,2'\text{-bpy})Pd\}_4]^{4+}$ (**9a**) was obtained by addition of $[Pd(2,2'\text{-bpy})\ (H_2O)_2]^{2+}$ to an aqueous solution of **1a** (r = 1). Increasing the pH to 10.5 and keeping the solution at 4°C gave, after roughly four weeks, rhombic yellow crystals of **9a**.

X-Ray Crystallography

The cation is a cyclic octanuclear complex consisting of four $(en)Pt^{II}$ entities, four Pd^{II}(2,2'-bpy) entities, four uracil dianions and four cytosine monoanions. The eight metal ions cross-linking the endocyclic N(1) and N(3) sites of the nucleobases form a cyclic Pt_4Pd_4 core unit, in which the sequence of nucleobases is similar to the Pt_2Pd_2 core of **7**. Unlike related metallacalix[n]arenes with n = 3, n = 4, n = 6, compound **9a** with n = 8 no longer has the shape of a ring, but rather adopts a strongly folded structure (Scheme 16).

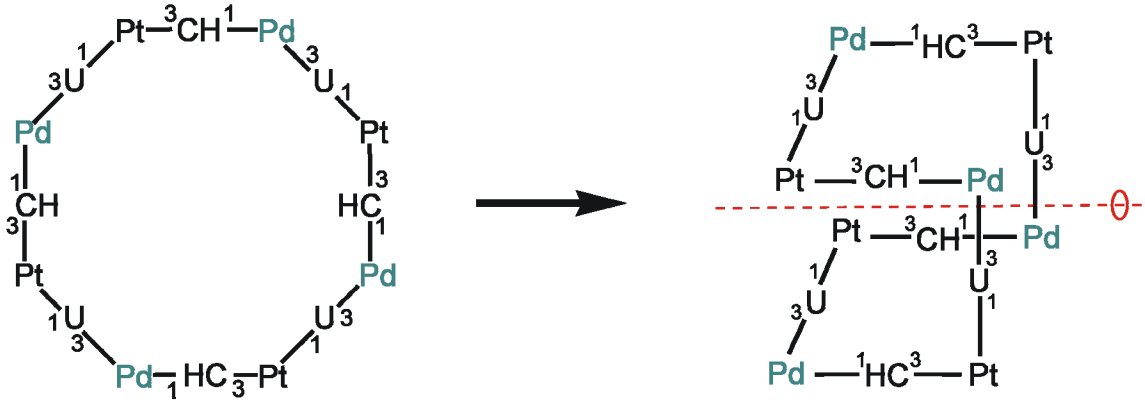

Scheme 16: Schematic representation of cyclic Pt_4Pd_4 (**9a**).

In Figure 27 the crystal structure of **9a** along its fourfold inversion axis is shown. The four uracilate ligands occupy the corners of the square and the four cytosines are oriented toward the center of the cation.

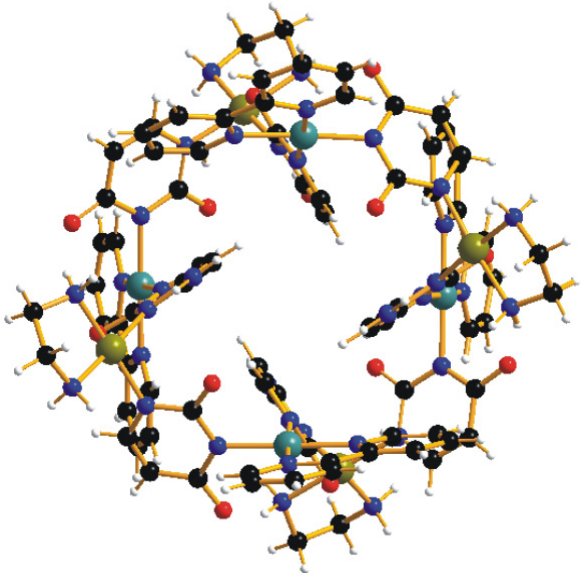

Figure 27: View of the cation (I) of [{(en)Pt(*N1*-U-*N3*)(*N3*-HC-*N1*)}$_4${(2,2'-bpy)Pd}$_4$](NO$_3$)$_3$(ClO$_4$)•56.1H$_2$O (**9**) along the fourfold inversion axis.

Complex **9a** crystalizes in the space group P4$_2$/n with one entire octanuclear cation (I) as well as a quarter of a second cation (II). The cytosine and the uracil nucleobases are clearly distinguishable by the means the length of the amide bonds as compared to the carbonyl bonds, as well as on the basis of the thermal displacement factor of N and O atoms. A view of the cation without the ethylenediamine ligands and bipyridine groups is depicted in Figure 28 and salient structural data are listed in Table 7.

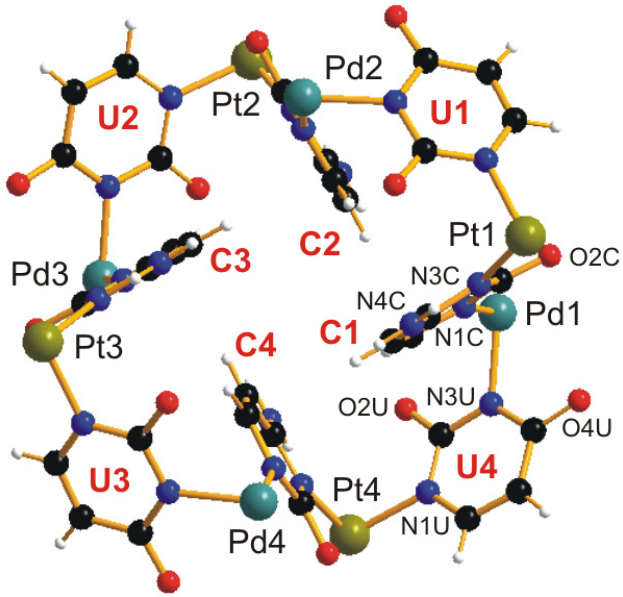

Figure 28: View of the cation (I) of [{(en)Pt(*N1*-U-*N3*)(*N3*-HC-*N1*)}$_4${2,2'-bpy)Pd}$_4$](NO$_3$)$_3$(ClO$_4$)•56.1H$_2$O (**9a**) along the inversion axis with 2,2'-bpy and en ligands omitted for clarity.

Table 7: Selected interatomic distances (Å) and angles (°) of [{(en)Pt(*N1*-U-*N3*)(*N3*-HC-*N1*)}$_4${2,2'-bpy)Pd}$_4$](NO$_3$)$_3$(ClO$_4$)•56.1H$_2$O (**9a**).

Pt-N(1)U	2.007(7) – 2.040(8)	N(en)-Pt-N(en)	83.4(1) – 84.1(3)
Pt-N(3)C	2.024(7) – 2.050(7)	N(1)U-Pt-N(3)C	88.5(3) – 90.2(3)
Pt-N(en)	1.994(7) – 2.041(8)	N(en)-Pt-N(1)U	92.4(3) – 93.5(3)
		N(en)-Pt-N(3)C	93.5(3) – 94.5(3)
Pd-N(3)U	2.019(7) – 2.025(7)	N(bpy)-Pd-N(bpy)	80.0(3) – 80.7(3)
Pd-N(1)C	2.021(7) – 2.038(8)	N(3)U-Pd-N(1)C	84.7(3) – 86.4(3)
Pd-N(bpy)	1.996(8) – 2.041(8)	N(bpy)-Pd-N(3)U	95.6(3) – 97.0(3)
		N(bpy)-Pd-N(1)C	97.3(3) – 98.1(3)

Within the cycle, uracilate- and cytosinate ligands alternate, leading to an alternation of the N(1) and the N(3) sites of the pyrimidine nucleobases (see Scheme 17). The four Pt atoms form a distorted tetrahedron with Pt···Pt distances of 9.579(1)-10.972(2) Å. The four Pd atoms have shorter Pd···Pd distances (7.789(2)-8.889(2) Å). The four metals "at the top" (Pt(1)-Pd(1)-Pt(2)-Pd(2)) and likewise the four metals "at the bottom" (Pt(3)-Pd(3)-Pt(4)-Pd(4)) each form a rhomboid with slight deviations of the metal atoms from planarity of approximately +/- 0.2 Å, resulting in a butterfly arrangement. The sides of each rhomboid are defined by two shorter and two longer Pt···Pd distances (5.789(1)-5.854(1) Å and 7.766(1)-8.210(1) Å, respectively). The diagonal intermetallic distances amount to 10.605(2)-10.972(2) Å (Pt···Pt) and 8.671(2)-8.889(2) Å (Pd···Pd).

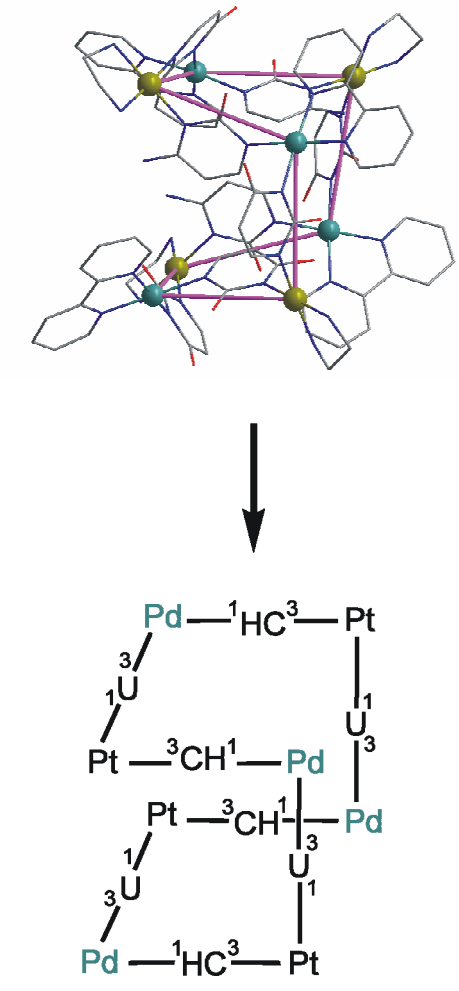

Scheme 17 : Schematic view of the cation of **9a** with nucleobase connectivities indicated.

The four cytosine monoanions orient their C(5) and C(6) faces into the interior of the cation, pointing up, down, up, down. The bulky bipyridine ligands could be the reason for this arrangement, due to the relatively short contacts between the C(5) atoms of the cytosine monoanions and the C(6) atoms of the neighbouring bpy ligands (ca. 3.4 Å). Consequently, a rotation of the nucleobases out of the inner cavity seems to be hindered. On the other hand, a rotation of the cytosines in the other direction would shorten the hydrogen bond between the $N(4)H_2$ groups of the cytosine and the O(2) positions of the neighbouring nucleobases. However, a steric hindrance between the O(2) atoms of the cytosines and the O(4) atoms of the neighbouring nucleobases is possibly present. The rotation of the cytosine, so that it points into the cavity of the cation (circled in yellow), is hindered by one bpy ligand as well as the two neighbouring uracils (lighter colored), as represented in Figure 29.

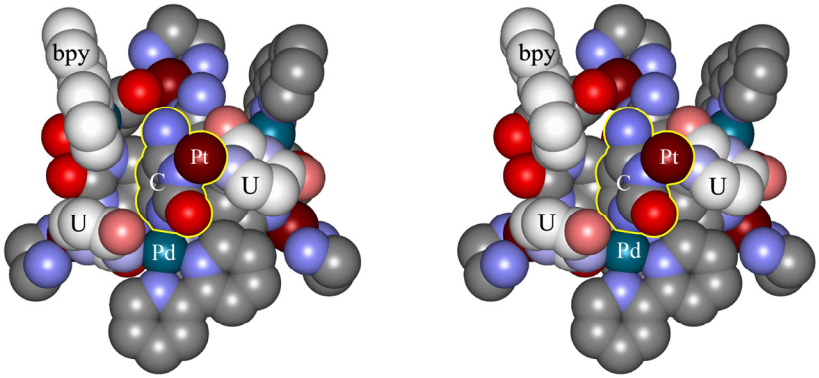

Figure 29: Space filling representation of the cation (I) of complex **9a** with the en ligand of the Pt atom pointing towards the front omitted for clarity.

Two water molecules are found on the top as well as on the bottom of the cation cavity (Figure 30).

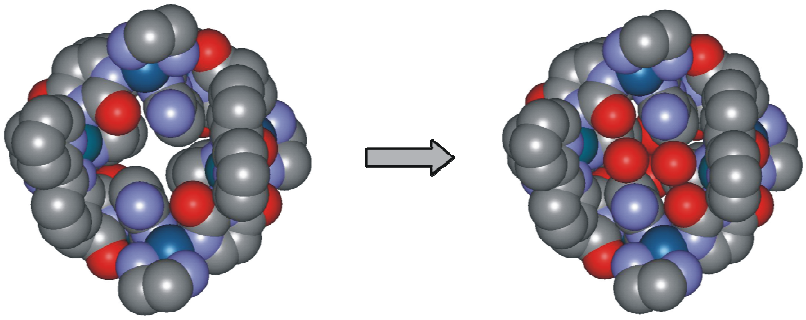

Figure 30: Space filling representation of the cation (I) of complex **9a** viewed along the fourfold inversion axis: without water molecules (left) and with two molecules included each at the top and at the bottom (right).

In Scheme 18, the coordination of the water molecules (O1, O2, O3, and O4, blue colored) to the nucleobases of complex **9a** is represented. The water molecules are bonded through hydrogen bonding interactions between the O(2) positions of the uracils ($H_2O\cdots O(2)$, mean distance 2.73(2) Å) and the N(4) positions of the cytosines ($H_2O\cdots N(4)H_2$, mean distance 2.92(2) Å). The two water molecules in each opening additionally form a hydrogen bond with each other ($H_2O\cdots H_2O$, mean distance 2.80(2) Å).

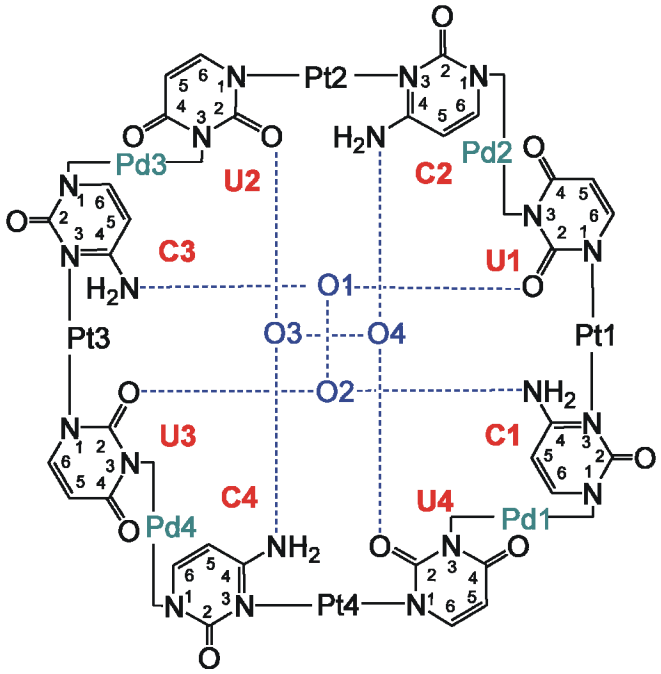

Scheme 18: Schematic representation of the cation of **9a** with two water molecules included each at the top (O1 and O2) and at the bottom (O3 and O4).

Crystal packing inspection of **9a** reveals that the fourfold inversion axis of the complex is parallel to the c-axis, thus the cations form infinite tubes along the c direction (Figure 31), which are only intersected by anions and water molecules. Perpendicular to the c-axis these tubes are connected by π-stacking interactions between bpy ligands of neighbouring cations (orange colored in Figure 31). Anions and water molecules are especially filling the holes between the cations arranged in tubes along the c-axis. It was found that 1.2 ClO_4^-, 3.8 NO_3^- and 70.1 water molecules complete the asymmetric unit. All atoms of the cations were refined anisotropically with the exception of one C(4) atom of one of the cytosine bases (non-positive refined). In Figure 31, cations (I) are shown in normal color code and cations (II) in green.

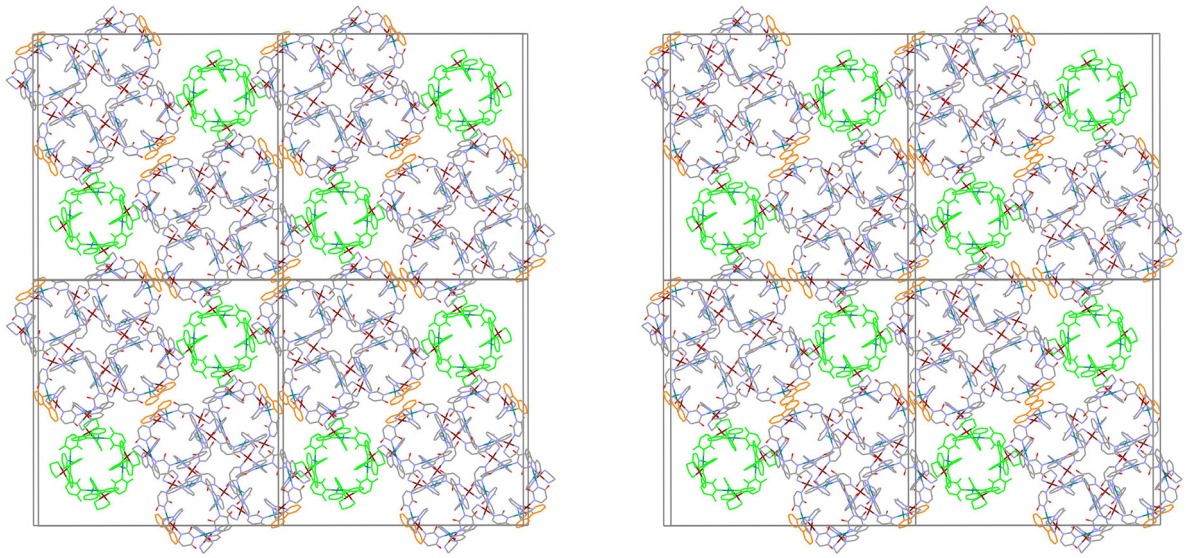

Figure 31: Crystal packing of **9a** along the *c*-axis and the fourfold inversion axes.

NMR Spectroscopy

The ^{1}H NMR spectrum of **9a** in D_2O is simple with only single doublets for H(5) and H(6) ($^{3}J_{H\text{-}H}$ = 6.8Hz) observed for the two nucleobases, eight resonances of the bpy ligands derived from the two non-equivalent halves of each 2,2'-bpy and a broad signal corresponding to the ethylenediamine groups. The relative intensities of the protons of the nucleobases and the 2,2'-bpy ligands are in agreement with expectations. One of the bpy resonances, a triplet at 6.95 ppm stands out amongst all bpy signals because of its high upfield shift. Inspection of the solid state structure of **9a** suggests that it could be the H5 proton of the pyridine ring *trans* to N(3)-uracil donor atom which gives rise to this upfield shift because of its disposition underneath a uracil ring (Figure 32a).

As can be seen in Figure 32b, spectral changes are observed within several hours at room temperature. Within two days, resonances of **9a** have disappeared completely, and two sets of uracil and cytosine resonances each of relative intensities of 2:1 have formed instead. They can be readily assigned to **4** and **1**, respectively, and indicate a clean conversion of **9a** into **4** and **1** according to:

$$3\ Pt_4Pd_4C_4U_4\ (\mathbf{9a}) \rightarrow 4\ Pt_2Pd_3C_2U_2\ (\mathbf{4}) + 4\ PtCU\ (\mathbf{1})$$

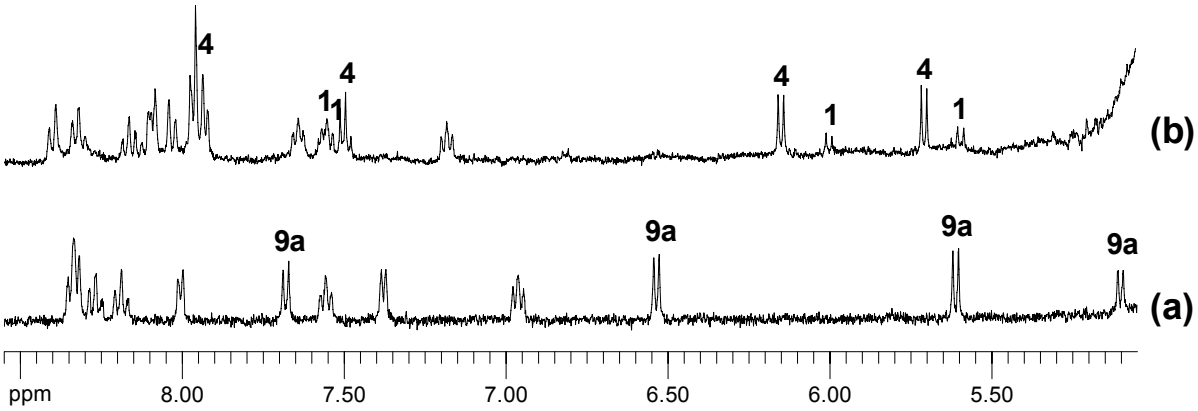

Figure 32: Lowfield sections of ^{1}H NMR spectra of compound **9a** when redissolved in D_2O and conversion into compound **4**: (a) Immediatelly after sample preparation; (b) after two days in solution.

4 Complexes with $[Pd(en)(H_2O)_2]^{2+}$

Here, a different *cis*-$Pd^{II}a_2$ entity (with a_2 = ethylenediamine) was reacted with the starting compound $[Pt(UH\text{-}N1)(CH_2\text{-}N3)(en)]^+$ (**1**), to give a variety of complexes. By addition of silver salts the chloride ions can be removed from $[PdCl_2(en)]$ to give the corresponding aqua species $[Pd(en)(H_2O)_2]^{2+}$. The steric effects of the ethylenediamine (en), which is not a planar ligand like bipyridine (2,2'-bpy), in the formation of these complexes will be studied.

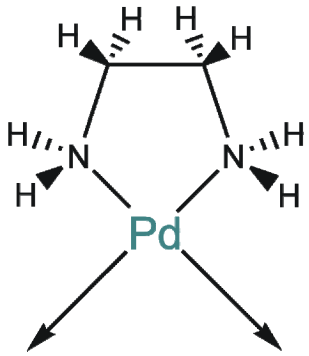

As has been mentioned in the introduction of this thesis, only two years ago a multicomponent reaction involving Pd^{II}(en) metal fragments, 2-pyrimidinol derivatives and 4,7-phenanthroline was reported. [73] The result was the formation of three different cyclic compounds (tri-, tetra, and hexanuclear cycles) of different size.

In this chapter, the formation of a serie of cyclic complexes with different numbers of metal ions will be discussed, as well as the reactivity patterns of the **1**/Pd^{II}(en) system. It should be noted that the compounds corresponding to the **1**/Pd^{II}(en) system are indicated with a prime.

Palladium(II) amine complexes have widely been used to understand the metal interaction ions with nucleobases. But in comparison with Pt(II) nucleobase complexes,[107] the number of characterized Pd(II) nucleobase complexes is limited.[101] The major advantage of Pd(II) over Pt(II) species are the considerably faster reaction kinetics of the former.[108]

4.1 Synthesis, characterization and reactivity.

To study a system of **1** with Pd^{II}(en) a ^{1}H NMR study in D_2O at different ratios of **1**:Pd was carried out. The reactions of **1** with solutions of $[Pd(D_2O)_2(en)]^{2+}$ took place at room temperature. As in the system with $[Pd(2,2'\text{-bpy})(D_2O)_2]^{2+}$, marked changes in the solutions were observed. The development of an intensive yellow color was observed, as was a rapid drop in pD of the solution down to roughly 2. Having adjusted the pD of the solutions to ca. 7.5, the reactions were followed by ^{1}H NMR spectroscopy.

In Figure 33 representative ^{1}H NMR spectra of the reaction of **1a** with a Pd^{II}(en) entity are shown. Some of the products (**Y'**, **12'**, **13'**) were isolated and one of these (**13'**) was characterized by X-ray crystal structure analysis. Starting from compound **13'**, it is possible to obtain product **12'**. Two major species present in the mixture of **1** and Pd^{II}(en) are assigned to the tetranuclear complex $[\{(en)Pt\}_2U_2(CH)_2\{(en)Pd\}_2]^{2+}$ "Pt_2Pd_2" (**Y'**) and to the hexanuclear complex $[\{(en)Pt(U\text{-}\textit{N1,N3,O2,O4})(C\text{-}\textit{N1,N3,N4,O2})\}_2\{(en)Pd\}_4]^{4+}$ "Pt_2Pd_4" (**12'**). A third compound, the octanuclear complex $[\{(en)Pt(U\text{-}\textit{N1,N3,O2,O4})(C\text{-}\textit{N1,N3,N4,O2})\}_2\{(en)Pd\}_6]^{8+}$, "$Pt_2Pd_6$" (**13'**), was eventually crystallized. It is detected in the reaction mixture in the presence of an excess of $enPd^{II}$ only (Figure 33d). The numerous minor species (c.f. in particular Figure 33b), are not identified.

Frequently a gradual isotopic exchange of the H(5) protons by deuterium of both uracil and cytosine resonances was observed, resulting in "pseudo-triplet" patterns of H(6) resonances or eventually in H(6) singlets (see, Figure 33c). In some cases (e.g. Figure 33b) more than 10 doublets for each of the H(5) and H(6) resonances were observed, representing numerous different species.

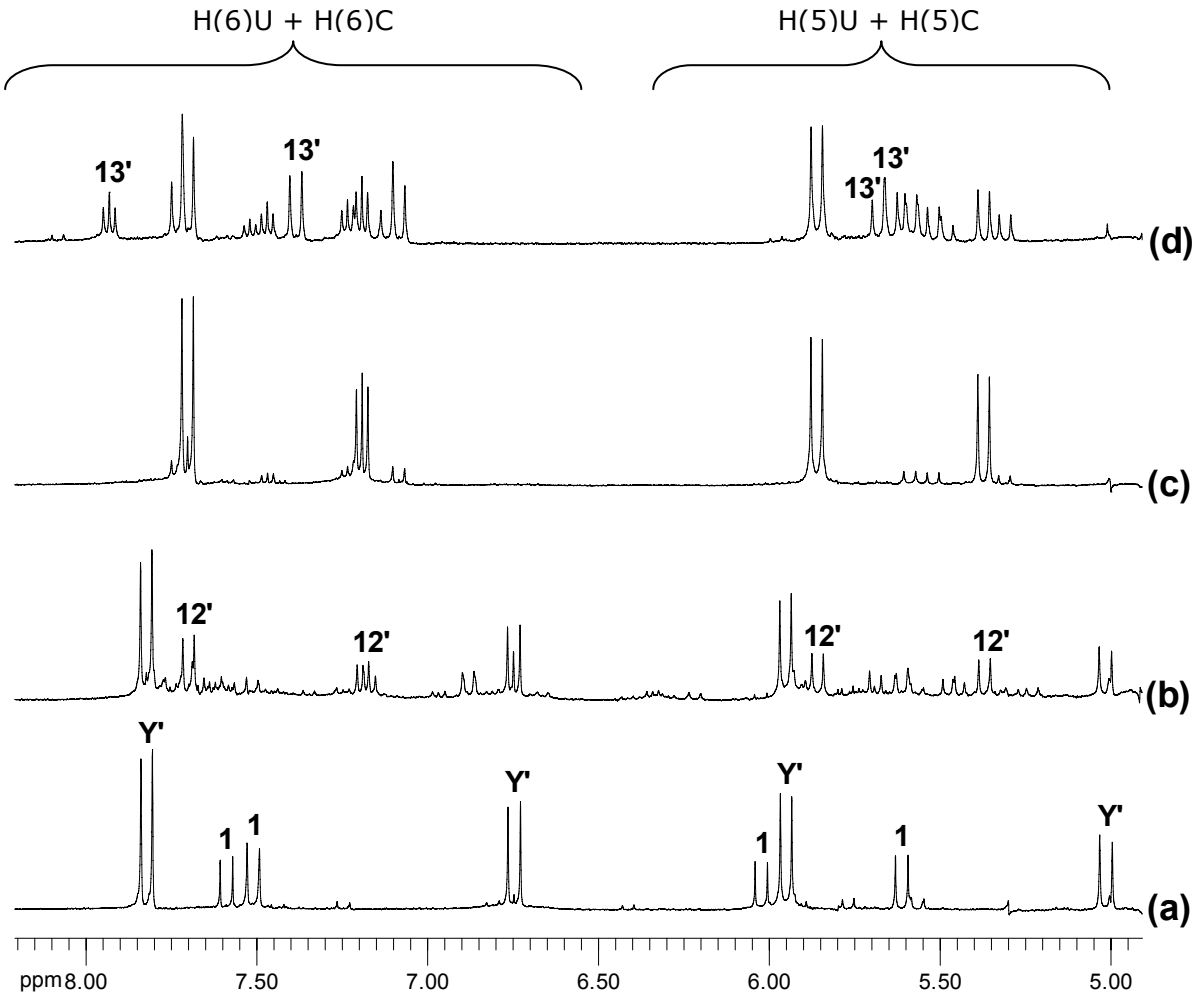

Figure 33: Low field section of ^{1}H NMR spectra of the reaction of [Pt(UH-*N1*)(CH$_2$-*N3*)(en)](ClO$_4$)•3H$_2$O (**1a**) with [Pd(D$_2$O)$_2$(en)]$^{2+}$ in D$_2$O where r = Pt:Pd is:
(a) r = 1:0.5, pD= 7.39;
(b) r = 1:1, pD = 7.40;
(c) r = 1:2, pD = 7.00;
(d) r = 1:3, pD = 7.02.

As for the system **1**/Pd^{II}(2,2'-bpy), after the ^{1}H NMR study of Pd^{II}(en) with **1a** in aqueous solution at different ratios (r), once again, the aim was to isolate each of the compounds observed to understand the reactivity patterns of the system. Preparations at different ratios were carried out and also in some cases the pH of the solutions was changed. In this part, the synthesis and characterization of all of the compounds isolated are reported. Possible reactivity patterns of the compounds isolated will be discussed following characterization of the products. This includes also intermediate species, which have not been detected by ^{1}H NMR spectroscopy.

4.1.1 Pt_2Pd_2 : $[\{(en)Pt\}_2U_2(CH)_2\{(en)Pd\}_2](NO_3)_2$ (Y')

The first compound isolated in the system of **1**/Pd^{II}(en) proved to be a cyclic tetramer, consisting of two Pt^{II}(en), two Pd^{II}(en), two uracilate dianions and two cytosinate monoanions, $[\{(en)Pt\}_2U_2(CH)_2\{(en)Pd\}_2](NO_3)_2$ (**Y'**), according to the mass spectrometric study (see below).

Compound **Y'** was obtained by addition of $[Pd(en)(H_2O)_2]^{2+}$ to an aqueous solution of **1b** at r = 0.5, pH =2.2. Following adjustment of the pH to 7.4 gave, after 10 days, a white precipitate.

ESI-Mass Spectrometry

Unfortunately, no crystals of the title compound could be obtained. However, **Y'** could be prepared on a preparative scale. An Electrospray ionization Fourier-transform ion-cyclotron-resonance (ESI-FTICR) mass spectrometry study of the precipitate was performed by Prof. Dr. C. A. Schalley (Berlin), which confirmed the composition of **Y'**. Quite intense signals for the doubly charged $[\mathbf{Y'}\text{- }2NO_3]^{2+}$ are detected at m/z 641.06. The isotope pattern of this ion is superimposed by a single charge fragment, which corresponds to half of the macrocycle and therefore appears at the same position. This isotope pattern is similar to a 4:1 superposition of the patterns calculated for $[\mathbf{Y'}\text{- }2NO_3]^{2+}$ and its singly charged half. Two other high intensive signals appear at m/z 559.08 and 477.10, corresponding to a trinuclear fragment $[(en)Pt\{U(CH)(en)Pd\}_2]^{2+}$ and a mononuclear fragment $[(en)PtU(CH)]^{+}$, respectively. The single charged ions $[\mathbf{Y'}\text{- }NO_3]^{+}$ (m/z 1344) and $[(en)Pt\{U(CH)(en)Pd\}_2]^{+}$ (m/z 1180) also appear in the mass spectrum, although with much lower intensities.

According to the mass spectrometric study, compound **Y'** proved to be a cyclic tetramer $[\{(en)Pt\}_2U_2(CH)_2\{(en)Pd\}_2]^{2+}$, but the nucleobase sequence in the tetranuclear complex can not be estabilished by this method. Two different geometries depending on the connectivity of the nucleobases (cytosine-uracil-uracil-cytosine or cytosine-uracil-uracil-cytosine) are possible. These two possibilities are represented in Scheme 19.

Scheme 19: Schematic representation of the two possible geometries adopted for compound **Y'** depending on the connectivities of the nucleobases: CUCU (left) and CUUC (right).

NMR Spectroscopy

The ^{1}H NMR spectrum in D_2O of this precipitate shows it to be a mixture of **Y'** (90%) and **1** (10%). The spectrum consists of discrete doublets ($^{3}J_{H\text{-}H}$ = 7.3Hz) for the uracil protons and for the cytosine protons ($^{3}J_{H\text{-}H}$ = 6.8Hz), as well as a broad signal for the CH_2-ethylenediamine protons (Figure 34a). On the other hand, addition of an excess of $[Pd(D_2O)_2(en)]^{2+}$ to this mixture leads to an important drop in the pD of the solution. The ^{1}H NMR spectrum shows the formation of a new compound **12'** and partial decomposition to the starting compound **1** due to the acidic pD (Figure 34b).The chemical shifts are given in Table 10 (see Chapter I: Summary).

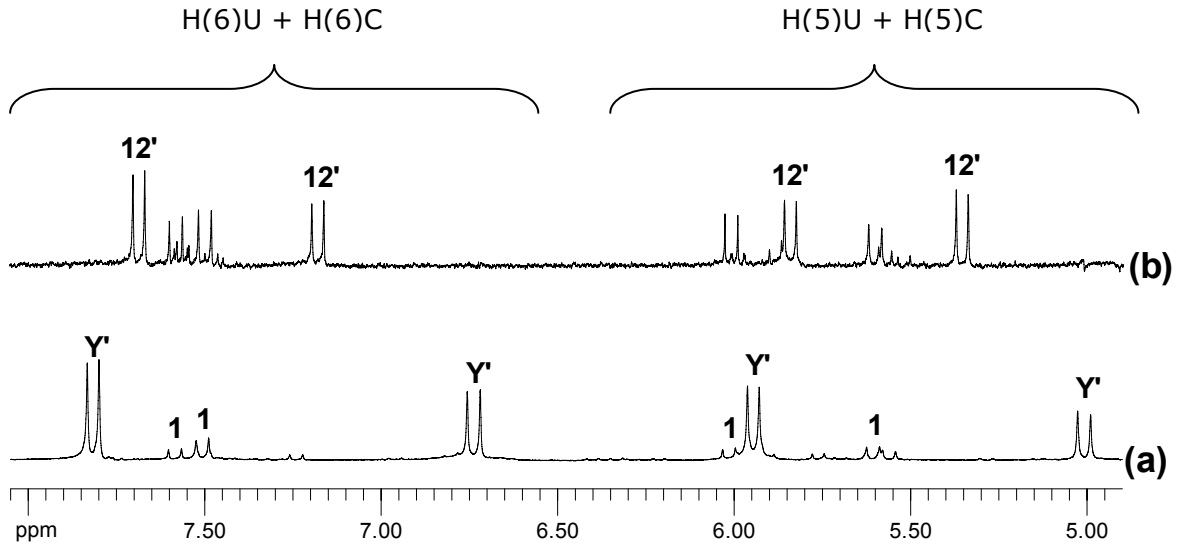

Figure 34: Low field section of ^{1}H NMR spectrum of $[\{(en)Pt\}_2U_2(CH)_2\{(en)Pd\}_2](NO_3)_2$ (**Y'**) in D_2O (a) after 15 min, pD = 7.68 and (b) after the addition of $[Pd(D_2O)_2(en)]^{2+}$, pD = 2.25.

The assignment of the ^{1}H NMR resonances of **Y'** with its two sets of uracil and cytosine resonances was achieved by a combination of a 2D $^{1}H,^{1}H$ NOESY and 2D $^{1}H,^{13}C$ COSY experiments (Figures 35 and 36, Table 8) and the help of direct (HSQC) as well as long range ^{1}H, ^{13}C coupling (HMBC). In the 2D ^{1}H, ^{1}H NOESY experiment the signal of proton H5 at 5.00 ppm shows cross-peaks to the signal of the H6 proton located at 6.73 ppm. Also intense cross-peaks between the H5 resonance at 5.93 ppm and H6 resonance at 7.81 ppm are detected. It should be noticed that TSP was not used as internal standard to adjust the chemical shifts of the signals in the 2D $^{1}H,^{1}H$ NOESY and $^{1}H,^{13}C$ COSY experiments. Consequently the shifts in Figure 35 are slightly different from the ones listed in Table 8.

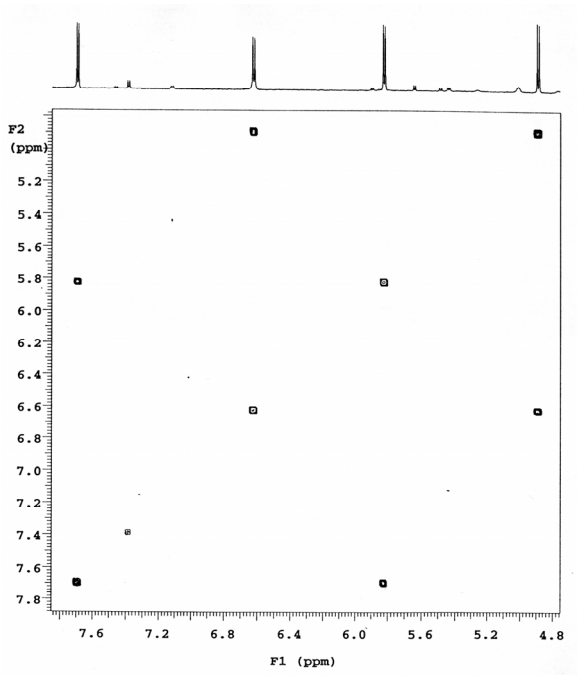

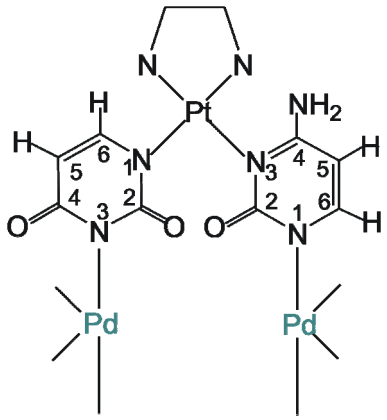

Figure 35: 2D ^{1}H, ^{1}H NOESY of compound **Y'** in D_2O.

To distinguish the uracil and cytosine resonances, a 2D ^{1}H, ^{13}C COSY was carried out. As can be seen in Figure 36, the signal of the H5 proton of uracil gives cross-peaks to the C5 and C6 signals. In the same way the H6 resonance of uracil shows cross-peaks to the C2, C4, C5 and C6 signals, which were assigned according to Pretsch et al.[105] Similarly, one observes cross-peaks between the signal of H5-cytosine and the C4, C5 and C6 signals, as well as between the H6 resonance and the C2, C4, C5 and C6 signals of the cytosine (see Table 8).

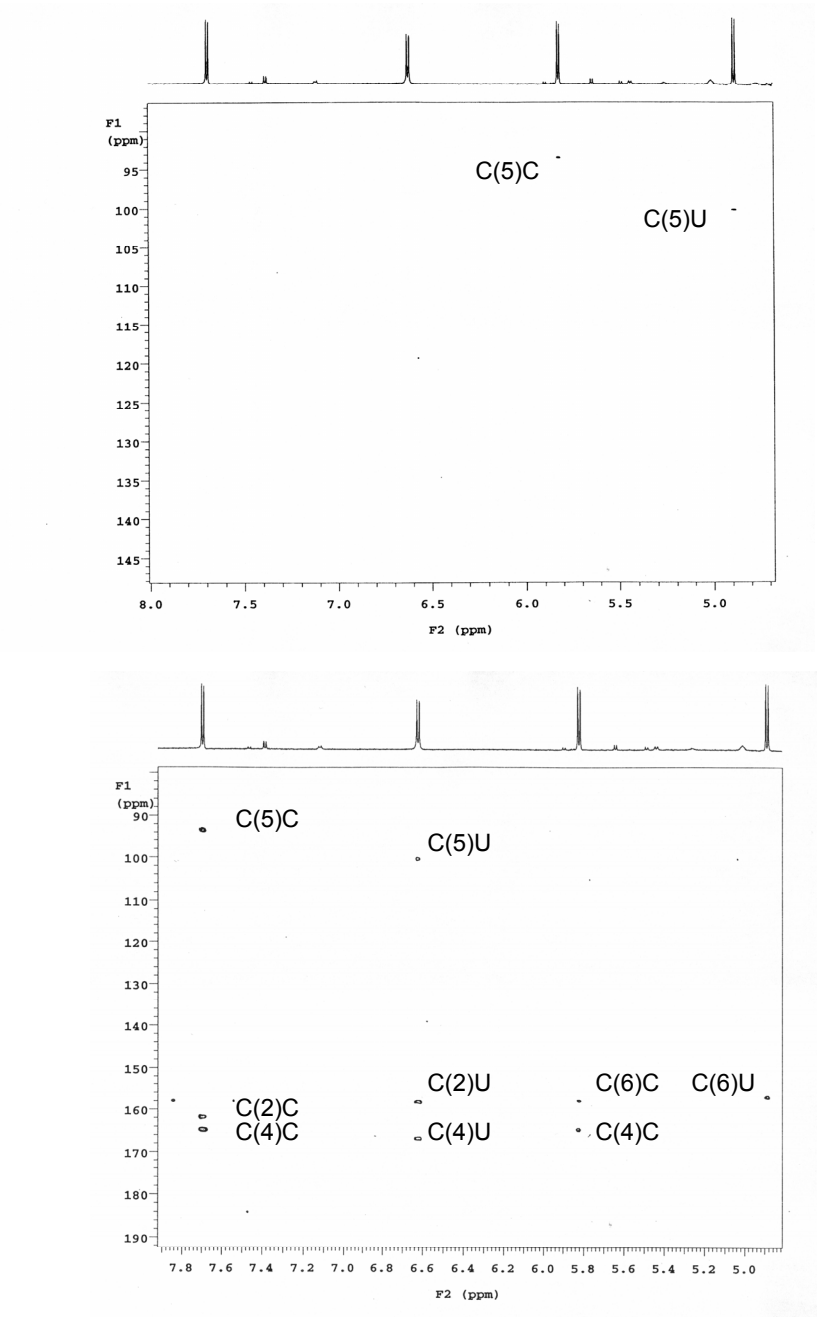

Figure 36: 2D ^{1}H, ^{13}C COSY of compound **Y'** in D_2O, HSQC (top) and HMBC (bottom).

Table 8: ^{1}H NMR of chemical shifts aromatic nucleobase protons and ^{13}C NMR resonances of carbon atoms of **Y'** (δ, D_2O).

	^{1}H NMR (ppm)	^{13}C NMR (ppm)
Uracil	5.00(H5) 6.73(H6)	158.5(C2), 167.3(C4), 100.6(C5), 157.7(C6)
Cytosine	5.94(H5) 7.81(H6)	162.1(C2), 165.3(C4), 93.7(C5), 158.1(C6)

Compound **Y'** is stable in neutral aqueous solution (pH = 7.68), even upon heating to 70°C (again with gradual isotopic exchange of uracil-H5). When the pD is increased up to 10.7, **Y'** remains stable in solution. In more basic conditions compound **Y'** starts to decompose to give **1** and $[Pd(D_2O)_2(en)]^{2+}$. At pD value of 12.4 a mixture of **Y'** and **1** (1:1) is present in the ^1H NMR spectrum and at pD values higher than 13 only compound **1** is observed in the spectrum. In DCl **1** forms. In the presence of a large excess of NaCl (more than 100 equivalents) the title compound remains stable in solution. However, in the presence of 2-4 equivalents of 9-methylguanine (9-MeGH), partial decomposition of **Y'** to **1** and some unidentified (en)Pd(9-MeGH) species takes place.

An interesting point is the possible conformation of the nucleobases in this metallocycle. Consistent with previous experimental findings[66] and with the model building of **Y'**, the cone conformer (O(2) groups of all four nucleobases pointing in the same direction, see Scheme 20) can be expected to provide access to anions from the side opposite to the O(2) oxygen atoms, hence might behave as a host for anionic guests. In order to probe such a possibility, increasing amounts of 3-(trimethylsilyl)-propanesulfonate (TSP) were added to an aqueous solution of **Y'**. There was no effect whatsoever on chemical shifts of any of the resonances, strongly suggesting that compound **Y'** does not adopt a cone structure, but rather is in a *1,3*-alternate conformation (see Scheme 20).

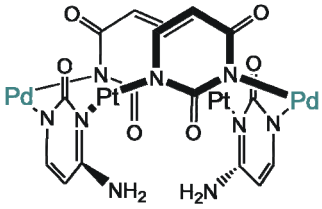

1,3-alternate

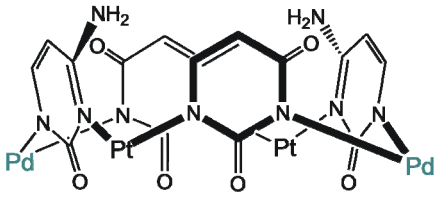

cone

Scheme 20: Possible conformers of **Y'** with the nucleobase secuence CUCU.

On the other hand, if an excess of $[Pd(en)(H_2O)_2]^{2+}$ is added to a solution of **Y'**, decomposition to **1** (because of the acidic pH) and formation of a new compound (**12'**), which is later assigned to the Pt_2Pd_4 species, takes place.

4.1.2 Pt_2Pd_4 and Pt_2Pd_6 :

$[\{(en)Pt(U\text{-}N1,N3,O2,O4)(C\text{-}N1,N3,N4,O2)\}_2\{(en)Pd\}_4]^{4+}$ (12') and $[\{(en)Pt(U\text{-}N1,N3,O2,O4)(C\text{-}N1,N3,N4,O2)\}_2\{(en)Pd\}_6](NO_3)_5(ClO_4)_3 \cdot 21.2H_2O$ (13') (Connectivity = cytosine-uracil-cytosine-uracil)

If the ratio of **1a**/Pd^{II}(en) is increased to 1:1, a new set of resonances is observed in the ^{1}H NMR spectrum (Figure 33b).

To isolate this new compound, $[Pd(en)(H_2O)_2]^{2+}$ was added to a solution of **1a** in H_2O (r =2). Then the pH was adjusted to 4.1 and after one week, orange cubic crystals were obtained from the yellow solution, which turned out to be suitable for X-ray crystallography.

X-Ray Crystallography

Compound **13'** is an octanuclear Pt_2Pd_6 species $[\{(en)Pt(U\text{-}N1,N3,O2,O4)(C\text{-}N1,N3,N4,O2)\}_2\{(en)Pd\}_6]^{8+}$. A view of the cation of compound **13'** is given in Figure 37 and selected interatomic distances are compiled in Table 9.

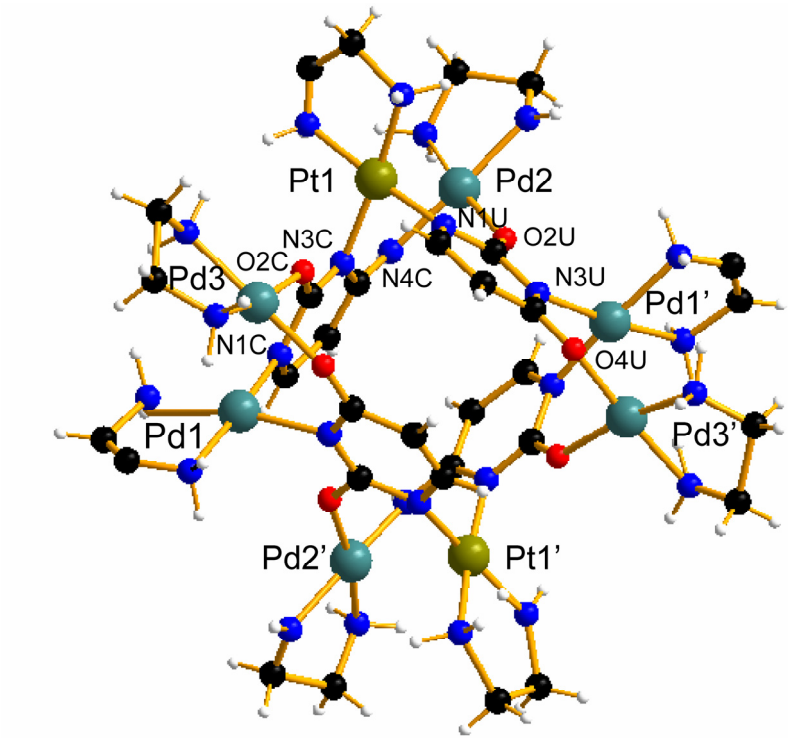

Figure 37: Crystal structure of the cation of $[\{(en)Pt(U\text{-}N1,N3,O2,O4)(C\text{-}N1,N3,N4,O2)\}_2\{(en)Pd\}_6](NO_3)_5(ClO_4)_3 \cdot 21.2H_2O$ (**13'**).

Table 9: Selected interatomic distances (Å) and angles (°) of [{(en)Pt(U-*N1,N3,O2,O4*)(C-*N1,N3,N4,O2*)}$_2${(en)Pd}$_6$]$(NO_3)_5(ClO_4)_3$•21.2H_2O (**13'**).

Pt(1)-N(1)U	2.032(7)	N(11)-Pt(1)-N(12)	83.5(4)
Pt(1)-N(3)C#1	2.033(7)	N(1)U-Pt(1)-N(3)C#1	87.6(3)
Pt(1)-N(11)	2.054(7)	N(11)-Pt(1)-N(1)U	95.3(3)
Pt(1)-N(12)	2.060(7)	N(12)-Pt(1)-N(3)C#	93.6(3)
Pd(1)-N(3)U'#1	2.032(8)	N(11)-Pd(1)-N(12)	83.3(4)
Pd(1)-N(1)C	2.036(8)	N(3)U'-Pd(1)-N(1)C#1	87.5(3)
Pd(1)-N(11)	2.058(8)	N(11)-Pd(1)-N(3)U'	95.2(4)
Pd(1)-N(12)	2.065(8)	N(12)-Pd(1)-N(1)C#	93.4(4)
Pd(3)-O(4)U'#1	1.989(8)	N(11)-Pd(3)-N(12)	83.4(4)
Pd(3)-O(2)C	2.024(8)	O(4)U'-Pd(3)-O(2)C#1	95.5(3)
Pd(3)-N(11)	2.039(6)	N(11)-Pd(3)-O(4)U'	90.1(3)
Pd(3)-N(12)	2.009(7)	N(12)-Pd(3)-O(2)C#	89.9(3)
Pt(1)···Pd(2)	3.04(1)		
Pd(1)···Pd(3)	2.96(3)		

#1: -y + $^7/_4$, x - $^1/_4$, -z + $^3/_4$

Compound **13'** crystallizes in the tetragonal space group $I4_1/a$ with a quarter of one octamer forming the asymmetric unit. The octamer is generated via the fourfold inversion axis in the center of the molecule. The four nucleobases of each cation enclose a cavity. The maximum diameter of the inner core of the complex can be estimated by the C(2)···C(2) distance of opposite nucleobase rings, which amounts to 5.68(2) Å. No guest molecules could be localized inside the cavity. Anions and water molecules fill the space between the complexes that are partially bonded to the outer sphere of the complex via the nitrogen atoms of the ethylenediamine ligands.

The oxygen atoms of all anions are disordered over multiple positions. The same is true for the 5.3 water molecules found per asymmetric unit. All atoms of the cation were refined anisotropically with the exception of one carbon atom of each

of the ethylenediamine ligands, which are disordered over two positions each, all with occupancies of 50%.

The cation of **13'** consists of a tetranuclear cyclic Pt_2Pd_2 core unit, in which all four nucleobases are cross-linked in an alternating *1,3*-fashion to the N ring atoms of the four nucleobases upon addition of four $(en)Pd^{II}$ residues to the eight available exocyclic sites. The four $Pd^{II}(en)$ residues are attached pairwise to the O(4)-uracil and the O(2)-cytosine sites as well as to the O(2)-uracil and the N(4)-cytosine sites, leading to *head-head* arrangements in all cases. All four nucleobases are dianions, with uracil deprotonated at N(1) and N(3), and cytosine deprotonated at N(1) and at the exocyclic amino group N(4) (see Scheme 21).

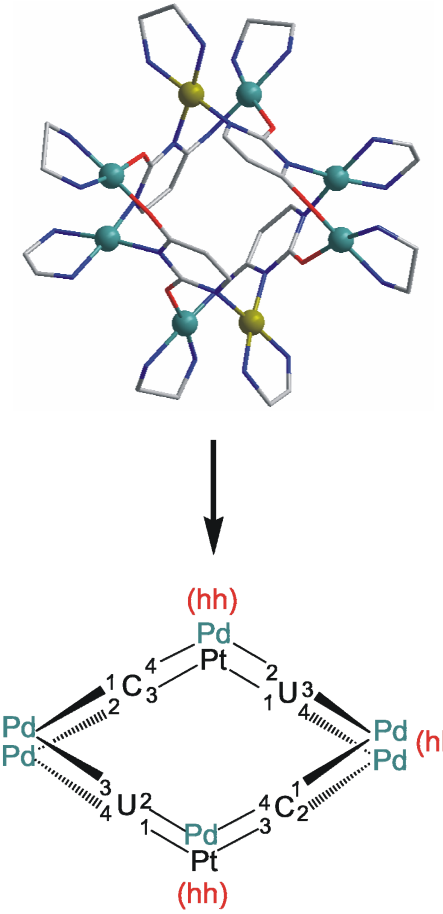

Scheme 21: Schematic view of the cation of compound **13'** with the nucleobase connectivities indicated.

Like compound **7** and **9** (with Pd^{II}(2,2'-bpy) entities) the sequence of nucleobases in the cycle is (*N1*-HC-*N3*)-Pt(*N1*-U-*N3*)Pd(*N1*-HC-*N3*)Pt(*N1*-U-*N3*)Pd. In **13'** all four bases act as tetradentate ligands. The cation of **13'**, which is defined as $Pt_2Pd_6C_2U_2$, presents a very close structural similarity with related Pt_8U_4 and $Pt_4Pd_4U_4$ complexes previously reported by our group.[40] This similarity includes intermetallic distances within the cation. The main difference between the U_4 and the C_2U_2 complexes is that the exocyclic O(4) oxygen atoms of the two uracil ligands in Pt_8U_4 are replaced by two isoelectronic N(4)H groups (to give two cytosine ligands) in $Pt_2Pd_6C_2U_6$ (**13'**), as shown in Figure 38.

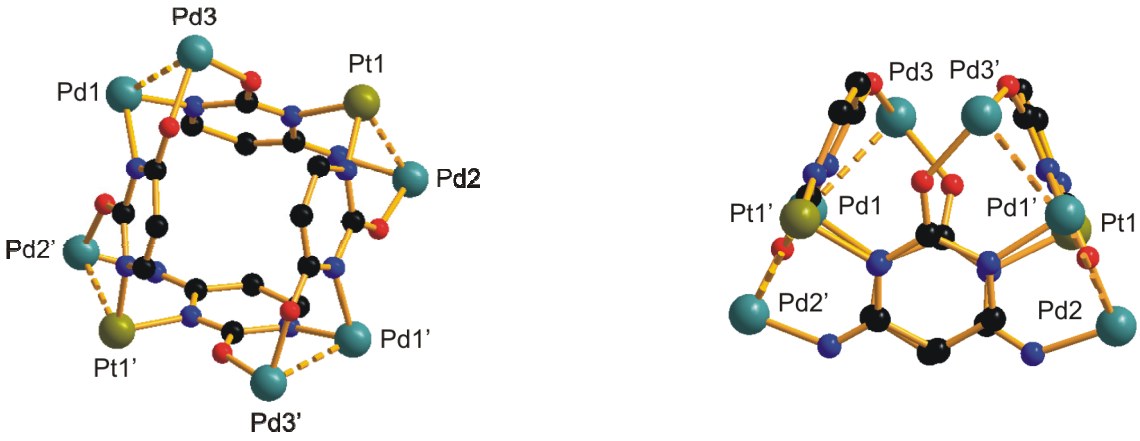

Figure 38: Two different views of the cation of **13'** with ethylenediamine groups omitted for clarity.

The four central metal ions cross-linking the endocyclic N(1) and N(3) sites of the four nucleobases are not in a plane. They form a distorted square, as can be seen in Figure 39 and rather adopt a flat butterfly structure, with two metals (Pt(1), Pt(1')) slightly above the best main plane (0.11(1) Å), and other two metals (Pd(1), Pd(1')) slightly below this plane (-0.11(1) Å). This feature has also been observed for **7**.

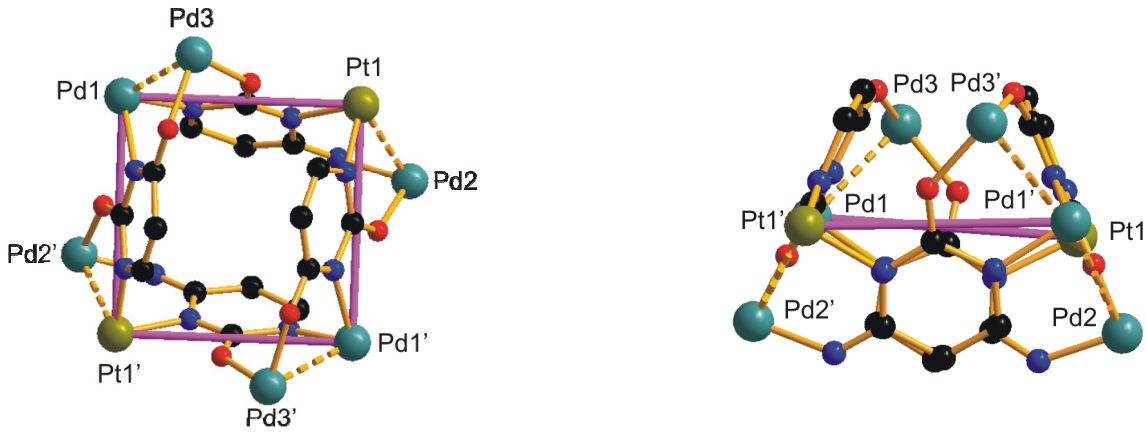

Figure 39: : Two different views of the cation of **13'** with ethylenediamine groups omitted for clarity. The Pt_2Pd_2 core unit (defined by the endocyclic coordination at the nucleobases) is indicated.

Compound **7** and compound **13'** have very close structural similarities. Both complexes have a Pt_2Pd_2 core unit, in which a pairwise sequence of nucleobases is present. The two exocyclic Pd^{II}(2,2'-bpy) entities of the hexanuclear compound **7** are bonded at O(2)-cytosine and O(4)-uracil sites, thus providing an intramolecular π-stacking interaction for the bipyridine rings. In complex **13'** two

Pd^{II}(en) moieties bonded at O(2)-cytosine and O(4)-uracil sites can also be observed, but in this case also two other Pd^{II}(en) moieties are bonded at N(4)H-cytosine and O(2)-uracil groups to form the octamer $Pt_2Pd_6C_2U_2$. The structures of both compounds are depicted in Figure 40.

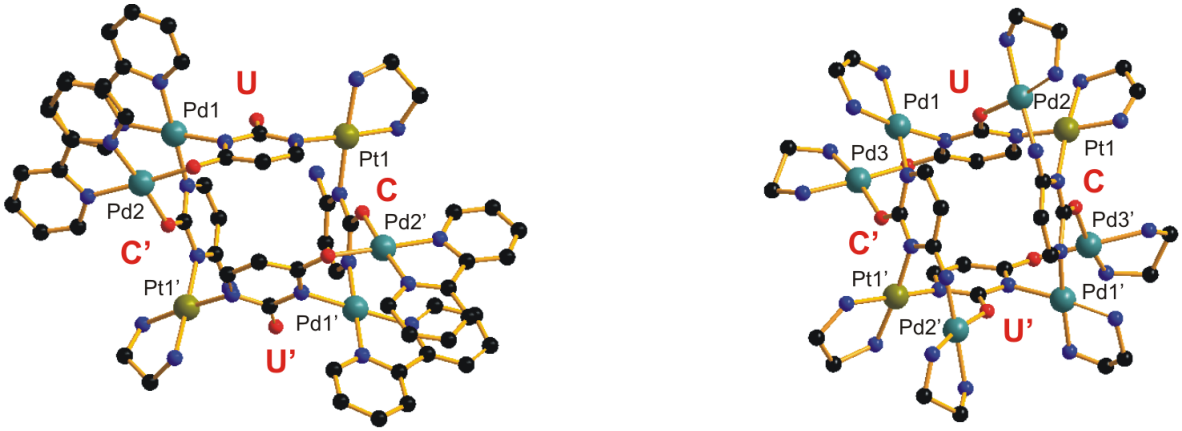

Figure 40: Views of the cation of [{(en)Pt}$_2$(*N1*-U-*N3,O4*)$_2$(*N3*-HC-*N1,O2*)$_2$}{(2,2'-bpy)Pd}$_4$](NO$_3$)$_6$ (**7**) (left) and of the cation of [{(en)Pt(U-*N1,N3,O2,O4*)(C-*N1,N3,N4,O2*)}$_2$ {(en)Pd}$_6$](NO$_3$)$_5$(ClO$_4$)$_3$•21.2H$_2$O (**13'**) (right).

A reason for this difference could be the propensity of the bipyridine rings to engage in intramolecular π-stacking interactions with each other. On the other hand, the addition of two further Pd^{II}(2,2'-bpy) entities to the exocyclic positions (N(4)H-cytosine and O(2)-uracil) seems not to be possible because of the sterical hindrance of the two Pt^{II}(en) moieties.

NMR Spectroscopy

Compound **7** is not stable in aqueous solution. The O-bonded Pd^{II}(2,2'-bpy) entities of the cation are lost under these conditions. When **13'** is redissolved in D_2O, a rapid formation (within a few minutes) of new ^{1}H NMR resonances due to the partial loss of Pd^{II}(en) from the cation is also detected. This is evident from the appearance of signals due to free $[Pd(D_2O)_2(en)]^{2+}$ (δ 2.51 ppm, pD = 4.65) in the ^{1}H NMR spectrum. In Figure 41 the ^{1}H NMR spectrum of **13'** in D_2O is shown and chemical shifts are given in Table 10 (see Chapter I: Summary).

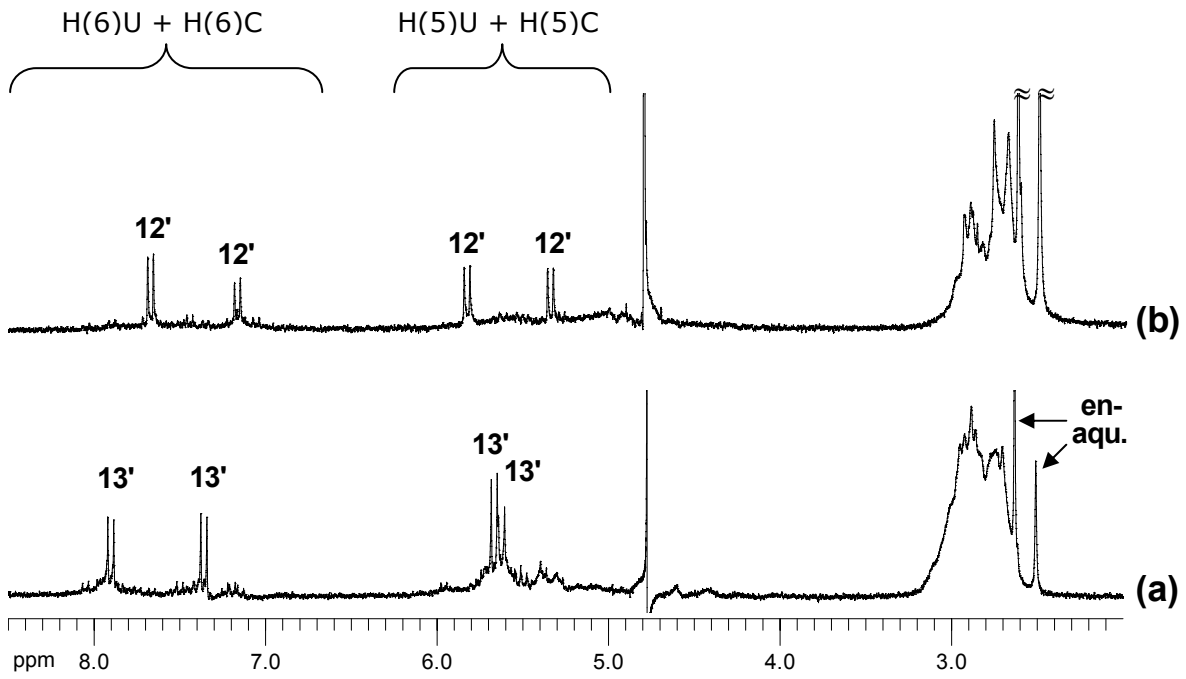

Figure 41: ^{1}H NMR spectra of compound **13'** when redissolved in D_2O and conversion into **12'**: (a) Immediatelly after sample preparation; (b) after 15 minutes (pD = 4.65).

The simplicity of the resulting spectrum, which consists of one type of uracil and one type of cytosine resonances only (Figure 41b), and the intensity of the resonance due to the uncoordinated $[Pd(D_2O)_2(en)]^{2+}$ reveal that two of the six $Pd^{II}(en)$ entities are lost.

It is assumed that the two Pd^{II} moieties bonded pairwise to O(2) of C and O(4) of U are displaced, whereas the Pd^{II} entities bonded to the deprotonated N(4) position of cytosine as well as O(2) of uracil remain associated with the cycle under these conditions. The compound obtained is therefore assigned to the Pt_2Pd_4 species (**12'**).

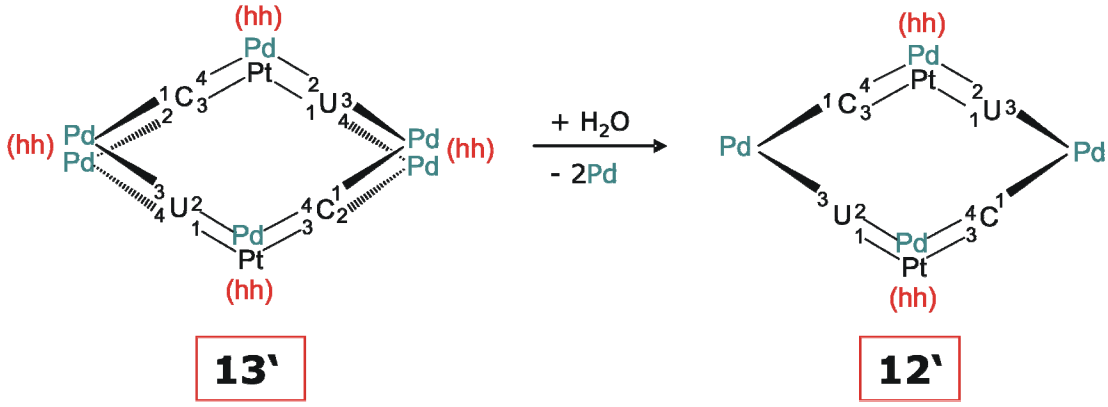

Schema 22: Proposed conversion process of **13'** to **12'**.

Concerning its formation, it has been seen previously, that **12'** can be derived from **Y'** by addition of two Pd^{II}(en) entities. These additional Pd moieties are coordinated to the exocylic O(2)-uracil and N(4)-cytosine positions adopting *head-head* arrangements of the nucleobases in the cycle. The nucelobase sequence in **Y'** can not be estabilished, hence two different mechanisms of conversion of the tetranuclear species **Y'** to the hexanuclear compound **12'** should be taken into account. In the following these interconversion mechanisms will be discussed.

In Scheme 23 a schematic diagram of these processes is shown, where the two possible structures of **Y'** (depending on the nucleobase sequence) are represented.

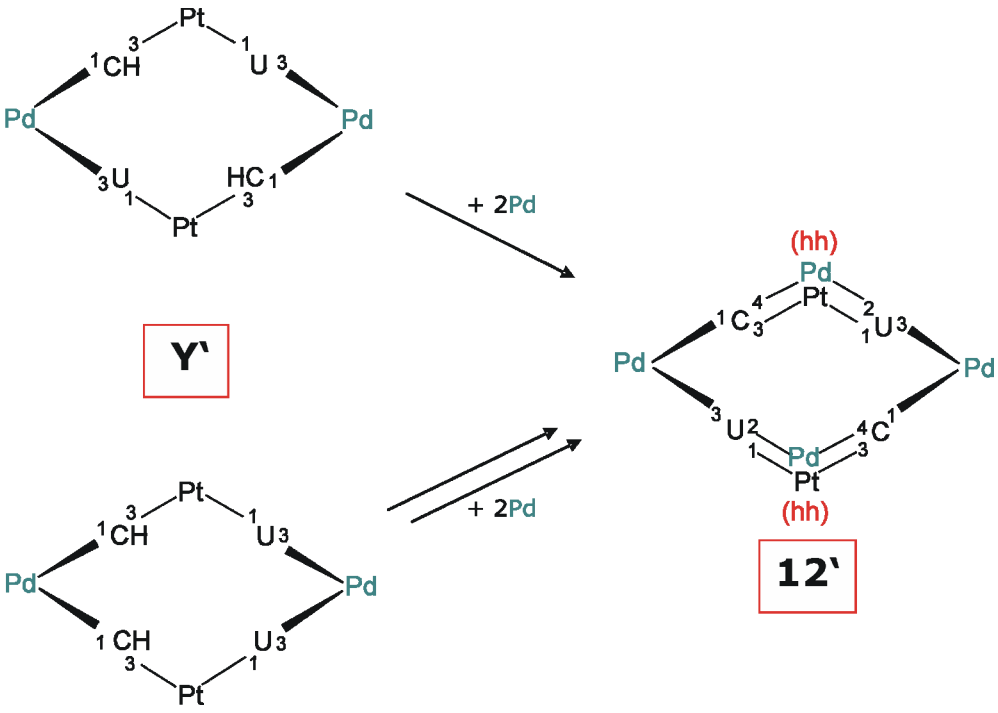

Scheme 23: Possible conversion processes of **Y'** to **12'**.

Compound **12'** is stable under moderately basic conditions (pD = 9.7), in the presence of a 50-fold excess of NaCl and even when heated to 70°C for 1d. As observed for other compounds, in the latter case, there is an accelerated exchange of the C5 protons by deuterium (with uracil exchange faster). Only with DCl (pD < 1) there is decomposition to the starting compound **1**, again accompanied by isotopic exchange of H5-uracil. In the presence of a large excess

of NaCl (100 equiv.), **12'** starts to decompose, leading to the starting compound **1** and **Y'**.

Given the rapid loss of two Pd^{II}(en) moieties from **12'** in aqueous solution, it did not come as a surprise to see that similar ^{1}H NMR spectroscopic changes occur in the presence of ligands such as 9-MeGH or AMP. Addition of two equivalents of 9-MeGH or one equivalent of AMP lead to **12'** and a mixture of Pd^{II}(en) complexes with these nucleobases (not further identified), with **12'** being stable for days. Only upon the addition of four equivalents 9-MeGH there is partial decomposition of **12'**, leading to **1** and **2**.

The cation of compound **12'** has free coordination sites (O(4) exocyclic atoms of uracil, as well as O(2) position of the cytosine), hence this metalla[4]calixarene could probably act as a guest for other molecules. Reactions of compound **12'** with different anions and cations were carried out. First, a solution of **13'** (after 2h decomposition to **12'** and Pd^{II}(en) takes place) was tried to react with cations such as Li^{+}, Na^{+}, K^{+}, Cu^{2+} or Ni^{2+}, and secondly **12'** was tested with anions such as NO_3^{-}, ClO_4^{-}, CO_3^{2-}, F^{-}, I^{-} or CH_3COO^{-}. The reactions were followed by ^{1}H NMR spectroscopy, but no spectroscopic changes were observed.

5 Complexes with $[Pd(H_2O)_2(tmeda)]^{2+}$

As discussed in the preceeding chapters, $[Pt(UH\text{-}N1)(CH_2\text{-}N3)(en)]^+$ (**1**), forms a series of metallacalix[n]arenes with two different a_2Pd^{II} entities, in which a_2 = (2,2'-bipyridine) and (ethylenediamine). The next step of this work was to use a bulky ligand such as *N,N,N',N'*-tetramethylethylenediamine (tmeda) and to study the influence of the steric bulk caused by the CH_3 groups of the tmeda ligand in the formation of the metallacalix[n]arenes.

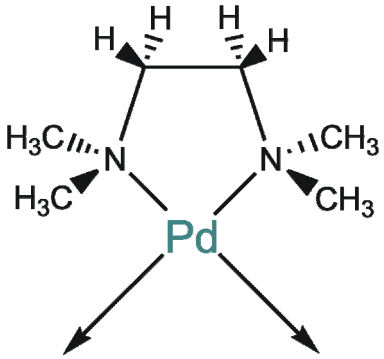

In related studies, the reactivity of the analoguous Pt^{II}(tmeda) entity with substituted pyrimidine nucleobases had been investigated. Preut et al.[109] reported on the structure of $[Pt(1\text{-}MeC)_2(tmeda)]^{2+}$ with 1-MeC = 1-methylcytosine. One year later, Frommer et al.[110] isolated the complex $[Pt(1\text{-}MeU)_2(tmeda)]$ (1-MeU = 1-methyluracil) as well as a trinuclear complex derived upon addition of Cu^{2+} to the 2:1 compound.

More recently, Shen et al. [111] showed the self-assembly of the Pd^{II}(tmeda) entity and 1-methylcytosine, which led to the formation of a trinuclear box. The usual *head-tail* dimer did not form presumably because of the steric bulk of the tmeda ligand, which prevents a close approach of two tmeda ligands.

It should be noted that the compounds corresponding to the **1**/Pd^{II}(tmeda) system are indicated with a double prime.

NMR Spectroscopy

Reactions of **1** with $[Pd(D_2O)_2(tmeda)]^{2+}$ at different ratios took place at room temperature and were followed by ^1H NMR spectroscopy. A rapid drop in the pD was detected in all reactions. Upon addition of NaOD (1M) the pD was brought to 7. In Figure 42 representative spectra of reactions at r = ½, 1 and 2 (where r = Pt:Pd) are shown.

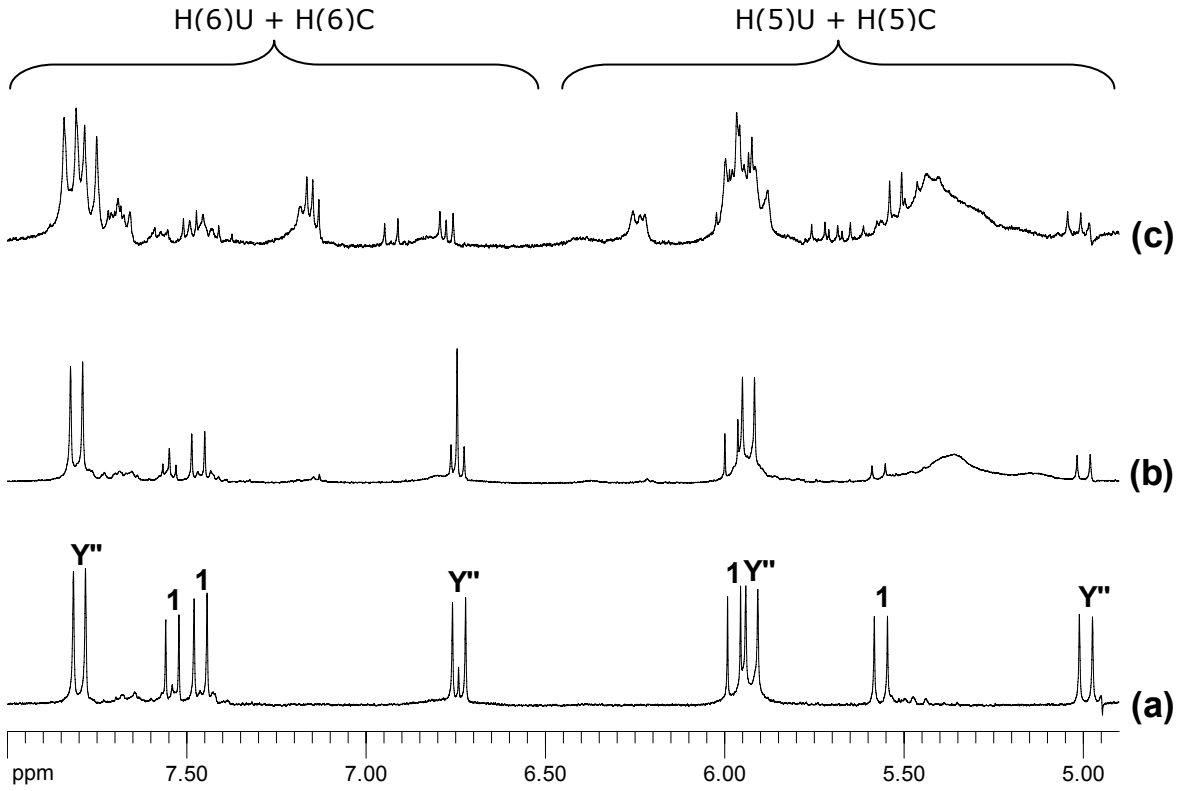

Figure 42: Low field section of ^1H NMR spectra of the reaction of $[Pt(UH\text{-}N1)(CH_2\text{-}N3)(en)](ClO_4)\cdot 3H_2O$ (**1a**) with $[Pd(D_2O)_2(tmeda)]^{2+}$ after 2d in D_2O where r = Pt:Pd is:
(a) r = 1:0.5, pD= 4.45;
(b) r = 1:1, pD = 5.27;
(c) r = 1:2, pD = 4.38.

In this system a gradual isotopic exchange of the proton at the C5 position of the uracil by deuterium takes place. For example, in Figure 42a it can be observed that the original signal at 5.03 ppm starts to disappear and the H6 resonance at 6.78 ppm is converted in a "pseudo-triplet". In Figure 42b, this process is more advanced because the doublet corresponding to the H5-uracil proton has almost disappeared whereas the H6-uracil resonance is nearly a singlet.

For the reaction of the system **1**/[Pd(D_2O)$_2$(tmeda)]$^{2+}$ when the ratio Pt:Pd is 1:0.5 (Figure 42a), resonances corresponding to the starting compound **1** as well as one set of signals corresponding to one unique product (Y''), can be seen. The reaction of **1**/[Pd(D_2O)$_2$(tmeda)]$^{2+}$ system at r = 1:1 shows the set of signals assigned to Y'' as well as the appearance of new signals in the ^{1}H NMR spectrum. At r = 1:2 (Figure 42c), a multitude of signals, which could not be assigned at this point, is detected in the spectrum.

The similarity of the chemical shifts of the nucleobases of this new species Y'' to compound **Y'**, previously obtained for the system **1**/[Pd(D_2O)$_2$(en)]$^{2+}$, is obvious (Figure 43). Therefore, it is suggested that compound Y'' is a tetramer. The chemical shifts are given in Table 10 (see Chapter I: Summary).

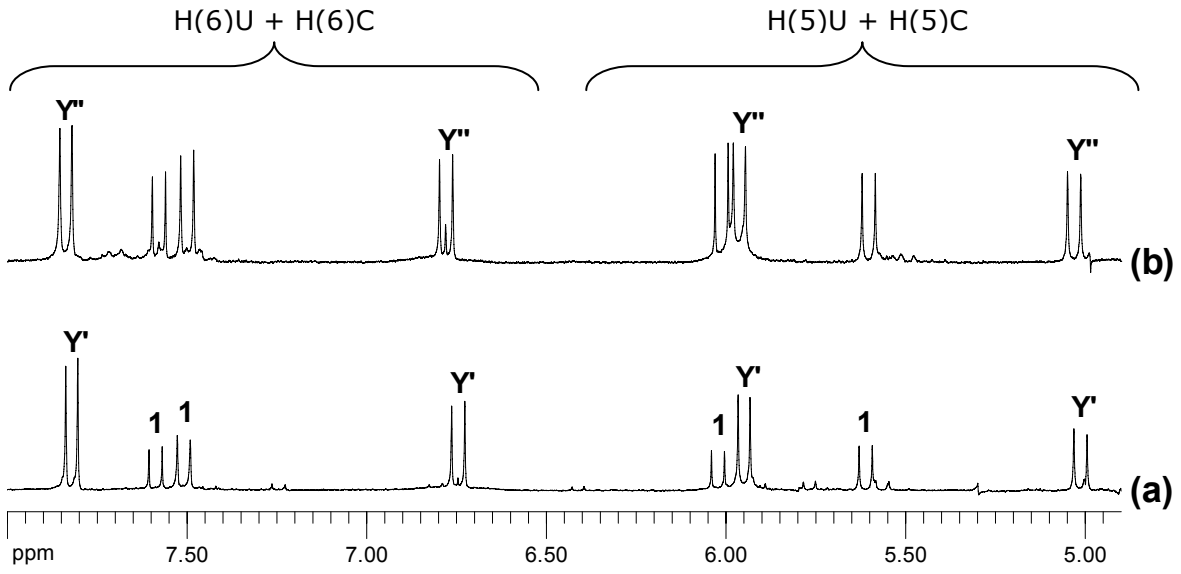

Figure 43: : Low field position of ^{1}H NMR spectra of the reaction of [(en)Pt(UH-*N1*)(CH_2-*N3*)](ClO_4)•3H_2O (**1a**) with:
(a) [Pd(D_2O)$_2$(en)]$^{2+}$ (r = 1:0.5, pD = 7.40);
(b)[Pd(D_2O)$_2$(tmeda)]$^{2+}$ (r = 1:0.5, pD = 4.45).

The nucleobase sequence in the tetranuclear complex **Y'** could not be estabilished, hence two different structures dependeing on the nucelobase connectivity are proposed. The structure of compound Y'' is, probably, similar to the tetranuclear species **Y'** because of the similar chemical schifts observed in the ^{1}H NMR spectrum. Thus, two possible geometries are also suggested for compound Y'' (Scheme 24).

Scheme 24 : Schematic representation of the two possible geometries adopted for compound Y'' depending on the connectivities of the nucleobases: CUCU (left) and CUUC (right).

6 Complexes with *cis*-$[Pt(H_2O)_2(NH_3)_2]^{2+}$

One aim of this thesis is to obtain information about the structural complexity of the so called "platinum pyrimidine blues", complexes derived from *cis*-$Pt^{II}(NH_3)_2$ with pyrimidine nucleobases (see Introduction).

The reactions discussed so far involve the mixed-pyrimidin nucleobase starting compound $[(en)Pt(UH\text{-}N1)(CH_2\text{-}N3)]^+$ (**1**) with different *cis*-$Pd^{II}a_2$ entities (a_2 = 2,2'-bpy, en, tmeda). Several compounds could be characterized by X-ray crystallography and their solution behavior could be understood. The next step was to test the reaction of **1** with *cis*-$Pt^{II}(NH_3)_2$ and to compare this result with the *cis*-$Pd^{II}a_2$ analogues.

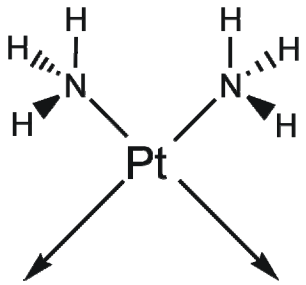

There are numerous studies in the literature on reactions of *cis*-$Pt^{II}(NH_3)_2$ containing pyrimidine and purine nucleobases (see, e.g. ref[112-115]) and also with substituted nucleobases, such as 1-Methylthymine,[33,116,117] 1-Methyl-cytosine,[116,118,119] 9-Ethylguanine,[116,118-120] 9-Methyladenine.[116]

NMR Spectroscopy

Reactions of **1** with *cis*-$[Pt^{II}(D_2O)_2(NH_3)_2]^{2+}$ at different ratios were carried out at room temperature and the reactions were followed by ^1H NMR spectroscopy. Several changes were observed in the solutions. For example, a development of an intensive blue color took place and a significant drop in the pD of the reaction mixtures was observed.

In Figure 44 selected spectra of reactions at r = ½, 1 and 2 are shown.

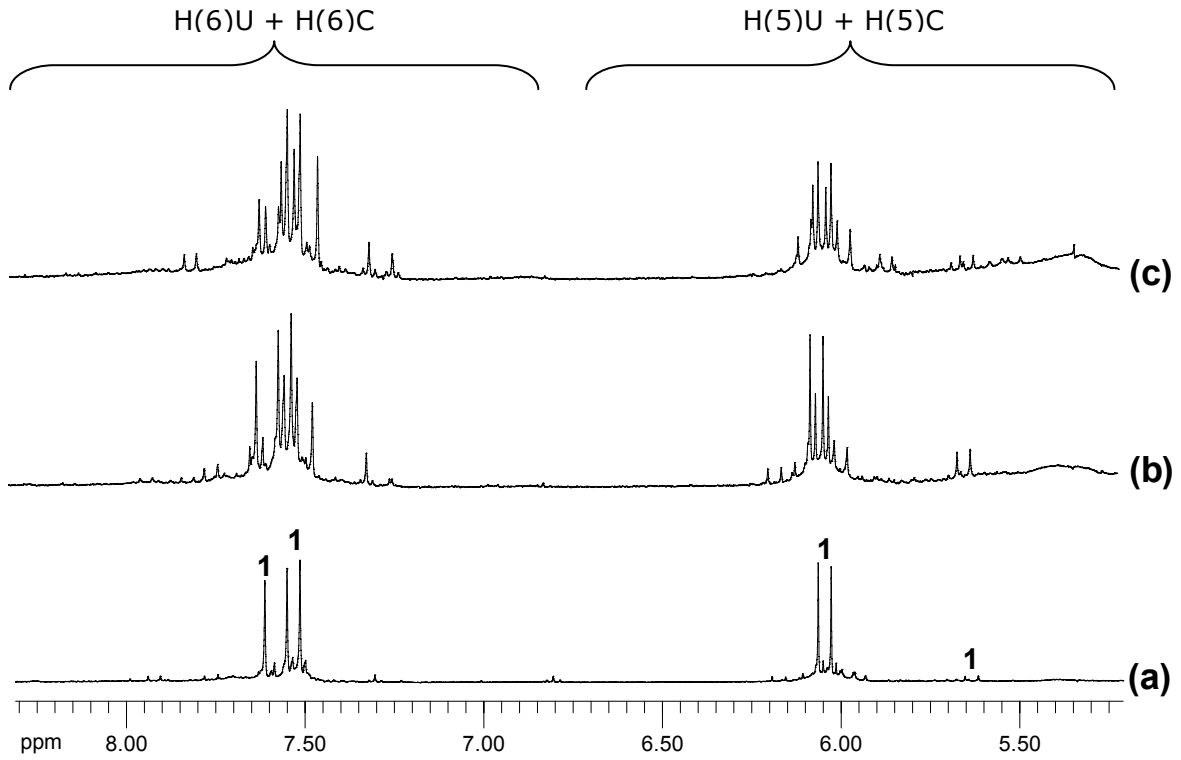

Figure 44: Low field section of ^{1}H NMR spectra of the reaction of [Pt(UH-*N1*)(CH$_2$-*N3*)(en)](ClO$_4$)•3H$_2$O (**1a**) with *cis*-[Pt(D$_2$O)$_2$(NH$_3$)$_2$]$^{2+}$ where r = Pt:Pd is:
(a) r = 1:0.5, pD= 7.23 (after 12d);
(b) r = 1:1, pD = 5.26 (after 5d);
(c) r = 1:2, pD = 5.84 (after 2d).

The ^{1}H NMR spectra of the reactions of **1** with *cis*-Pd^{II}a$_2$ are recorded after a few minutes in solution and new products could already be detected in the spectra. On the other hand, the slowly reacting *cis*-(NH$_3$)$_2$Pt^{II} does not show any reaction after one day in solution. Then the pD was increased to roughly 5-7 upon addition of NaOD (1 M) and few days later, new signals appeared in the ^{1} HNMR spectra of **1** with *cis*-(NH$_3$)$_2$Pt^{II}.

After 12 days in solution, the ^{1}H NMR spectrum of the system **1**/*cis*-[Pd(D$_2$O)$_2$[(NH$_3$)$_2$]$^{2+}$ when the ratio Pt:Pd is 1:0.5, shows almost only the signals corresponding to the starting compound with the usual isotopic exchange of the H5-uracil proton by deuterium (Figure 44a). At r > 1, a multitude of species can be detected in the spectra, as well as the signals corresponding to the starting compound **1**. The isotopic exchange of the H(5)-uracils proton by deuterium can also be seen in the spectrum after only two days in solution.

No compound of this system could be isolated or characterized. Although the intense blue color of the solutions suggest that mixed-valence state species are formed (presumably under the influence of air oxygen), the sharpness of the resonances indicate that these compounds are present in very small amounts only.

7 Reactivity Patterns and Interconversion Mechanisms

Based on the established structures discussed so far, mechanisms of formation can be proposed. It is assumed that Pd^{II}(2,2'-bpy) or Pd^{II}(en) behave very similarly. Therefore, the proposed interconversion mechanisms, if not specifed, are common for both *cis*-$Pd^{II}a_2$ entities.

The X-ray crystal structures of [(2,2'-bpy)Pd{(en)Pt(UH-*N1*)(*N3*-CH-*N1*)}$_2$](ClO_4)(NO_3)•4.9H_2O (**2a**) and [{(2,2'-bpy)Pd}$_3${(en)Pt(*N1*-U-*N3,O4*)(*N3*-CH-*N1*)}$_2$](NO_3)$_4$•5H_2O (**4**) on one hand, and [{(2,2'-bpy)Pd}$_4${(en)Pt(*N1*-U-*N3,O4*)(*N3*-HC-*N1,O2*)}$_2$](NO_3)$_6$ (**7**), [{(2,2'-bpy)Pd}{(en)Pt(*N1*-U-*N3*)(*N3*-HC-*N1*)}]$_4$(NO_3)$_3$(ClO_4)•56.1H_2O (**9a**) and [{(en)Pt(U-*N1,N3,O2,O4*)(C-*N1,N3,N4,O2*)}$_2${(en)Pd}$_6$](NO_3)$_5$(ClO_4)$_3$•21.2H_2O (**13'**) on the other clearly indicate that there are two different pathways to families of compounds, which involve different connectivities. Although it was impossible to isolate intermediates with the exception of the trinuclear species Pt_2Pd (**2a**), there are several feasible routes to the cyclic compounds, depending on whether the starting compound [Pt(UH-*N1*)(CH_2-*N3*)(en)] (**1**) reacts with the *cis*-diamine palladium entity to give initially a Pt_2Pd product or a PtPd species.

It appears that cyclic, tetranuclear species are central to the various routes of formation and probably also the routes of interconversion. There are two different Pt_2Pd_2 compounds as far as the connectivity is concerned. The first tetramer (3) consists of four nucleobases with the sequence uracil-uracil-cytosine-cytosine and the second one (**Y'**) is formed of an alternating sequence of nucleobases, namely uracil-cytosine-uracil-cytosine. Whereas 3 can lead to the formation of **4**, the tetranuclear compound **Y'** can lead to the formation of **7**, **9a** and **13'**.

Possible pathways to different connectivities and at the end to different compounds are depicted in the Scheme 25. Metal coordination sites at the nucleobases (N(1) and N(3)) are indicated.

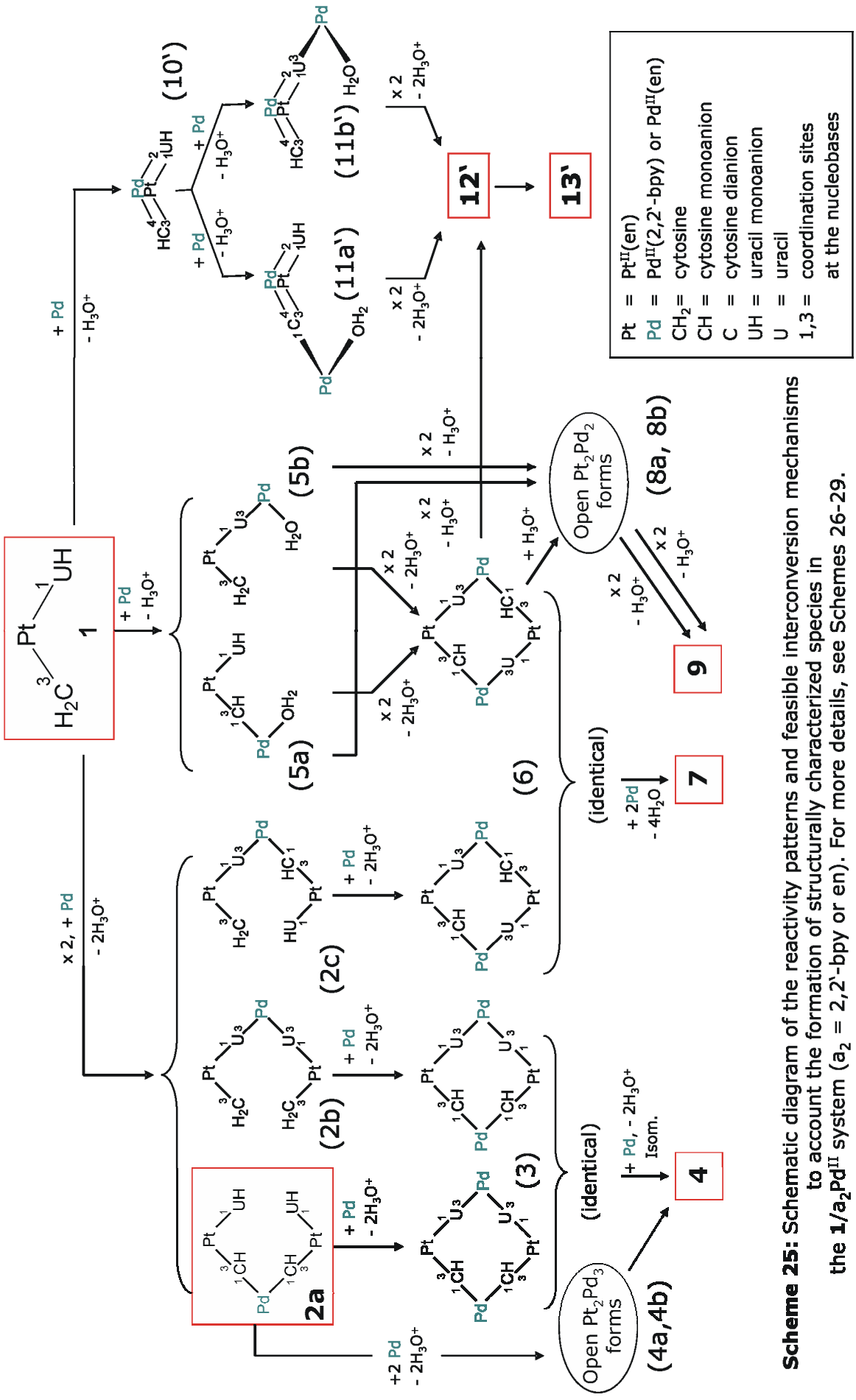

Scheme 25: Schematic diagram of the reactivity patterns and feasible interconversion mechanisms to account the formation of structurally characterized species in the **1**/a_2Pd^{II} system (a_2 = 2,2'-bpy or en). For more details, see Schemes 26-29.

As can be seen on the left side of the Scheme 25 and also in Scheme 26, the formation of **2a** is the result of two cations of **1** being cross-linked by an $Pd^{II}a_2$ (a_2 = 2,2'-bpy or en) entity via the N(1) position of each of the two cytosine ligands. Alternatively, cross-linking via the N(3) position of each of the two uracilate ligands (2b) or via the N(3)-cytosine and N(1)-uracil sites is possible (2c). Formation of **4** conceivably could take place from the "open" complex **2** upon addition of two Pd^{II}(2,2'-bpy) entities, to the N(3) site or to the O(4) site of the terminal uracilate ligands (4a and 4b, respectively), followed by *head-tail* ring closure. Alternatively, a stepwise addition of Pd^{II}(2,2'-bpy) to **2a** or 2b with formation of the closed intermediate 3 is feasible. The latter pathway would initially involve the *head-head* species $[\{(2,2'\text{-bpy})Pd\}_2\{U\text{-}N3,O4\}_2]$ and would require an isomerization to a *head-tail* arrangement (not shown in Scheme 26).

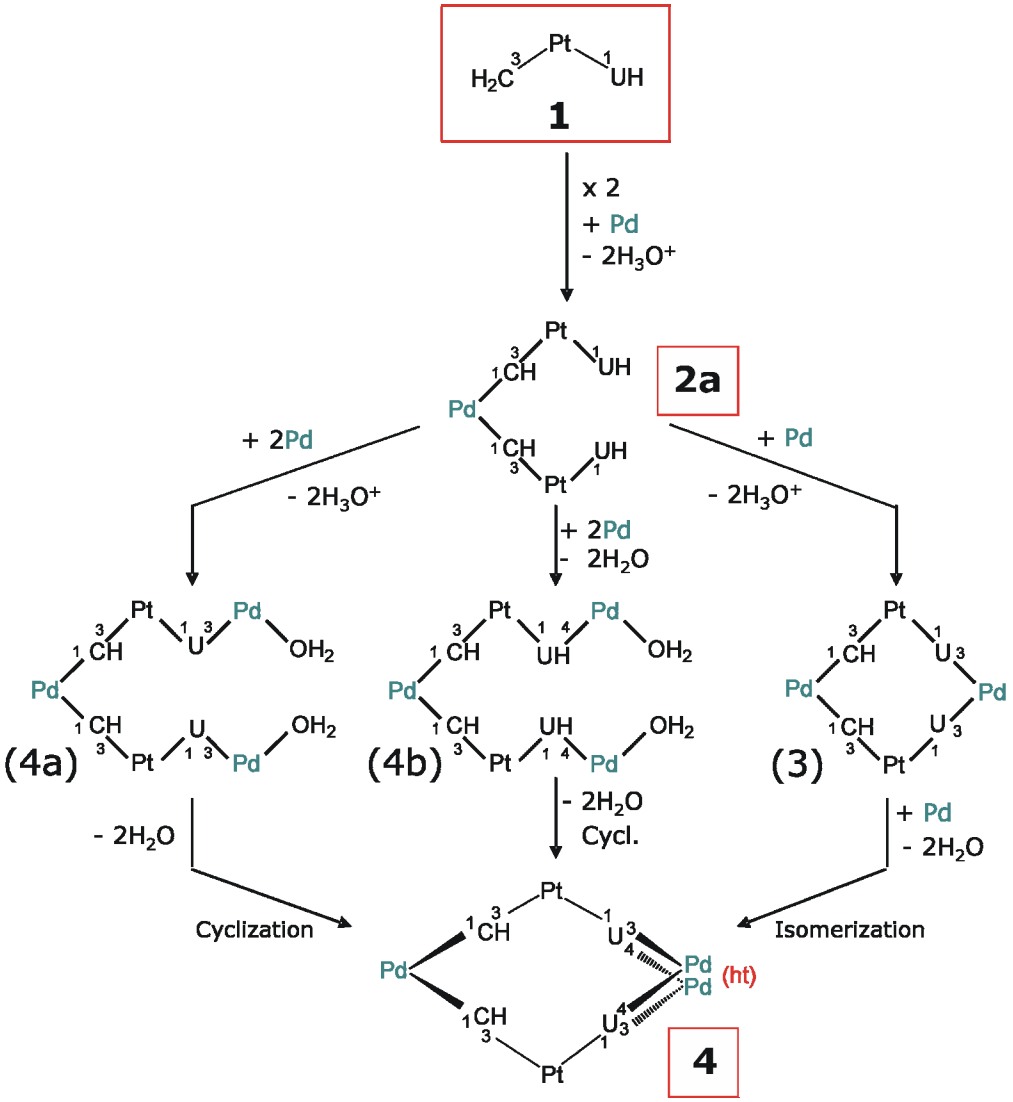

Scheme 26: Proposed pathway from **1** to **4**.

On the other hand, a stepwise addition of $Pd^{II}a_2$ to 2c leads to the formation to the closed intermediate 6. Alternatively, cyclic complex 6 can also be formed from the PtPd (5) species (Scheme 27).

Formation of 5 could take place by addition of one molecule of $Pd^{II}a_2$ to the starting compound **1**, depending on the Pd binding either at the N(1) site of the cytosine (5a) or at the N(3) position of the uracilate ligand (5b). A following "self-sorting" dimerization of both dinuclear species leads to compound 6 (Scheme 27). However, if a hetero-condensation of 5a and 5b takes place, the complex obtained is 3 (not shown in Scheme 27). Therefore, the way by which open products condense ("self-sorting" or hetero-dimerization) has an influence on the connectivity of the resulting macrocyclic ring.

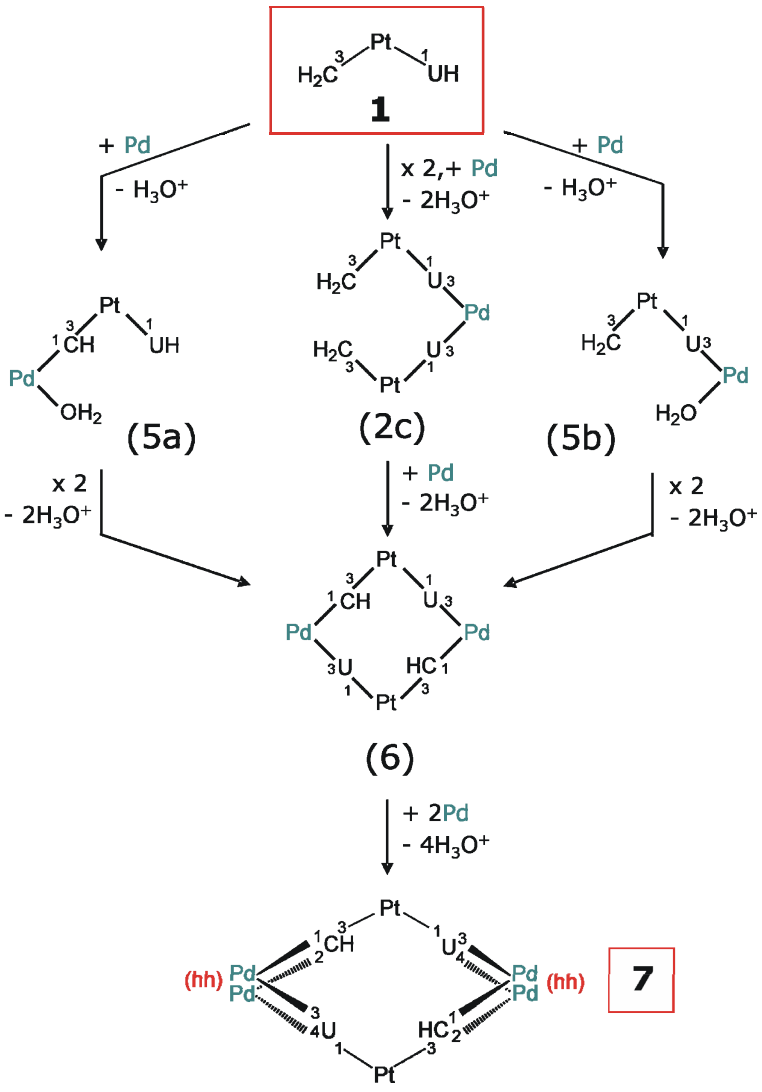

Scheme27: Proposed pathway from **1** to **7**.

The hexanuclear complex **7** could be derived from 6 by addition of two Pd^{II}(2,2'-bpy) entities at the exocyclic sites of the pyrimidine nucleobases, namely O(4) position of the uracilate dianions and O(2) position of the cytosine monoanions, leading to *head-head* arrangement (Scheme 27).

Furthermore, the opening of the cycle 6 could give two different tetranuclear species Pt_2Pd_2 (8a, 8b). Formation of the octanuclear box **9a** conceivably takes place via intramolecular "self-sorting" condensation of 8a (Scheme 28). Whereas "self-sorting" of 8b leads to a species (9b) with identical connectivities as seen in **9a**, yet a different folding topology of the Pt_4Pd_4 ring. Numerous foldamers other than **9a** and 9b are feasible, but it appears unlikely that rapid interconversion between the various forms is possible. On the other hand, hetero-condensation between 8a and 8b leads to foldamers with connectivities different form those in **9a** and 9b.

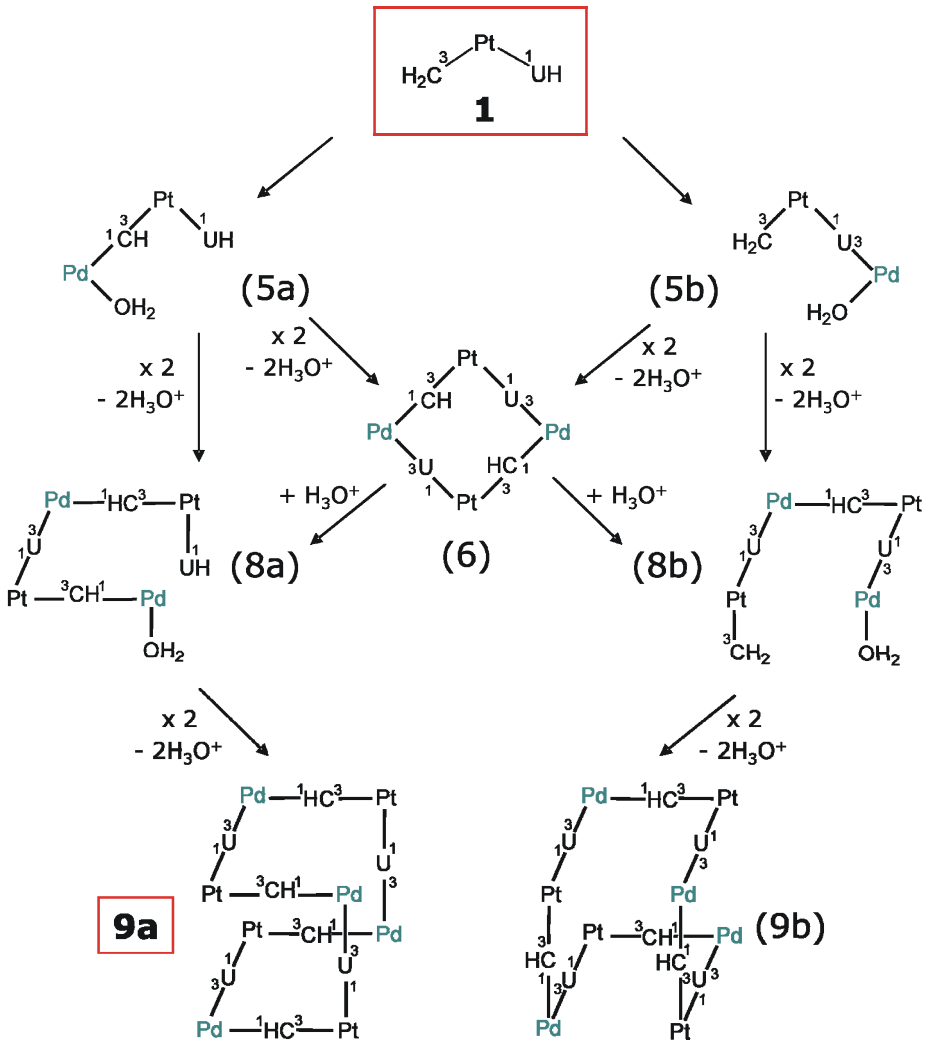

Scheme 28: Proposed pathway from **1** to **9**.

The main difference between the **1**/Pd^{II}(2,2'-bpy) and the **1**/Pd^{II}(en) system is the formation of compound **13'**.

In the first pathway for the **1**/Pd^{II}(en) system (Scheme 25, left) no intermediate compounds could be detected and no final compounds, such as **4'**, which has an alternating sequence of nucleobases, could be isolated.

The second possibility, which leads to the tetranuclear compound 6' with a pairwise sequence of nucleobases, is also similar to the pathway previously observed for the **1**/Pd^{II}(2,2'-bpy) system. Formation of 6' could take place from the "self-sorting" dimerization of each dinuclear species (5a' and 5b') or by addition of an Pd^{II}(en) entity to the trinuclear compound 2c'. Addition of two more Pd^{II}(en) entities to the exocyclic sites of the nucleobases in 6' (O(2) of the uracilate ligands and N(4) of the cytosines) leads to compound **12'** (Scheme 29).

The third pathway (Scheme 25, right), which was not detected in the Pd^{II}(2,2'-bpy) system, is the initial formation of an *head-head* dimer (10'). According to it, Pd^{II}(en) can interact with **1** at the exocyclic positions of the nucleobases (O(2)-uracil and N(4)-cytosine) to give a dinuclear PtPd species with stacked metals (10') (for more details, see Scheme 29). Another possibility is the initial formation of a different *head-head* dimer, which is bonded at O(4)-uracil and O(2)-cytosine sites (not shown in Scheme 29). The interaction of a second Pd^{II}(en) moiety with 10' at N(1) position of the cytosine leads to the formation of 11a' or at the N(3) site of the uracil to give 11b'. Following "self-sorting" dimerization of each trinuclear species leads to the hexanulear species **12'** (Scheme 29), whereas condensation of 11a' with 11b' would lead to a product with some of the connectivities being different from those seen in **12'**.

The octanuclear complex **13'** could then be formed by addition of two further Pd^{II}(en) moieties to the free coordination sites of **12'** (O(4)-uracil and O(2)-cytosine).

In the following Scheme 29 the three different routes are represented, as well as the resulting intermediates, which could possibly lead to **13'**.

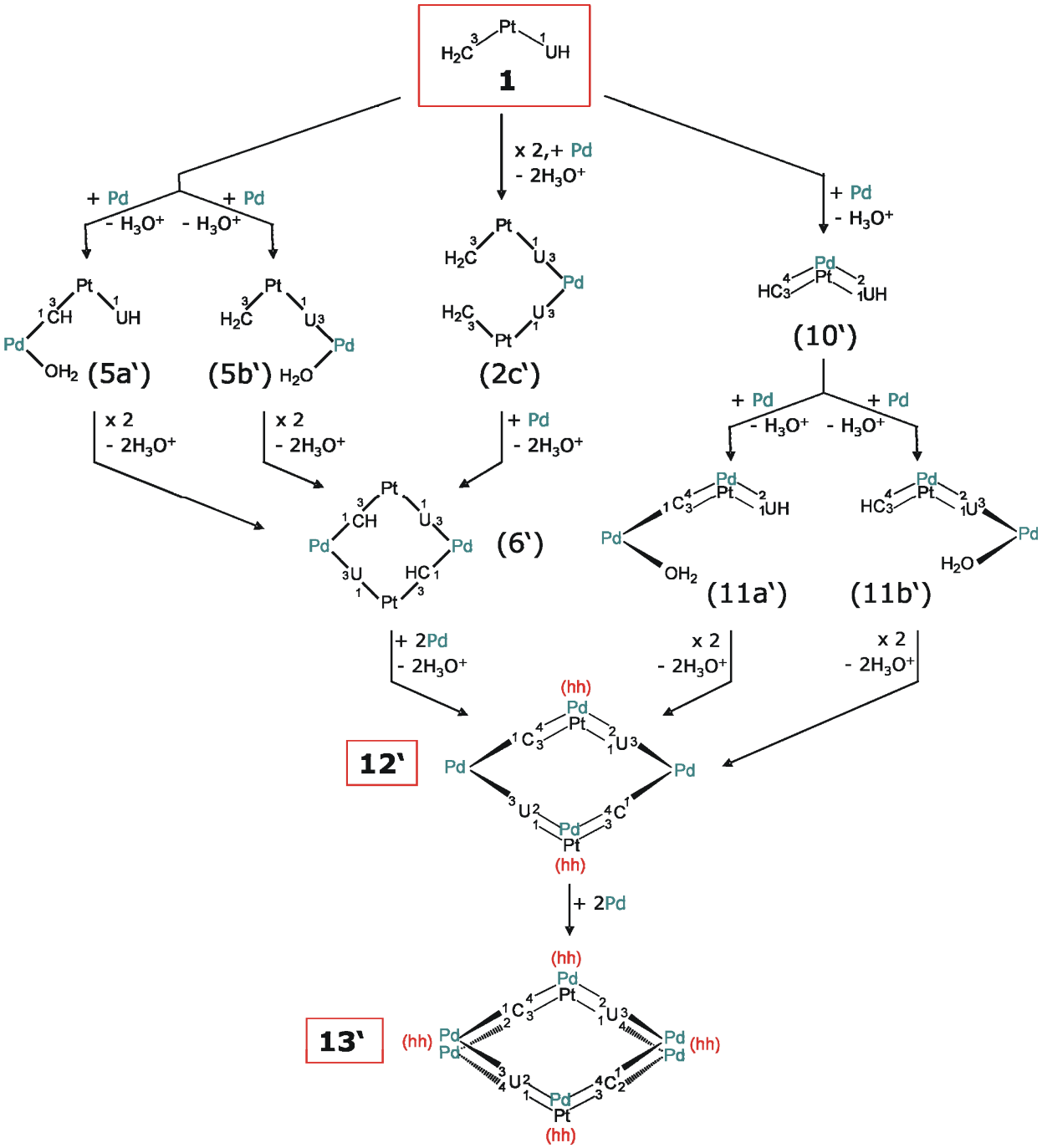

Scheme 29: Possible pathway from **1** to **13'**.

8 Summary

The mixed-nucleobase cation of the starting compound [(en)Pt(UH-*N1*)(CH_2-*N3*)]$^+$ (**1**) was reacted with Pd^{II}(2,2′-bpy), Pd^{II}(en), Pd^{II}(tmeda) and *cis*-$Pt^{II}(NH_3)_2$ entities to give a multitude of species. Several of them could be isolated and characterized, which greatly helped to understand the reactivity patterns of these systems. All compounds disscused so far were characterized by ^{1}H NMR spectroscopy. In Table 10 the ^{1}H NMR resonances (δ, D_2O) of aromatic nucleobase protons of **1** and adducts of **1** with Pd^{II}(2,2′-bpy), Pd^{II}(en) and Pd^{II}(tmeda) are listed.

Table 10: ^{1}H NMR resonances (δ, D_2O) of aromatic nucleobase protons of **1** and adducts of **1** with Pd^{II}(2,2'-bpy), Pd^{II}(en) and Pd^{II}(tmeda), with no differentiation of protonation state of uracil (U) and cytosine (C) considered.

	H(6)U	H(6)C	H(5)C	H(5)U	Others	pD
1	7.59	7.51	6.02	5.61	2.73 (en)	5.45
2a	6.82	8.00	6.11	5.16	2.6-2.8(en) 8.4-7.6(bpy)	8.55
X	7.62	7.86	5.90	5.51	2.68(en) 8.4-7.5(bpy)	7.51
4	7.50	7.97	6.16	5.70	2.7-2.8(en) 8.4-7.1(bpy)	9.23
7	7.81	8.26	6.33	6.07	2.7-2.8(en) 8.4-7.2(bpy)	4.45
Y′	6.73	7.81	5.94	5.00	2.7-2.8(en)	7.68
12′	7.17	7.67	5.83	5.35	2.5-3.0(en)	4.65
13′	7.36	7.90	5.66	5.62	2.5-3.2(en)	5.32
Y′′	6.77	7.83	5.95	5.02	2.4-2.9(tmeda)	4.43

The solution behavior as well as the solid state structure of each of the isolated complexes was studied in detail. In most of the cases cyclic metallacalix[n]arenes with different number of metal entities were formed.

The ability of the Pd^{II}(2,2'-bpy) moiety to provide intramolecular π-stacking interactions seems to play an important role in the formation of the different complexes. Two different kinds of compounds were found as far as connectivity is concerned. First, a cyclic complex consisting of four nucleobases with the sequence uracil-uracil-cytosine-cytosine (**4**) was isolated and secondly, cyclic comlexes with an alternating sequence of nucleobases, namely uracil-cytosine-uracil-cytosine (**7**, **9a**) were also isolated. An intermediate of the way from **1** to **4** could be isolated (**2a**) and possible pathways of formation of the families of compounds could be rationalized. In Scheme 30 all of the compounds characterized with Pd^{II}(2,2'-bpy) moiety, as well as proposed routes of their formation are represented.

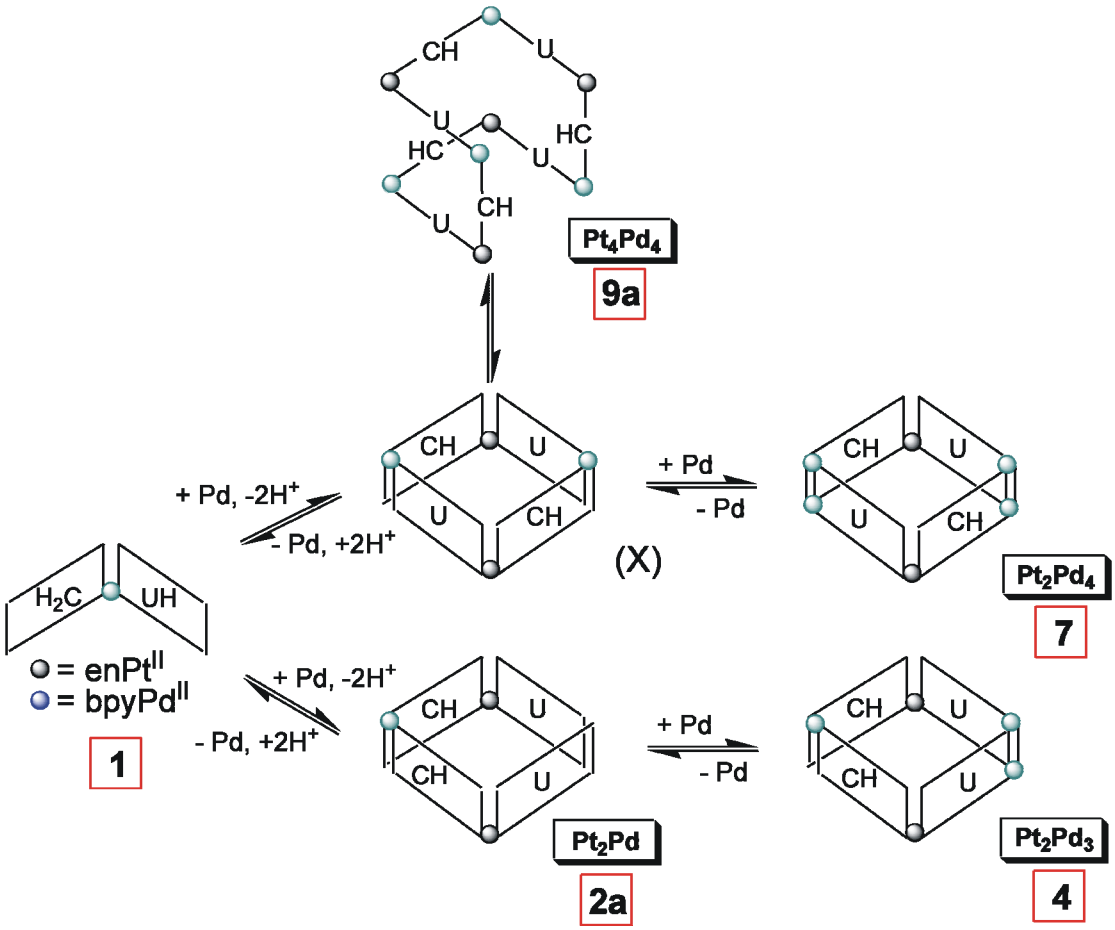

Scheme 30: Schematic representation of the system **1**/Pd^{II}(2,2'-bpy).

In the case of the Pd^{II}(en) entity, three different metallacalix[4]arenes could be characterized (**Y'**, **12'** and **13'**). The nucleobase sequence in **12'** and **13'** is cytosine-uracil-cytosine-uracil. Compound **12'**, which is a hexanuclear complex, could be obtained by addition of two Pd^{II}(en) entities to the tetranuclear compound **Y'**. Finally **13'** (octanuclear complex) could be obtained from **12'**. For the tetramer **Y'** $Pt_2Pd_2U_2(CH)_2$, however, the nucleobase connectivity could not be estabilished. In Scheme 31 the interrelationship of the compounds is depicted. Possible "shortcuts" between individual species are not considered.

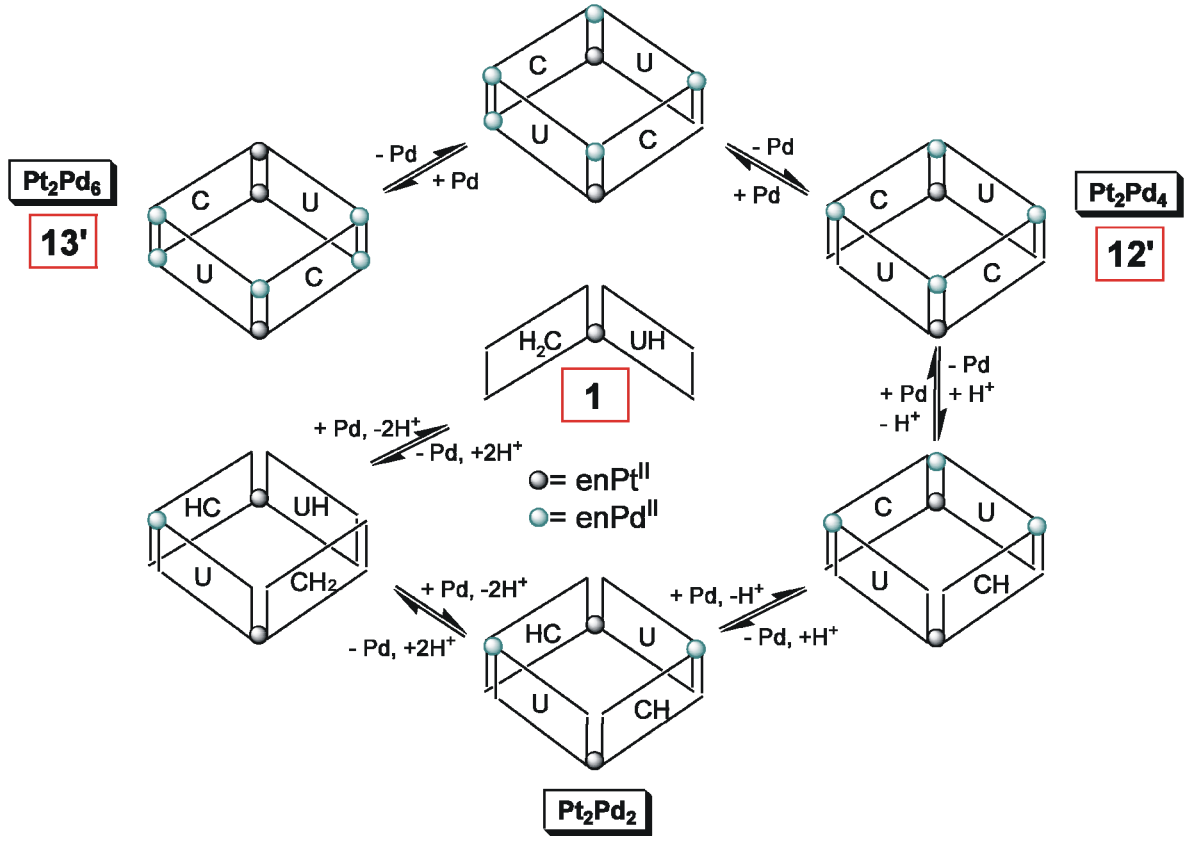

Scheme 31: Schematic representation of interrelationships of the various compounds the system **1**/Pd^{II}(en).

The bulky Pd^{II}(tmeda) entity seems to react very similar to the previously studied Pd^{II}(2,2'-bpy) and Pd^{II}(en) metal fragments, at least in the early stage of the reaction.

In all structurally studied examples of metallacalix[4]arenes reported here (**4**, **7**, **11'**), four nucleobases adopt *1,3*-alternate conformations in the solid state, irrespective of nucleobase connectivity. As a consequence of this conformation, the interior of the metallacalix[4]arene does not have any space for inclusion of an anion or of solvent molecules, unlike a cone conformer, which provides a suitable hydrophobic cavity (Scheme 32).

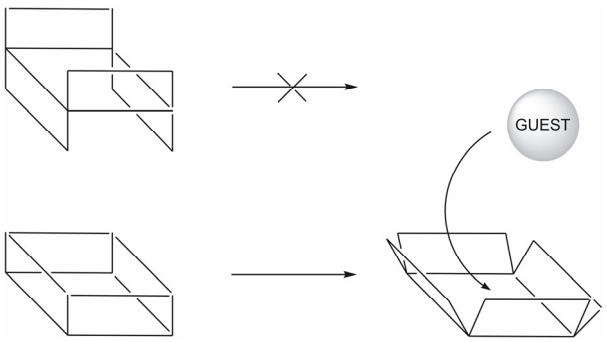

Scheme 32: Schematic representation of the *1,3*-alternate conformer (top) and cone conformer (bottom) in the metallacalix[4]arenes.

The solution study with the Pt_2Pd_2 complex **Y'** does not show evidence of ligand rotation to a cone conformer. It is possible that steric hindrance between the exocyclic amino group of the cytosine nucleobase and H(6) of the uracil nucleobase, which is to be expected both for UCUC and UCCU connectivities, prevents the cone conformation to be easily realized.

Chapter II:
Bis-Uracil Complexes

1 Introduction

In chapter I, the mixed-nucleobase complex [Pt(UH-*N1*)(CH_2-*N3*)(en)](ClO_4) •3H_2O (**1a**) has been used as starting material for the formation of different metalalcalix[n]arenes. In chapter II, these results will be compared with the formation of metalalcalix[n]arenes derived from the starting compound *cis*-Na_2[Pt(U-*N1*)$_2$(NH_3)$_2$]•10H_2O (**14b**), in which only one type of nucleobase is present.

It should be noted that apart from their function as counter ions for the charge neutralization of nucleic acids, alkali metal ions play important roles in stabilizing particular multistranded nucleic acids, e.g. guanine quartets in telomeres and uracil or thymine quartets. Several compounds with a series of alkali metal ions (Na^+, K^+, Rb^+, Cs^+) with the model bases *1*-methylthymine and *1*-ethylthymine were reported by E. Freisinger et al.[121] as well as three complexes of model nucleobases with exocyclic oxygen atoms (1-methyluracilate, 1-methylcytosine, 9-methylguanine) which contain Pt^{II} bonded to a ring N atom and an in addition comprises an alkali metal ion (Na^+, K^+, Cs^+).[122]

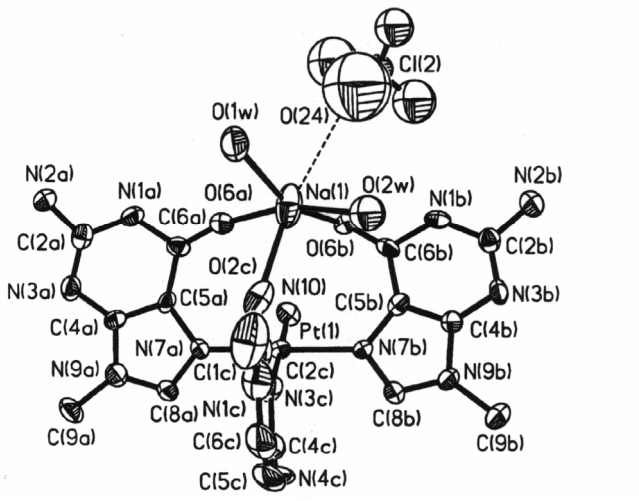

Figure 45: Section of *trans*-[Pt(NH_3)(9-MeGH-*N7*)$_2$(1-MeC-*N3*)Na(H_2O)$_2$] (ClO_4)$_3$•0.5H_2O.[121]

There are also some examples of N(3) platinated uracil and thymine model bases with alkali ions bonded to the exocyclic oxygen atoms of the nucleobases.[123,124] The deprotonation of thymine and uracil bases at the N(3) position and subsequent binding of Pt^{II} to this site leads to an electronic distribution that leaves substantial basicity at the exocyclic oxygen atoms. Therefore, it is not surprising to see alkali ions bonded to these sites.

Another interesting complex derived from *trans*-$Pt^{II}I_2$ and unsubstituted uracil was reported by O. Renn et al.[124] The anionic complex *trans*-[PtI_2(1-MeU-N3)]$^{2-}$ is formed by supramolecular assembly with anionic entities linked via K^+ cations and bridging H_2O molecules. Pt binding takes place via the deprotonated N(3) positions of two 1-MeU anions and the two K^+ ions are coordinated pairwise by exocyclic O(2) and O(4) oxygen atoms of the two uracils, which are coplanar. The coordination sphere of K is completed by bonding water molecules, which serve as bridges to adjacent potassiums (Figure 46).

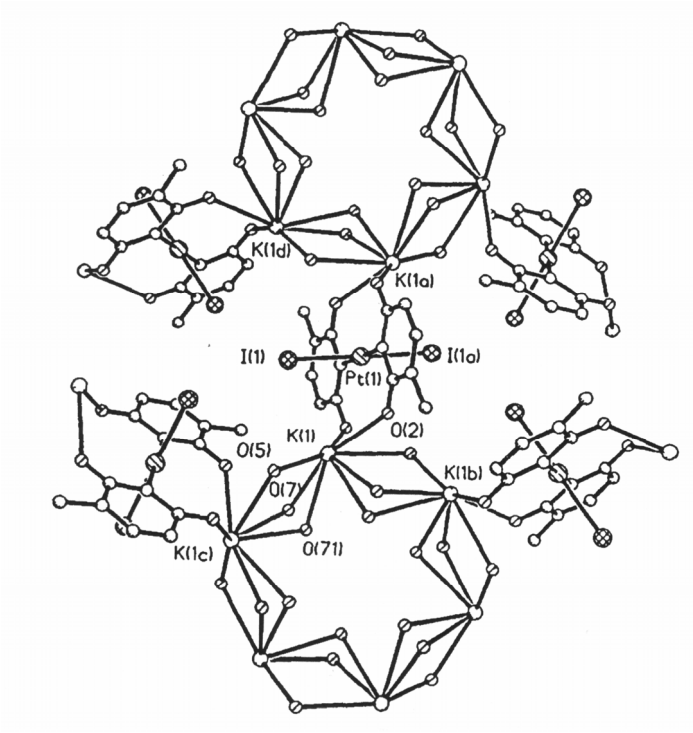

Figure 46: Crystal arrangement of trans-$K_2[PtI_2(1\text{-}MeU)_2]\cdot 4H_2O$.[124]

Several clusters of alkali ions with very different ligands and metal entities have already been reported (see e.g. Na ions[125,126] or K ions[127]). An example that is related to this work is the Na_8 cluster in the structure of a novel oxamato-bridged Na^ICu^{II}.[125] The core skeleton of the cationic Na_8 cluster is composed of six sodium atoms linked by ten bridging oxygen atoms: four carboxylate-O and four carbonyl amide-O from the oxamato groups and only two water molecules. Bis(aquo) bridges connect the two external sodium ions outside the ring to the central Na_6 skeleton.

In both starting compounds of this thesis (**1a** and **14**), the uracil nucleobase is bonded to platinum via the N(1) position. The characteristics of N(1) and N(3) tautomer complexes of uracil have already been discussed[91,128] and it has been shown that N(3) complexes are more readly protonated than the corresponding N(1) complexes. B. Lippert published an article, in which three important differences between complexes containing N(1) and N(3) bonded uracil were deduced by ^{1}H NMR spectroscopy and by Raman spectroscopy.[41] It was found

that the coupling constants of H5 and H6 with ^{195}Pt were different, that the stabilities of the complexes in strongly acidic medium were also different and finally, that the two types of complexes showed quite different tendencies to undergo isotopic $^{1}H/^{2}D$ exchange at the C(5) position in acidic medium. However, some fundamental questions like the assignment of the donor atoms in the uracil-bridged species still remained unanswered and these can eventually be answered by X-ray crystallography only. One of the goals of this part of the work is to answer the question concerning the different ways of bridging and to obtain X-ray crystal structures, which give a solid proof of the binding patterns of the N(1) uracil complexes.

As could be seen in the last chapter, the combination of the 90° angles of the metal fragments with the 120° angles of the uracil ligand can lead to the formation of many different molecules. Some of these molecular entities are shown in Scheme 33.

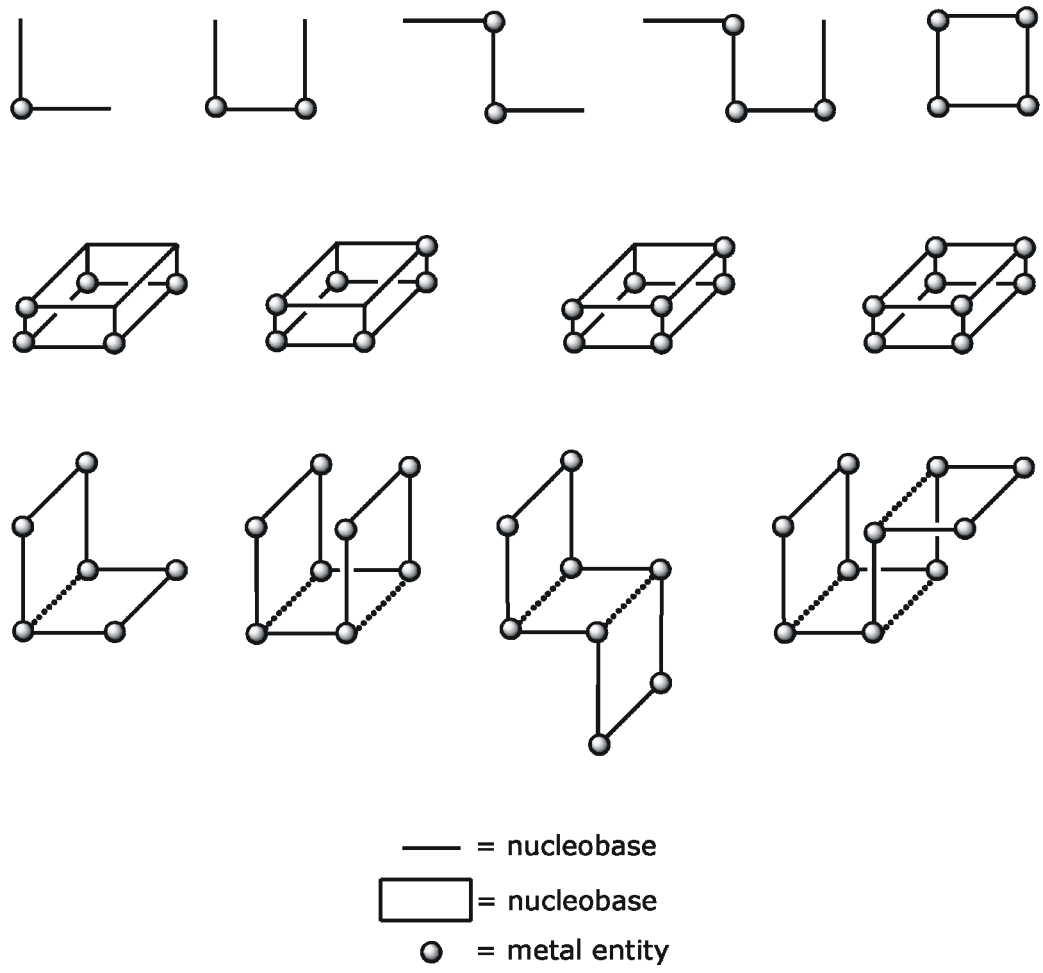

Scheme 33: Schematic representation of fragments of molecular squares, molecular boxes, and larger aggregates.

2 Starting compound: *cis*-$Na_2[Pt(U\text{-}N1)_2(NH_3)_2]\cdot 10H_2O$ (14b)

Crystals of the 2:1 complex *cis*-$Na_2[Pt(U\text{-}N1)_2(NH_3)_2]\cdot 10H_2O$ (**14b**), were obtained by addition of an excess of NaOH (1 M) to a suspension of *cis*-$Pt(UH\text{-}N1)_2(NH_3)_2\cdot 2H_2O$ (**14a**)[41] in H_2O and cooling at 4 °C for 10 days.

Compound **14b** was previously prepared in our group,[41] but it could not be charaterized by X-ray crystallography. Luckily, in the present work, the crystals of compound **14b** could be isolated and characterized.

X-Ray Crystallography

Compound **14b** crystallizes in the triclinic space group P-1. The unit cell contains two crystallographically different *cis*-$[Pt(U\text{-}N1)_2(NH_3)_2]^{2-}$ anions (I, II), both of which display N(1) binding of the uracil dianion and a *head-tail* arrangement of the two nucleobases. The two anions do not differ significantly in bond lengths and angles within the coordination spheres of Pt, but do show differences in dihedral angles between U and PtN_4 coordination planes and between the nucleobases. The structure of the two cations of **14b** are depicted in Figure 47 and the selected bond distances and angles of the structure are given in Table 11.

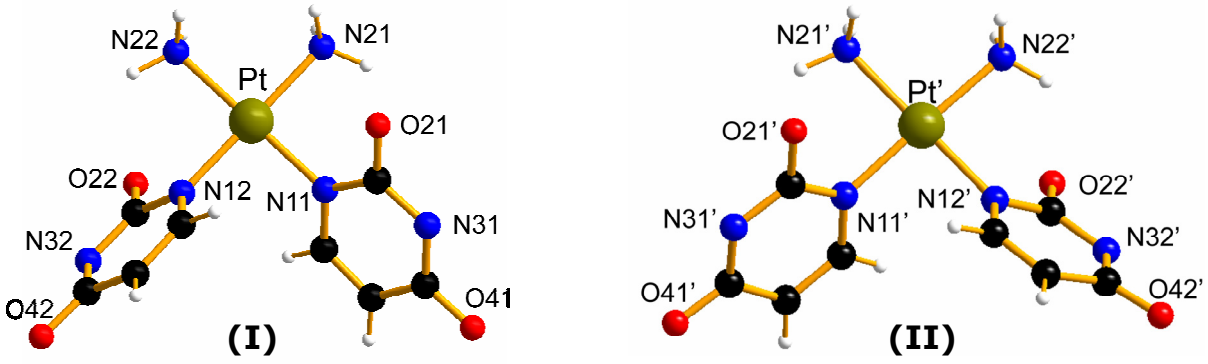

Figure 47: View of the two crystallographic independent anions of *cis*-$Na_2[Pt(U\text{-}N1)_2(NH_3)_2]\cdot 10H_2O$ (**14b**).

Table 11: Selected interatomic distances (Å) and angles (°) of *cis*-$Na_2[Pt(U\text{-}N1)_2(NH_3)_2]\cdot 10H_2O$ (**14b**).

Pt-N(11)U1	2.025(8)	N(21)-Pt-N(22)	90.6(3)
Pt-N(12)U2	2.024(8)	N(11)U1-Pt-N(12)U2	92.7(4)
Pt-N(21)	2.062(7)	N(21)-Pt-N(11)U1	88.8(3)
Pt-N(22)	2.049(10)	N(22)-Pt-N(12)U2	88.0(4)
Pt'-N(11')U1'	2.024(8)	N(21')-Pt'-N(22')	89.1(3)
Pt'-N(12')U2'	2.029(7)	N(11')U1'-Pt'-N(12')U2'	89.1(3)
Pt'-N(21')	2.063(9)	N(21')-Pt'-N(11')U1'	90.9(3)
Pt'-N(22')	2.052(8)	N(22')-Pt'-N(12')U2'	91.0(3)
Na-O(21)U1	2.57(1)		
Na-O(41')U1'	2.44(2)		
Na-O(42')U2'	2.32(1)		

Geometries of the uracilate dianion ligands differ from those of uracil monoanion ligands in the following way: The angle C(2)-N(3)-C(4) in the uracil monoanion complexes is larger than the angle in the uracil dianion complexes. The effect of the proton at the N(3) position of the uracil makes this angle to be around 125-129°, as has been observed for other platinum uracilate monoanion complexes, such as $[Pt(UH\text{-}N1)(CH_2\text{-}N3)(en)]NO_3\cdot 3.5H_2O$ (125.8(9)° and 128.8(9)°, for the two cations in the asymmetric unit, see Chapter I), $[Pt(UH\text{-}N1)(en)(H_2O)]NO_3\cdot H_2O$ (126.1(9)°),[38] $PtCl(UH\text{-}N1)(en)\cdot(H_5O_2)Cl$ (125.2(8)°) or in the case of the related thyminate monoanion complex $PtCl(TH\text{-}N1)(en)$ (127.2(7)°).[37] However, if the N(3)-uracil position is deprotonated, the effect of the increased electron density ("free" pair) at this position makes the C(2)-N(3)-C(4) angle smaller. Hence, the angles observed for **14b** are 119.9(8)° and 119.7(8)° in (I) and 120.5(9)° and 121.0(8)° in (II). Going along with this trend, C···O distances in the uracilate

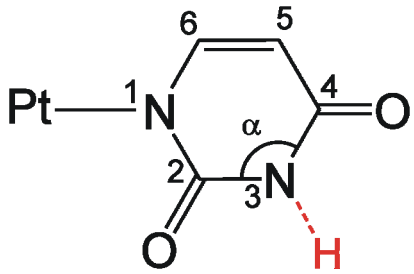

Scheme 34: Schematic diagram of the binding pattern of Pt with uracil via N(1).

monoanion complexes, which range from 1.238(13) Å to 1.257(12) Å for the complexes cited above, are shorter than in the uracilate dianion complex **14b** (1.262(12) Å – 1.289(12) Å).

Anions (I) and (II) of **14b** are cross-linked by Na^+ cations to give infinite chains as follows (Figure 48): Na1 is bonded via O(2) of **U2** of anion (I) and O(4) of **U3** of anion (II), while Na2 is bonded symmetrically via the O(4) sites of uracil ligands of two anions (II). The two other Na^+ ions are disordered over multiple positions and could not be refined anisotropically. The Na^+ ions complete their octahedral coordination spheres by water molecules, some of which bridge to other Na^+ ions not directly associated with the *cis*-$[Pt(U\text{-}N1)_2(NH_3)_2]^{2-}$ anions.

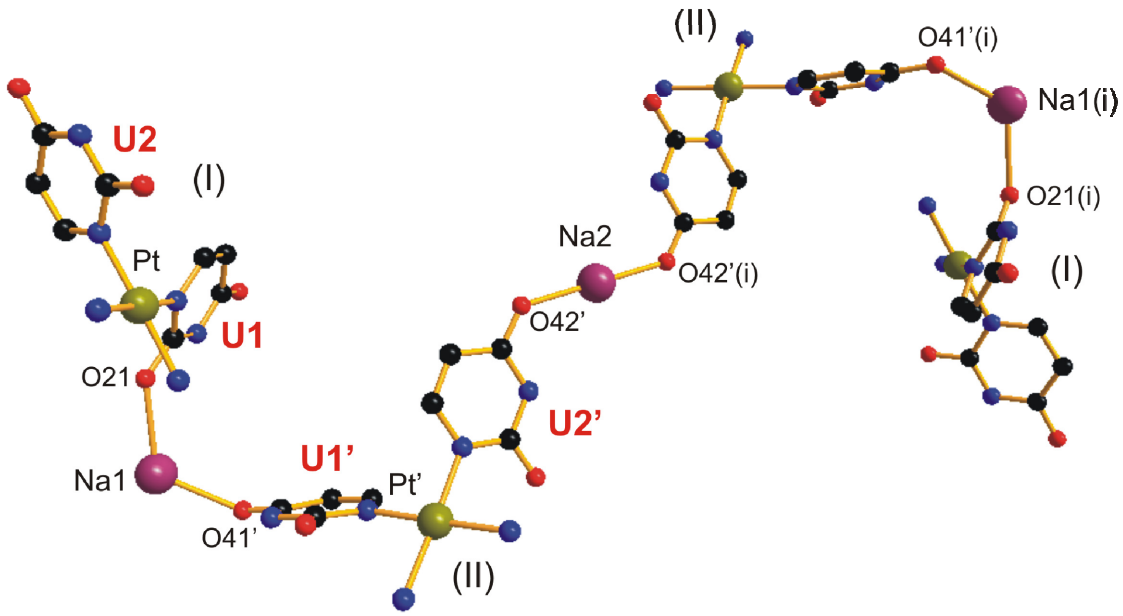

Figure 48: View of the anions of compound **14b** coordinated to the Na^+ ions. The rest of the Na^+ ions is omitted, as well as the water molecules that complete the coordination spheres of the Na^+ ions.

Distances and angles about the platinum and within the nucleobases are not unexpected. Dihedral angles between the PtN_4 coordination plane and the nucleobase planes are 59.2(2)° and 52.3(2)° in (I) and 55.1(3)° and 54.3(3)° in (II). The angle between the two bases is 73.1(1)° and 88.7(2)°, for complex I and complex II, repectively.

Each Na^+ ion is bonded to six oxygen atoms, which provide an octahedral coordination for the alkali ion. Some of the Na^+ ions are binding to exocyclic sites of the uracil and complete their coordination sphere with water molecules (Figure 49, Na2). On the other hand, other Na ions are only bonded to water molecules (Figure 49, Na3, Na3(i)). Aquo bridges connect the two exterior sodium atoms to the central Na2. The rest of the Na ions in the unit cell are disordered over multiple positions with different occupancies.

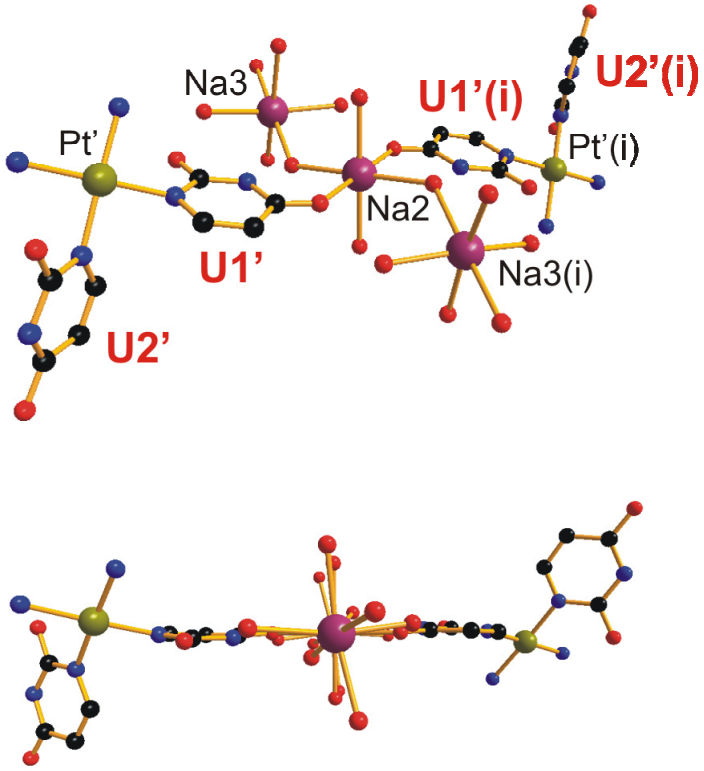

Figure 49: : View of the coordination spheres of sodium ions Na2, Na3 and Na3(i) of compound **14b** (anion (II)).

NMR Spectroscopy

As could be observed previously for complexes formed by Pt^{II} with uracil bonded at the N(1) position,[41] the ^1H NMR resonances of the uracilate ligand in **14b** at pD = 13.3 consist of a well resolved "six-line pattern" for H6 (7.50 ppm) and a doublet for H5 (5.51 ppm) (Figure 50). The expected "six-line pattern" for H(5) could not be detected in the spectrum at these conditions. The multiplets of both signals are due to the coupling between H5 and H6 ($^3J_{H\text{-}H} \approx 6.8$ Hz) and from

coupling between the ^{195}Pt isotope (33.8 % natural abundance, spin ½) and the ^{1}H nucleus. Since N(1) is the site of Pt binding, the platinum coordination site is closer to H6 than to H5. This is the reason for the ^{195}Pt-^{1}H coupling constant for the H6 resonance (38.3 Hz) to be considerably larger than that of the H5 resonance (4.3 Hz).[41]

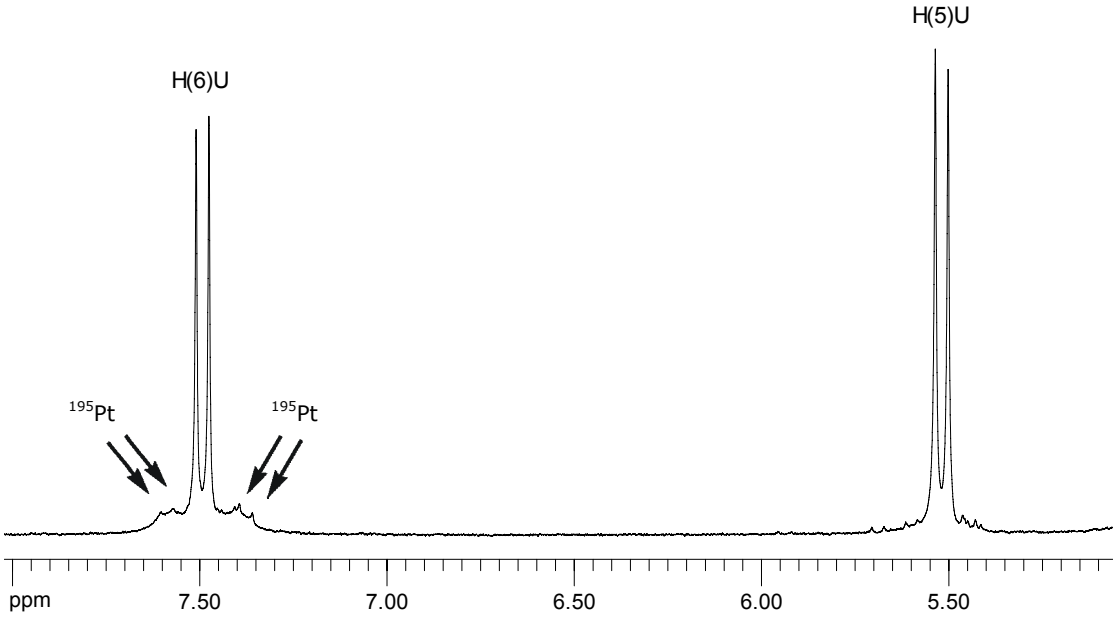

Figure 50: Low field section of the ^{1}H NMR spectrum of *cis*-$Na_2[Pt(U\text{-}N1)_2(NH_3)_2]\cdot 10H_2O$ (**14b**) in D_2O, pD = 13.3.

Upon isotopic exchange at 5-position of the uracil, the original H5 signal disappears and the H6 "sextet" is reduced to a triplet. The relative intensities of this triplet are 1:4:1 and correspond to the expected distribution according to the natural abundance of ^{195}Pt.[41]

3 Complexes with $[Pd(2,2'\text{-bpy})(H_2O)_2]^{2+}$

As has been done before for the mixed-nucleobase starting compound $[Pt(UH\text{-}N1)(CH_2\text{-}N3)(en)]^+$(**1**), reactions of *cis*-$[Pt(U\text{-}N1)_2(NH_3)_2]^{2-}$ (**14**) with $Pd^{II}a_2$ (with a_2 = 2,2'-bipyridine, *N,N*-ethylenediamine and *N,N,N',N'*-tetramethylethylenediamine) were carried out. The influence of the different ligands bonded to the palladium ion on the formation of the metallacalix[n]arenes with the bis-uracilate platinum compound (**14**) was investigated. In this and the following chapters reactions of the $Pd^{II}a_2$ entities will be discussed individually.

3.1 Synthesis, characterization and reactivity.

Reactions were initially followed by ^{1}H NMR spectroscopy. Typically, to a solution of *cis*-$Pt(UH\text{-}N1)_2(NH_3)_2 \cdot 2H_2O$ (**14a**) in D_2O/NaOD at a pD value higher than 13 (to ensure deprotonation of the N(3) positions of the uracil) $[Pd(2,2'\text{-bpy})(D_2O)_2]^{2+}$ was added at different ratios and the reaction was followed by ^{1}H NMR spectroscopy. Representative spectra at pD>13 are shown in Figure 51.

In general, the samples were kept at high pD for two days. Afterwards, the pD was decreased to 5-6 by addition of DNO_3 (1 M), yielding yellow products or orange crystals in some cases. Two different compounds, $[\{(2,2'\text{-bpy})Pd\}_3\{cis\text{-}[(NH_3)_2Pt(N1\text{-U-}N3)(N1\text{-U-}N3,O4)]\}_2](NO_3)_2 \cdot 23.1H_2O$ (**17**) and $[\{(2,2'\text{-bpy})Pd\}_4\{cis\text{-}[(NH_3)_2Pt(N1\text{-U-}N3,O4)_2]\}_2](NO_3)_4 \cdot 17H_2O$ (**24**), could be isolated this way and were characterized.

As can be seen from Figure 51, multiple new uracil resonances appear, especially at higher ratios of Pt:Pd.

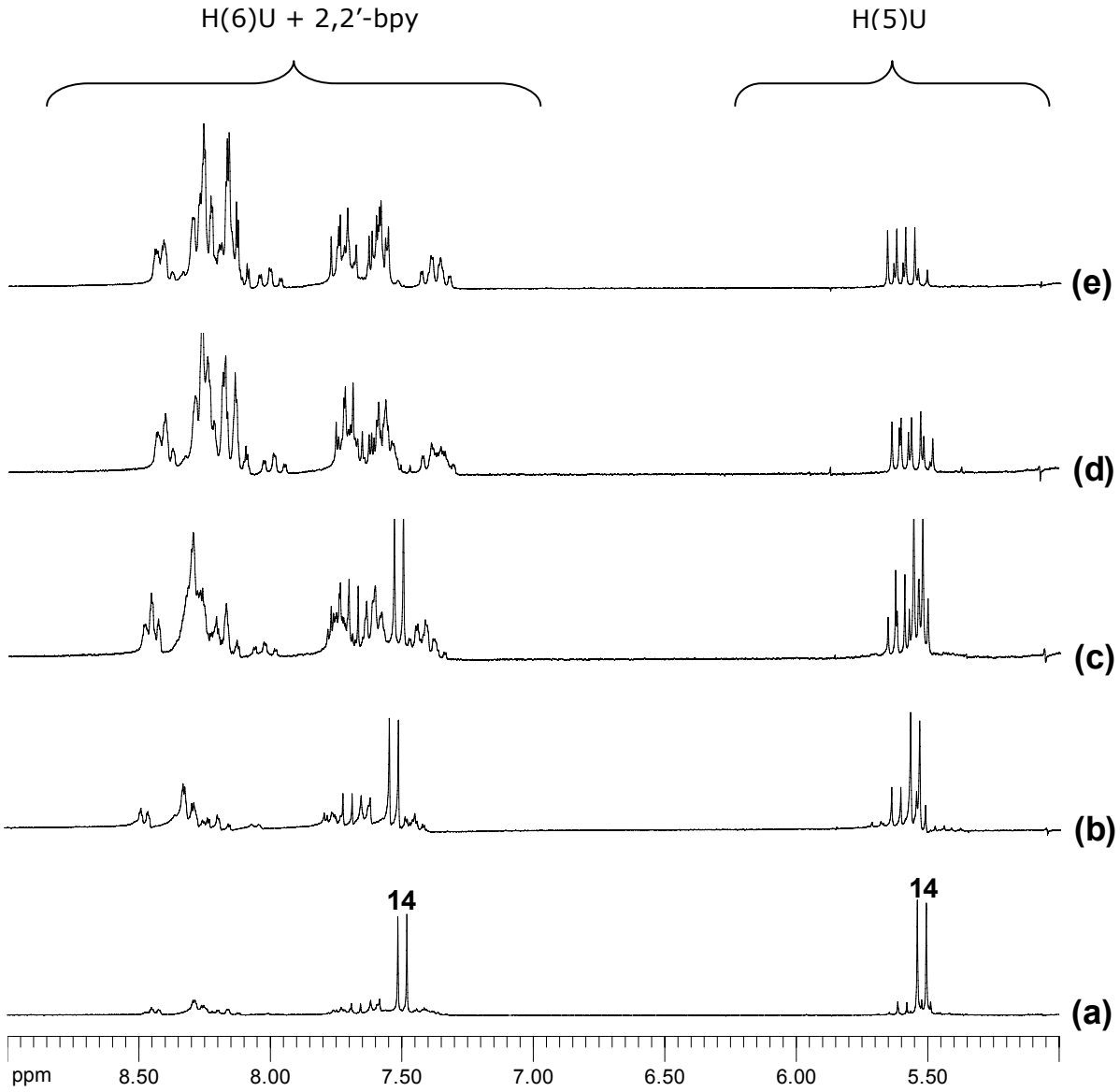

Figure 51: : Low field section of the ^{1}H NMR spectra of the reaction of *cis*-Pt(UH-*N1*)$_2$(NH$_3$)$_2$•2H$_2$O (**14a**) with [Pd(2,2'-bpy)(D$_2$O)$_2$]$^{2+}$ in D$_2$O where r = Pt:Pd is:
(a) r = 1:0.25, pD = 13.2;
(b) r = 1:0.5, pD = 13.4;
(c) r = 1:1, pD = 13.5;
(d) r = 1:2, pD = 13.3;
(e) r = 1:3, pD = 13.4.

3.1.1 Pt_2Pd_3 : [{(2,2'-bpy)Pd}$_3${*cis*-[$(NH_3)_2$Pt(*N1*-U-*N3*)(*N1*-U- *N3,O4*)]}$_2$]$(NO_3)_2$•23.1H_2O (17)

Compound **17** was obtained by addition of $[Pd(2,2'\text{-bpy})(D_2O)_2]^{2+}$ to a solution of *cis*-Pt(UH-*N1*)$_2(NH_3)_2$•2H_2O (**14a**) in D_2O (r = 1:0.25). The solution was stirred for two days at a pD higher than 13 without observing changes in the ^{1}H NMR spectrum. Afterwards, the pD was adjusted to 5.6 by addition of DNO_3 (1M). Orange cubic crystals, which turned out to be suitable for X-ray crystallography, were collected from a sample kept in D_2O for NMR characterization.

X-Ray Crystallography

The X-ray crystal structural analysis of [{(2,2'-bpy)Pd}$_3${*cis*-[$(NH_3)_2$Pt(*N1*-U-*N3*)(*N1*-U-*N3,O4*)]}$_2$]$^{2+}$ (**17**) showed that the solid state structure consists of a pentanuclear complex with two *cis*-diammineplatinum entities and three bipyridine palladium entities, in which two of latter are stacked (3.4-4.0 Å). The nucleobases adopt a *head-tail* arrangement.

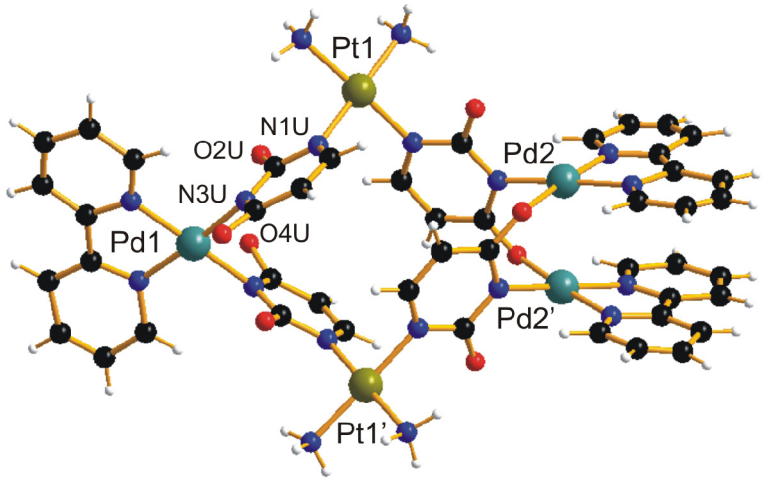

Figure 52: Crystal structure of the cation of [{(2,2'-bpy)Pd}$_3${*cis*-[$(NH_3)_2$Pt(*N1*-U-*N3*)(*N1*-U-*N3,O4*)]}$_2$]$(NO_3)_2$•23.1H_2O (**17**).

As can be seen in Figure 52, the cyclic cation is derived from two molecules of the anion *cis*-[Pt(U-*N1*)$_2(NH_3)_2]^{2-}$ cross-linked by three Pd^{II}(2,2'-bpy) entities. One Pd metal fragment is bonded via the N(3) position of two uracilate ligands, whereas the two other Pd moieties are bonded via N(3) and O(4) of the uracil

dianions in *head-tail* fashion. The Pd···Pd distance of the two stacked Pd^{II}(2,2'-bpy) entities is 2.863(3) Å, which is very similar to the Pd···Pd distances observed in Chapter I for the structurally related compounds [{(2,2'-bpy)Pd}$_3${(en)Pt(*N1*-U-*N3,O4*)(*N3*-CH-*N1*)}$_2$](NO$_3$)$_4$•5H$_2$O (**4**) and [{(2,2'-bpy)Pd}$_4${(en)Pt(*N1*-U-*N3,O4*)(*N3*-HC-*N1,O2*)}$_2$](NO$_3$)$_6$ (**7**) (2.819(2) Å and 2.844(10) Å, respectively). The distances and angles of the molecule are given in Table 12.

Table 12: Selected interatomic distances (Å) and angles (°) of [{(2,2'-bpy)Pd}$_3${*cis*-[(NH$_3$)$_2$Pt(*N1*-U-*N3*)(*N1*-U-*N3,O4*)]}$_2$](NO$_3$)$_2$•23.1H$_2$O (**17**).

Pt(1)-N(1)U1	1.982(15)	N(11)-Pt(1)-N(12)	88.4(6)
Pt(1)-N(1)U2	1.980(16)	N(1)U1-Pt(1)-N(1)U2	90.5(6)
Pt(1)-N(11)	1.968(14)	N(11)-Pt(1)-N(1)U1	90.9(6)
Pt(1)-N(12)	2.022(13)	N(12)-Pt(1)- N(1)U2	90.3(6)
Pd(1)-N(3)U1	2.024(16)	N(11)-Pd(1)-N(12)	80.1(8)
Pd(1)-N(3)U1'	2.049(15)	N(3)U1-Pd(1)-N(3)U1'	86.4(6)
Pd(1)-N(11)	2.004(16)	N(11)-Pd(1)-N(3)U1	96.4(6)
Pd(1)-N(12)	2.040(20)	N(12)-Pd(1)-N(3)U1'	96.9(7)
Pd(2)-N(3)U2	2.014(13)	N(11)-Pd(2)-N(12)	80.9(6)
Pd(2)-O(4)U2'	2.021(13)	N(3)U2-Pd(2)-O(4)U2'	87.0(5)
Pd(2)-N(11)	2.044(13)	N(11)-Pd(2)-N(3)U2	98.0(6)
Pd(2)-N(12)	2.019(14)	N(12)-Pd(2)-O(4)U2'	94.2(6)
Pd(2) ···Pd(2')	2.863(3)		

The effect of the Pd coordination at the O(4) position of the uracilate ligands is not reflected in the C–O bond lengths of the nucleobases. C(4)–O(4) bond lenghts of the uracil nucleobases coordinated to the metal entities at N(1) and N(3) positions (U1 and U1', Figure 53) are in the normal range (1.22(3) Å and 1.24(2) Å, respectively). On the other hand, C(4)–O(4) bond lengths of the uracil ligands coordinated to the metal entities at N(1), N(3) and O(4) positions (U2 and U2', Figure 53) are slightly but not significally larger with values of 1.29(2) Å for U2 and for U2'.

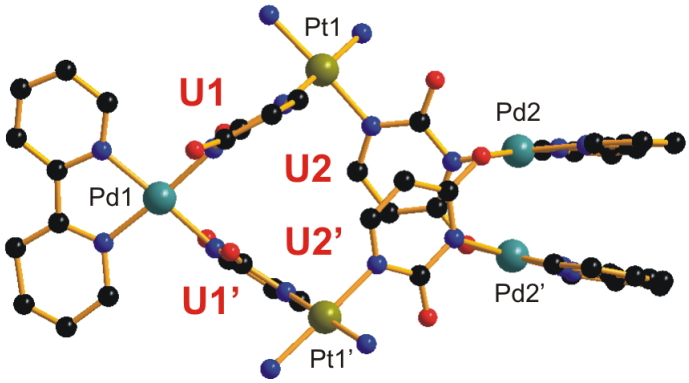

Figure 53: View of the cation of [{(2,2'-bpy)Pd}$_3${*cis*-[(NH$_3$)$_2$Pt(*N1*-U-*N3*)(*N1*-U-*N3,O4*)]}$_2$](NO$_3$)$_2$•23.1H$_2$O (**17**).

Compound **17** can be described as an extended metallacalix[4]arene with an additional metal added to one of the four corners. As consequence of this change of the basic metallacalix[4]arene structure, the mixed-metal distances Pt···Pd are very different from each other depending on whether the Pd is bonded at N(3) or O(4) positions of the uracil. In the first case, the distances range from 5.805(2) Å – 5.863(3) Å and in the latter case the Pt···Pd distances range from 7.270(3) Å – 7.355(3) Å. The intermetallic Pt···Pt distance is 7.705(3) Å. In Scheme 35 a simplified version of the crystal structure of the cation of **17** is shown (with Pt = *cis*-Pt^{II}(NH$_3$)$_2$ and Pd = Pd^{II}(2,2'-bpy)).

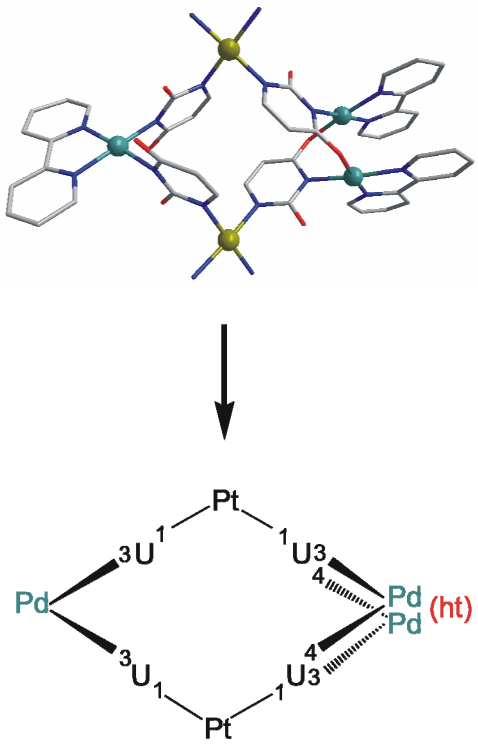

Scheme 35: Schematic view of the cation of compound **17**.

The structure of [{(2,2'-bpy)Pd}$_3${*cis*-[(NH$_3$)$_2$Pt(*N1*-U-*N3*)(*N1*-U- *N3,O4*)]}$_2$]$^{2+}$ (**17**) is reminiscent of a structure discussed previously. In the last chapter, it was described that compound [{(2,2'-bpy)Pd}$_3${(en)Pt(*N1*-U-*N3,O4*)(*N3*-CH-*N1*)}$_2$]$^{4+}$ (**4**) is a pentanuclear box consisting of two uracilate ligands and two cytosines. Formation of **4** arises from the reaction of two molecules of the cation [Pt(UH-

N1)(CH_2-*N3*)(en)]$^+$ (**1**) with three Pd^{II}(2,2'-bpy) moieties. One Pd ion is bonded via the N(1) positions of each of the the two cytosine ligands and the other two Pd ions are bonded trough N(3) and O(4) of each of the uracil dianions, adopting a *head-tail* arrangement. Hence, the two main differences with **17** are the ethylenediamine groups bonded to the platinum and the NH_2-goups in the (4)-position of the cytosine nucleobases, which are replaced by oxygen atoms in the uracil nucleobases. The connectivity of the nucleobases to the metal entities has slightly changed. Whereas in **4** the cytosine nucleobases are bonded at N(3) position to platinum, in **17** all of the urailate ligands are bonded at N(1) position to platinum. The cations of **4** and **17** are compared in Figure 54.

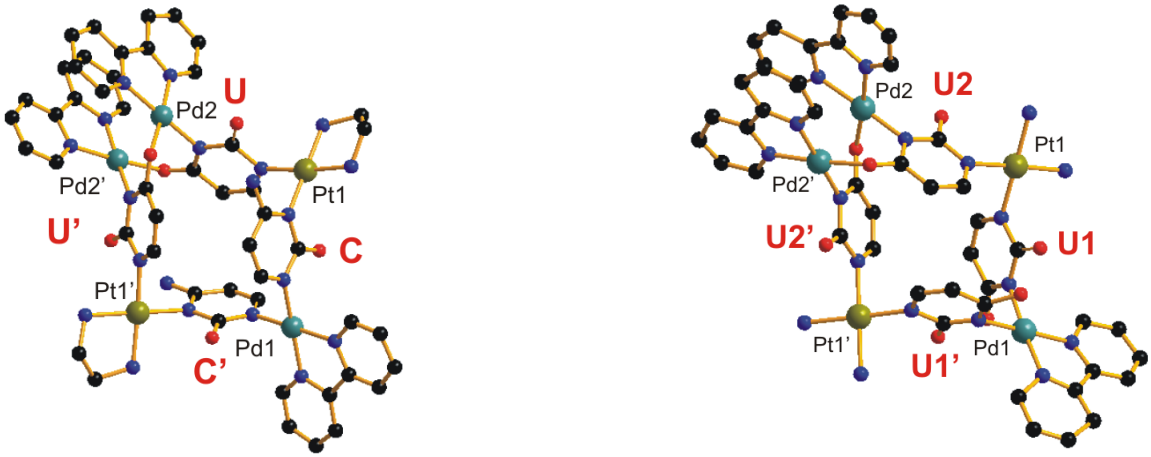

Figure 54: Crystal structures of the cations of [{(2,2'-bpy)Pd}$_3${(en)Pt(*N1*-U-*N3,O4*)(*N3*-CH-*N1*)}$_2$](NO$_3$)$_4$•5H$_2$O (**4**) (left) and [{(2,2'-bpy)Pd}$_3${*cis*-[(NH$_3$)$_2$Pt(*N1*-U-*N3*)(*N1*-U-*N3,O4*)]}$_2$](NO$_3$)$_2$•23.1H$_2$O (**17**) (right).

NMR Spectroscopy

The four uracilate (U) ligands in **17** are pairwise equivalent. However, the ^{1}H NMR spectrum of **17** in D_2O (pD = 7.65) displays more than the two anticipated pairs of uracil H5 and H6 doublets (Figure 55a). Within 5 minutes after dissolving **17** in D_2O, at least four sets of H5 resonances are observed, consistent with a rearrangement process going on (Figure 55b). The two H5 doublets of equal intensity at 5.63 and 5.74 ppm are tentatively assigned to **17**, as well as the 2,2'-bpy resonance at 7.18 ppm, which is characteristic for the H5 proton of a stacked bpy ligand (see Chapter I: 3.1.2). The doublet at 5.60 ppm corresponds to the starting compound **14** and the signal observed at 5.95 ppm is assigned to

a new compound **24**. The chemical shifts of the species are given in Table 15 (see Chapter II: Summary).

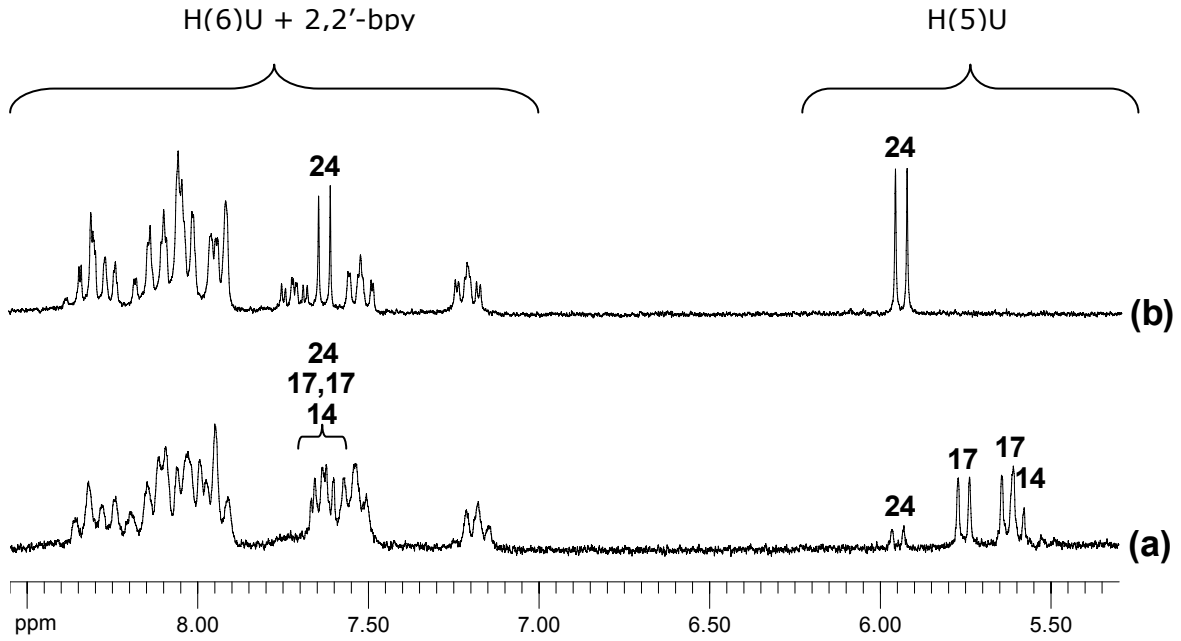

Figure 55: Low field section of the ^{1}H NMR spectrum of [{(2,2'-bpy)Pd}$_3${*cis*-[$(NH_3)_2$Pt(*N1*-U-*N3*)(*N1*-U-*N3,O4*)]}$_2$]$(NO_3)_2$•23.1H_2O (**17**) (a) after 5 min and (b) after the addition of 0.5 equiv. of $[Pd(2,2'\text{-bpy})(D_2O)_2]^{2+}$.

Addition of a small excess of $[Pd(2,2'\text{-bpy})(D_2O)_2]^{2+}$ to this mixture simplifies the spectrum greatly. Only one doublet is detected for H5 and H6 proton resonances of the uracils at 5.95 and 7.63 ppm, respectively (Figure 55b). This result indicates the formation of compound **24**, in which all uracils are equivalent. Again an upfield signal of the bpy resonance at 7.22 ppm is detected, suggestive of bpy stacking in **24**.

3.1.2 Pt_2Pd_4 : $[\{(2,2'\text{-bpy})Pd\}_4\{cis\text{-}[(NH_3)_2Pt(N1\text{-U-}N3,O4)_2]\}_2](NO_3)_4 \cdot 17H_2O$ (24)

In most cases, the study of the **14**/Pd^{II}(2,2'-bpy) system at different ratios (pD>13) showed that a yellow compound precipitated when the pD was decreased into the neutral range.

Additional reactions of **14** with $[Pd(2,2'\text{-bpy})(D_2O)_2]^{2+}$ at different ratios (r = ½, 1, 2, 3) were carried out at pD values higher than 13. After two days the pD was adjusted to 5-6 and in all cases a precipitate was separated from the neutral solutions. ^{1}H NMR spectroscopy proved the yellow powder to be the identical compound in all reactions. Recrystalization of the yellow precipitate gave orange rhombic crystals, which were separated from the solution, but a rapid loss of water molecules from the crystals took place and made them useless for X-ray crystallography.

ESI-Mass Spectrometry

To determine the composition of **24**, an Electrospray ionization Fourier-transform ion-cyclotron-resonance (ESI-FTICR) mass spectrometry study of compound **24** was performed by Prof. Dr. C. A. Schalley (Berlin). Two intensive signals corresponding to $[\mathbf{24} - 3NO_3]^{3+}$ and $[\mathbf{24} - 4NO_3]^{4+}$ are detected at m/z 669.99 and 487.24, respectively. Another high intensive signal appears at m/z 1035.98 corresponding to the dication $[\mathbf{24} - 2NO_3]^{2+}$. The isotope patterns of this ion is superimposed by a quadruply charged fragment $[2\ \mathbf{24} - 4NO_3]^{4+}$. Thus, this analysis is fully consistent with the expected hexanuclear cyclic complex **24**.

NMR Spectroscopy

The ^{1}H NMR spectrum of this product showed one doublet for the H5 proton of uracil at 5.95 ppm, as well as one doublet for the H6 resonance of uracil at 7.63 ppm with a coupling constant of $^3J_{H\text{-}H} \approx 6.8$ Hz. According to the relative integrals of the resonances, uracil and 2,2'-bpy are present in a 1:1 ratio. A representative

spectrum of this compound (**24**) is shown in Figure 56 and chemical shifts are given in Table 15 (see Chapter II: Summary).

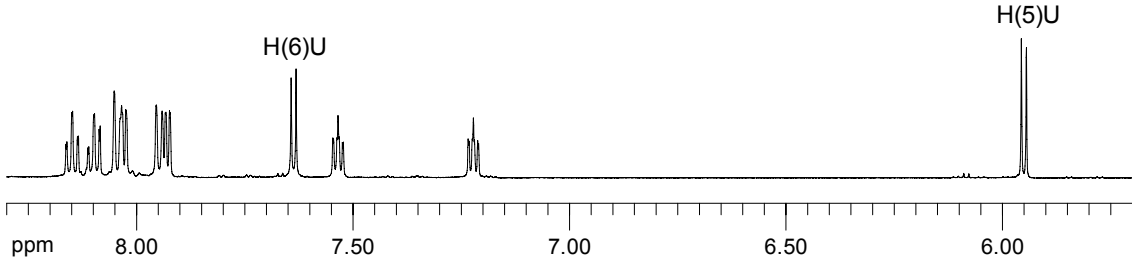

Figure 56: Low field section of the ^{1}H NMR spectrum of [{(2,2'-bpy)Pd}$_4${*cis*-[(NH$_3$)$_2$Pt(*N1*-U-*N3,O4*)$_2$]}$_2$](NO$_3$)$_4$•17H$_2$O (**24**) in D$_2$O at pD = 6.30.

As could be observed for compound [{(2,2'-bpy)Pd}$_3${(en)Pt(*N1*-U-*N3,O4*)(*N3*-CH-*N1*)}$_2$](NO$_3$)$_4$•5H$_2$O (**4**), an interesting point of the ^{1}H NMR spectrum of **24** in D$_2$O is the remarkable upfield shift of one of the 2,2'-bpy resonances (the triplet at 7.22 ppm). To analyze the 2,2'-bpy resonances in more detail, 1D TOCSY experiments were carried out for compound **24**. The spectra with the irradiated signal indicated, are shown in Figure 57.

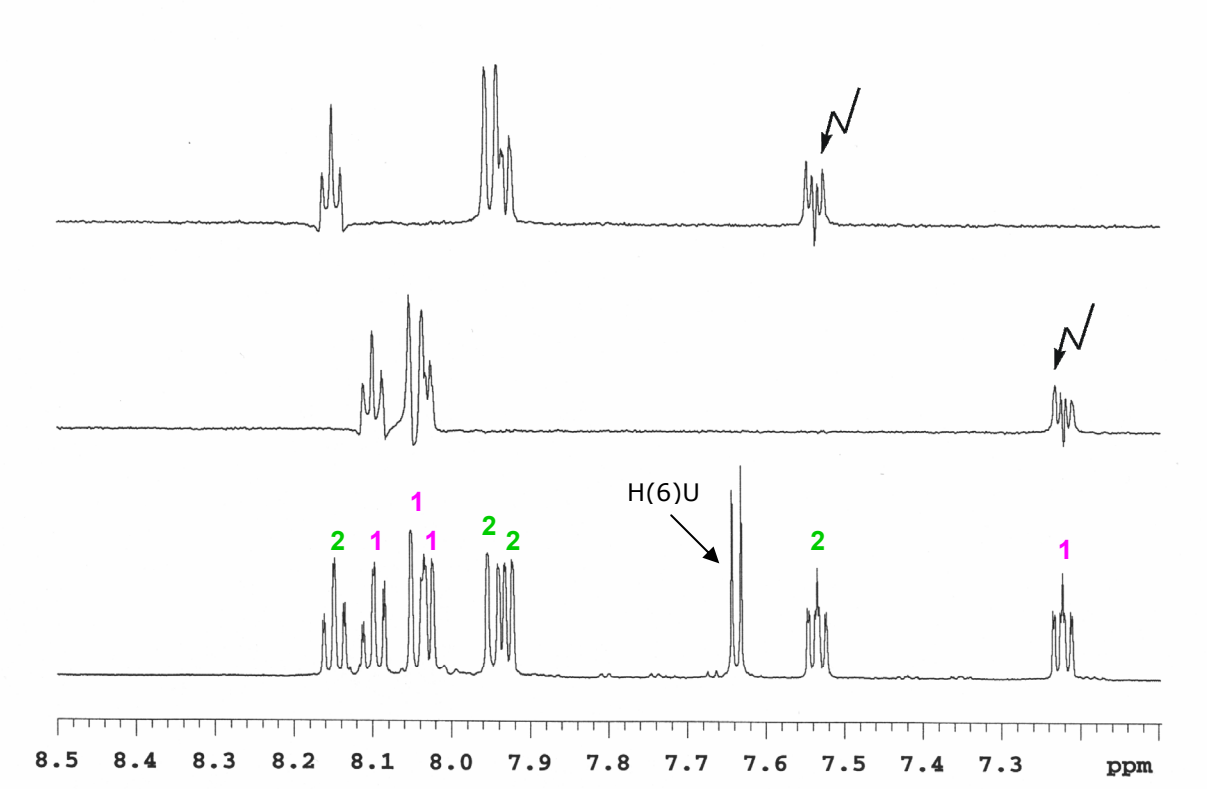

Figure 57: Low field section of the ^{1}H NMR spectrum of **24** (bottom) and 1D TOCSY experiments (top) applied to separate the bipyridine resonances.

The bpy resonances in the ^{1}H NMR spectrum show similar chemical shifts as the bpy resonances observed for compound **4**, but this time only two sets of the bpy resonances can be observed. The two sets of four 2,2'-bpy resonances are grouped at δ [ppm] = 7.22 (t), 8.03 (d), 8.05 (d) and 8.10 (t) (indicated with pink color in Figure 57); as well as 7.54 (t), 7.93 (d), 7.95 (d) and 8.15 (t) (green color in Figure 57). The 7.22 ppm signal exhibits the highest upfield shift of all bpy resonances, clearly reflecting the bpy stacking. For comparison with the ^{1}H NMR spectrum of the structurally characterized compound **4** (page 34), the first set of bpy resonances (pink, Figure 57) is assigned to the bipyridine rings *trans* to the N(3) positions of the uracil ligands and the second set of resonances (green) is assigned to the bipyridine rings *trans* to the exocyclic O(4) positions of uracil. However, this assumption is according to two different geometries depending on the orientation of the 2,2'-bpy units (*head-head* or *head-tail*). These two possibilities are represented in Scheme 36.

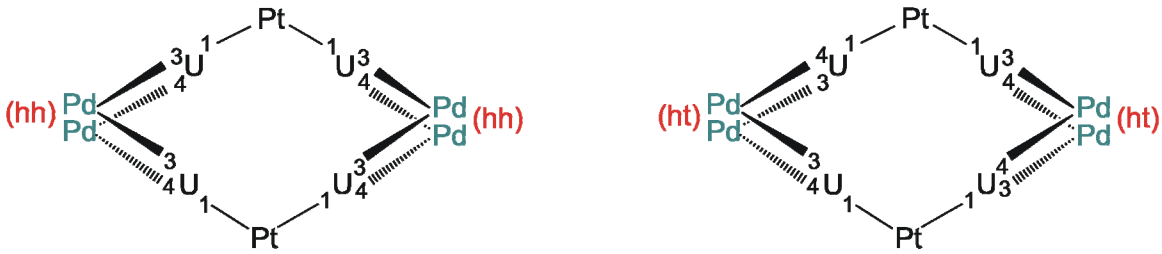

Scheme 36: Schematic representation of the two possible geometries adopted for compound **24** depending on the orientation of the nucleobase ligands: *head-head* (left) and *head-tail* (right).

According to the mass spectrometry study and the elemental analysis, it can be concluded that compound **24** is a metallacalix[4]arene with two *cis*-diammineplatinum entities, four bipyridine palladium entities and four nucleobases.

Concerning its formation, it has been seen previously, that **24** can be derived from **17** by addition of one Pd^{II}(2,2'-bpy) entity (Scheme 37). The pentanuclear compound **17** shows a *head-tail* arrangement of the uracil nucleobases coordinated to the two stacked Pd^{II}(2,2'-bpy) moieties. At first, only an attachment of the new Pd entity at the O(4)-sites of the other two uracils leading to a *head-head* arrangement seems to be possible. However, this postulated product (24a) has two different Pd binding patterns and therefore, according to

the ^{1}H NMR spectrum of **24**, it is feasible that an isomerization of 24a takes place. The isomerization process leads to a *head-tail* arrangement of all uracil nucleobases, hence to a symmetric product with the four equivalent uracilate ligands. A schematic picture of this process is depicted in Scheme 37.

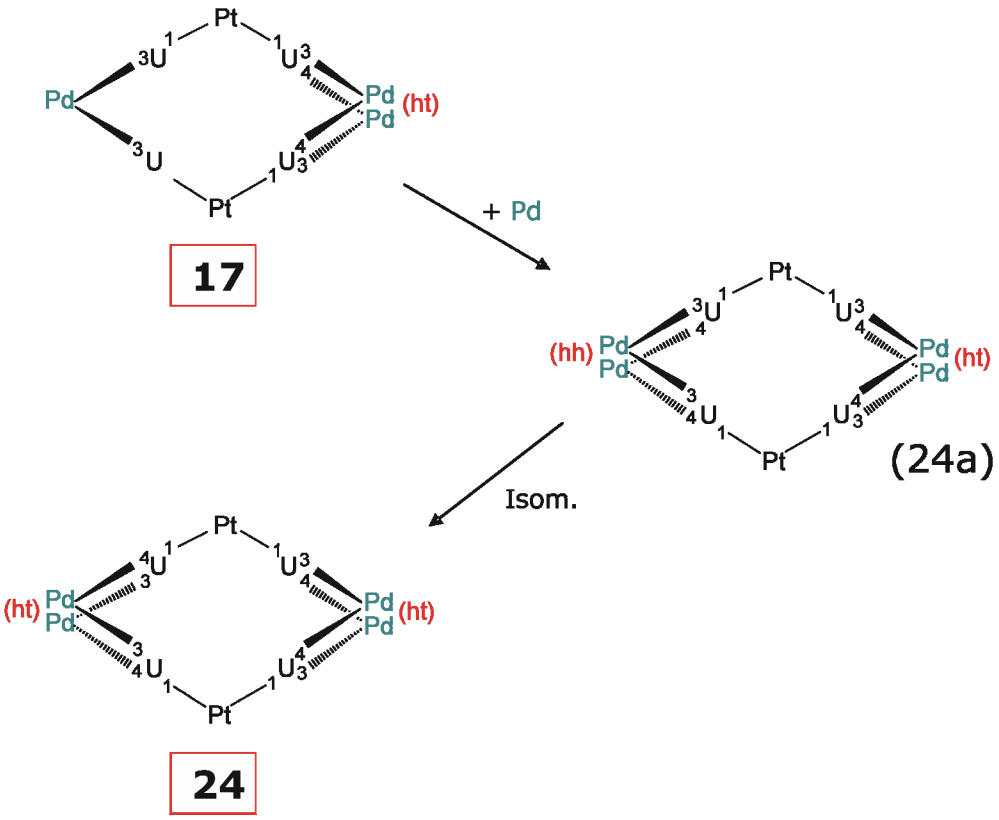

Scheme 37: Proposed process to obtain compound **24** from compound **17**.

3.1.3 Solution Behavior of Pt_2Pd_4: $[\{(2,2'\text{-bpy})Pd\}_4\{cis\text{-}[(NH_3)_2Pt(N1\text{-}U\text{-}N3,O4)_2]\}_2](NO_3)_4 \cdot 17H_2O$ (24)

The solution behavior of compound **24** was also studied in detail. For example, it was observed that by upon heating a solution of **24** in D_2O at 70°C (pD = 4.53) for three days or by addition of an large excess of NaCl at 40°C, compound **24** remains stable in solution. Compound **24** is also stable in solution at pD value of 9.5. As in all compound discussed so far, compound **24** decomposes to the starting compound in strongly acidic conditions (pD<1).

In the presence of two equivalents of a good ligand, such as 9-methylguanine in D_2O (pD =6.2), a partial decomposition of **24** to the starting compound **14** (50%) is observed after 30 min. The same reaction was carried out with four equiv. of 9-methylguanine and in this case immediately partial decomposition of **24** takes place. After two days almost only the signals corresponding to the starting compound **14** are present in the ^{1}H NMR spectrum.

On the other hand, increasing amounts of NaOD lead to the disappearance of the signals of **24** in the ^{1}H NMR spectrum and to the formation of two new doublets for each of the uracil protons (Figure 58). The doublets for the H6 resonances are overlapped by the bipyridine resonances, hence, only the H5 resonances of uracil will be analyzed in detail. To identifiy the new compound (16), solutions of **24** at different pD values are investigated by ^{1}H NMR spectroscopy. At pD = 9.58 (Figure 58b) compound **24** starts to decompose to give the pentanuclear compound **17** (5.63 and 5.74 ppm for H(5)). Further addition of NaOD to the solution leads to the formation of new signals in the ^{1}H NMR spectrum, located at 5.54 and 5.62 ppm (H5). It can be observed that the doublet at 5.63 ppm, which corresponds to **17**, is overlapped with the doublet at 5.62 ppm, which is assigned to the new product 16 (Figure 58d). Finally, at pD = 11.5-12.0, only the doublets of 16 can be observed (Figure 58f and Figure 58g). Within one week, the compound still remains stable in solution.

Another interesting point is the reversibility of this reaction. If the pD is decreased to ca. 9, compound **24** is regenerated.

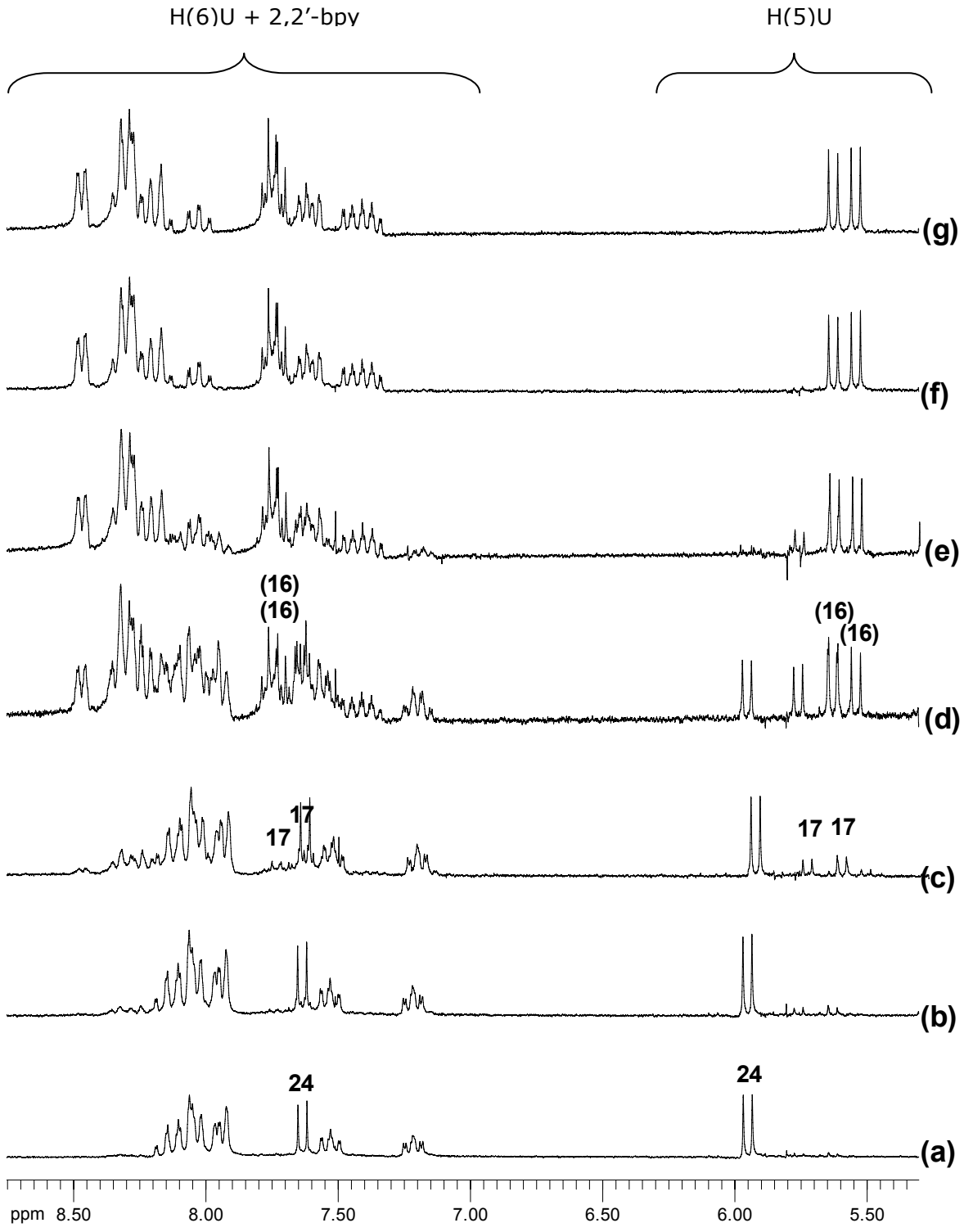

Figure 58: Low field section of the ^{1}H NMR spectrum (200 MHz) of [{(2,2'-bpy)Pd}$_4${*cis*-[$(NH_3)_2$Pt(*N1*-U-*N3,O4*)$_2$]}$_2$]$(NO_3)_4$•$17H_2O$ (**24**) in D_2O at:

(a) pD = 9.02,
(b) pD = 9.58,
(c) pD = 10.2,
(d) pD = 10.6,
(e) pD = 11.0,
(f) pD = 11.5,
(g) pD = 12.0.

From the ^{1}H NMR spectrum of **24** at pD> 11.5, important conclusions can be drawn. First, the new product probably does not have bipyridine groups stacked, because the typical upfield shift resonances of bpy at ca. 7.22 ppm is not present. Secondly, this compound has two chemically different uracil nucleobases, since two doublets for the H5-uracil resonances can be detected in the spectrum. Under these conditions two different products can be envisaged (16 and 22), which are depicted in Scheme 38.

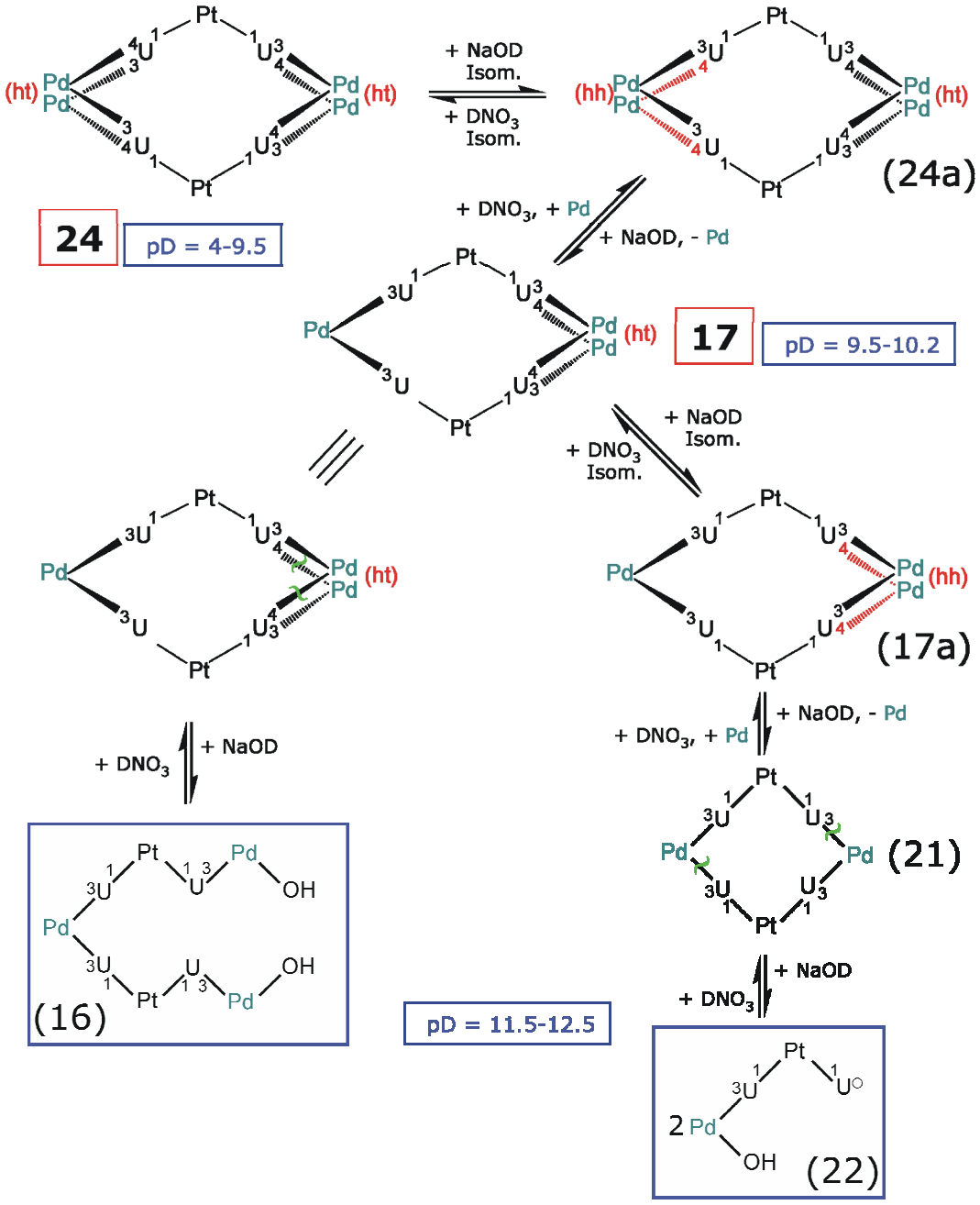

Scheme 38: Proposed process for the decomposition of **24** under strongly basic conditions suggested by the results of the ^{1}H NMR experiments (pD = 9.5-12.5).

The proposed process (Scheme 38) indicates the loss of one Pd entity of the hexanuclear complex **24** to give the pentanuclear complex **17** at ca. pD = 9.5-10.2. This conversion can take place by an isomerization process that first leads to a *head-head/head-tail* hexanuclear product (24a). Further loss of the (2,2'-bpy)Pd^{II} entity bonded at the O(4) exocyclic positions of the uracilate dianions then leads to formation of **17**. Upon further increase of the pD, **17** starts to decompose. In Scheme 38 two different possibilities are indicated. First, an isomerization process of **17** to give a pentanuclear compound (17a) with a *head-head* arrangement of the Pd ions can take place. Further loss of the Pd entity bonded at the O(4)-uracil positions can give the tetranuclear compound 21. Under more basic conditions, complex fragmentation with Pd-N(3) (uracil) bond breakage can take place leading to the dinuclear species 22. Secondly, Pd-O(4) (uracil) bond breakage in **17** is possible, leading to the "open" pentanuclear species 16.

Both compounds (16 and 22) have neither bipyridine ligands stacked nor all uracil ligands identically coordinated to the metal entities, hence both complexes are feasible derivatives **24** under basic conditions according to the ^{1}H NMR spectrum. To determine which species is present at pD = 11.5-12.5 (Figure 58f and 58g), 1D TOCSY experiments were carried out to analyze the 2,2'-bpy resonances of this compound. The spectra are shown in Figure 59.

The ^{1}H NMR spectrum consists of two doublets for the H5-uracil resonances (5.54 and 5.62 ppm), two doublets for the H6-uracil resonances (7.71 and 7.74 ppm) and four sets (each with four signals; H(3),H(4),H(5) and H(6)) of the 2,2'-bpy resonances. Four signals corresponding to the 2,2'-bpy resonances of the "aqua" species $[Pd(2,2'\text{-bpy})(D_2O)_2]^{2+}$ are located at δ [ppm] = 7.65 (t), 8.21 (t), 8.25 (d) and 8.33 (d) (indicated with red asterisks in Figure 59,*****). The other three sets of bpy resonances are located at [ppm] = 7.38 (t), 7.58 (d), 8.17 (t) and 8.30 (d) (pink, Figure 59); 7.44 (t), 7.62 (d), 8.02(t) and 8.18(d) (green, Figure 59); and finally, 7.75(t), 8.28 (d), 8.33 (d) and 8.47 (t) (blue, Figure 59). Therefore, the compound derived from **24** under basic conditions (16 oder 22) has three different coordinated rings of the bipyridine ligands.

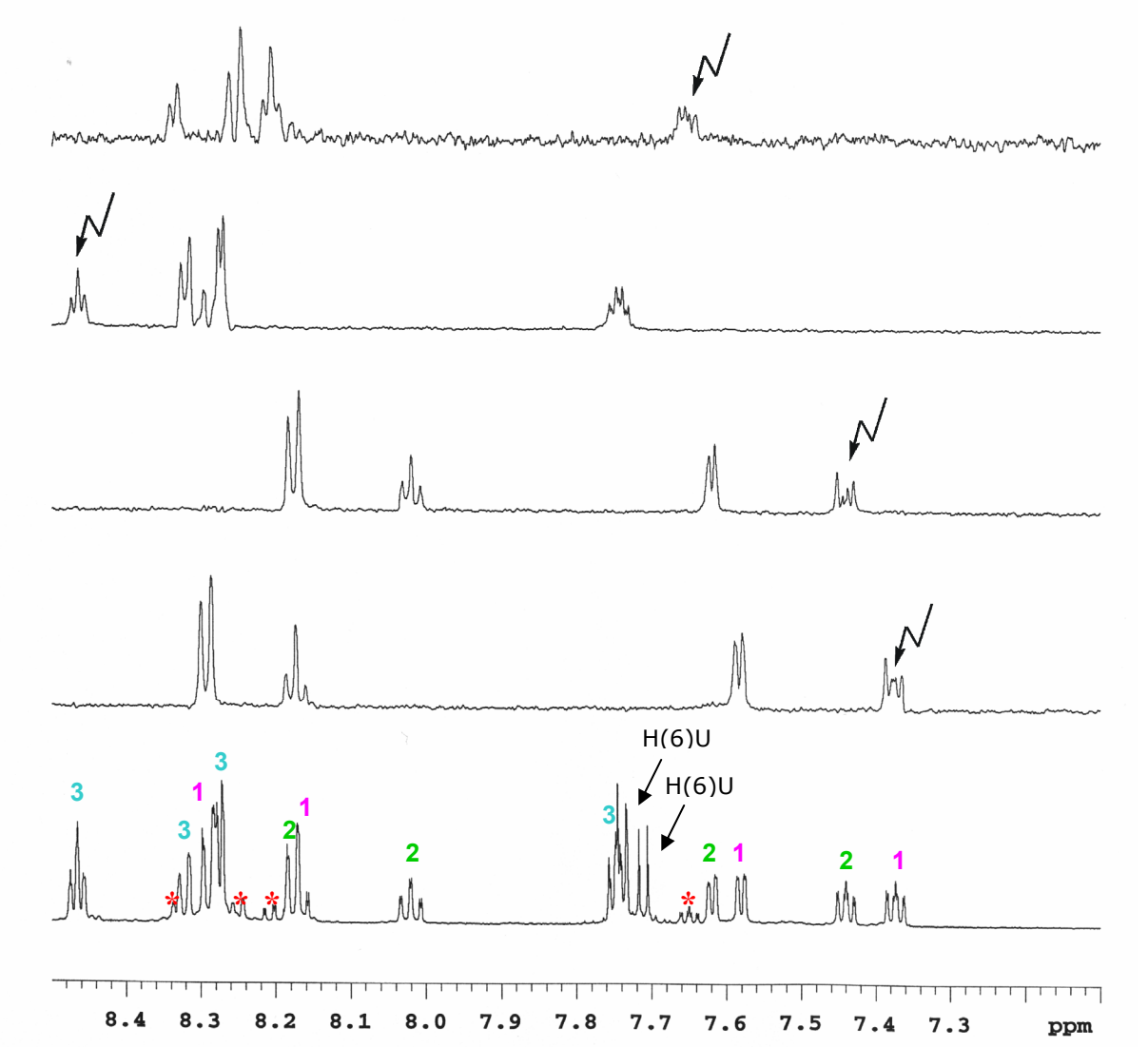

Figure 59: Low field section of the ^{1}H NMR spectrum (600 MHz) of **24** at pD = 11.96 (bottom) and 1D TOCSY experiments (top) applied to separate the bipyridine resonances.

However, compound 22 could be excluded, because its ^{1}H NMR spectrum should contain two sets of the bpy resonances due to the non-equivalence of the two pyridine "halves" as a consequence of different *trans*-positioned Pd donor atoms (N(3)-uracil and OH-group). On the other hand, the ^{1}H NMR spectrum of 16 should show three different sets of resonances. One set corresponding to the 2,2'-bpy ring symmetrically bonded to Pd and *trans* to N(3)-uracil sites and two times four signals of the two other bpy rings due to the non-equivalence bpy "halves" because of the two different *trans*-positioned Pd donor atoms (N(3)-uracil and OH-group), see Scheme 38.

The expected ^{1}H NMR spectrum of the postulated compound 16 seems to agree with the ^{1}H NMR spectrum of **24** (pD = 11.5-12.5), however, the relative intensities of the 2,2'-bpy resonances of the "aqua" species [Pd(2,2'-bpy)$(D_2O)_2]^{2+}$ (indicated with red asterisks in Figure 59,*****) are smaller than expected. Unfortunately, it was not possible to study the sample present at high pD by mass spectrometry because of the presence of high salt concentration.

Host-guest chemistry reactions with cations and anions were carried out for compound **24** and followed by ^{1}H NMR spectroscopy. In the first case, a solution of **24** was tried to react with Li^+, Na^+, or K^+, as well as with Cu^{2+} or Ni^{2+}, but no changes are detected in the solution. Reactions with anions such as NO_3^-, ClO_4^-, CO_3^{2-}, F^-, I^- or CH_3COO^- also show no sign of reaction in the ^{1}H NMR spectra.

4 Complexes with $[Pd(en)(H_2O)_2]^{2+}$

4.1 Synthesis, Characterization and Reactivity.

As a general method in the system **14**/$Pd^{II}a_2$, the reactions initially is carried out in strongly basic conditions so that the uracil N(3) positions are deprotonated. This way, several reactions of *cis*-Pt(UH-*N1*)$_2$(NH$_3$)$_2$•2H$_2$O (**14a**) in D$_2$O (pD>13) with $[Pd(D_2O)_2(en)]^{2+}$ at different ratios were carried out. After two days the pD of the solutions was adjusted to roughly 6-7 and in some cases (r = 1:0.25 and r = 1:0.5) a white precipitate corresponding to the starting compound **14** appears in the NMR tubes, as it does not react completely (Figure 60).

When the ratio of the system **14**/$[Pd(D_2O)_2(en)]^{2+}$ when the ratio Pt:Pd is 1:0.25 (Figure 60a), at least four different resonances for H(5)- as well as for H(6)-uracil protons are found in the spectrum (5.29, 5.53, 5.54 and 5.55 ppm for the H(5)-uracil proton, as well as 7.32, 7.41, 7.53 and 7.54 ppm for H(6)-uracil proton). It should be noted that the resonances corresponding to the free uracil ligand at pD =6-7 (5.79 ppm and 7.52 ppm, for H(5)- and H(6)-uracil, respctively) are not detected in the spectra.

When the ratio is increased to r =1:0.5 (Figure 60b), five additional resonances for the H(5)- and H(6)-uracil protons appear in the spectrum.

Further addition of Pd^{II}(en) to the solution (r = 1:1) leads to a different mixture of products. The ^{1}H NMR spectrum (Figure 60c) shows only five of the eight resonances observed at r = 1:0.5. The resonances corresponding to the early product(s) are not present in the spectrum.

If the ratio Pt:Pd is increased to r = 1:2, one major species is found (5.44 ppm and 7.45 ppm). The resonances corresponding to the X-ray structurally characterized compound [{(en)Pd}$_4${*cis*-[(NH$_3$)$_2$Pt(*N1*-U-*N3,O4*)$_2$]}$_2$](NO$_3$)$_4$ •13.8H$_2$O (**24'**) (5.49 ppm and 7.36 ppm) appear at r = 1:3.

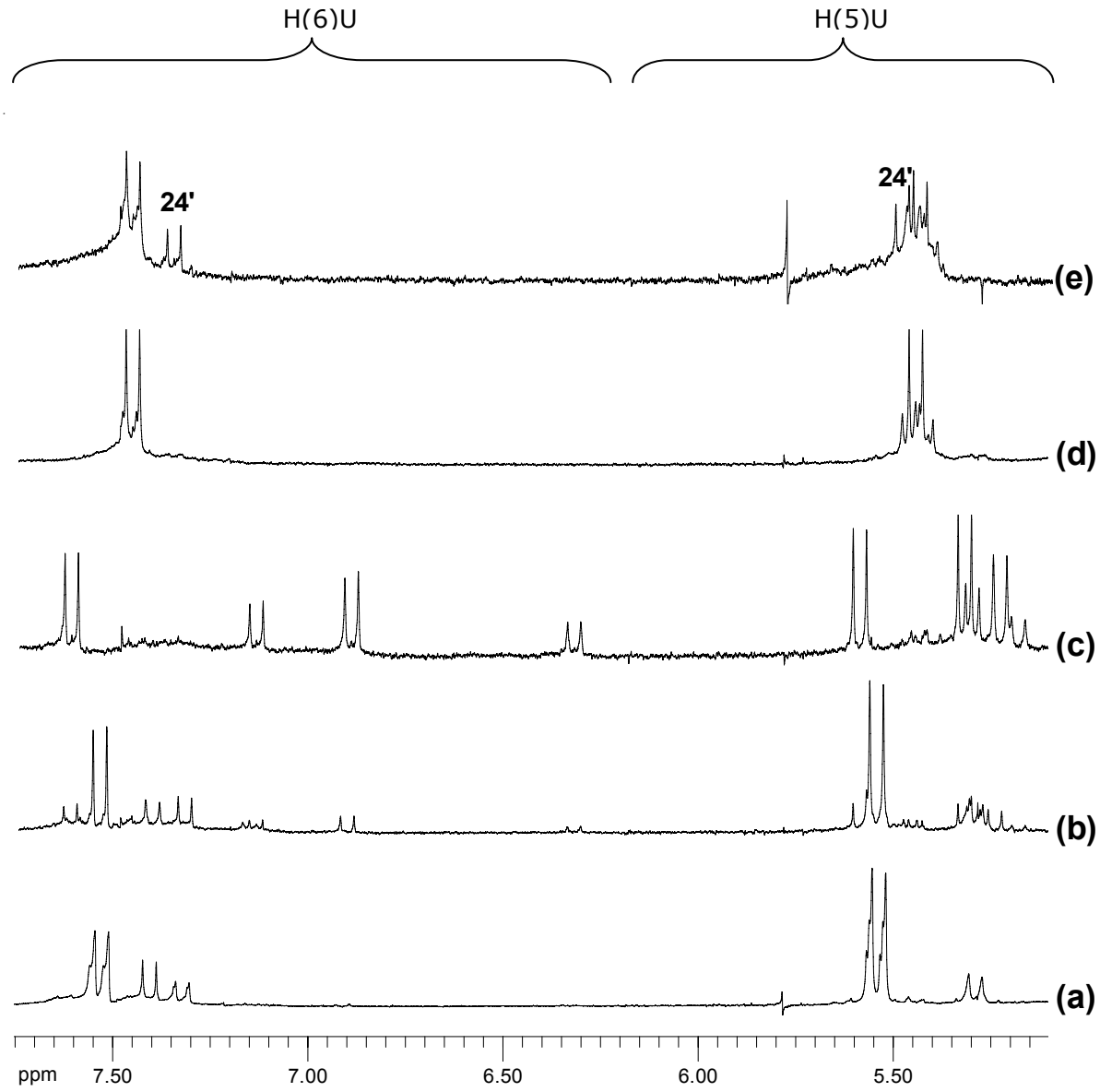

Figure 60: Low field section of the ^{1}H NMR spectra of the reaction of *cis*-Pt(UH-*N1*)$_2$(NH$_3$)$_2$•2H$_2$O (**14a**) with [Pd(D$_2$O)$_2$(en)]$^{2+}$ in D$_2$O where r = Pt:Pd is:
(a) r = 1:0.25, pD = 6.43;
(b) r = 1:0.5, pD = 6.59;
(c) r = 1:1, pD = 6.20;
(d) r = 1:2, pD =7.07;
(e) r = 1:3, pD = 6.27.

4.1.1 Pt_2Pd_4: $[\{(en)Pd\}_4\{cis\text{-}[(NH_3)_2Pt(N1\text{-}U\text{-}N3,O4)_2]\}_2](NO_3)_4 \cdot 13.8H_2O$ (24')

The title compound was obtained by addition of $[Pd(D_2O)_2(en)]^{2+}$ to a solution of *cis*-$Pt(UH\text{-}N1)_2(NH_3)_2 \cdot 2H_2O$ (**14a**) in H_2O (r = 1:2, pH>13) and subsequent decrease of the pH to 8.5. Upon slow evaporation of the solution at room temperature, orange blocks of a product were isolated after four days. The crystals turned out to be suitable for X-ray crystallography.

X-Ray Crystallography

Compound **24'** crystallizes in the triclinic space group P-1. The cation of **24'** consists of two molecules of the anion *cis*-$[(NH_3)_2Pt(U\text{-}N1)_2]^{2-}$ connected by four $Pd^{II}(en)$ entities. All Pd entities are bonded via N(3) and O(4) of the uracil dianions, thus leading to *head-tail* fashion. The metal-donor atom distances range from 2.017(9) to 2.045(9) Å for Pd bonded at N(3) and from 2.033(9) to 2.053(6) Å for Pd bonded at O(4). The Pd(1)···Pd(2) distance is 2.985(3) Å long and the Pd(1')···Pd(2') distance 2.975(1) Å. These are very similar to the Pd···Pd distances observed in Chapter I for the structurally related compound $[\{(en)Pt(U\text{-}N1,N3,O2,O4)(C\text{-}N1,N3,N4,O2)\}_2\{(en)Pd\}_6](NO_3)_5(ClO_4)_3 \cdot 21.2H_2O$ (**13'**) (2.96(3) Å). The solid state structure of **24'** is depicted in Figure 61. As can be seen the compound is analoguous to **24**, with 2,2'-bpy replaced by en. Selected interatomic distances and angles are given in Table 13.

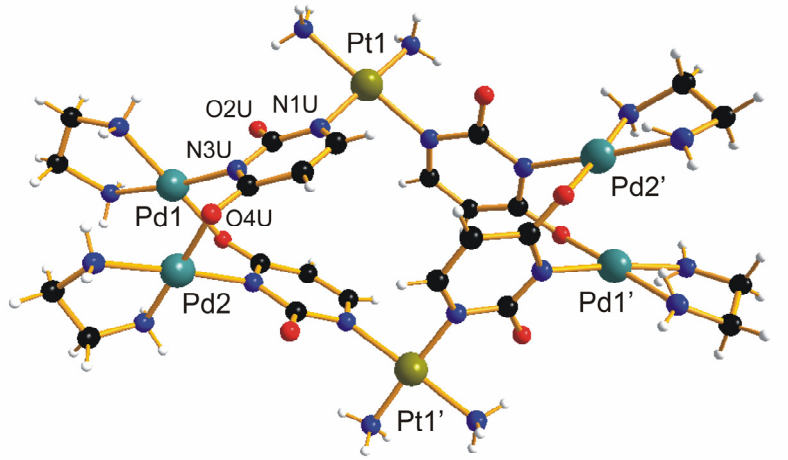

Figure 61: Crystal structure of the cation (I) of $[\{(en)Pd\}_4\{cis\text{-}[(NH_3)_2Pt(N1\text{-}U\text{-}N3,O4)_2]\}_2](NO_3)_4 \cdot 13.8H_2O$ (**24'**).

Table 13: : Selected interatomic distances (Å) and angles (°) of [{(en)Pd}$_4${*cis*-[(NH$_3$)$_2$Pt(*N1*-U-*N3,O4*)$_2$]}$_2$](NO$_3$)$_4$•13.8H$_2$O (**24'**).

Pt(1)-N(1)U1	2.008(8)	N(11)-Pt(1)-N(12)	89.1(5)
Pt(1)-N(1)U2	2.009(9)	N(1)U1-Pt(1)-N(1)U2	91.1(4)
Pt(1)-N(11)	2.037(11)	N(11)-Pt(1)-N(1)U1	90.2(4)
Pt(1)-N(12)	2.022(12)	N(12)-Pt(1)-N(1)U2	89.5(5)
Pd(1)-N(3)U1	2.039(8)	N(11)-Pd(1)-N(12)	83.2(4)
Pd(1)-O(4)U1'	2.053(6)	N(3)U1-Pd(1)-O(4)U1'	89.1(3)
Pd(1)-N(11)	2.009(8)	N(11)-Pd(1)-N(3)U1	94.2(4)
Pd(1)-N(12)	1.990(9)	N(12)-Pd(1)-O(4)U1'	93.4(3)
Pd(1) ···Pd(2)	2.985(1)		
Pd(1') ···Pd(2')	2.975(1)		

Compound **24'** can be described as an extended metallacalix[4]arene with two additional metals added to two of the four corners. The Pt···Pd distances, which involve the endocyclic sites of the nucleobases, are about 5.727(1) – 5.818(2) Å long. The Pt···Pd distances defined by the coordination of Pd to the exocyclic O(4) of each of the uracilate ligands range from 7.327(2) Å to 7.391(3) Å. The diagonal intermetallic Pt···Pt distance is 7.921(2) Å.

In Scheme 39 a simplified version of the crystal structure of the cation of **24'** is shown, together with a schematic representation of the nucleobase coordination sites (with Pt = *cis*-Pt^{II}(NH$_3$)$_2$ and Pd = Pd^{II}(en)).

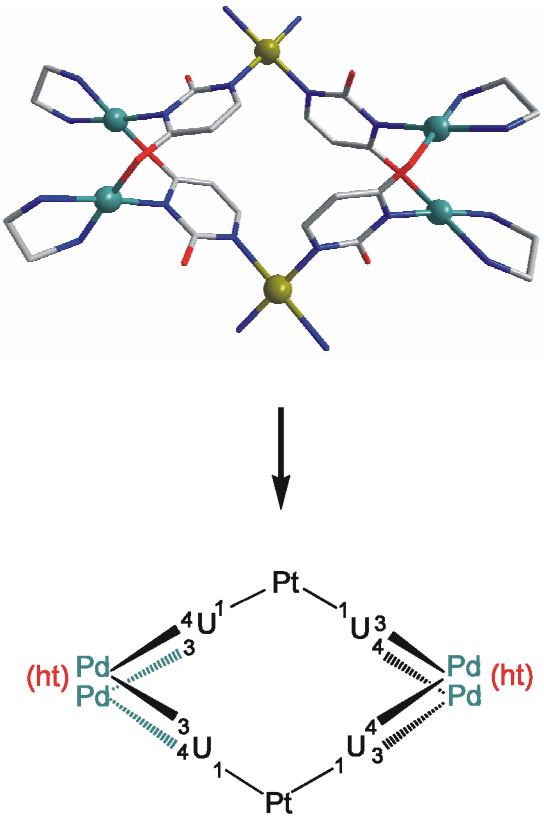

Scheme 39: Schematic view of the cation of compound **24'**.

The solid state structure of **24'** can be compared to another compound discussed previously. Compound **13'**, which was discussed in the previous chapter, consists of a Pt_2Pd_2 core unit and four additional Pd ions bonded at the exocyclic sites of the nucleobases (uracil and cytosine). The metallacalix[4]arene **13'** can be abbreviated $Pt_2Pd_6C_2U_2$ and shows a *head-head* arrangement of the nucleobases. In the metallacallix[4]arene **24'**, which can be abbreviated $Pt_2Pd_4U_4$, the nucleobases (only uracil) adopted a *head-tail* arrangement. Although in principle these are possible coordination sites for other metal fragments, the O(2) position of the uracilate dianions in **24'**are not able to bind other metal ions in a chelating fashion due to the *head-tail* arrangement adopted for the uracil rings. The two compounds are compared in the Figure 62.

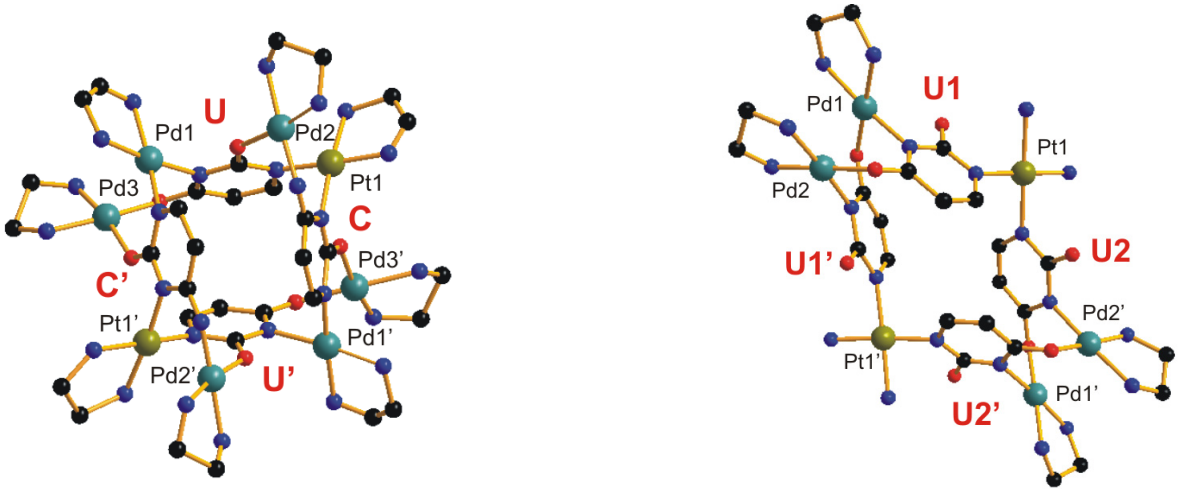

Figure 62: Views of the cation of [{(en)Pt(U-*N1,N3,O2,O4*)(C-*N1,N3,N4,O2*)}$_2$ {(en)Pd}$_6$](NO$_3$)$_5$(ClO$_4$)$_3$•21.2H$_2$O (**13'**) (left) and of the cation of [{(en)Pd}$_4${*cis*-[(NH$_3$)$_2$Pt(*N1*-U-*N3,O4*)$_2$]}$_2$](NO$_3$)$_4$•13.8H$_2$O (**24'**) (right).

NMR Spectroscopy

The ^{1}H NMR spectrum of **24'** shows one doublet for the H(5) proton and one doublet for the H(6) proton of uracil ($^3J_{H\text{-}H}$ = 6.8Hz). The spectrum is shown in Figure 63 and the chemical shifts are given in Table 15 (see Chapter II: Summary).

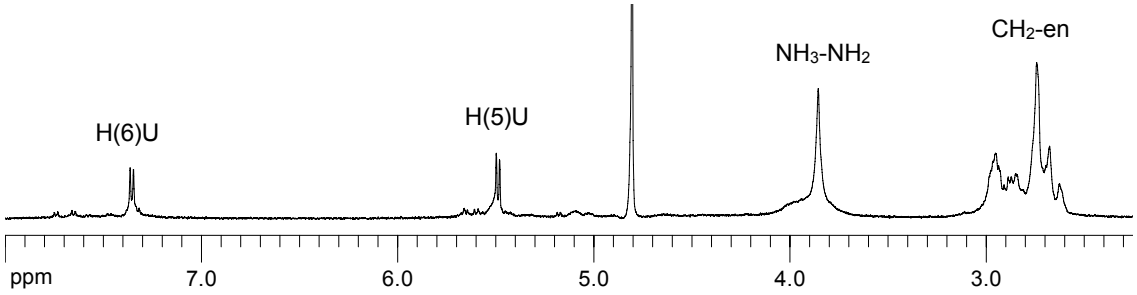

Figure 63: ^{1}H NMR spectum of [{(en)Pd}$_4${*cis*-[(NH$_3$)$_2$Pt(*N1*-U-*N3,O4*)$_2$]}$_2$](NO$_3$)$_4$•13.8H$_2$O (**24'**) in D$_2$O, pD = 5.66.

In complex **24'**, all metal ions are bonded in an identical fashion to the nucleobases. Therefore, all four uracil ligands are identical in the ^{1}H NMR spectrum with only one doublet for H5-uracil and one doublet for H6-uracil observed, at 5.36 ppm and at 7.45 ppm, respectively. The crystals of compound **24'** were obtained on a preparative scale when the ratio Pt:Pd was 1:2. However, the chemical shifts corresponding to **24'** are detected in the ^{1}H NMR study of the **14**/[Pd(en)(D$_2$O)$_2$]$^{2+}$ system when the ratio Pt:Pd was 1:3 (Figure 60e), which is probably due to the low concentration of the reaction.

4.1.2 Pt_4Pd_{10}: [{(en)Pd}$_{10}$(U-*N1,N3,O4*)$_2$(U-*N1,N3,O2,O4*)$_6${*cis*-[$(NH_3)_2$Pt]}$_4$]$(NO_3)_{12}$•30H_2O (28')

In the ^{1}H NMR study of the system **14b**/[Pd$(D_2O)_2$(en)]$^{2+}$ at r = 1:2 only one structurally characterized product (**24'**) is detected in the spectra. However, an attempt to synthetize **24'** on a preparative scale at r = 1:3 gave an unexpected result.

To a solution of *cis*-Pt(UH-*N1*)$_2$$(NH_3)_2$•2$H_2O$ (**14a**) in H_2O (pH = 13.3) three equivalents of [Pd$(D_2O)_2$(en)]$^{2+}$ were added and the solution was stirred for 2 days. Afterwards the pH was decreased to ca. 9 and after slow evaporation of the solution at room temperature, orange blocks were obtained. Although these crystals at first glance appeared to be identical with those of compound **24'**, X-ray crystal structure analysis proved this product to be different, however.

X-Ray Crystallography

In fact, the solid state structure of the title compound shows it to be a 14-nuclear complex, composed of four *cis*-diammineplatinum entities, ten ethylenediamine palladium entities and eight uracilate dianions. It should be noted that only a preliminary structure of compound **28'** could be obtained due to the poor crystal quality.

As has been observed previously for compound **9,** and unlike related metallacalix[n]arenes with n ≤ 6, compound **28'** no longer has the shape of a ring, but rather adopts a strongly folded structure. In Scheme 40 a schematic representation of the crystal structure of **28'** is shown.

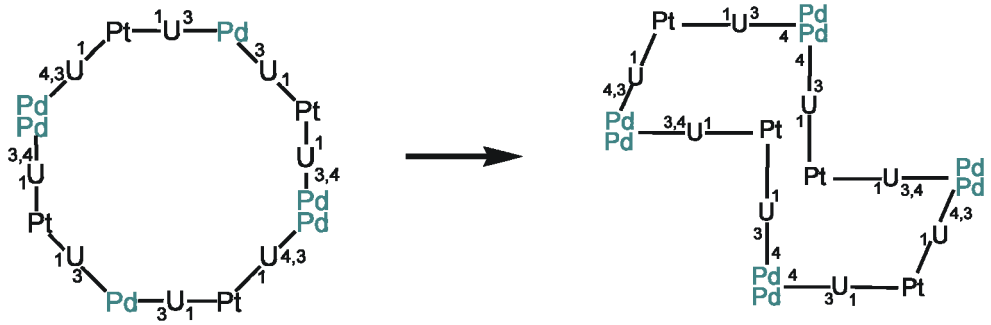

Scheme 40: Schematic representations of the Pt_4Pd_6 core of compound **28'**. The four Pd^{II}(en) entities bonded only via O(4)-uracil or O(2)-uracil are not shown.

Compound **28'** crystalizes in the monoclinic space group $P2_1/c$. A view of the complete cation is depicted in Figure 64.

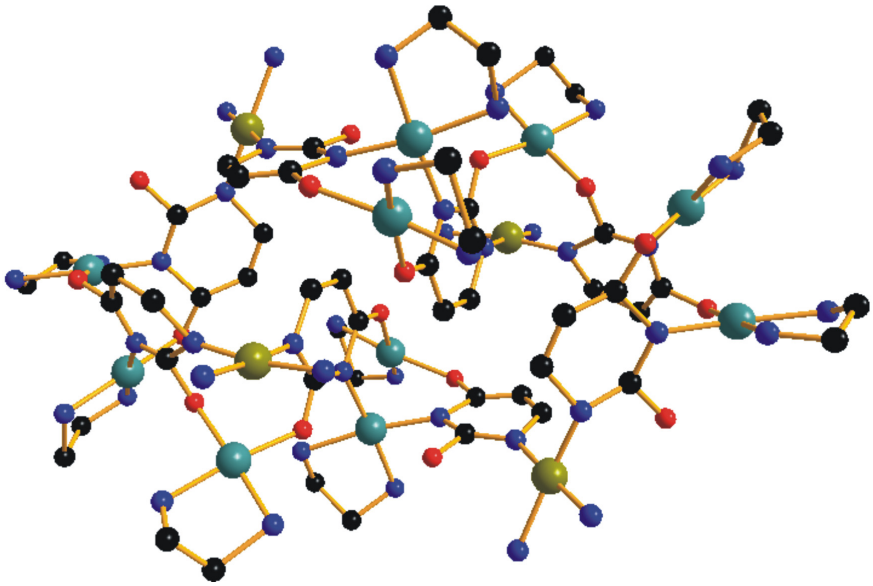

Figure 64: Crystal structure of the cation of $[\{(en)Pd\}_{10}(U\text{-}N1,N3,O4)_2(U\text{-}N1,N3,O2,O4)_6\{cis\text{-}[(NH_3)_2Pt]\}_4](NO_3)_{12}\cdot 30H_2O$ (**28'**).

The 14-nuclear complex is composed of four anions of the starting compound **14b** cross-linked by Pd^{II}(en) entitites. Compound **28'** consists of two identical halves, which contain of two different sorts of platinum environments and five different sorts of Pd environments, depending on the coordination to the nucleobases. In Figure 65 the cation of **28'** is shown, with the ethylenediamine groups bonded to palladium and the *cis*-diammine groups of platinum omitted for clarity. Salient structural data are listed in Table 14.

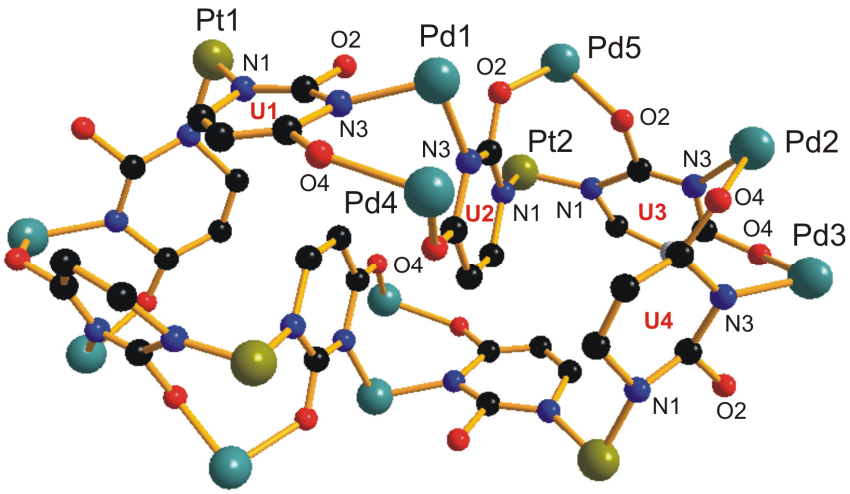

Figure 65: View of the cation of $[\{(en)Pd\}_{10}(U\text{-}N1,N3,O4)_2(U\text{-}N1,N3,O2,O4)_6\{cis\text{-}[(NH_3)_2Pt]\}_4](NO_3)_{12}\cdot 30H_2O$ (**28'**) with bipyridine and ethylenediamine groups omitted.

Table 14: Selected interatomic distances (Å) and angles (°) of $[\{(en)Pd\}_{10}(U\text{-}\textit{N1,N3,O4})_2(U\text{-}\textit{N1,N3,O2,O4})_6\{\textit{cis}\text{-}[(NH_3)_2Pt]\}_4](NO_3)_{12}\bullet 30H_2O$ (**28'**).

Pt(1)-N(1)U1	1.77(4)	N(1)U1-Pt(1)- N(1)U8	94.4(18)
Pt(1)-N(1)U8	1.82(4)		
Pt(2)-N(1)U2	1.91(3)	N(1)U2-Pt(2)- N(1)U3	87.1(15)
Pt(2)-N(1)U3	1.80(4)		
Pd(1)-N(3)U1	2.01(3)	N(3)U1-Pd(1)-N(3)U2	96.2(13)
Pd(1)-N(3)U2	1.96(3)		
Pd(2)-N(3)U3	1.93(4)	N(3)U3-Pd(2)-O(4)U4	98.0(14)
Pd(2)-O(4)U4	1.98(4)		
Pd(3)-N(3)U4	2.04(5)	N(3)U4-Pd(3)-O(4)U3	88.4(15)
Pd(3)-O(4)U3	1.96(3)		
Pd(4)-O(4)U1	2.13(3)	O(4)U1-Pd(4)-O(4)U2	96.9(11)
Pd(4)-O(4)U2	2.00(3)		
Pd(5)-O(2)U2	2.04(3)	O(2)U2-Pd(5)-O(2)U3	91.2(10)
Pd(5)-O(2)U3	2.00(3)		
Pt-N(a_2)	1.70(3)-	N(a_2)-Pt-N(a_2)	84.7(15)-
	2.04(4)		90.6(12)
Pd-N(en)	1.82(5)-	N(en)-Pd-N(en)	78.8(18)-
	2.21(5)		92.1(19)
Pt(2)···Pd(5)	2.977(4)		
Pd(1) ···Pd(4)	3.000(6)		
Pd(2) ···Pd(3)	3.004(6)		

Pt(1) is bonded to two uracilate dianions, which have the O(2) exocyclic sites free. Pt(2), on the other hand, is bonded to two uracilate ligands with all exocyclic positions bonded to Pd^{II}(en) entities. The endocyclic sites of the four uracilate dianions, forming the symmetric half, are arranged in the sequence Pt1(*N1*-**U1**-*N3*)Pd1(*N3*-**U2**-*N1*)Pt2(*N1*-**U3**-*N3,O4*)Pd2Pd3(*O4,N3*-**U4**-*N1*). Pd(4) and Pd(5) are bonded at the exocyclic positions of uracil (O(4) and O(2), respectively).

U1 and U2 are connected by two palladium entities (Pd(1) and Pd(4)), adopting a head-head arrangement and U2 and U3 are connected by one platinum entity and one palladium entity (Pt(2) and Pd(5)), adopting also a *head-head* arrangement. In contrast, U3 and U4 are connected by two palladium entities (Pd(2) and Pd(3)), adopting a *head-tail* arrangement (Figure 65).

In Scheme 41 the four different metal coordination motifs observed in **28'** are schematically depicted.

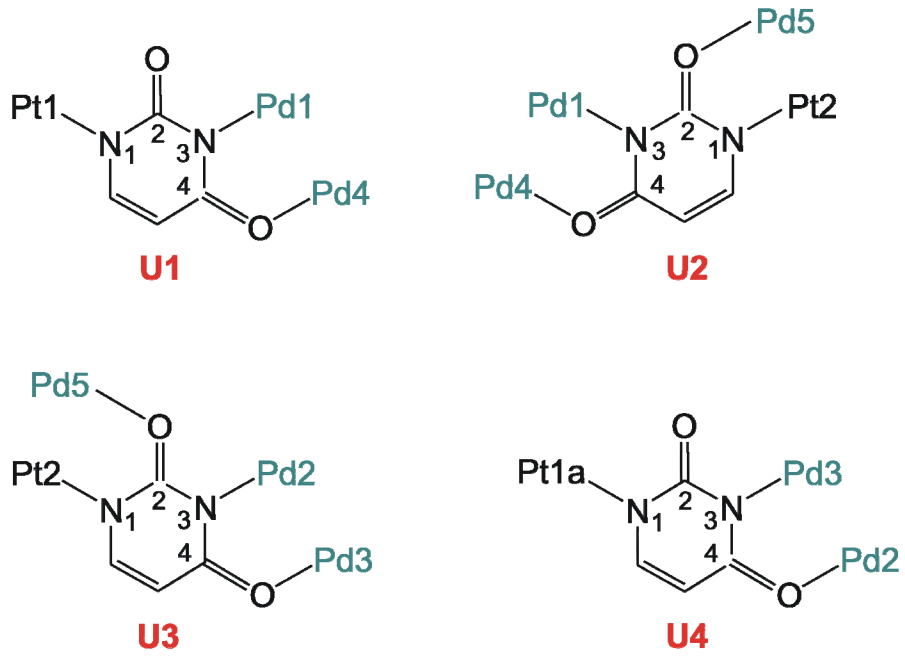

Scheme 41: Schematic diagram of U1, U2, U3, U4 with the metal coordination patterns of $[\{(en)Pd\}_{10}(U\text{-}N1,N3,O4)_2(U\text{-}N1,N3,O2,O4)_6\{cis\text{-}[(NH_3)_2Pt]\}_4](NO_3)_{12}\cdot 30H_2O$ (**28'**).

Unfortunately, the crystal was of poor quality and consequently the resolution of the structure is low. Only the metal ions could be refined anisotropically in the cation. The counter anions could not be defined within the remaining electronic density. Elemental analysis of the crystals is consistent with a structure of **28'**

composed of fourteen metal ions, twelve nitrate anions, as well as thirty crystal water molecules.

The metals "at the top" and likewise the metals "at the bottom", which are bonded to the endocyclic sites of the nucleobases form a distorted square (Scheme 42). The sides of each square involving the endocyclic binding pattern Pt(N1-U-N3)Pd range from 5.794(5) Å to 5.881(4) Å.

Pt···Pd distances involving the *head-tail* coordination Pt(N1-U-O4)Pd range between 7.179(6) Å and 7.360(5) Å. Alternatively, Pt···Pd distances involving the *head-head* coordination Pt(N1-U-O4)Pd range from 7.514(6) Å to 7.589(4) Å as well as from 4.713(5) Å to 4.762(6) Å for Pd(N3-U-O2)Pd.

The intermetallic distance Pt···Pt in the asymmetric half is 12.204(4) Å.

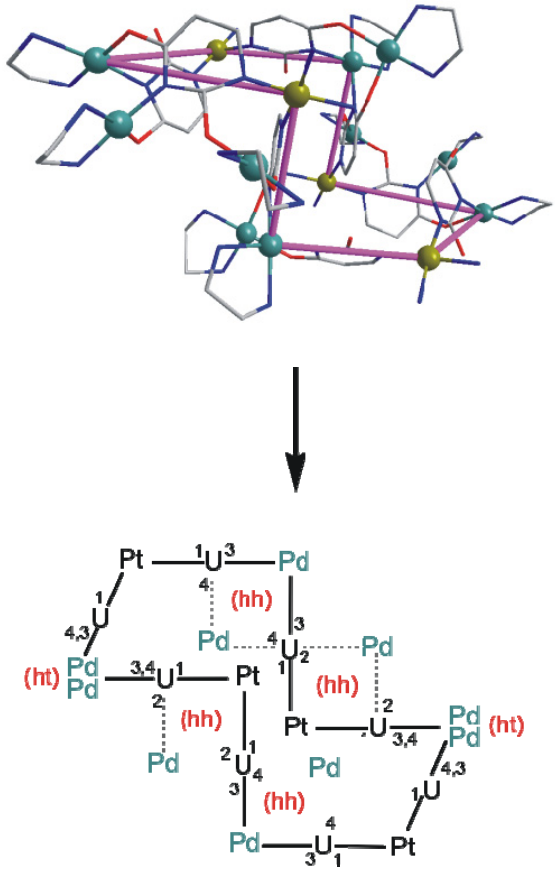

Scheme 42: Schematic diagram of the cation of compound **28'**.

NMR Scpectroscopy

The ^{1}H NMR study of compound **28'** shows the complex to be unstable in solution. The crystals were dissolved in D_2O and the spectrum was immediatly recorded. According to the solid state structure of **28'**, four different signals for the H5 proton and H6 proton of uracil (due to the four non-equivalent uracilate ligands) are expected. However, the ^{1}H NMR spectrum shows one set of intensive doublets corresponding to H(5) and H(6)-uracil resonances, previously assigned to compound **24'**, and three additional sets of doublets of equal intensity

(Figure 66). After 30 min a second spectrum is recordered. This time only the signals corresponding to **24'** are detected.

It is suggested that **28'** decomposes very fast, leading to the formation of two cations of **24'**. The six doublets observed in the spectrum probably belong to intermediate species.

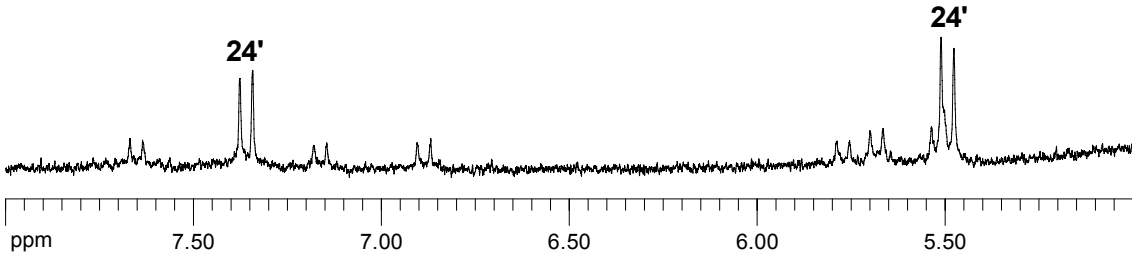

Figure 66: Low field section of the ^{1}H NMR spectrum of $[\{(en)Pd\}_{10}(U\text{-}N1,N3,O4)_2(U\text{-}N1,N3,O2,O4)_6\{cis\text{-}[(NH_3)_2Pt]\}_4](NO_3)_{12}\bullet 30H_2O$ (**28'**) in D_2O, at pD = 7.12, shortly after sample preparation.

There are three ways to explain the conversion of **28'** to **24'**. These processes are represented in Scheme 43 (bond-breakages indicated in green color).

First, loss of the four exocyclic Pd^{II} entities that are bonded at the O(4) and O(2) sites of the uracilate dianions can take place in solution to give 26' (Scheme 43, left). Then, complex fragmentation of the 10-nuclear cycle (26') can ocurr, leading to the formation of two pentanuclear boxes (17'). A further coordination of another Pd^{II}(en) entity at the exocyclic O(4) positions of each of the cycles and a subsequent isomerization leading to a *head-tail* arrangement result in the formation of **24',** as was observed for compounds **17** and **24** with (2,2-bpy)Pd^{II}. The second possibility (Scheme 43, center), involves also the decomposition of the 10-nuclear cycle (26'), but this time, to give two "open" species (18'). Next, attachment of one Pd entity to the deprotonated N(3) position of the uracilate dianion and a subsequent cyclization that leads to a *head-tail* arrangement is also possible.

Finally (Scheme 43, right), loss of only the two exocyclic Pd^{II}(en) entities that are bonded at the O(2) positions of the uracilate nucleobases can take place to give 27'. The following complex fragmentation with Pd-N(3) and Pd-O(4) bond breakages leads to the formation of two "open" hexanuclear species (20').

Subsequent cyclization of these species with formation of a *head-tail* arrangement give compound **24'**.

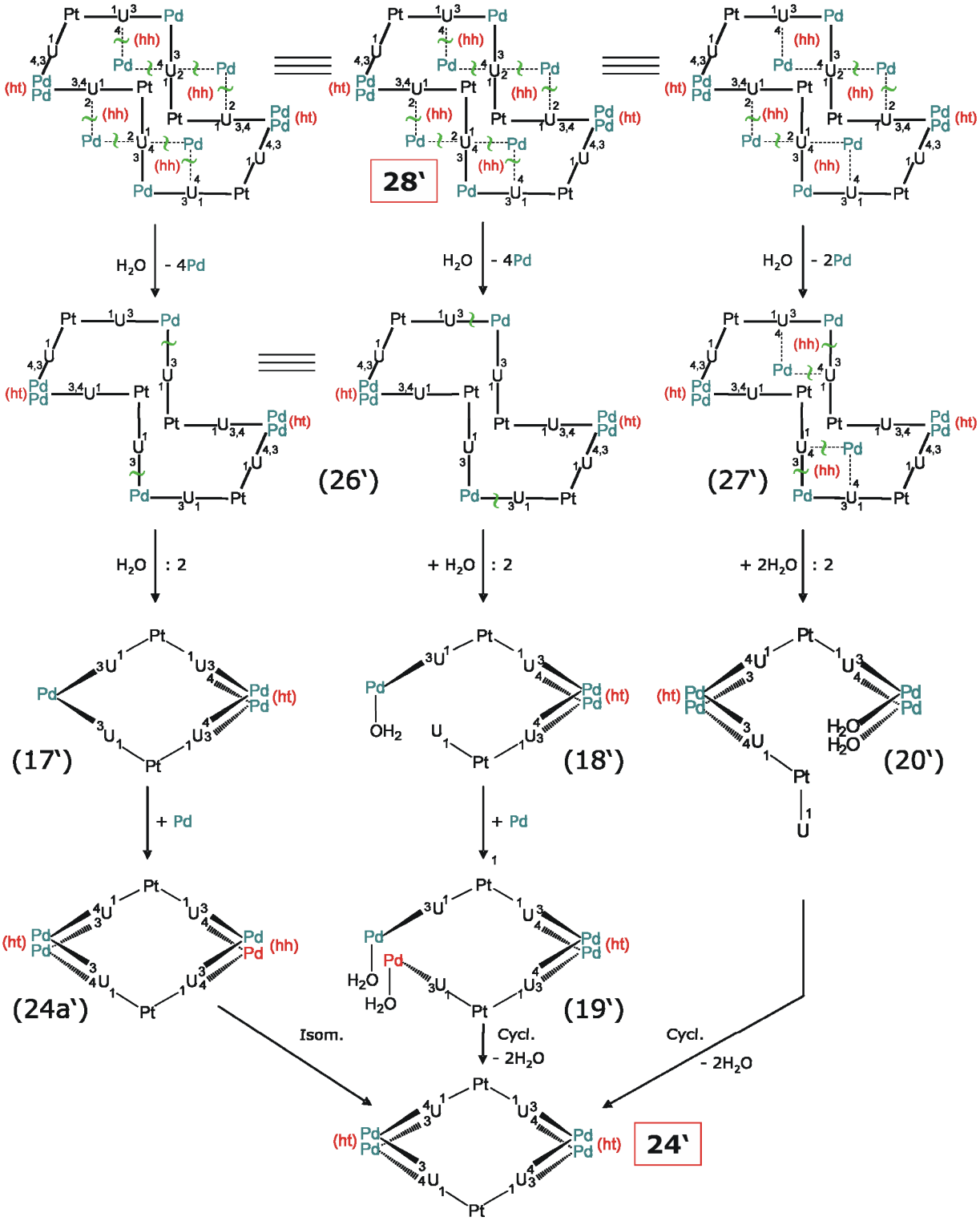

Scheme 43: Possible ways of the decomposition of compound **28'** to compound **24'**.

5 Complexes with $[Pd(H_2O)_2(tmeda)]^{2+}$

To understand the reactivity properties of the **14**/$[Pd(D_2O)_2(tmeda)]^{2+}$ system, different reactions of the bis-uracilate platinum compound **14** with (tmeda)Pd^{II} entity were carried out.

^{1}H NMR Spectroscopy

To solutions of *cis*-Pt(UH-*N1*)$_2$(NH$_3$)$_2$•2H$_2$O (**14a**) in D_2O (pD>13), $[Pd(D_2O)_2(tmeda)]^{2+}$ was added at different ratios and the reactions are monitored by ^{1}H NMR spectroscopy. The pD was kept at strongly basic conditions for one day, then the pD was decreased to roughly 4-5. Representative ^{1}H NMR spectra are shown in Figure 67.

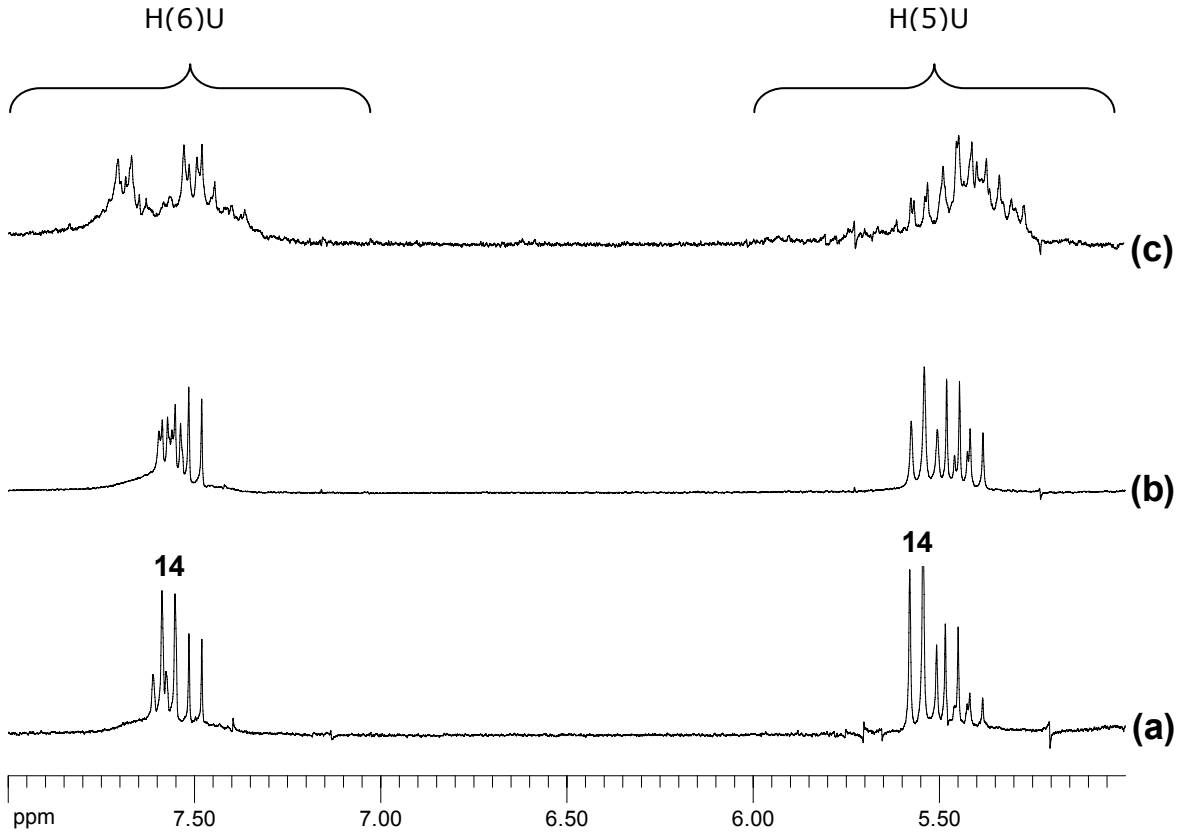

Figure 67: Low field section of the ^{1}H NMR spectra of the reaction of *cis*-Pt(UH-*N1*)$_2$(NH$_3$)$_2$•2H$_2$O (**14a**) with $[Pd(D_2O)_2(tmeda)]^{2+}$ in D_2O, after 2 days, where r = Pt:Pd is:
(a) r = 1:0.5, pD = 5.55;
(b) r = 1:1, pD = 4.59;
(c) r = 1:2, pD = 5.23.

At r = 1:0.5, several new signals in addition to those of the starting compound **14b** appear in the ^{1}H NMR spectrum (Figure 67a). When the ratio is increased to 1:1, the overall intensitiy of the new sets of signals grows and likewise the intensity of the doublets corresponding to the H5 and H6 resonances of **14** decreases. At r = 1:2, the starting compound can no longer be detected in the spectrum and several sets of overlapping signals appear (Figure 67c). Unfortunately, no compound of this system could be isolated.

6 Reactivity Patterns and Interconversion Mechanisms

Based on the isolated complexes discussed in this chapter (**17**, **24'** and **28'**), mechanisms of formation for these compounds can be proposed. It is assumed that Pd^{II}(2,2'-bpy) or Pd^{II}(en) behave very similar. Therefore, the proposed interconversion mechanisms, if not specifed, are proposed to be common to both $Pd^{II}a_2$ entities.

The starting compound $[Pt(U\text{-}\mathit{N1})_2(NH_3)_2]^{2-}$ (**14**) consisting of two uracilate dianions is very different from the starting compoun $[Pt(UH\text{-}\mathit{N1})(CH_2\text{-}\mathit{N3})(en)]^+$ (**1**), which is composed of one uracilate monoanion and one neutral cytosine. In the latter, families of compounds have been observed that display different connectivities of the nucleobases. In the case of **14** with only N(1) bonded uracilate ligands present, such a possibility is ruled out.

The metallacalix[4]arenes $[\{(2,2'\text{-bpy})Pd\}_3\{\mathit{cis}\text{-}[(NH_3)_2Pt(\mathit{N1}\text{-}U\text{-}\mathit{N3})(\mathit{N1}\text{-}U\text{-}\mathit{N3,O4})]\}_2](NO_3)_2 \bullet 23.1H_2O$ (**17**), $[\{(2,2'\text{-bpy})Pd\}_4\{\mathit{cis}\text{-}[(NH_3)_2Pt(\mathit{N1}\text{-}U\text{-}\mathit{N3,O4})_2]\}_2](NO_3)_4 \bullet 17H_2O$ (**24**) and $[\{(en)Pd\}_4\{\mathit{cis}\text{-}[(NH_3)_2Pt(\mathit{N1}\text{-}U\text{-}\mathit{N3,O4})_2]\}_2](NO_3)_4 \bullet 13.8H_2O$ (**24'**), show a *head-head* arrangement of the nucleobases. Possible isomerization processes of the species will also be discussed in detail. The fourteen-nuclear complex $[\{(en)Pd\}_{10}(U\text{-}\mathit{N1,N3,O4})_2(U\text{-}\mathit{N1,N3,O2,O4})_6\{\mathit{cis}\text{-}[(NH_3)_2Pt]\}_4](NO_3)_{12} \bullet 30\ H_2O$ (**28'**) shows several different types of metal environments and therefore, there are several ways of its formation feasible.

It appears that the stoichiometry of the first species formed (PtPd or Pt_2Pd, Scheme 44) is central to the various routes of formation and probably also the routes of interconversion.

Possible pathways to different compounds are depicted in the Scheme 44. Metal coordination positions at the nucleobases (N(1) and N(3)) are indicated.

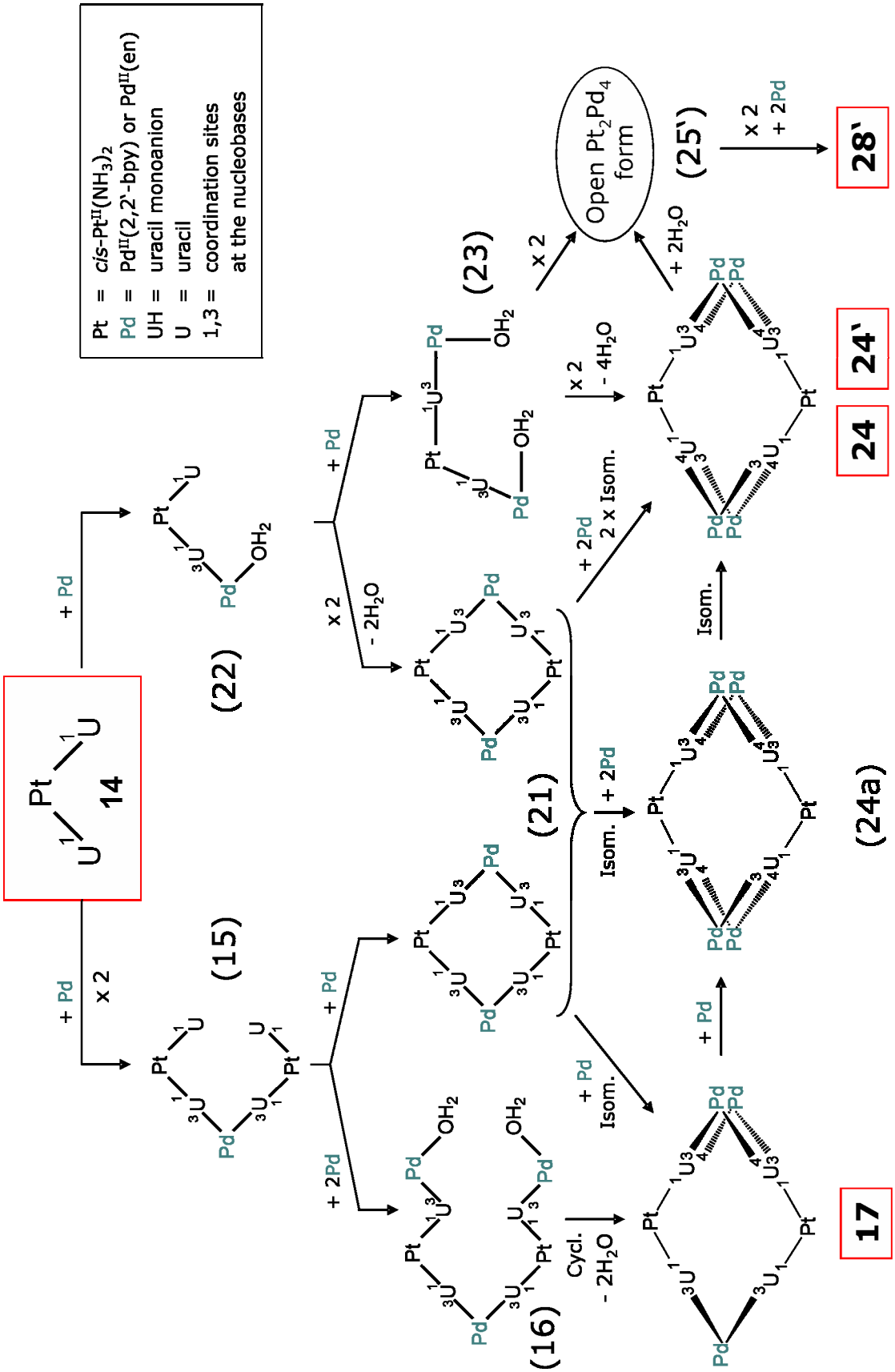

Scheme 44: Schematic diagram of the reactivity patterns and feasible interconversion mechanisms to account the formation of structurally characterized species in the **14**/a_2Pd^{II} system (a_2 = 2,2'-bpy or en). For more details, see Schemes 45-46.

As can be seen on the left side of the Scheme 44, formation of **15** is the result of two anionic **14b** being cross-linked by a $Pd^{II}a_2$ entity via the N(3) positions of the uracilate dianions. The subsequent formation of **17** could take place from the "open" complex 15 upon addition of two Pd^{II} moieties to the N(3) sites of the terminal uracilate ligands to give 16, followed by *head-tail* ring closure. On the other hand, addition of only a single Pd^{II} entity to 15, might leads to the formation of the closed tetramer 21.

Alternatively, the cyclic complex 21 could conceivably form by a dimerization of the PtPd species (22), as is indicated on the right side of Scheme 44. Formation of the pentanuclear compound **17** could also take place by a further addition of one Pd entity to the Pt_2Pd_2 species (21), followed by isomerization to a *head-tail* arrangement.

The intermediate compound 23 is the result of the reaction of one Pd^{II} entity at the deprotonated N(3) positions of the uracil dianions in the dinuclear compound 22. A posterior dimerization of compound 23 could lead to the formation of the hexanuclear compound **24**.

There are several routes that could lead to the formation of **24**. In Scheme 45 three possible pathways as well as the interconversion mechanisms of the species are depicted.

In the first one (Scheme 45, left), addition of one Pd entity to the free O(4) sites of the uracilate ligands in **17** leads to compound 24a with *head-head/head-tail* arrangements. Posterior isomerization of 24a to *head-tail/head-tail* arrangements gives **24**.

The second possibility (Scheme 45, center) involves the formation of a pentanuclear box (17a) from the tetranuclear compound 21, resulting in a *head-head* arrangement of the nucleobases. Attachment of yet another Pd entity to the O(4) positions of the uracilate dianions in 17a leads to the hexanuclear species 24b with *head-head/head-head* arrangements. Assuming two isomerization steps to *head-tail* arrangements at boh sides, formation of **24** is feasible.

The third pathway (Scheme 45, right), which involves a dimerization of the trinuclear species 23, has already been discussed.

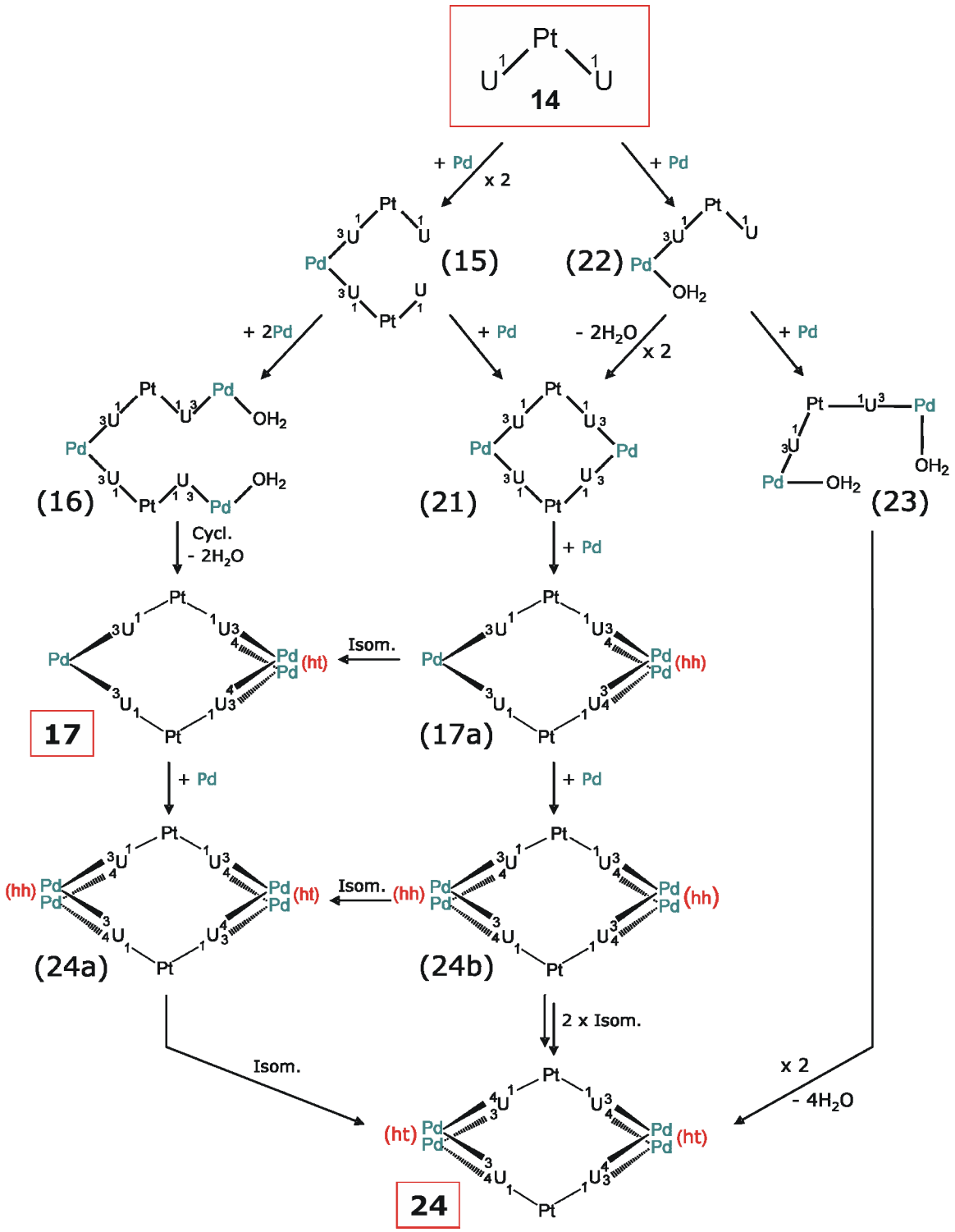

Scheme 45: Proposed pathways from **14** to **17** and **24**.

The main difference between the **14**/Pd^{II}(2,2'-bpy) on ane hand and the **14**/Pd^{II}(en) system on the other is the formation of compound **28'** in the latter.

The "open" species 23' is derived from two Pd^{II}(en) entities cross-linked by an entity of the starting compound **14**. As can be seen in Scheme 46, a dimerization of 23' could take place, leading to the formation of a Pt_2Pd_4 species (25') with a *head-tail* arrangement of the Pd_2 unit. A further dimerization of the hexanuclear species 25' could give a large closed macrocycle Pt_4Pd_8 (27'), in which two pairs of Pd entities are a *head-head* arrangement of the nucleobases and the other two pairs of Pd entities involve a *head-tail* arrangement. The orientation of the nucleobases in the cycle allows the addition of another two Pd^{II}(en) moieties at the exocyclic O(2) positions of the uracil dianions also adopting a *head-head* arrangement (**28'**). Addition of any further palladium entity does not seem to be possible.

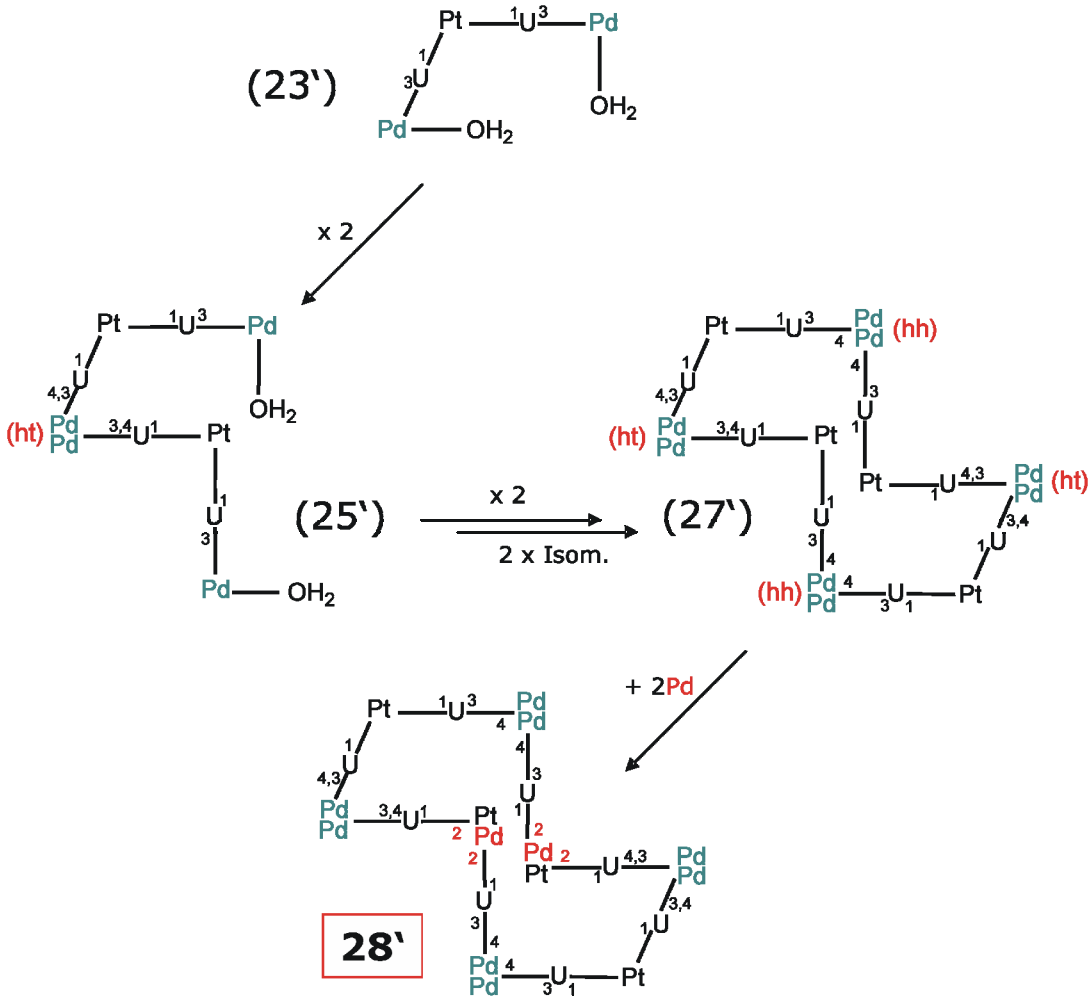

Scheme 46: Proposed pathway of the formation of **28'**.

7 Summary

The compound *cis*-Pt(UH-*N1*)$_2$(NH$_3$)$_2$•2H$_2$O (**14a**) reacted with Pd^{II}(2,2'-bpy), Pd^{II}(en) and Pd^{II}(tmeda) entities to give different products. The estabilished structures of the isolated complexes helped to understand the reactivity patterns of these systems. Some compounds discussed in this chapter were characterized by ^{1}H NMR spectroscopy. In Table 15 the ^{1}H NMR resonances (δ, D$_2$O) of the aromatic uracil protons of **14** as well as its derivatives with Pd^{II}(2,2'-bpy) and Pd^{II}(en) are given.

Table 15: ^{1}H NMR resonances (δ, D$_2$O) of aromatic nucleobase protons of **14b** and adducts of **14** with Pd^{II}(2,2'-bpy) and Pd^{II}(en), with no differentiation of protonation state of uracil (U) considered.

	H(6)U	H(5)U	Others	pD
14	7.50 7.65	5.51 5.60	- -	13.3 6-8
17	7.59 7.64	5.63 5.74	7.17-8.35 (bpy)	7.65
24	7.63	5.95	7.18-8.20 (bpy)	6.30
24'	7.36	5.49	2.70-3.0 (en)	5.66

In most cases, metallacalix[4]arenes were obtained and their solution behavior was studied.

With the mixed-nucleobase starting compound [Pt(UH-*N1*)(CH$_2$-*N3*)(en)]$^+$ (**1**) composed of two different nuclebases (uracil and cytosine), there are numerous possible combinations for the reaction with additional metal entities. Two different connectivities are possible depending on the coordination sites at the nucleobases. The starting compound *cis*-[Pt(U-*N1*)$_2$(NH$_3$)$_2$]$^{2-}$ (**14**) consists of only

one type of nucleobase (uracil bonded to platinum via N(1)), hence no differentiation in the sequence of the nucleobases is possible.

The Pd^{II}(2,2'-bpy) entity reacts with **14** to give a hexanuclear metallacalix[4]arene composed of four Pd entities and two platinum entities (**24**). It was found that the Pd^{II}(2,2'-bpy) entities are stacked in two corners of the cylce giving a *head-tail* arrangement of the nucleobases. Isolation of the pentanuclear compound **17** suggests a possible way to **24**. Complex **17** consists of one Pd^{II}(2,2'-bpy) moiety less than **24**, hence forms a pentanuclear metallacalix[4]arene. Two of the Pd^{II}(2,2'-bpy) metal fragments are stacked in a corner of the cycle leading to a *head-tail* arrangement of the nucleobases. The third Pd entity is bonded to each of the uracilate dianions via the N(3) position of the nucleobase. Therefore, an isomerization process that leads to the formation of **24** is proposed (Scheme 47).

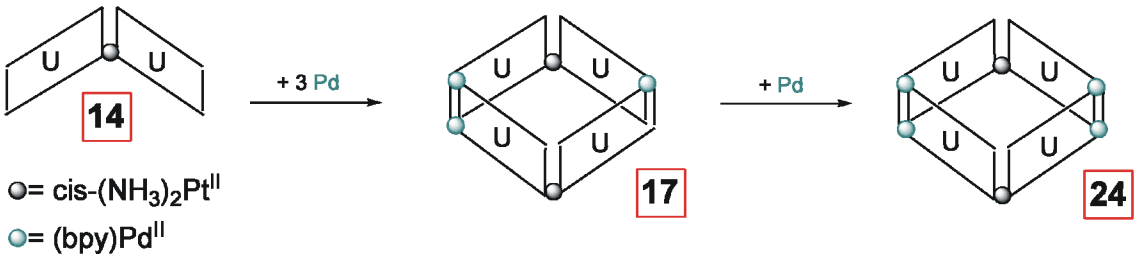

Scheme 47: : Schematic representation of relationship of the structurally characterized compounds in system **14**/Pd^{II}(2,2'-bpy).

In the case of the Pd^{II}(en) moiety, a hexanuclear metallacalix[4]arene closely related to **24** was isolated, in which the Pd^{II}(en) metal fragments are in two corners of the cycle leading to *head-tail* arrangement of the uracilate dianions (**24'**). None of the intermediate compounds observed in the ^{1}H NMR spectrum could be isolated for this system. However, a second complex (**28'**)could be isolated and characterized by X-ray crystallography from the **14**/Pd^{II}(en) system. **28'** turned out to be a 14-nuclear cycle. The solution behavior of **24'** and **28'**, as well as their solid state structures, provided some idea about the pathways of formation of **28'**. It was found that **28'** can formally be derived from two molecules of **24'** by addition of more Pd metal fragments (Scheme 48).

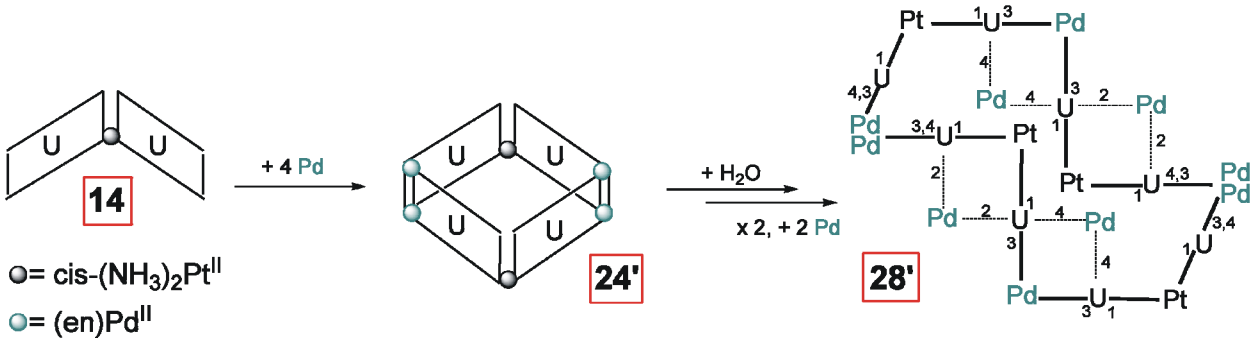

Scheme 48: : Schematic representation of relationship of the structurally characterized compounds in the system **14**/Pd^{II}(en).

The use of the Pd^{II}(tmeda) entity gave a mixture of different products, which could not be isolated.

All compounds isolated for the **14**/$Pd^{II}a_2$ systems show an *1,3*-alternate configuration of the uracil nucleobase. Therefore, it does not come as a surprise to see that all attempts with regard to a host-guest chemistry with **24** failed. The size of the complex cavity is simply too small.

Chapter III:
Attempts to Obtain a Metallacalix[3]arene with Unsubstituted Uracil

1 Introduction

As has been outlined at the beginning of this thesis, self-assembled metallomacrocycles presently receive a great deal of attention. The possibility of combining *cis*-protected metal entities and N-heterocycles with flexible bond angles to build metal analogues of calix[n]arenes with n = 3,[65,72,74,129-131] 4,[38,39,62,66-70] 6[64,71], has previously been shown. The Navarro group[74] has reported the synthesis of these macrocycles involving *cis*-protected palladium (II) metal fragments with 2-pyrimidinol derivatives and 4,7-phenanthroline. This starting materials can lead to the formation of a wide variety of species, such as trinuclear, tetranuclear and hexanuclear species. Such complex reaction mixture resulted, among others, in the formation of the trinuclear metallacalix[3]arene $[Pd_3(en)_3(\mu\text{-N,N'-4,6-dimethyl-2-pymo})(\mu\text{-N,N'-4,7-phen})_2]^{5+}$. In favourable cases, selection of a specific product can be achieved by appropriately chosen reaction conditions, stoichiometry and pyrimidine functionalisation.[73]

A goal of this thesis was the formation of a metallacalix[3]arene composed of a metal fragment such as a Pt^{II} or Pd^{II} entity and an unsubstituted nucleobase.

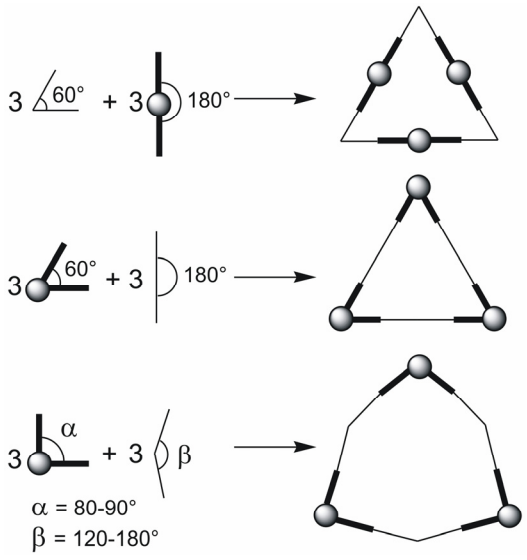

Scheme 49: Possible synthesis that lead to the formation of molecular triangles.

As outlined by Puddephatt et al.,[65] molecular triangles can be obtained in three different ways shown in the Scheme 49. These three methods involve the combination of metal units as well as bridging ligands with different bond angles, which lead to the formation of different kinds of molecular triangles.

In our case, the strategy of forming the molecular triangle is a combination of a metal entity with 90° bond angle and an organic ligand with 120° bond angle (Scheme 49, bottom). This situation is ideally met by d^8 square planar metal fragments, like *cis*-$Pt^{II}(NH_3)_2$, Pt^{II}(en), Pd^{II}(en) or Pd^{II}(2,2'-bpy) and pyrimidine nucleobases like uracil.

The number of examples corresponding to the situation sketched in Scheme 46, bottom, is very rare. To the best of our knowledge there are only two examples in the literature:

The existence of Pd_3-macrocycles, such as the bowl-like molecular triangle [{Pd-(bu_2bpy)(μ-pm)}]$^{3+}$ (with pm as the deprotonated form of 4(3H)-pyrimidone (Hpm) and bu_2bpy = 4,4'-di-*tert*-butyl-2,2'-bipyridine), was reported by Puddephatt et al.[65] in 2002.

Only two years ago, Krebs et al.[131] reported another interesting compound. The pentanuclear complex [$Pt_5(dpk)_2(dpkOH_2)_3(U)_3$]$^{4+}$ is composed of five Pt^{II}(dpk) entities (with dkp = 2,2'-dipyridylketone) and three uracilate dianions. The complex consists of a Pt_3 core unit, which involves the endocyclic N(1) and N(3) coordination sites of the nucleobases. Two additional Pt^{II}(dkp) entities are bonded to the exocyclic O(4) and O(2) positions of two uracilate ligands.

2 Results and discussion

The goal of this part of the work was the preparation of a molecular triangle, composed of *cis*-$M^{II}a_2$ (with a_2 = $(NH_3)_2$, (en) or (bpy) and M = Pt^{II} or Pd^{II}) and, as bridging ligand, unsubstituted uracil.

Several strategies of formation were considered and carried out with different metal fragments, which will be explained below.

First of all, the self-assembly of Pt^{II}(en) or Pd^{II}(en) entitites with uracilate dianion in aqueous solution was investigated.

$$x[MCl_2(en)] + UH_2 + 2\ NaOD \xrightarrow{D_2O}$$

M = Pt^{II}, Pd^{II}
x = 2, 3, 4

The product formation was followed in each case by ^{1}H NMR spectroscopy. Strongly basic conditions were applied. In the case of Pt^{II}(en), the reactions were carried out for x = 2, 3, 4 at 40°C and at 80°C for several days. When two equivalents of $PtCl_2$(en) are present at pD > 13 and the solution is stirred for 4 days at 80°C, no reaction takes place. It is to be assumed that the uracil dianion can not react with the hydroxo species $Pt(OH)_2$(en) as a consequence of the known inertness of Pt-OH groups. At a pD of approximately 9 and x = 3, the appearance of new signals is observed, but the major part of the free uracilate ligand remains unreacted. Only when x = 4 and after 6 days at 40°C, the set of signals corresponding to the free nucleobase has disappeared and a mixture of products is present in solution.

In addition it was tried to react Pd^{II}(en) with uracil nucleobase under basic conditions, this time with x = 2 and at 40°C. After one day, the signals corresponding to the free uracil nucleobase could no longer be detected and several sets of new signals were observed in the spectrum. The new signals remained in the spectrum after several days, but they could neither be assigned to any compound nor could any of the compounds be isolated.

As it was not possible to isolate any self-assembled products, the next idea was to isolate an intermediate like $[(a_2M^{II})_2(U)]$, which can possibly lead to the formation of a metallacalix[3]arene upon addition of compound **14**, as outlined in Scheme 50.

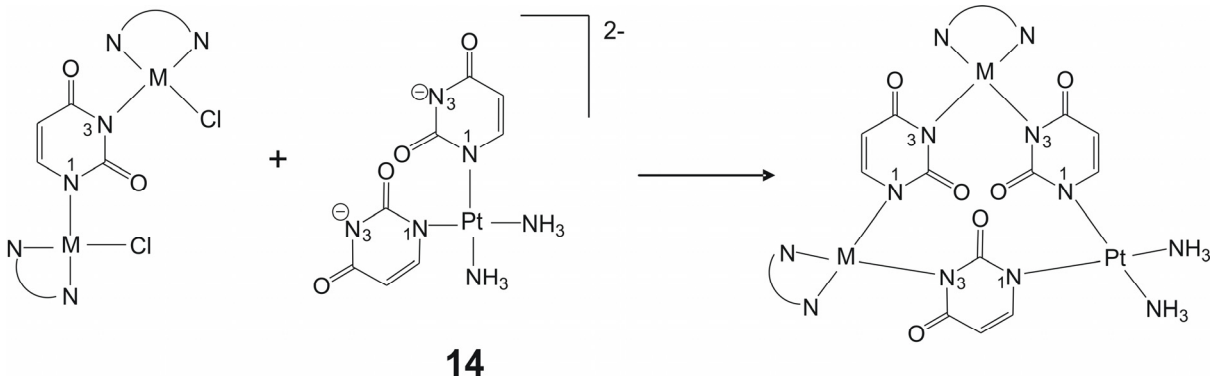

Scheme 50: Proposed synthesis of a metallacalix[3]arene.

To this end, it was attemped to prepare $[\{(en)_2M^{II}\}_2(U)]$ by reacting the 1:1 complex $[MCl(en)(DMF)]^+$ with uracilate in a DMF/water mixture (1:1) according to:

$$2\ [MCl(DMF)(en)]^+ \quad + \quad KUH \bullet \tfrac{1}{2}\ H_2O \xrightarrow{DMF\text{-}d^7/D_2O}$$

$$M = Pt^{II}, Pd^{II}$$

The reaction (M = Pt) was followed by ^{1}H NMR spectroscopy over a period of several days. However, no changes were observed in the spectrum. The same reaction was carried out at 40°C, but only an accelerated isotopic exchange of the H5-uracil resonance by deuterium was detected. A third reaction was carried out with M = Pd at room temperature. After 30 minutes the signals of the uracilate ligand as well as additional sets of resonances were observed in the spectrum. There are no spectral changes within the following six days, only an isotopic exchange was observed. This reaction at 40°C gives the same result as at room temperature, but with an accelerated isotopic exchange. Unfortunatelly, none of the products detected in the ^{1}H NMR spectra could be isolated.

The next strategy was to synthesize the intermediate [{(en)$_2$M^{II}}$_2$(U)] derived from the neutral compound PtCl(UH-*N1*)(en)•H$_2$O[41] by addition of the M^{II}(en) entity in aqueous solution. As a general method, the reactions were carried out under strongly basic conditions to deprotonate the N(3) position of PtCl(UH-*N1*)(en)•H$_2$O. Three different kinds of reactions were performed.

$$\text{PtCl(UH-}N1\text{)(en)}\bullet H_2O + MCl_2(en) \xrightarrow{D_2O}$$

$$\text{PtCl(UH-}N1\text{)(en)}\bullet H_2O + [MCl(D_2O)(en)]^+ \xrightarrow{D_2O}$$

$$\text{PtCl(UH-}N1\text{)(en)}\bullet H_2O + x\,[M(D_2O)_2(en)]^{2+} \xrightarrow{D_2O}$$

M = Pt^{II}, Pd^{II}

x = ¼, ½, 1, 2

Addition of PtCl$_2$(en) to a solution of PtCl(UH-*N1*)(en)•H$_2$O at pD>13 was followed by ^{1}H NMR spectroscopy. After 4 days at 40°C only the isotopic exchange of the H5 proton of PtCl(UH-*N1*)(en)•H$_2$O by deuterium could be detected.

Next, the reaction of [PtCl(D$_2$O)(en)]$^+$ with PtCl(UH-*N1*)(en)•H$_2$O under strongly basic conditions was carried out at 40°C for four days, but in this case also no reaction was detected. On the other hand, [PdCl(D$_2$O)(en)]$^+$ reacts with the PtCl(UH-*N1*)(en)•H$_2$O. The reaction took place at room temperature and likewise at 40°C. In both cases a mixture of several products was observed in the spectrum, which could not be isolated.

Finally the addition of [Pd(D$_2$O)$_2$(en)]$^{2+}$ to an aqueous solution of PtCl(UH-*N1*)(en)•H$_2$O was carried out. Since many possible products can be formed the reaction was performed at different ratios. The ^{1}H NMR spectra at strongly basic conditions are shown in Figure 68.

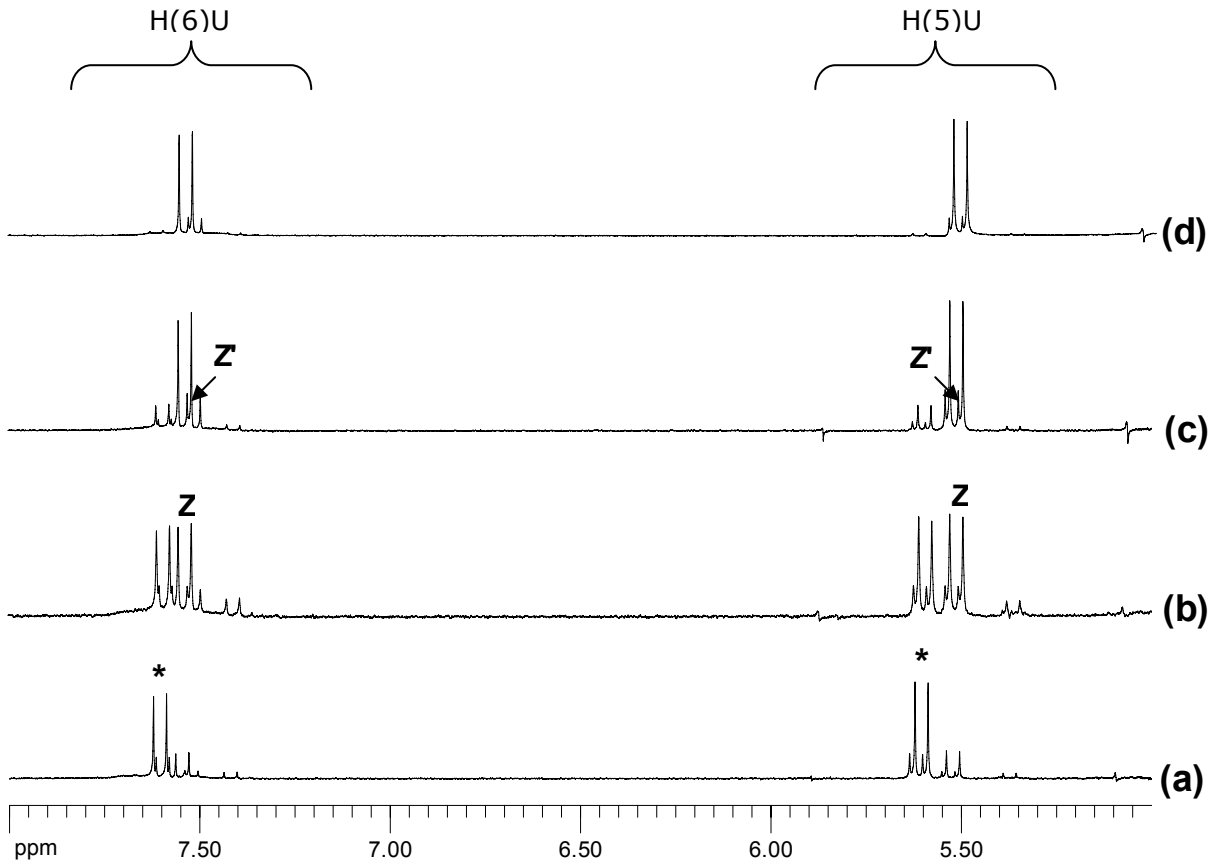

Figure 68:Low field position of ^{1}H NMR spectra of the reaction of [(en)Pt(UH-*N1*)Cl] H_2O (*****) with $[Pd(D_2O)_2(en)]^{2+}$ in D_2O at pD>13 where r = Pt:Pd is
(a) r = 0.25,
(b) r = 1:0.5,
(c) r = 1:1,
(d) r = 1:2.

At r = 1:0.25 (Figure 68a), the resonances corresponding to PtCl(UH-*N1*)(en)•H_2O and formation of different new products can be observed in the spectrum. When the ratio was increased to 1:0.5 (Figure 68b), the signals assigned to the starting compound PtCl(UH-*N1*)(en)•H_2O (5.63 ppm and 7.62 ppm for H(5)- and H(6)-uracil protons, respectively) remained in the spectrum and at least four different products could be detected. In the third case (Figure 68c), one equivalent of the Pd^{II}(en) aqua species was added to a solution of PtCl(UH-*N1*)(en)•H_2O and a rapid reaction took place. The result was a mixture of the starting compound, secondary products and a major species (Z) with ^{1}H NMR resonances at 5.51 ppm and 7.54 ppm. Finally, at r = 1:2 the resonances corresponding to PtCl(UH-*N1*)(en)•H_2O disappeared and the major product observed at r = 1:1 was predominant in solution (Figure 68d). Surprisingly,

compound Z does not remain stable in solution. After one day, another species (Z'), with chemical shifts of 5.52 ppm and 7.51 ppm, is the main product (Figure 69b). Z' could already be detected in small amounts at the beginning of the reactions.

After one day under strong basic conditions, the pD of the reaction of PtCl(UH-*N1*)(en)•H_2O with two equivalents of $[Pd(D_2O)_2(en)]^{2+}$ was decreased to 7.32 (Figure 69). The ^1H NMR spectrum shows again a mixture of different species (Figure 69c). The new products can be due to the hydroxo species of the free Pd^{II}(en) entity, which is present in excess and therefore can lead to the formation of various products when reacting with the starting compound. Even under these conditions, not a single compound can be isolated from the solution.

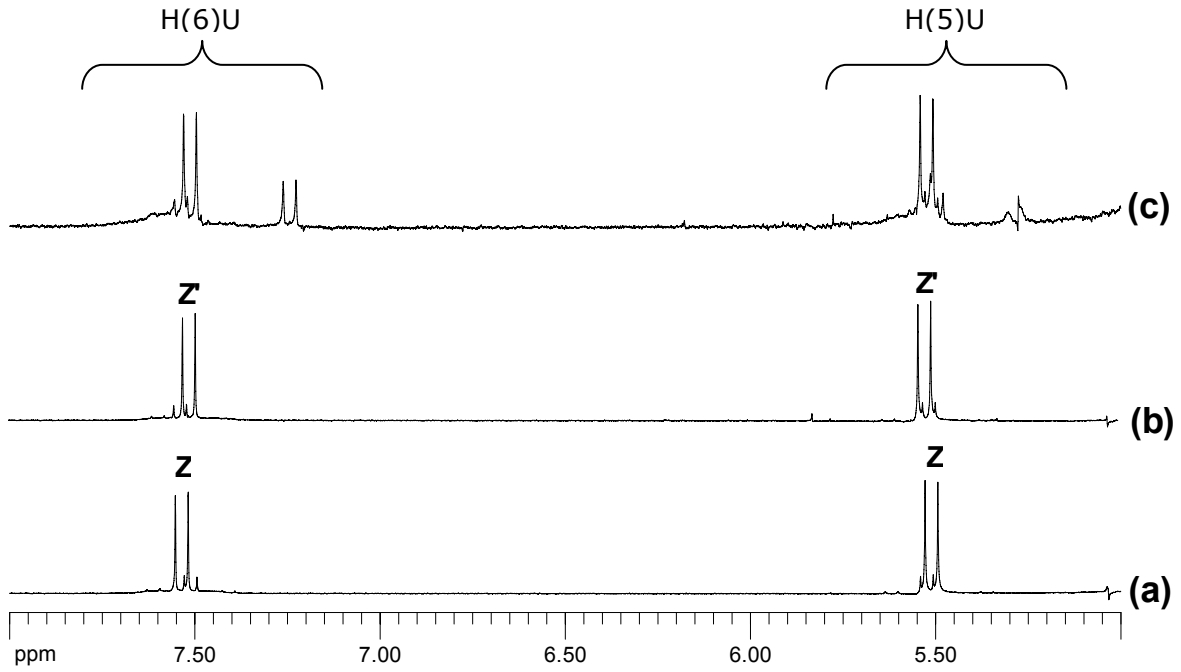

Figure 69: Low field section of ^1H NMR spectra recorded during the reaction of PtCl(UH-*N1*)(en)•H_2O with 2 equiv.of $[Pd(D_2O)_2(en)]^{2+}$ in D_2O:
(a) Immediately after dissolving (pD>13),
(b) After 1d (pD>13),
(c) After 1d (pD = 7.32).

To isolate Z', the basic solution was kept in a closed crystallization dish at 4 °C for several days, but neither a precipitate nor crystals were formed under these conditions.

3 Summary

Different ways of formation were investigated to obtain the desired metallacalix[3]arene with unsubstituted uracil. The proposed syntheses discussed in this chapter were unsuccessfull. One reason for this result can be the high pH of the reactions and the resulting inertness of the $Pd^{II}(OH)_2(en)$ entity.

D EXPERIMENTAL SECTION

1 Instrumentation and Methods

1.1 pH/pD Measurements

The pH values were measured with the help of a glass electrode Typ "SenTix Mic" on a pH meter WTW Walheim "Ino-Lab pH Level 1". The pD values of the solutions in D_2O were determined by addition of 0.4 units to the uncorrected pH meter reading (pH^*).[132] Due to the limitations of the AgCl glass electrode, it was not possible to obtain reliable measurements at pH values close to 14.

1.2 NMR Spectroscopy

One-dimensional ^1H NMR spectra were recorded on a Varian mercury 200 FT NMR and/or on a Bruker DRX 400 spectrometer. One-dimensional ^1H NOE spectra as well as two-dimensional ^1H, ^1H NOESY and ^1H, ^{13}C COSY spectra were recorded on a Varian Inova 600. TSP (sodium-3-(trimethylsilyl)-propanesulfonate) (δ= 0 ppm) or TMA (tetramethylammonium tetrafluoroborate) (δ= 3.18ppm) were used as internal standards in D_2O. All of the samples were measured in collaboration with Prof. Dr. Burkhard Costisella and Annette Danzmann and were processed using MestReC.[133]

1.3 IR Spectroscopy

IR spectra were recordered on a Bruker IFS 28 spectrometer. Measurements (KBr pellets) were carried out from 250 to 4000 cm^{-1}. The spectra were processed with Opus-IR.

1.4 Elemental Analysis

Elemental analyses were performed on a CHNS-932 Element Analyzer by Markus Hüffner.

1.5 ESI-Mass Spectrometry

The mass spectrometric experiments were performed on a Bruker APEX IV FT-ICR mass spectrometer equipped with a superconducting 7 Tesla magnet and an Apollo ESI source utilizing a nickel-coated glass capillary with a 0.5 mm inner diameter. This ESI source had three differential pumping stages. Ions were continuously generated from 150 μM solutions of the sample in water/methanol (ca. 1:1) which was introduced into the source with a syringe pump (Cole Parmer Instruments, Series 74900) at flow rates of ca. 3 μL/min. The ions were then introduced into the FT-ICR analyzer cell, which was operated at pressures below 10^{-10} mbar, and detected by a standard excitation and detection sequence. In the APEX IV, the ICR cell is a cylindrical "infinity" cell with equipotential-line-segmented trapping plates. For each measurement 32 – 256 scans were averaged to improve the signal-to-noise ratio. The measurements were done by Prof. Dr. Christoph Schalley (Berlin).

1.6 X-Ray Crystallography

Data collection was carried out on an Enraf-Nonius Kappa CCD diffractometer using graphite-monochromated Mo-Kα radiation (λ= 0.7169Å).[134] The measurements recorded at low temperature (150K) were carried out using a "Oxford Cryostream 700".[135] Data reduction and cell refinement were performed using the programs DENZO and SCALE-PACK[136] or with the program EvalCCD.[137,138] All of the structures were solved by standard Patterson methods[139] and refined by full-matrix least-squares methods based on F^2 using the SHELXTL-PLUS[140] and SHELXL-97[141] programs. All non-hydrogen atoms of the crystals, if not specified, were refined anisotropically and all of the hydrogen atoms except those of the water molecules were included in geometrically calculated positions. Absorption corrections were carried out with the program SADABS.[142] The distances and angles were calculated by using PLATON[106] and the CIF files[143] were generated using the Software WinGX.[144] The graphics were generated using Ortep-3,[145] POV-Ray[146] and Diamond 3[147] programs. The crystal structures were solved in collaboration with Dr. Eva Freisinger (Zurich).

2 General Work Descriptions

2.1 Starting Materials

The following compounds were purchased: K_2PtCl_4 and K_2PdCl_4 (Heraeus), $PdCl_2$ (Heraeus), 9-Methylguanine (Kemogen, Konstantz), Adenosine Monophosphate (Sigma), Cytosine (CH_2) and Uracil (UH_2) (Fluka), and 2,2'-bipyridine (Aldrich). The following starting compounds were synthesized according to published methods: *cis*-$PtCl_2(NH_3)_2$,[148] $PtCl_2$(en),[149] $PdCl_2$(en),[150] $PdCl_2$(2,2'-bpy),[150] and $PdCl_2$(tmeda)[151]. The Pt^{II} complexes PtCl(UH-*N1*)(en)•H_2O,[41] *cis*-Pt(UH-*N1*)$_2$$(NH_3)_2$•$2H_2O$[41] (**14a**), *cis*-$Na_2$[Pt(UH-*N1*)$_2$$(NH_3)_2$]•$10H_2O$[41] and [Pt(UH-*N1*)($CH_2$-*N3*)(en)]$ClO_4$•$3H_2O$[84] (**1a**) were also synthesized according to published methods.

2.2 Synthesis of Compounds

2.2.1 [Pt(UH-*N1*)(CH_2-*N3*)(en)]NO_3•$3.5H_2O$ (1b)

The compound was synthesized in analogy to [Pt(UH-*N1*)(CH_2-*N3*)(en)](ClO_4)•$3H_2O$ (**1a**). PtCl(UH-*N1*)(en)•H_2O (302 mg, 0.720 mmol) and cytosine (CH_2) (80 mg, 0.72 mmol) were mixed in H_2O (80 mL) and kept at 40°C for 4 d. After filtration from some elemental Pt, $AgNO_3$ (120 mg, 0.706 mmol, 0.98 eq) was added to the filtrate. The mixture was stirred in the dark for 12 h at room temperature, then filtered from AgCl and concentrated by rotary evaporation to 1/10 of the original volume. Then $NaNO_3$ (61 mg, 0.72 mmol) was added and the solution kept at 4 °C. Within 7 d, colorless cubes formed, which were filtered off, washed with a small amount of ice water and dried in air. X-ray crystal structure analysis showed the water content of freshly prepared **1b** to be higher (3.5-hydrate) than the one obtained by elemental analysis.

Yield: 217 mg (0.377 mmol, 53%)
Elemental analysis:
(calc. for 2 molecules of crystal water)
$C_{10}H_{16}N_8O_6Pt$•$2H_2O$
M = 575.4 g/mol

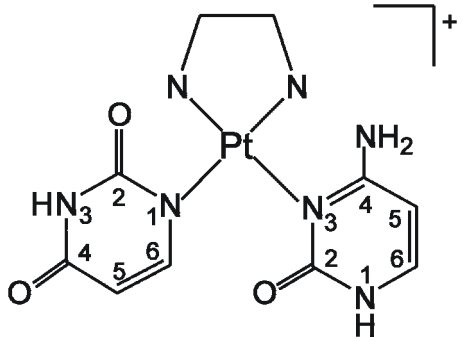

Calc.: C 20.8% H 3.5% N 19.5%
Found: C 20.6% H 3.3% N 19.5%

^{1}H NMR: (D_2O, pD = 5.45, δ in ppm)
7.59 (d, 1H, H6U); 7.51 (d, 1H, H6C); 6.02 (d, 1H, H5C); 5.61 (d, 1H, H5U); 2.73 (m, 4H, en)

2.2.2 [(2,2'-bpy)Pd{(en)Pt(UH-*N1*)(*N3*-CH-*N1*)}$_2$](ClO$_4$)(NO$_3$)•4.9H$_2$O (2a)

$PdCl_2$(2,2'-bpy) (13.3 mg, 39.6 μmol) was added to a solution of $AgClO_4$•H_2O (16.2 mg, 77.9 μmol, 1.96 eq) in 4 mL of H_2O and the suspension was stirred overnight in the dark at 40 °C. The resulting mixture was kept in an ice bath for 1 h, then the AgCl precipitate was centrifuged off. Subsequently, [Pt(UH-*N1*)(CH_2-*N3*)(en)](ClO_4)•3H_2O (**1a**) (50.5 mg, 80.0 μmol) was added to the filtrate and the mixture was stirred for 1 d. The pH was adjusted to 10 by means of NaOH (1 M) and a small amount of $NaNO_3$ was added to improve crystallization. The solution was kept at room temperature in a crystallization dish covered with parafilm. After 3 d, a mixture consisting of **1a** (40%) and light yellow crystals of **2a** (60%) were determined by ^{1}H NMR spectroscopy. The crystals corresponding to **2a** were separated by hand under a microscope. X-ray crystallography showed a slightly lower H_2O content (4.9-hydrate) than the elemental analysis.

Elemental analysis:
(calc. for 6 molecules of crystal water)
$C_{30}H_{38}N_{17}O_{13}ClPt_2Pd$•6$H_2O$
M = 1484.8 g/mol
Calc.: C 24.2% H 3.4% N 16.0%
Found: C 24.1% H 3.5% N 16.2%

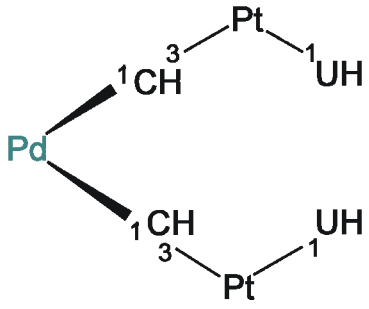

^{1}H NMR: (D_2O, pD = 8.55, δ in ppm)
8.00 (d, 2H, 2 x H6C); 6.82 (d, 2H, 2 x H6U); 6.11 (d, 2H, 2 x H5C); 5.11 (d, 2H, 2 x H5U); 8.42-7.60 (m, 8H, 2,2'-bpy); 2.6-2.8 (m, 8H,2 x en)

2.2.3 [{(2,2'-bpy)Pd}$_3${(en)Pt(*N1*-U-*N3,O4*)(*N3*-CH-*N1*)}$_2$](NO$_3$)$_4$•5H$_2$O (4) and [{(2,2'-bpy)Pd}$_4${(en)Pt(*N1*-U-*N3,O4*)(*N3*-HC-*N1,O2*)}$_2$](NO$_3$)$_6$ (7)

$PdCl_2$(2,2'-bpy) (302 mg, 0.901 mmol) was added to a solution of $AgNO_3$ (301 mg, 1.77 mmol, 1.96 eq.) in 15 mL of H_2O and the suspension was stirred overnight in the dark at 40 °C. The resulting mixture was kept in an ice bath for 1 h before the AgCl precipitate was filtered off. Then [Pt(UH-*N1*)(CH_2-*N3*)(en)](ClO_4)•3H_2O (**1a**) (283 mg, 0.448 mmol) was added to the filtrate, and the solution was stirred for 2 d. The pH was adjusted to 7.5 by means of NaOH (1 M) and the solution was kept at 4 °C. After roughly two weeks the solution was dry and a mixture of a small amount of orange blocks (**7**) and a large amount of yellow precipitate was recovered. The orange crystals **7** were separated by hand under a microscope and turned out to be suitable for X-ray crystallography. The yellow precipitate was recrystallized from 0.1 M KNO_3 solution and the pH was adjusted to 9.5 by addition of NaOH (1 M). After 3 d at room temperature crystals suitable for X-ray crystal structural analysis were obtained (**4**).

[{(2,2'-bpy)Pd}$_3${(en)Pt(*N1*-U-*N3,O4*)(*N3*-CH-*N1*)}$_2$](NO$_3$)$_4$•5H_2O (**4**):

Yield: 134 mg (63.0 μmol, 28%)

Elemental analysis:

(calc. for 8 molecules of crystal water)

$C_{50}H_{52}N_{24}O_{18}Pt_2Pd_3$•8$H_2O$

M = 2130.7 g/mol

Calc.: C 28.1% H 3.2% N 15.8%

Found: C 28.1% H 3.1% N 15.9%

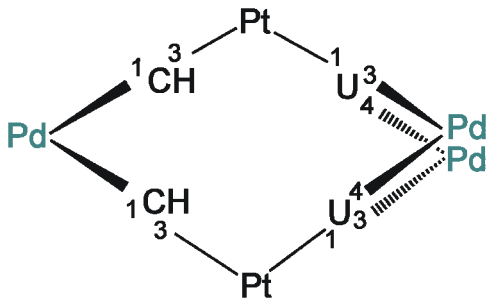

^{1}H NMR: (D_2O, pD = 9.23, δ in ppm)

7.97 (d, 2H, 2 x H6C); 7.50 (d, 2H, 2 x H6U); 6.16 (d, 2H, 2 x H5C); 5.70 (d, 2H, 2 x H5U); 8.43-7.15 (m, 24H, 3 x 2,2'-bpy); 2.70-2.73 (m, 8H, 2 x en)

[{(2,2'-bpy)Pd}$_4${(en)Pt(*N1*-U-*N3,O4*)(*N3*-HC-*N1,O2*)}$_2$](NO$_3$)$_6$ (**7**):

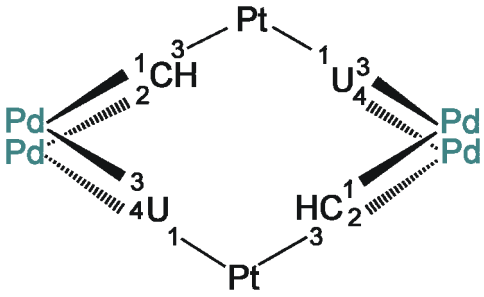

^{1}H NMR: (D_2O, pD = 4.4, δ in ppm)

8.26 (d, 2H, 2 x H6C); 7.81 (d, 2H, 2 x H6U); 6.33 (d, 2H, 2 x H5C); 6.07 (d, 2H, 2 x H5U); 8.42-7.16 (m, 32H, 4 x 2,2'-bpy); 2.73-2.70 (m, 8H, 2 x en)

2.2.4 [{(2,2'-bpy)Pd}{(en)Pt(*N1*-U-*N3*)(*N3*-HC-*N1*)}]$_4$(NO$_3$)$_3$(ClO$_4$) •56.1H$_2$O (9)

$PdCl_2$(2,2'-bpy) (102 mg, 0.303 mmol) was added to a solution of $AgNO_3$ (102 mg, 0.597 mmol, 1.96 eq.) in 4 mL of H_2O. The suspension was stirred overnight in the dark at 40 °C. The resulting mixture was kept in an ice bath for 1 h before the AgCl precipitate was filtered off. Then [Pt(UH-*N1*)(CH_2-*N3*) (en)](ClO$_4$)•3H$_2$O (**1a**) (189 mg, 0.300 mmol) was added to the filtrate, and the solution was stirred for 2 d. The pH was adjusted to 10.5 using NaOH (1 M) and the solution was kept closed at 4 °C. After roughly four weeks yellow crystals suitable for X-ray crystallography were obtained in low yield. Further concentration of the filtrate resulted in a precipitate which, according to its ^{1}H NMR spectrum, consisted mostly of **4**.

Elemental analysis:

(calc. for 16 molecules of crystal water)

$C_{80}H_{88}N_{39}O_{25}ClPt_4Pd_4$•16$H_2O$

M = 3525.52 g/mol

Calc.: C 27.2% H 3.4% N 15.5%

Found: C 27.1% H 3.1% N 15.5%

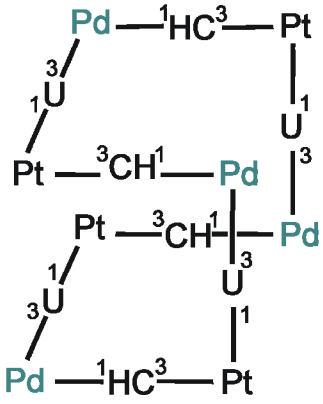

^{1}H NMR: (D_2O, δ in ppm)
7.68 (d, 4H); 6.54 (d, 4H); 5.61 (d, 4H); 5.10 (d, 4H);8.33 (d, 4H, 2,2'-bpy); 8.30 (d, 4H, 2,2'-bpy); 8.24 (t, 4H, 2,2'-bpy); 8.16 (t, 4H, 2,2'-bpy); 7.99 (d, 4H, 2,2'-bpy); 7.53 (t, 4H, 2,2'-bpy); 7.35 (d, 4H, 2,2'-bpy); 6.94 (t, 4H, 2,2'-bpy); 2.79-2.70 (m, 16H, 4 x en)

2.2.5 [{(en)Pt(*N1*-U-*N3*)(*N3*-CH-*N1*)}{(en)Pd}]$_2$(NO$_3$)$_2$ (Y')

$PdCl_2$(en) (20.2 mg, 85.1 μmol) was added to a solution of $AgNO_3$ (28.5 mg, 168 μmol, 1.96 eq) in 5 mL of H_2O and the suspension was stirred overnight in the dark at 40 °C. The resulting mixture was kept in an ice bath for 1 h before the AgCl precipitate was centrifuged off. Then [Pt(UH-*N1*)(CH_2-*N3*)(en)](NO_3)•3.5H_2O (**1b**) (98.1 mg, 0.170 mmol) was added to the filtrate, and the solution was stirred for 2 d. The pH was adjusted to 7.4 by means of NaOH (1 M) and the solution was kept at room temperature. After 10 d a mixture (40.3 mg) was recovered as a precipitate. According to its ^{1}H NMR spectrum, the mixture consisted of **1b** (10 %) and **Y** (90%). The mixture was characterized by ESI mass spectrometry.

^{1}H NMR: (D_2O, pD= 7.68, δ in ppm)
7.81 (d, 2H, 2 x H6C); 6.73 (d, 2H, 2 x H6U); 5.94 (d, 2H, 2 x H5C); 5.00 (d, 2H, 2 x H5U); 2.80-2.69 (m, 16H, 4 x en)

2.2.6 [{(en)Pt(U-*N1,N3,O2*)(C-*N1,N3,N4*)}$_2$}{(en)Pd}$_4$]$^{6+}$ (12')

Some crystals of [{enPt}$_2$(U-*N1,N3,O2,O4*)$_2$(C-*N1,N3,N4,O2*)$_2$}{enPd}$_6$](NO_3)$_5$(ClO_4)$_3$•21.2H_2O (**13'**) (see below) were disolved in D_2O. The ^{1}H NMR of the solution showed the decomposition of **13'** into **12'**, which was not isolated.

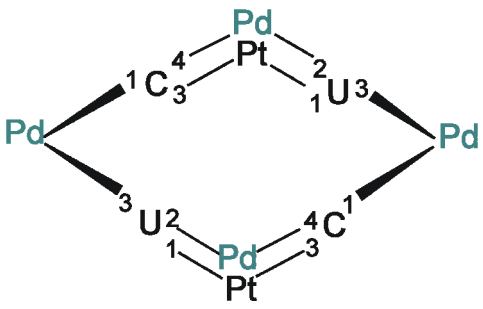

^{1}H NMR: (D_2O, pD = 4.65, δ in ppm)
7.67 (d, 2H, 2 x H6C); 7.17 (d, 2H, 2 x H6U); 5.83 (d, 2H, 2 x H5C); 5.35 (d, 2H, 2 x H5U); 2.5-3.0 (m, 24H, 6 x en)

2.2.7 [{(en)Pt(U-*N1,N3,O2,O4*)(C-*N1,N3,N4,O2*)}$_2${(en)Pd}$_6$](NO$_3$)$_5$(ClO$_4$)$_3$•21.2H$_2$O (13')

$PdCl_2$(en) (213 mg, 0.898 mmol) was added to a solution of $AgNO_3$ (301 mg, 1.77 mmol, 1.96 eq) in 15 mL of H_2O and the suspension was stirred overnight in the dark at 40 °C. The resulting mixture was kept in an ice bath for 1 h before the AgCl precipitate was filtered off. Then [Pt(UH-*N1*)(CH_2-*N3*) (en)](ClO_4)•3H_2O (**1a**) (284 mg, 0.450 mmol) was added to the filtrate, and the solution was stirred for 2 d. The pH was adjusted to 4.1 by means of NaOH (1 M) and the solution was kept at 4 °C in an open beaker. Within 7 d, orange cubes of **13'** formed, which were filtered off, washed with a small amount of ice water and dried in air. The crystals turned out to be suitable for X-ray crystallography.

Yield: 216 mg (79.0 μmol, 35%)
Elemental analysis:
(calc. for 10 molecules of crystal water)
$C_{32}H_{74}N_{31}O_{33}Cl_3Pt_2Pd_6$•10$H_2O$
M = 2736.3 g/mol

Calc.:	C 14.1%	H 3.4%	N 15.8%
Found:	C 14.1%	H 3.6%	N 15.7%

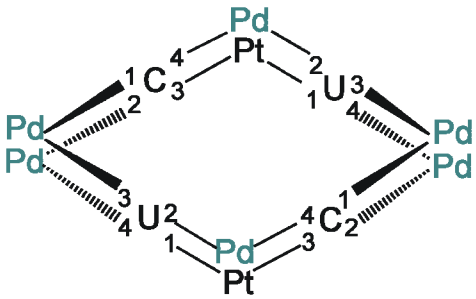

^{1}H NMR: (D_2O, pD = 5.32, δ in ppm)
7.90 (d, 2H, 2 x H6C); 7.36 (d, 2H, 2 x H6U); 5.66 (d, 2H, 2 x H5C); 5.62 (d, 2H, 2 x H5U); 2.5-3.2 (m, 32H, 8 x en)

2.2.8 *cis*-Na$_2$[Pt(U-*N1*)$_2$(NH$_3$)$_2$]•10H$_2$O (14b)

cis-Pt(UH-*N1*)$_2$(NH_3)$_2$•2H_2O (229 mg, 0.469 mmol) was added to 1.5 mL of a solution of NaOH (1 M). The suspension was centrifuged and the filtrate was kept in a closed crystallizing dish at 4 °C. After 10 d colorless blocks suitable for

X-crystallography formed, which were filtered off, washed with a small amount of ice water and dried in air.

Yield: 81 mg (0.12 mmol, 26%)

Elemental analysis:

(calc. for 10 molecules of crystal water)

$C_8H_{10}N_6O_4Na_2Pt \cdot 10H_2O$

M = 675.42 g/mol

Calc.: C 14.2% H 4.5% N 12.4%

Found: C 14.1% H 4.5% N 12.3%

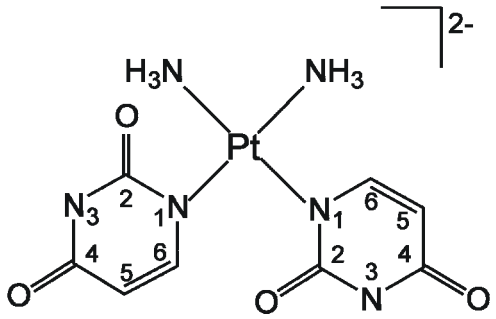

^{1}H NMR: (D_2O, pD = 13.3, δ in ppm)

7.50 (d, 2H, 2 x H6U); 5.51 (d, 2H, 2 x H5U)

^{1}H NMR: (D_2O, pD = 6.75, δ in ppm)

7.65 (d, 2H, 2 x H6U); 5.60 (d, 2H, 2 x H5U)

2.2.9 [{(2,2'-bpy)Pd}$_3${*cis*-[$(NH_3)_2$Pt(*N1*-U-*N3*)(*N1*-U-*N3,O4*)]}$_2$] $(NO_3)_2 \cdot 23.1H_2O$ (17)

To a suspension of $PdCl_2$(2,2'-bpy) (7.8 mg, 23 μmol) in 550 μL D_2O 45 μL of a $AgNO_3$ solution (1 M) in D_2O (45 μmol, 1.96 eq) were added and the suspension was stirred overnight in the dark at 40 °C. Afterwards, the resulting mixture was centrifuged and *cis*-Pt(UH-*N1*)$_2$$(NH_3)_2 \cdot 2H_2O$ (21 mg, 43 μmol) was added to the filtrate. The pD was adjusted to 13.3 using NaOD (10 M) and then the solution was stirred for 1 d. The suspension was centrifuged and the pD was adjusted to 5.6 using DNO_3 (1 M). After 1 d at room temperature orange cubes suitable for X-ray crystallography were obtained in low yield.

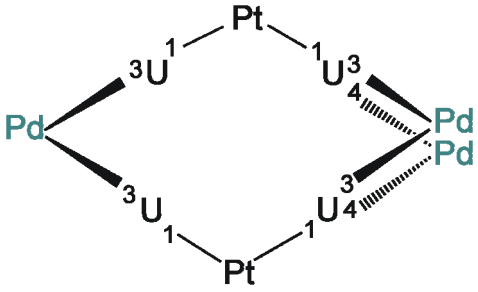

^{1}H NMR: (D_2O, pD= 8.85 , δ in ppm)
7.64 (d, 2H, H6U); 7.59 (d, 2H, H6U); 7.76 (d, 2H, H5U); 5.63 (d, 2H, H5U); 8.88-7.18 (m, 24H, 2,2'-bpy)

2.2.10 [{(2,2'-bpy)Pd}$_4${*cis*-[$(NH_3)_2$Pt(*N1*-U-*N3,O4*)$_2$]}$_2$]$(NO_3)_4$•17H_2O (24)

$PdCl_2$(2,2'-bpy) (338 mg, 1.01 mmol) was added to a solution of $AgNO_3$ (335 mg, 1.97 mmol, 1.96 eq) in 10 mL of H_2O and the suspension was stirred overnight in the dark at 40 °C. The resulting mixture was kept in an ice bath for 1 h before the AgCl precipitate was filtered off. Afterwards *cis*-Pt(UH-*N1*)$_2(NH_3)_2$•2H_2O (244 mg, 0.501 mmol) was dissolved in 5 mL of H_2O and the pD was adjusted to 13.2 by means of NaOH (1 M). The solution was added to the filtrate and it was stirred for 2 d. The resulting suspension was filtered off and the pH was adjusted to 5.5 by means of HNO_3 (1 M). After 4 d at 4 °C yellow rhombic blocks were obtained, which were filtered off, washed with a small amount of ice water and dried in air.

Yield: 193 mg (77.2 μmol, 31%)
Elemental analysis:
(calc. for 17 molecules of crystal water)
$C_{56}H_{52}N_{24}O_{20}Pt_2Pd_4$•17$H_2O$
M = 2503.28 g/mol
Calc.: C 26.8% H 3.4% N 13.4%
Found: C 26.7% H 3.2% N 13.4%

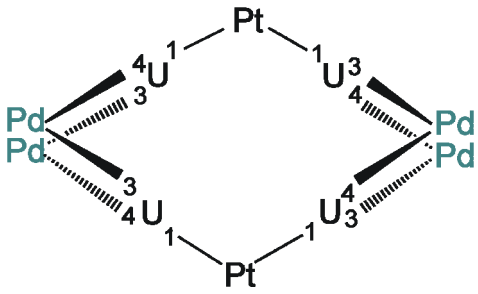

^{1}H NMR: (D_2O, pD= 6.30, δ in ppm)
7.63 (d, 4H, 4 x H6U); 5.95 (d, 4H, 4 x H5U); 8.28-7.22 (m, 32H, 4 x 2,2'-bpy)

2.2.11 [{(en)Pd}$_4${*cis*-[$(NH_3)_2$Pt(*N1*-U-*N3,O4*)$_2$]}$_2$]$(NO_3)_4$•13.8H_2O (24')

$PdCl_2$(en) (214 mg, 0.901 mmol) was added to a solution of $AgNO_3$ (301 mg, 1.77 mmol, 0.96 eq) in 10 mL of H_2O and the suspension was stirred overnight in the dark at 40 °C. The resulting mixture was kept in an ice bath for 1 h before

the AgCl precipitate was filtered off. Afterwards *cis*-Pt(UH-*N1*)$_2$(NH$_3$)$_2$•2H$_2$O (219 mg, 0.449 mmol) was dissolved in 5 mL of H$_2$O and the pD was adjusted to 13.5 by means of NaOH (1 M). The solution was added to the filtrate and it was stirred for 2 d. The resulting suspension was filtered off and the pH was adjusted to 8.5 by means of HNO$_3$ (1 M). The filtrate was concentrated in a water bath at 40 °C to a volume of roughly 4 mL. After 4 d at room temperature the solution was completely evaporated and orange crystals suitable for X-ray crystallography were obtained in low yield

Elemental analysis:
(calc. for 14 molecules of crystal water)
$C_{24}H_{52}N_{24}O_{20}Pt_2Pd_4 \cdot 14H_2O$
M = 2064.88 g/mol
Calc.: C 14.0% H 3.9% N 16.2%
Found: C 14.1% H 2.8% N 15.9%

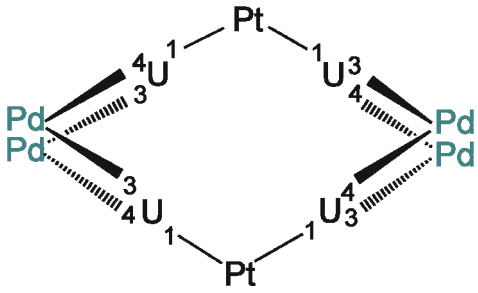

^{1}H NMR: (D$_2$O, pD= 5.66, δ in ppm)
7.36 (d, 4H, 4 x H6U); 5.49 (d, 4H, 4 x H5U); 2.70-3.0 (m, 16H, 4 x en)

2.2.12 [{(en)Pd}$_{10}$(U-*N1,N3,O4*)$_2$(U-*N1,N3,O2,O4*)$_6${*cis*-[(NH$_3$)$_2$Pt]}$_4$](NO$_3$)$_{12}$•30H$_2$O (28')

PdCl$_2$(en) (143 mg, 0.602 mmol) was added to a solution of AgNO$_3$ (200 mg, 1.18 mmol, 1.96 eq) in 5 mL of H$_2$O and the suspension was stirred overnight in the dark at 40 °C. The resulting mixture was kept in an ice bath for 1 h before the AgCl precipitate was filtered off. Afterwards, *cis*-Pt(UH-*N1*)$_2$(NH$_3$)$_2$•2H$_2$O (98.4 mg, 0.202 mmol) was dissolved in 2 mL of H$_2$O and the pD was adjusted to 13.3 by means of NaOH (1 M). The solution was added to the filtrate and it was stirred for 2 d. The resulting suspension was filtered off and the pH was adjusted to 9.1 by means of HNO$_3$ (1 M). The filtrate was concentrated in a water bath at 40 °C until only 4 mL were remained. After 4 d at room temperature the solution was completely evaporated and orange crystals suitable for X-ray crystallography were obtained in low yield.

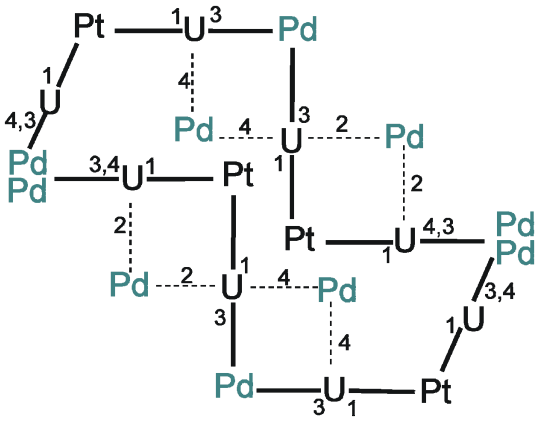

Elemental analysis:

(calc. for 30 molecules of crystal water)

$C_{52}H_{120}N_{56}O_{52}Pt_4Pd_{10}\cdot 30H_2O$

M = 4746.85 g/mol

Calc.:	C 13.1%	H 3.8%	N 16.5%
Found:	C 12.9%	H 3.0%	N 16.5%

E SUMMARY

1 English Version

Supramolecular transition metal chemistry has attracted a great deal of attention in the last years since self-assembly has proven to be a powerful tool for building two- and three-dimensional supramolecular units with diverse structures and properties. Particularly, the interest of this thesis includes the chemistry of metalla-analogues of the classical calix[n]arenes. In the metallacalix[n]arenes, metal fragments replace the methylene groups and likewise pyrimidine ligands replace the phenol rings of the calixarenes (Scheme S1). There is a structural and functional analogy between both types of compounds, however, the metal entities introduce a wide range of novel applications.

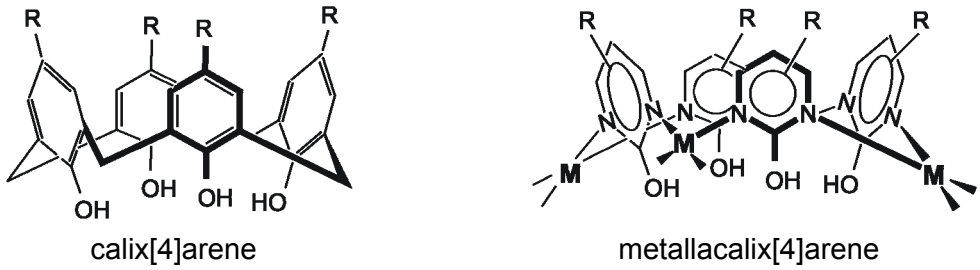

Scheme S1: Analogy between calix[4]arenes and metallacalix[4]arenes.

Square-planar metal centers *cis*-$M^{II}a_2$ (a_2 = 2,2'-bipyridine, ethylenediamine, *N,N,N',N'*-tetramethylethylenediamine, diammine, and M = Pt, Pd) and unsubstituted pyrimidine nucleobases (uracil, cytosine) have been applied in this work to synthetize metallacalix[n]arenes. Through the synthesis and the X-ray structural characterization of these complexes further information on their relationships and ways of formation has been obtained.

As described in the first chapter, a series of multinuclear, mixed-metal (Pt, Pd), mixed-nucleobase (uracil, cytosine) and in part, mixed-amine (2,2'-bpy, en) complexes has been characterized. In only one case, an open-chain compound could be isolated [(2,2'-bpy)Pd{(en)Pt(UH-*N1*)(*N3*-CH-*N1*)}$_2$](ClO$_4$)(NO$_3$)•4.9H$_2$O (**2a**), (Figure S1).

The other adducts derived from the reaction of the starting compound [(en)Pt(UH-*N1*)(CH_2-*N3*)]$ClO_4 \cdot 3H_2O$ (**1**) with Pd^{II}(2,2'-bpy) or Pd^{II}(en) moieties are cyclic compounds, hence metallacalix[n]arenes. Several examples with n = 4 have been characterized by X-ray crystallography, as well as an unprecedented one with n = 8, [{(2,2'-bpy)Pd}$_4${(en)Pt(*N1*-U-*N3*)(*N3*-HC-*N1*)}$_4$]$(NO_3)_3$ (ClO_4)•$56.1H_2O$ (**9**).

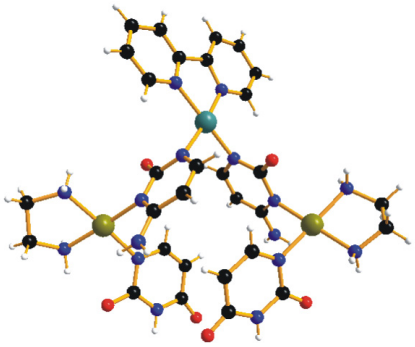

Figure S1: Crystal structure of one of the crystallographically independent cations of of compound **2a**.

The availability of exocyclic functions of the nucleobases, O(2) and O(4) in uracil as well as O(2) and N(4) in cytosine, capable of chelating additional square-planar metal fragments, permits formation of metallacalix[4]arenes with more metal entities bonded, namely a total of five in [{(2,2'-bpy)Pd}$_3${(en)Pt(*N1*-U-*N3,O4*)(*N3*-CH-*N1*)}$_2$]$(NO_3)_4$•$5H_2O$ (**4**), six in [{(2,2'-bpy)Pd}$_4${(en)Pt(*N1*-U-*N3,O4*)(*N3*-HC-*N1,O2*)}$_2$]$(NO_3)_6$ (**7**), and even eight in [{(en)Pt(U-*N1,N3,O2,O4*)(C-*N1,N3,N4,O2*)}$_2${(en)Pd}$_6$]$(NO_3)_5(ClO_4)_3$•$21.2H_2O$ (**13'**) (Figure S2).

Binding of these additional metal fragments can occur via exocyclic groups leading to a *head-head* arrangement (**7**, **13'**), or in a mixed fashion (endocyclic N, exocyclic O) leading to a *head-tail* arrangement, which is realized in **4**. Major structural differences between the characterized compounds are their different nucleobase connectivities, such as CUCU in **7**, **9**, **13'** or CUUC in **2a**, and **4**.

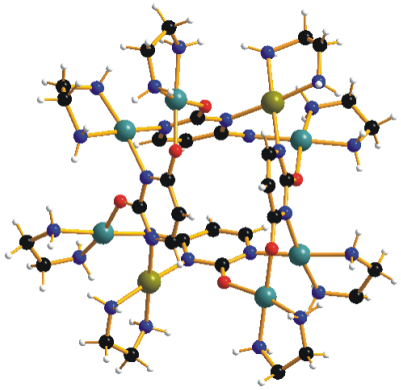

Figure S2: Crystal structure of the cation of compound **13'**.

The nucleobase connectivity is determined by three main factors:

- the binding pattern of the first Pd^{II} species that reacts with **1** (reaction at N(3)-uracil or N(1)-cytosine sites),
- the stoichiometry of the first species formed (PtPd or Pt_2Pd),
- the dimerization patterns of these early products.

Moreover, connectivities can also be reversed. Conversion of **7** to **4** (Figure S3), as well as conversion of **9** to **4** has been observed. Possible interconversion mechanisms are discussed. It is proposed that complex fragmentation with Pd-N and/or Pd-O (nucleobase) bond breakage takes place, while Pt-N bonds are kinetically robust.

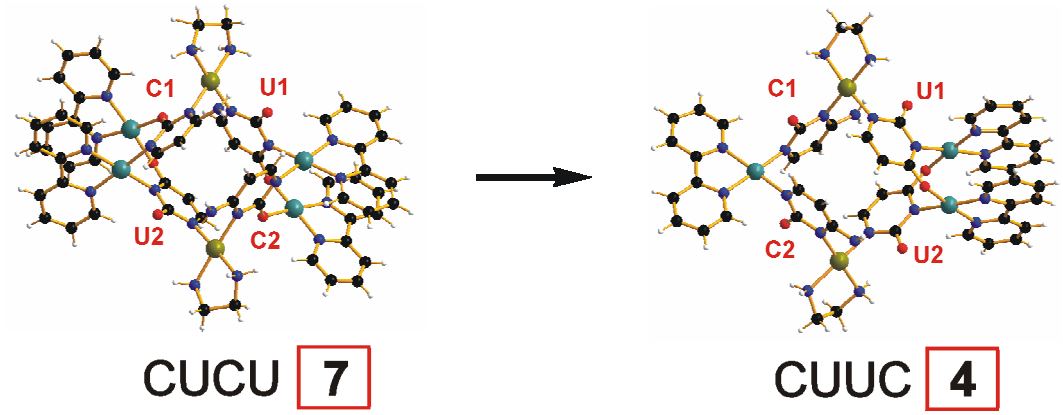

Figure S3: Crystal structures of the cations of **7** and **4**, in which the nucleobase sequences are indicated.

In the second chapter, four multinuclear, mixed-metal (Pt, Pd), mixed-amine (diammine, en, 2,2'-bpy) uracil complexes are described and characterized.

The adducts derived from the reaction of the starting compound *cis*-Pt(UH-*N1*)$_2$(NH$_3$)$_2$•H$_2$O (**14a**) with the square-planar metal fragments Pd^{II}(2,2'-bpy) or Pd^{II}(en) are again cyclic complexes. The two products, [{(2,2'-bpy)Pd}$_3${*cis*-[(NH$_3$)$_2$Pt(*N1*-U-*N3*)(*N1*-U-*N3,O4*)]}$_2$](NO$_3$)$_2$•23.1H$_2$O (**17**) and [{(en)Pd}$_4${*cis*-[(NH$_3$)$_2$Pt(*N1*-U-*N3,O4*)$_2$]}$_2$] (NO$_3$)$_4$•13.8H$_2$O (**24'**), have been characterized by X-ray crystallography. Compound **28'**, [{(en)Pd}$_{10}$(U-*N1,N3,O4*)$_2$(U-*N1,N3,O2,O4*)$_6${*cis*-[(NH$_3$)$_2$Pt]}$_4$](NO$_3$)$_{12}$•30H$_2$O, has been found to be a fourteen-nuclear complex. The three metallacalix[4]arenes (abbreviated Pt$_2$Pd$_3$ (**17**) and Pt$_2$Pd$_4$ (**24**, **24'**)) show additional metal entities bonded at the exocyclic O(4)-uracil positions, leading to a *head-tail* arrangement in all cases.

Interconversion of the species is allowed upon addition of more metal entities, suggesting that isomerization processes leading to different metal-nucleobase arrangements (namely, *head-head* or *head-tail*) can take place (see, e.g. conversion of **17** to **24**).

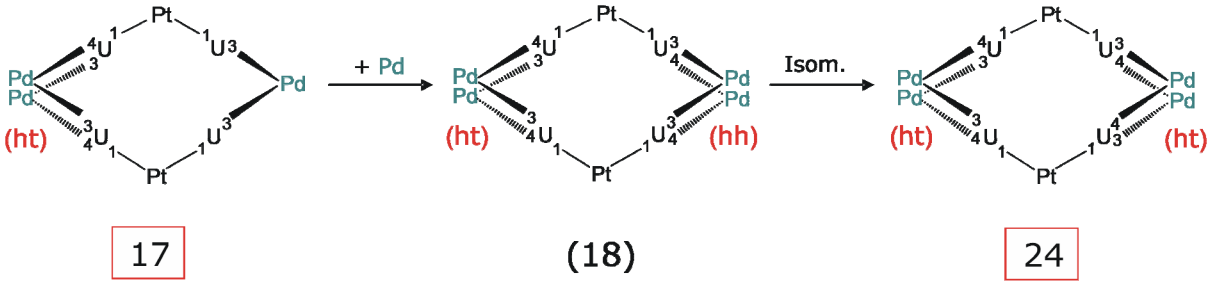

Scheme S2: Proposed conversion process of **17** to **24**.

On the other hand, loss of the Pd^{II} entities bonded to the exocyclic positions of the nucleobases, followed by complex fragmentation takes place, as has been seen for the conversion of **28'** to **24'**.

Several interconversion mechanisms are discussed in this thesis: The formation of metallacalix[n]arenes is likely to be reversible and proceeds under thermodynamic control. Therefore, these systems might be adequately described in terms of Dynamic Combinatorial Chemistry.

In all structurally characterized examples of metallacalix[4]arenes reported in this thesis (**4**, **7**, **13'**, **17**, and **24'**) the four nucleobases adopt a *1,3*-alternate conformation in the solid state, irrespective of the nucleobase connectivity. In the interior of the metallacalix[4]arenes no anion or solvent molecules were found. This feature seems to be due to the conformation adopted by the nucleobases, which does not permit any space for guest molecules in their cavities.

"Platinum Pyrimidine Blues", complexes derived from *cis*-$Pt^{II}(NH_3)_2$ with unsubstituted uracil, have received a great deal of attention due to their versatile properties and due to their, insufficiently understood behavior. In this thesis, *cis*-$Pd^{II}a_2$ entities have been used as faster reacting analogues of *cis*-$Pt^{II}(NH_3)_2$, which at the same time prevent Pt redox chemistry. In spite of the several questions about the "blues" which still remain unanswered, a better understanding of the structural complexity of these kinds of compounds has been obtained.

2 German Version

Supramolekulare Übergangsmetallchemie hat in den letzten Jahren große Aufmerksamkeit auf sich gezogen, da Selbstassoziation ein exzellenter Weg zur Erzeugung zwei- und drei dimensionaler supramolekularer Einheiten mit verschiedenen Strukturen and Eigenschaften ist. Von besonderem Interesse für diese Dissertation war die Chemie von Metall-Analoga der klassischen Calix[n]arene. In den Metallacalix[n]arenen ersetzen Metallfragmente die Methylengruppen, und gleicherweise ersetzen Pyrimidin-Liganden die Phenolringe der Calixarene (Schema S1). Es existiert daher eine strukturelle and funktionelle Analogie zwischen den beiden Typen von Verbindungen. Die Metalleinheiten führen zu einer großen Reihe von neuen Anwendungsmöglichkeiten.

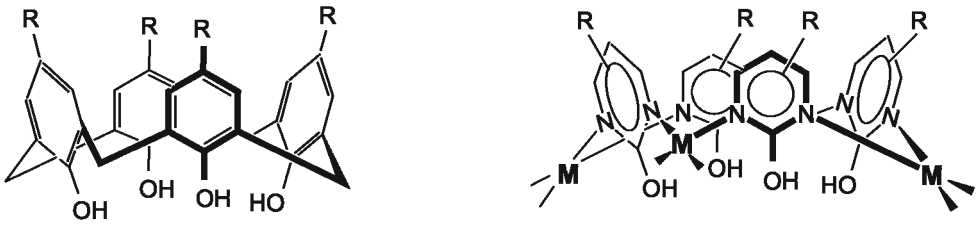

Schema S1: Analogie zwischen Calix[4]aren und Metallacalix[4]aren.

Für die Synthese der Metallacalix[n]aren wurden im dieser Arbeit quadratisch-planare Metallzentren *cis*-$M^{II}a_2$ (a_2 = 2,2'-Bipyridin, Ethylendiamin, *N,N,N',N'*-Tetramethylethylendiamin, Diammin) und unsubstituierte Pyrimidinenukleobasen (Uracil, Cytosin) verwendet. Durch Synthese und strukturelle Charakterisierung der Komplexe wurden weitere Informationen über die Verbindungen und die Reaktionenmechanismen ihre Entstehung erhalten.

Im ersten Kapitel wurden eine Reihe multinuklearer Komplexe mit verschiedenen Metallen (Pt, Pd) Nukleobasen (Uracil, Cytosin) und zum Teil auch verschiedenen Aminliganden (2,2'-bpy, en) charakterisiert. [(2,2'-bpy)Pd{(en)Pt(UH-*N1*)(*N3*-CH-*N1*)}$_2$](ClO_4)(NO_3)•4.9H_2O (**2a**) konnte als einziger offenkeltiger Vertreter isoliert werden (Abbildung S1).

Alle weiteren Addukte, die sich von Reaktionen der Ausgangsverbindung [(en)Pt(UH-*N1*)(CH_2-*N3*)]ClO_4·3H_2O (**1**) mit Pd^{II}(2, 2'-bpy) oder Pd^{II}(en) Baueinheiten ableiten lassen, sind cyclische Verbindungen. Es handelt sich um Metallacalix[n]arene. Mehrere Beispiele mit n = 4 wurden kristallographisch charakterisiert, ebenso wie ein Beispiel mit n = 8, nämlich [{(2,2'-bpy)Pd}$_4$}{(en)Pt(*N1*-U-*N3*)(*N3*-HC-*N1*)}$_4$]$(NO_3)_3$ (ClO_4)•56.1H_2O (**9**).

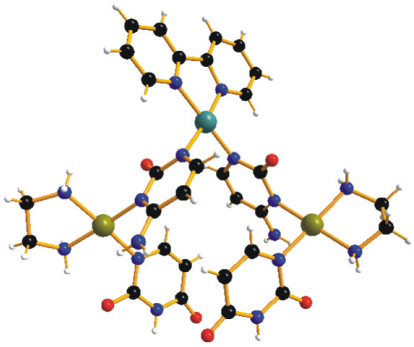

Abbildung S1: Kristallstruktur von einer der kristallographisch unabhängigen Kationen von Verbindung **2a.**

Die Verfügbarkeit der exocyclischen Funktionen der Nukleobasen (O(2) und O(4)) im Uracil bzw. O(2) und N(4) im Cytosin) können als Chelatbildner für zusätzliche quadratisch-planare Metallfragmente agieren und erlauben so die Bildung von Metallacalix[n]arenen, die mehrere Metalleinheiten binden. Das [{(2,2'-bpy)Pd}$_3$}{(en)Pt(*N1*-U-*N3,O4*)(*N3*-CH-*N1*)}$_2$]$(NO_3)_4$•5H_2O (**4**) enthält fünf Metalleinheiten, das [{(2,2'-bpy)Pd}$_4$}{(en)Pt(*N1*-U-*N3,O4*)(*N3*-HC-*N1,O2*)}$_2$]$(NO_3)_6$ (**7**) sechs und das [{(en)Pt(U-*N1,N3,O2,O4*)(C-*N1,N3,N4,O2*)}$_2$}{(en)Pd}$_6$]$(NO_3)_5(ClO_4)_3$•21.2H_2O (**13'**) sogar acht (Abbildung S2).

Diese zusätzlichen Metallfragmente können über die exocyclischen Gruppen binden und so zu einen Kopf-Kopf Anordnung (**7**, **13'**) oder in der gemischten Form (N-endocyclisch und O-exocyclisch) zu einer Kopf-Schwanz Anordnung (**4**) führen. Die unterschiedliche Reihenfolge der Nukleobasen, wie zum Beispiel CUCU in **7**, **9**, **13'** order CUUC in **2a**, und **4**, führt zu großen strukturellen Unterschieden zwischen den charakterisierten Verbindungen.

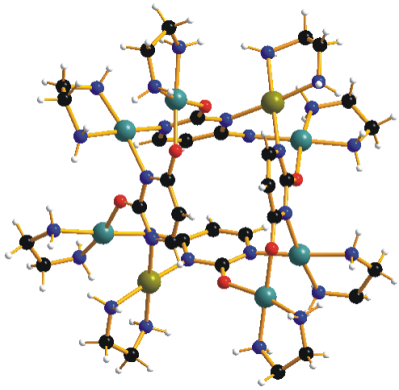

Abbildung S2: Kristallstructure des Kations von Verbindung **13'**.

Die Abfolge der Nukleobasen wird durch drei Hauptfaktoren bestimmt:

- Die Bindungsposition der ersten Pd^{II}-Species, die mit **1** reagiert (Reaktion an N(3)-Uracil oder N(1)-Cytosin),
- Die Stöchiometrie der ersten gebildete Species (PtPd oder Pt_2Pd),
- Das Dimerisierungschema der zu erst gebildeten Produkte.

Die Reihenfolge der Nukleobasen kann auch umgedreht werden. So wurde etwa die Umwandlung von **7** zu **4** (Abbildung S3) bzw. von **9** zu **4** beobachtet. Dernkbare Mechanismen der Umwandlung werden diskutiert. Die Fragmentierungsreaktion findet möglicherweise durch einen Bindungsbruch an Pd-N oder Pd-O Nukleobase-Bindungen statt, wohingegen die Pt-N-Bindungen kinetisch robust sind.

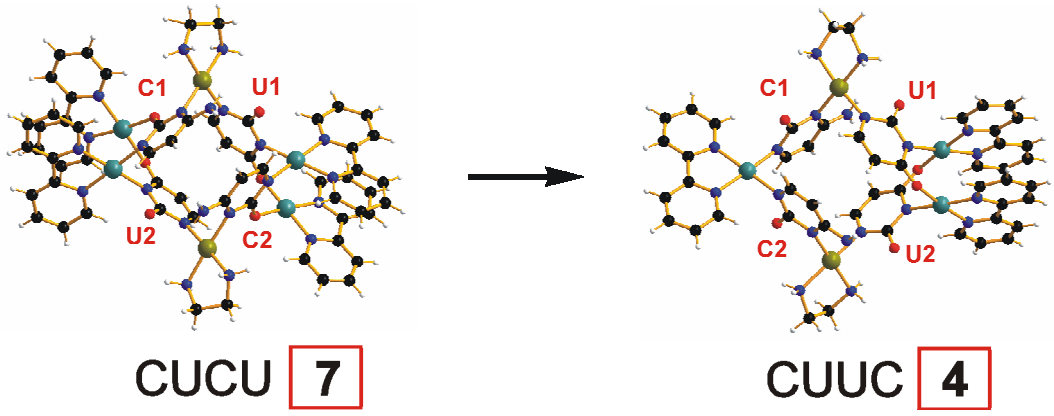

Abbildung S3: Kristallstrukturen der Kationen von **7** und **4**.
Die Abfolge der Nukleobasen ist ebenfalls angezeigt.

Im zweiten Kapitel wurden vier multinukleare Uracil Komplexe mit verschiedenen Metallen (Pt, Pd) und verschiedenen Aminliganden (Diammin, 2,2'-Bipyridin, Ethylendiamin) isoliert und charakterisiert.

Die Reaktion der Ausgangsverbindung *cis*-Pt(UH-*N1*)$_2$(NH_3)$_2$•H_2O (**14a**) mit den quadratisch-planaren Metallfragmenten Pd^{II}(2,2'-bpy) oder Pd^{II}(en) führt wiederum zu cyclischen Komplexen. Die beiden Produkte [{(2,2'-bpy)Pd}$_3${*cis*-[(NH_3)$_2$Pt(*N1*-U-*N3*)(*N1*-U-*N3,O4*)]}$_2$](NO_3)$_2$•23.1H_2O (**17**) und [{(en)Pd}$_4${*cis*-[(NH_3)$_2$Pt(*N1*-U-*N3,O4*)$_2$]}$_2$](NO_3)$_4$•13.8H_2O (**24'**) wurden strukturell charakterisiert. Verbindung[{(en)Pd}$_{10}$(U-*N1,N3,O4*)$_2$(U-*N1,N3,O2,O4*)$_6${*cis*-[(NH_3)$_2$Pt]}$_4$](NO_3)$_{12}$•30H_2O (**28'**) ist ein 14-nuklearer Komplex. Die drei

Metallacalix[4]arene (abgekürzt Pt_2Pd_3 (**17**) und Pt_2Pd_4 (**24**, **24'**)) besitzen zusätzliche Metalleinheiten, die an die exocyclische O(4)-Uracil Position gebunden sind und in jedem Fall zu einer Kopf-Schwanz Anordnung führen.

Die Umwandlung diese Species wird durch Zugabe weitere Metalleinheiten begünstigt. Möglicherweise finden Isomerisierungsprozess statt, die zu einer anderen Metall-Nukleobase Konformation (Kopf-Kopf zu Kopf-Schwanz) führen (zum Beispiel Umwandlung von **17** zu **24**).

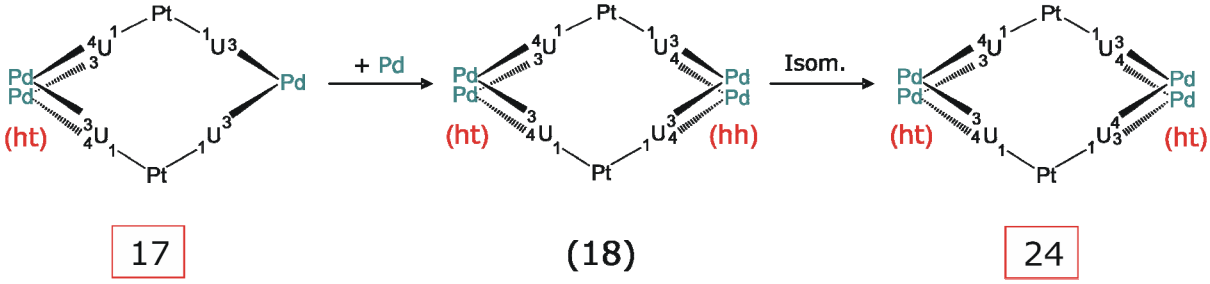

Schema S2: Vorgeschlagener Umwandlungsprozess von **17** zu **24**.

Andererseits erfolgt leicht ein Verlust solcher Pd^{II} Einheiten, die an exocyclische Positionen von Nukleobasen gebunden sind. Auschließend gibt es eine Komplexfragmentation, was auch bei die Umwandlung von **28'** zu **24'** beobachtet wird.

Verschiedene Umwandlungsmechanismen werden in dieser Arbeit diskutiert: Das Bilden von Metallacalix[n]arene ist wahrscheinlich reversibel und thermodynamisch kontrolliert. Daher könnten diese Systeme adäquat durch Konzepte der Dynamischen Kombinatorischen Chemie beschrieben werden.

In allen strukturell charakterisierten Beispielen von Metallacalix[n]arenen, die in diesem Arbeit beschrieben werden (**4**, **7**, **13'**, **17** und **24'**), findet man eine 1,3-alternierende Anordnung der Nukleobasen in der festen Phase. Die Anordnung ist unabhängig von der Reihenfolge der Nukleobasen. In Inneren der Metallacalix[4]arene werden weder Anionen noch Lösungsmittelmoleküle gefunden. Der Grund hierfür ist die von den Nukleobasen angenommene Konformation, die in dem Hohlraum keinen Platz für Gast-Moleküle lässt.

Bei “Platin-Pyrimidin-Blau” handelt es sich um Komplexe, die aus der Reaktion von *cis*-$Pt^{II}(NH_3)_2$ mit unsubstituerten Uracil entstehen. Aufgrund ihrer vielseitigen Eigenschaften und ihres bis heute nicht voll verstandenen Reaktionsverhaltens haben sie große Aufmerksamkeit auf sich gezogen. In dieser Arbeit wurden *cis*-$Pd^{II}a_2$ Einheiten als schneller reagierende Analoga für *cis*-$Pt^{II}(NH_3)_2$ verwendet. Zugleich kann hierdurch Pt-Redoxchemie vermieden werden. Ungeachtet der vielen Fragen zu “Platin-Pyrimidin-Blau”, die immer noch unbeantwortet sind, konnte das Wissen über die strukturelle Komplexität dieser Art von Verbindungen erweitet werden.

3 Spanish Version

La Química Supramolecular de los metales de transición ha despertado gran atención en los últimos años ya que el autoensamblaje ha provado ser una poderosa herramienta para construir unidades supramoleculares bi- y tridimensionales con diversas estructuras y propiedades. En particular, el interés de ésta tesis incluye la química de metal-análogos de los clásicos calix[n]arenos. En los metalcalix[n]arenos, fragmentos metálicos reemplazan los grupos metilenos y los ligandos orgánicos reemplazan los anillos fenoles de los calix[n]arenos (Esquema S1). Entre ambos tipos de compuestos existe una analogía estructural y funcional, sin embargo las entidades metálicas introducen un amplio rango de nuevas aplicaciones.

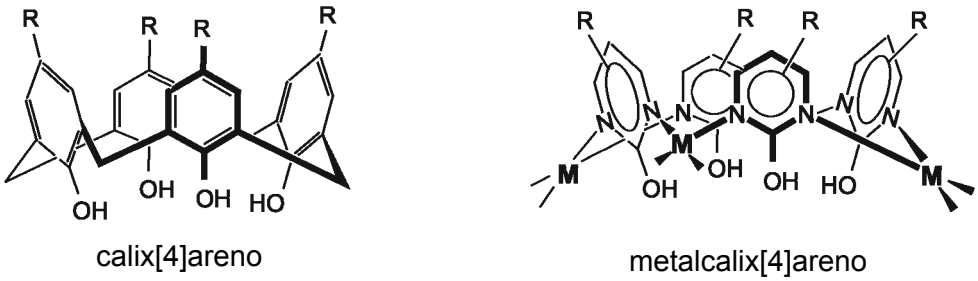

Esquema S1: Analogía entre calix[4]arenos y metalcalix[4]arenos.

Centros metálicos plano cuadrados como *cis*-$M^{II}a_2$ (a_2 = 2,2'-bipiridina, etilendiamina, N,N,N',N'-tetrametiletilendiamina) y nucleobases pirimidínicas no substituidas (uracilo, citosina) han sido usados en este trabajo para sintetizar metalcalix[n]arenos. A través de la síntesis y la caracterización estructural por difracción de rayos X de estos complejos, se ha obtenido informacion adicional sobre sus mechanismos de formación e intercoversión.

En el primer capítulo han sido caracterizados una serie de complejos multinucleares con differentes metales (Pt, Pd), nucleobases (uracilo, citosina) y en parte también con differentes ligandos nitrogenados (2,2'-bpy, en). Sin embargo, sólo un compuesto intermedio se ha podido aislar [(2,2'-bpy)Pd{(en)Pt(UH-*N1*)(*N3*-CH-*N1*)}$_2$](ClO_4)(NO_3)•4.9H_2O (**2a**) (Figura S1).

Los otros productos derivados de la reacción del compuesto de partida [(en)Pt(UH-*N1*)(CH_2-*N3*)]$ClO_4 \cdot 3H_2O$ (**1**) con Pd^{II}(2, 2'-bpy) o con Pd^{II}(en) son compuestos cíclicos, que presentan la estructura de los metalcalix[n]arenos. Varios ejemplos con n = 4 han sido caracterizados por difracción de rayos X, así como un ejemplo con n = 8, [{(2,2'-bpy)Pd}$_4${(en)Pt(*N1*-U-*N3*)(*N3*-HC-*N1*)}$_4$] $(NO_3)_3(ClO_4) \cdot 56.1H_2O$ (**9**).

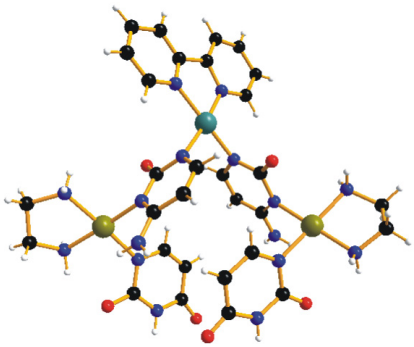

Figura S1: Estructura cristalina de uno de los dos cristallográficamente independientes cationes del compuesto **2a.**

La disponibilidad de los groupos exocíclicos de las nucleobases (O(2) y O(4) en el uracilo así como O(2) y N(4) en la citosina) capaces de adicionar fragmentos metálicos plano cuadrados, permite la formación de metalcalix[n]arenos con más entidades metálicas enlazadas. El compuesto [{(2,2'-bpy)Pd}$_3${(en)Pt(*N1*-U-*N3,O4*)(*N3*-CH-*N1*)}$_2$]$(NO_3)_4 \cdot 5H_2O$ (**4**) contiene cinco centros metálicos, [{(2,2'-bpy)Pd}$_4${(en)Pt(*N1*-U-*N3,O4*)(*N3*-HC-*N1,O2*)}$_2$]$(NO_3)_6$ (**7**) contiene seis y [{(en)Pt(U-*N1,N3,O2,O4*)(C-*N1,N3,N4,O2*)}$_2${(en)Pd}$_6$]$(NO_3)_5(ClO_4)_3 \cdot 21.2H_2O$ (**13'**) incluso ocho (Figura S2).

Estos fragmentos metálicos adicionales pueden enlazarse a través de los grupos exocíclicos dando lugar a una configuración cabeza-cabeza (**7**, **13'**) o bien en forma mixta (N-endocíclico, O-exocíclico) dando lugar a una configuración cabeza-cola (**4**). La diferente conectividad de las nucleobases, como por ejemplo CUCU en **7**, **9**, **13'** o bien CUUC en **2a** y **4**, da lugar a grandes diferencias estructurales entre los compuestos caracterizados.

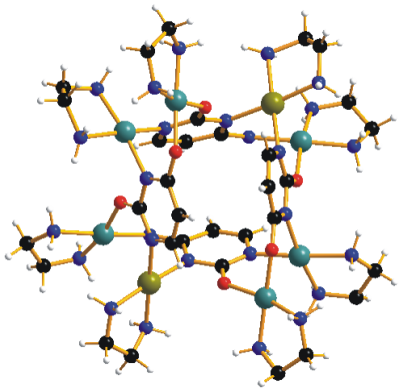

Figura S2: Estructura cristalina del catión del compuesto **13'.**

La conectividad de las nucleobases está determinada por tres factores principales:

- la posición de enlace del primer Pd^{II} que reaciona con **1** (reacción en N(3) del uracilo o en N(1) de la citosina),
- la estequiometría de las primeras especies formadas (PtPd o Pt_2Pd),
- la dimerización de los primeros productos formados.

La conectividad de las nucleobases puede ser también invertida. La conversión de **7** en **4** así como la conversión de **9** en **4** han sido observadas y los mecanismos de interconversión han sido discutidos. La reacción de fragmentación tiene lugar probablemente a través de la ruptura de los enlaces Pd-N o Pd-O (nucleobase) ya que los enlaces Pt-N son cinéticamente robustos.

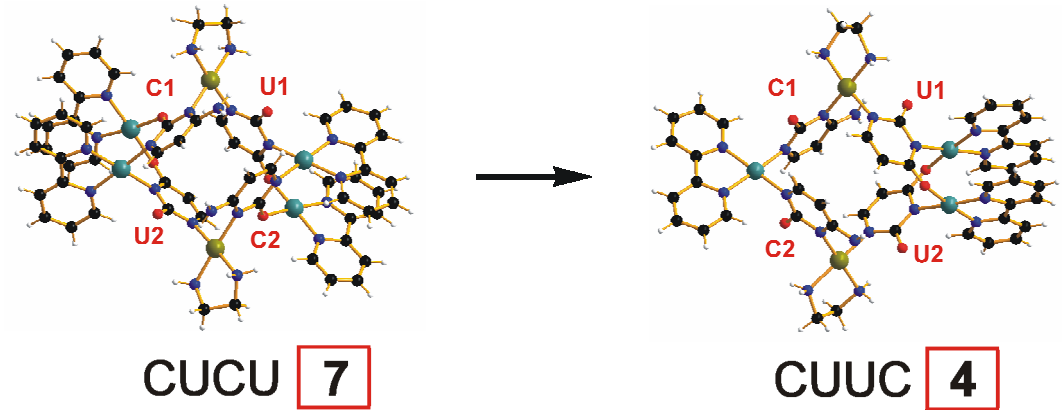

Figura S3: Estructuras cristalinas de los cationes de **7** y **4** con la connectividad de las nucleobases indicada.

En el segundo capítulo han sido aislados y caracterizados cuatro complejos multinucleares de uracilo con differentes metales (Pt, Pd) y con differentes ligandos nitrogenados (diamina, 2,2'-bpy, en).

Los productos derivados de la reacción del compuesto de partida *cis*-$Pt(UH\text{-}N1)_2(NH_3)_2 \cdot H_2O$ (**14a**) con Pd^{II}(2, 2'-bpy) o con Pd^{II}(en) son compuestos cíclicos. Los compuestos $[\{(2,2'\text{-bpy})Pd\}_3\{cis\text{-}[(NH_3)_2Pt(N1\text{-}U\text{-}N3)(N1\text{-}U\text{-}N3,O4)]\}_2](NO_3)_2 \cdot 23.1H_2O$ (**17**) y $[\{(en)Pd\}_4\{cis\text{-}[(NH_3)_2Pt(N1\text{-}U\text{-}N3,O4)_2]\}_2](NO_3)_4 \cdot 13.8H_2O$ (**24'**) han sido caracterizados por difracción de rayos X. El compuesto $[\{(en)Pd\}_{10}(U\text{-}N1,N3,O4)_2(U\text{-}N1,N3,O2,O4)_6\{cis\text{-}[(NH_3)_2Pt]\}_4](NO_3)_{12} \cdot 30H_2O$ (**28'**) ha resultado ser un complejo compuesto de catorce centros metálicos. Los tres metalcalix[4]arenos (abreviadamente Pt_2Pd_3 (**17**) y Pt_2Pd_4 (**24** y **24'**)) muestran entidades metálicas adicionales enlazadas a través de las

posiciones exocíclicas del uracilo (O(4)) dando lugar a una configuración cabeza-cabeza en todos los casos.

La interconversión de especies es posible a través de la adición de más entidades metálicas. Probablemente, un proceso de isomerización tiene lugar ya que los productos obtenidos presentan una configuración diferente de las nucleobases (de cabeza-cabeza a cabeza-cola), como por ejemplo en la conversión de **17** en **24**.

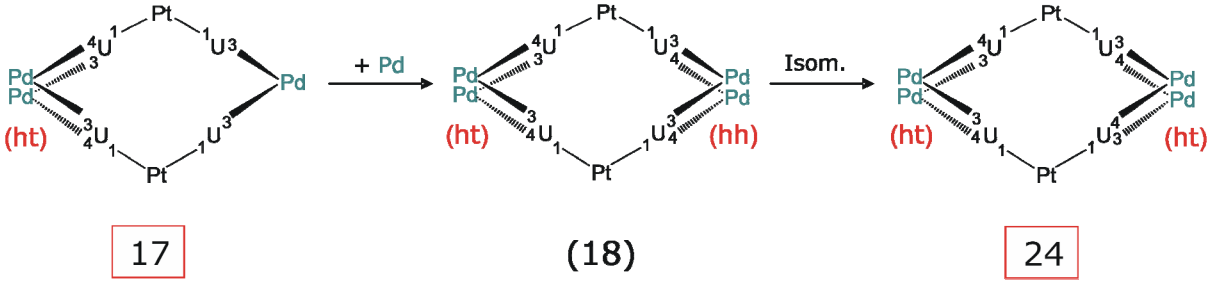

Esquema S2: Proceso propuesto para la conversión de **17** en **24**.

Por otro lado, la pérdida de entidades Pd^{II} enlazadas a las posiciones exocíclicas de las nucleobases seguida de una reacción de fragmentación puede tener lugar, como se ha podido observar en la conversión de **28'** en **24'**.

Varios mecanismos de interconversión han sido discutidos en esta trabajo de investigación y se ha podido observar que la formación de los metalcalix[n]arenos es reversible y ocurre bajo control termodinámico. Por consiguiente, estos sistemas pueden ser adecuadamente discutidos en términos de Química Combinatorial Dinámica.

En todos los ejemplos de metalcalix[4]arenos estructuralmente caracterizados que se han expuesto en esta tesis (**4**, **7**, **13'**, **17** y **24'**), las cuatro nucleobases adoptan una conformación *1,3*-alternada en estado sólido independientemente de la concectividad de las mismas. En el interior de los metalcalix[4]arenos no se han encontrado aniones o moleculas de disolvente. Esta característica parece ser debida a la conformación adptada por las nucleobases, la cual no deja espacio disponible en la cavidad del ciclo para moléculas invitadas.

"Los azules de platino con pirimidinas" son complejos derivados de *cis*-$Pt^{II}(NH_3)_2$ con nucleobases pirimidínicas, como por ejemplo uracilo no substituido. Estos compuestos reciven gran atención debido a sus differentes propiedades y a que su comportamiento en disolución no se ha podido comprender totalmente hasta el momento. En esta trabajo se han utilizado entidades *cis*-$Pd^{II}a_2$ como análogos de *cis*-$Pt^{II}(NH_3)_2$, ya que los primeros reaccionan más rápidamente y al mismo tiempo se previene la química redox del platino. A pesar de que muchas cuestiones relacionadas con los "azules" permanecen todavía sin respuesta, se ha podido obetener una mayor comprensión de la complejidad estructural de este tipo de compuestos.

F APENDIX

1 Crystallographic Tables

Table F1: Crystallographic data for compound **1b**.

Crystal Data		
Empirical Formula	$C_{10}H_{23}N_8O_{9.5}Pt$	
Molar Weight	595.40	
Crystal color and habit	colorless, cube	
Space system	Triclinic	
Space group	P-1	
Cell constants (Å and °)	a = 10.226(2)	α = 96.20(3)
	b = 12.792(3)	β = 91.20(3)
	c = 15.027(3)	γ = 94.13(3)
Cell volume ($Å^3$)	1948.3(7)	
Z	4	
ρ_{calc} (g/cm^3)	2.030	
μ (MoK_α)(1/mm)	7.266	
F (000)	1144	
Data collection		
Temperature (K)	150(2)	
Crystal-detector distance (mm)	34	
Oscillation in ω	2.0	
Frames	188	
Time per picture (s)	200	
θ range (°)	3-27.5	
No. of reflections collected	6776	
No. of reflections observed	3063	
Completion till θ = 27.5	98.5 %	
Structure refinement		
No. of parameters refined	436	
R_1 (total data)	0.1242	
R_1 (observed data)	0.0409	
wR_2 (total data)	0.0771	
wR_2 (observed data)	0.0622	
GooF	7.266	
Residual	ρ_{min} ($e/Å^3$) = -1.062	
	ρ_{max} ($e/Å^3$) = 1.110	

Table F2: Crystallographic data for compound **2a**.

Crystal Data		
Empirical Formula	$C_{30}H_{48.13}ClN_{17}O_{18.06}PdPt_2$	
Molar Weight	1457.80	
Crystal color and habit	Yellow, cube	
Space system	Triclinic	
Space group	P-1	
Cell constants (Å and °)	a = 13.639(3)	α = 79.32(3)
	b = 16.802(3)	β = 77.93(3)
	c = 22.453(4)	γ = 73.23(3)
Cell volume ($Å^3$)	4774.5(16)	
Z	4	
ρ_{calc} (g/cm^3)	2.028	
μ (MoK_α)(1/mm)	6.361	
F (000)	2802	
Data collection		
Temperature (K)	298(2)	
Crystal-detector distance (mm)	34	
Oscillation in ω	1.0	
Frames	423	
Time per picture (s)	300	
θ range (°)	3-27.5	
No. of reflections collected	12406	
No. of reflections observed	5592	
Completion till θ = 27.5	99.8 %	
Structure refinement		
No. of parameters refined	804	
R_1 (total data)	0.1256	
R_1 (observed data)	0.0496	
wR_2 (total data)	0.1205	
wR_2 (observed data)	0.1058	
GooF	0.803	
Residual	ρ_{min} ($e/Å^3$) = -0.709	
	ρ_{max} ($e/Å^3$) = 1.491	

Table F3: Crystallographic data for compound **4**.

Crystal Data		
Empirical Formula	$C_{50}H_{62}N_{24}O_{23}Pd_3Pt_2$	
Molar Weight	2082.04	
Crystal color and habit	Orange, block	
Space system	Triclinic	
Space group	P-1	
Cell constants (Å and °)	a = 12.270(2)	α = 87.24(3)
	b = 13.385(3)	β = 75.76(3)
	c = 21.199(4)	γ = 80.87(3)
Cell volume ($Å^3$)	3331.7(11)	
Z	2	
ρ_{calc} (g/cm^3)	2.075	
μ (MoK_α)(1/mm)	5.075	
F (000)	2012	
Data collection		
Temperature (K)	150(2)	
Crystal-detector distance (mm)	34	
Oscillation in ω	0.7	
Frames	445	
Time per picture (s)	450	
θ range (°)	3-25.5	
No. of reflections collected	9865	
No. of reflections observed	4149	
Completion till θ = 27.5	97.6 %	
Structure refinement		
No. of parameters refined	601	
R_1 (total data)	0.1553	
R_1 (observed data)	0.0554	
wR_2 (total data)	0.1093	
wR_2 (observed data)	0.0919	
GooF	0.780	
Residual	ρ_{min} ($e/Å^3$) = -0.779	
	ρ_{max} ($e/Å^3$) = 1.318	

Table F4: Crystallographic data for compound **7**.

Crystal Data		
Empirical Formula	$C_{60}H_{60}N_{28}O_{24}Pd_4Pt_2$	
Molar Weight	2001.08	
Crystal color and habit	Orange, cube	
Space system	Triclinic	
Space group	P-1	
Cell constants (Å and °)	a = 13.478(3)	α = 79.12(3)
	b = 14.940(3)	β = 82.05(3)
	c = 23.317(5)	γ = 70.17(3)
Cell volume ($Å^3$)	4323.4(15)	
Z	2	
ρ_{calc} (g/cm^3)	1.537	
μ (MoK_α)(1/mm)	4.089	
F (000)	1924	
Data collection		
Temperature (K)	150(2)	
Crystal-detector distance (mm)	34	
Oscillation in ω	1.3	
Frames	331	
Time per picture (s)	25	
θ range (°)	3-27.5	
No. of reflections collected	19691	
No. of reflections observed	10944	
Completion till θ = 27.5	99.0 %	
Structure refinement		
No. of parameters refined	845	
R_1 (total data)	0.1192	
R_1 (observed data)	0.0577	
wR_2 (total data)	0.1267	
wR_2 (observed data)	0.1130	
GooF	0.920	
Residual	ρ_{min} ($e/Å^3$) = -2.644	
	ρ_{max} ($e/Å^3$) = 3.055	

Table F5: Crystallographic data for compound **9a**.

Crystal Data		
Empirical Formula	$C_{80}H_{200.2}ClN_{39}O_{81.1}Pd_4Pt_4$	
Molar Weight	4246.68	
Crystal color and habit	Yellow, block	
Space system	Tetragonal	
Space group	$P4_2/n$	
Cell constants (Å and °)	a = 41.132(6)	α = 90.00
	b = 41.132(6)	β = 90.00
	c = 23.372(5)	γ = 90.00
Cell volume ($Å^3$)	39542(12)	
Z	10	
ρ_{calc} (g/cm^3)	1.783	
μ (MoK_α)(1/mm)	4.090	
F (000)	21144	
Data collection		
Temperature (K)	150(2)	
Crystal-detector distance (mm)	70.2	
Oscillation in ω	0.30	
Frames	3577	
Time per picture (s)	250	
θ range (°)	3-27.5	
No. of reflections collected	29178	
No. of reflections observed	15473	
Completion till θ = 27.5	99.2%	
Structure refinement		
No. of parameters refined	2195	
R_1 (total data)	0.1102	
R_1 (observed data)	0.0424	
wR_2 (total data)	0.0968	
wR_2 (observed data)	0.0851	
GooF	0.879	
Residual	ρ_{min} ($e/Å^3$) = -1.079	
	ρ_{max} ($e/Å^3$) = 0.818	

Table F6: Crystallographic data for compound **13'**.

Crystal Data		
Empirical Formula	$C_{32}H_{116.40}Cl_3N_{31}O_{54.20}Pd_6Pt_2$	
Molar Weight	2938.09	
Crystal color and habit	orange, cube	
Space system	Tetragonal	
Space group	$I4_1/a$	
Cell constants (Å and °)	a = 19.775(3)	α = 90.00
	b = 19.775(3)	β = 90.00
	c = 23.921(5)	γ = 90.00
Cell volume ($Å^3$)	9354(3)	
Z	4	
ρ_{calc} (g/cm^3)	2.086	
μ (MoK_α)(1/mm)	4.302	
F (000)	5864	
Data collection		
Temperature (K)	150(2)	
Crystal-detector distance (mm)	34	
Oscillation in ω	2.0	
Frames	454	
Time per picture (s)	90	
θ range (°)	3-27.5	
No. of reflections collected	3358	
No. of reflections observed	2321	
Completion till θ = 27.5	99.7 %	
Structure refinement		
No. of parameters refined	304	
R_1 (total data)	0.0839	
R_1 (observed data)	0.0484	
wR_2 (total data)	0.1466	
wR_2 (observed data)	0.1296	
GooF	1.010	
Residual	ρ_{min} ($e/Å^3$) = -1.046	
	ρ_{max} ($e/Å^3$) = 0.695	

Table F7: Crystallographic data for compound **14b**.

Crystal Data		
Empirical Formula	$C_8H_{30}N_6O_{14}Na_2Pt$	
Molar Weight	1386.93	
Crystal color and habit	Transparent, cube	
Space system	Triclinic	
Space group	P-1	
Cell constants (Å and °)	a = 12.301(3)	α = 76.00(3)
	b = 14.090(3)	β = 80.40(3)
	c = 14.339(3)	γ = 85.70(3)
Cell volume ($Å^3$)	2376.1(8)	
Z	2	
ρ_{calc} (g/cm^3)	1.939	
μ (MoK_α)(1/mm)	6.018	
F (000)	1368	
Data collection		
Temperature (K)	150(2)	
Crystal-detector distance (mm)	34	
Oscillation in ω	2.0	
Frames	244	
Time per picture (s)	125	
θ range (°)	3-27.5	
No. of reflections collected	10780	
No. of reflections observed	8528	
Completion till θ = 27.5	98.7%	
Structure refinement		
No. of parameters refined	559	
R_1 (total data)	0.0754	
R_1 (observed data)	0.0542	
wR_2 (total data)	0.1501	
wR_2 (observed data)	0.1375	
GooF	1.176	
Residual	ρ_{min} ($e/Å^3$) = -1.378	
	ρ_{max} ($e/Å^3$) = 1.150	

Table F8: Crystallographic data for compound **17'**.

Crystal Data		
Empirical Formula	$C_{46}H_{90.2}N_{20}O_{37.1}Pd_3Pt_2$	
Molar Weight	2226.56	
Crystal color and habit	Orange, block	
Space system	Triclinic	
Space group	P-1	
Cell constants (Å and °)	a = 13.715(3)	α = 108.74(3)
	b = 15.548(3)	β = 90.60(3)
	c = 19.902(4)	γ = 105.64(3)
Cell volume ($Å^3$)	3848.1(14)	
Z	2	
ρ_{calc} (g/cm^3)	1.922	
μ (MoK_α)(1/mm)	4.411	
F (000)	2194	
Data collection		
Temperature (K)	150	
Crystal-detector distance (mm)	34	
Oscillation in ω	1.0	
Frames	524	
Time per picture (s)	50	
θ range (°)	3-27.5	
No. of reflections collected	7924	
No. of reflections observed	2957	
Completion till θ = 27.5	98.4 %	
Structure refinement		
No. of parameters refined	500	
R_1 (total data)	0.1519	
R_1 (observed data)	0.0494	
wR_2 (total data)	0.1047	
wR_2 (observed data)	0.0916	
GooF	0.709	
Residual	ρ_{min} ($e/Å^3$) = -0.636	
	ρ_{max} ($e/Å^3$) = 0.661	

Table F9: Crystallographic data for compound **24'**.

Crystal Data		
Empirical Formula	$C_{24}H_{79.6}N_{24}O_{33.8}Pd_4Pt_2$	
Molar Weight	2061.30	
Crystal color and habit	Orange, block	
Space system	Monoclinic	
Space group	$P2_1/c$	
Cell constants (Å and °)	a = 21.947(4)	α = 90.00
	b = 15.729(3)	β = 96.39(3)
	c = 17.811(4)	γ = 90.00
Cell volume ($Å^3$)	6110(2)	
Z	4	
ρ_{calc} (g/cm^3)	2.241	
μ (MoK_α)(1/mm)	5.822	
F (000)	4008	
Data collection		
Temperature (K)	150(2)	
Crystal-detector distance (mm)	34	
Oscillation in ω	1.2	
Frames	225	
Time per picture (s)	250	
θ range (°)	3-27.5	
No. of reflections collected	7696	
No. of reflections observed	4710	
Completion till θ = 27.5	99.9 %	
Structure refinement		
No. of parameters refined	658	
R_1 (total data)	0.0779	
R_1 (observed data)	0.0411	
wR_2 (total data)	0.0908	
wR_2 (observed data)	0.0844	
GooF	0.862	
Residual	ρ_{min} ($e/Å^3$) = -0.900	
	ρ_{max} ($e/Å^3$) = 1.771	

Table F10: Crystallographic data for compound **28'**.*

Crystal Data		
Empirical Formula	$C_{52}H_{180}N_{56}O_{82}Pt_4Pd_{10}$	
Molar Weight	3486.53	
Crystal color and habit	Orange, block	
Space system	Monoclinic	
Space group	$P2_1/c$	
Cell constants (Å and °)	a = 16.490(3)	α = 90.00
	b = 31.763(6)	β = 115.70(3)
	c = 15.070(3)	γ = 90.00
Cell volume ($Å^3$)	7112(2)	
Z	4	
ρ_{calc} (g/cm^3)	2.322	
μ (MoK_α)(1/mm)	5.195	
F (000)	4728	
Data collection		
Temperature (K)	150(2)	
Crystal-detector distance (mm)	44.1	
Oscillation in ω	0.60	
Frames	864	
Time per picture (s)	60	
θ range (°)	3-27.5	
No. of reflections collected	7013	
No. of reflections observed	2209	
Completion till θ = 27.5	91.7% %	
Structure refinement		
No. of parameters refined	372	
R_1 (total data)	0.2509	
R_1 (observed data)	0.1017	
wR_2 (total data)	0.2747	
wR_2 (observed data)	0.2514	
GooF	1.091	
Residual	ρ_{min} ($e/Å^3$) = -0.745	
	ρ_{max} ($e/Å^3$) = 1.687	

*Preliminary Structure

2 References

(1) Rosenberg, B.; Van Camp, L.; Krigas, T. "Inhibition of Cell Division in Escherichia Coli by Electrolysis Products from a Platinum Electrode". *Nature* **1965**, *205*, 698-699.

(2) Silver, R. T.; Lauper, R. D.; Jarowski, C. I. *"A Synopsis of Cancer Chemotherapy"*; 2d ed., Yorke Medical Books, Reed Publishing: New York: New York, 1987.

(3) Carter, S. K. *"Cisplatin"*; Academic Press Inc.: New York: New York, 1980.

(4) Loehrer, P.; Einhorn, L. "Drugs five years later. Cisplatin". *Ann. Intern. Med* **1984**, *100*, 704-713.

(5) Takahara, P. M.; Rosenzweig, A. C.; Frederick, C. A.; Lippard, S. J. "Crystal structure of double-stranded DNA containing the major adduct of the anticancer drug cisplatin". *Nature* **1995**, *377*, 649-652.

(6) Takahara, P. M.; Frederick, C. A.; Lippard, S. J. "Crystal Structure of the Anticancer Drug Cisplatin Bound to Duplex DNA". *J. Am. Chem. Soc.* **1996**, *118*, 12309-12321.

(7) Mansy, S.; Chu, G. Y. H.; Duncan, R. E.; Tobias, R. S. "Heavy Metal nucleotide interactions. Competitive recognition in systems of four nucleotides with *cis*- or *trans*diammineplatinum(II). Raman difference spectrophotometry of the relative nucleophilicity of guanosine, cytidine, adenosine, and uridine monophosphates and analogous DNA bases". *J. Am. Chem. Soc.* **1978**, *100*, 607-616.

(8) Chan, H.-L.; Ma, D.-L.; Yang, M.; Che, C.-M. "Bis-intercalativedinuclear platinum(II) 6-phenyl-2,2'-bypiridine complexes exhibit enhanced DNA affinity but similar cytotoxicity compared to the mononuclear unit". *J. Biol. Inorg. Chem.* **2003**, *8*, 761-769.

(9) Lippert, B. *"Cisplatin-Chemistry and Biochemistry of a Leading Anticancer Drug"*; Wiley-VCH: Weinheim, 1999.

(10) Wong, E.; Gianodomenico, C. M. "Current Status of Platinum-Based Antitumor Drugs". *Chem. Rev.* **1999**, *99*, 2451-2466.

(11) Weiss, R. B.; Christian, M. C. "New cisplatin analogues in development. A review". *Drugs* **1993**, *46*, 360-377.

(12) Kelland, L. R. "Preclinical Perspectives on Platinum Resistance". *Drugs* **2000**, *59*, 1-8.

(13) Giaccone, G. "Clinical perspectives on Platinum Resistance". *Drugs* **2000**, *59*, 9-17.

(14) Judson, I.; Kelland, L. R. "New Developments and Approaches in the Platinum Arena". *Drugs* **2000**, *59*, 29-36.

(15) Wastaff, A. J.; Ward, A.; Benfield, P.; Heel, R. C. "Carboplatin. A preliminary review of its pharmacodynamic and pharmacokinetic properties and therapeutic efficacy in the treatment of cancer". *Drugs* **1989**, *37*, 162-190.

(16) Teuben, J. M.; Bauer, C.; Wang, A. H.; Reedijk, J. "Solution Structure of a DNA Duplex Containing a *cis*-Diammineplatinum(II) 1,3-d(GTG) Intrastrand Cross-Link, a Major Adduct in Cells Treated with the Anticancer Drug Carboplatin". *Biochemistry* **1999**, *38*, 12305-12312.

(17) Raymond, E.; Chaney, S. G.; Taamma, A.; Cvitkovic, E. "Oxaliplatin: A review of preclinical and clinical studies". *Ann. Oncol.* **1998**, *9*, 1053-1071.

(18) Spingler, B.; Whittington, D. A.; Lippard, S. J. "2.4 Å Crystal Structure of an Oxaliplatin 1,2-d(GpG) Intrastrand Cross-Link in a DNA Dodecamer Duplex". *Inorg. Chem.* **2001**, *40*, 5596-5602.

(19) Piccart, J. M.; Lamb, H.; Vermorken, J. B. "Current and future potential roles of the platinum drugs in the treatment of ovarian cancer". *Ann. Oncol.* **2001**, *12*, 1195-1203.

(20) Kratz, F.; Schütte, M. T. "Anticancer metal complexes and tumour targeting strategies". *Cancer J.* **1998**, *38*, 176-182.

(21) Erkkila, K. E.; Odom, D. T.; Barton, J. K. "Recognition and Reaction of Metallointercalators with DNA". *Chem. Rev.* **1999**, *99*, 2777-2796.

(22) Lippert, B. "Platinum Pyrimidine Blues–Nature and Possible Structure". *J. Clin. Hemat. Oncol.* **1977**, *7*, 26-42.

(23) Flynn, C. M.; Viswanthan, T. S.; Martin, R. B. "The constitution of platinum blues". *J. Inorg. Nucl. Chem.* **1977**, *39*, 437-439.

(24) Chu, G. Y. H.; Duncan, R. E.; Tobias, R. S. "Heavy metal-nucleoside interactions. Binding of *cis*-diammineplatinum(II) to cytidine and uridine in aqueous solution: necessary conditions for formation of platinum-uridine `blues´ ". *Inorg. Chem.* **1977**, *16*, 2625-2636.

(25) Hofmann, K. A.; Bugge, G. "Platinblau". *Ber. Chem. Ges.* **1908**, *41*, 312.

(26) Davidson, J. P.; Faber, P. J.; Fischer, j. R. G.; Mansy, S.; Peresie, H. J. et al. "Platinum-pyrimidine blues and related complexes. A new class of antitumor agents". *Cancer Chemother. Rep. Part I* **1975**, *59*, 287-300.

(27) Speer, R. J.; Ridgway, H.; Hall, L. M.; Stewart, D. P.; Howe, K. E. et al. "Coordination complexes of platinum as antitumor agents". *Cancer Chemother. Rep. Part I* **1975**, *59*, 629-641.

(28) Burness, J. H.; Bandurski, M. J.; Passman, L. J.; Rosenberg, B. "The Interaction of Platinum -Containing Polycations and Polyanions with Biomacromolecules". *J. Clin. Hemat. Oncol.* **1977**, *7(2)*, 508-521.

(29) Aggarwal, S. K.; Wagner, R. W.; McAllister, P. K.; Rosenberg, B. "Cell-surface-associated nucleic acid in tumorigenic cells make visible with platinum-pyrimidine complexes by electron microscopy". *Proc. Natl. Acad Sci. U.S.A.* **1973***, 12*, 928-932.

(30) Barton, J. K.; Rabinowitz, H. N.; Szalda, D. J.; Lippard, S. J. "Synthesis and Crystal Structure of *cis*-Diammineplatinum a-Pyridone Blue". *J. Am. Chem. Soc.* **1977***, 99*, 2827-2829.

(31) Lippert, B.; Neugebauer, D.; Raudaschl, G. "Formation of Dinuclear (*Head-Head*, *Head-Tail*, m-Hydroxo) Complexes of *cis*-$(NH_3)_2$Pt(II) with 1-Methyluracil". *Inorg. Chim. Acta* **1983***, 78*, 161-170.

(32) Lippert, B.; Neugebauer, D.; Schubert, U. "A Platinum(II) Dimer with Bridging 1-Methylthyminato Ligands in *Head*-to-*Head* Arrangement". *Inorg. Chim. Acta* **1980***, 46*, L11-L14.

(33) Schöllhorn, H.; Thewalt, U.; Lippert, B. "Crystal Structure of Bis(m-1-methylthyminato-N3,O4)bis-(*cis*-diammin-platinum(II)) Dinitrate (*Head-Head*). Comparison with Related Compounds". *Inorg. Chim. Acta* **1984***, 93*, 19-26.

(34) Dohta, Y.; Browning, S.; Rekonen, P.; Kodaka, M.; Okada, T. et al. "Preparation, structure and cytotoxicity of cis-diammineplatinum(II) dinuclear complexes with 1-alkyluracil and imidate ligands". *Inorg. Chim. Acta* **1997***, 263*, 69-79.

(35) Mascharak, P. K.; Williams, I. D.; Lippard, S. J. "Characterization of a platinum pyrimidine blue: synthesis, structure, and physical properties of *cis*-diammineplatinum 1-methyluracil blue". *J. Am. Chem. Soc.* **1984***, 106*, 6428-6430.

(36) O´Halloran, T. V.; Mascharak, P. K.; Williams, I. D.; Roberts, M. M.; Lippard, S. J. "Synthesis, structure determination, and electronic structure characterization of two mixed-valence tetranuclear platinum blues with bridging, a-pyridonate or 1-methyluracilate ligands". *Inorg. Chem.* **1987***, 26*, 1261-1270.

(37) Faggiani, R.; Lippert, B.; Lock, C. J. L. "Heavy Transition Metal Complex of Biologically Important Molecules. Crystal and Molecular Structure of Pentahydrodioxonium Chloro-(uracilato-*N1*)(ethylenediamine)platinum(II)Chloride and Chloro-(thyminato-*N1*)(ethylenediamine)platinum(II)". *Inorg. Chem.* **1980***, 19*, 295-300.

(38) Rauter, H.; Hillgeris, E. C.; Erxleben, A.; Lippert, B. "$[(en)Pt(uracilate)]_4^{4+}$, A Metal Analogue of Calix[4]arene. Similarities and Differences With Classical Calix[4]arenes". *J. Am. Chem. Soc.* **1994***, 116*, 616-624.

(39) Rauter, H.; Hillgeris, E. C.; Lippert, B. "A cyclic Tetranuclear Platinum Complex of Uracil". *J. Chem. Soc., Chem. Commun.* **1992**, 1385-1386.

(40) Rauter, H.; Mutikainen, I.; Blomberg, M.; Lock, C. J. L.; Amo-Ochoa, P. et al. "Cyclic Metal Complexes of Nucleobases and Other Heterocycles: Molecular Boxes, Rectangles and Hexagons". *Angew. Chem., Int. Ed. Engl.* **1997**, *36*, 1296-1301.

(41) Lippert, B. "Platinum Complexes of Uracil. Multiplicity and Interconversion of Binding Sites". *Inorg. Chem.* **1981**, *20*, 4326-4343.

(42) Pfab, R.; Jandik, P.; Lippert, B. "Pt(II) Complexes of Thymine: Factors Influencing Binding Sites and Methods of Differentiation". *Inorg. Chim. Acta* **1982**, *66*, 193-204.

(43) Barker, J.; Kilner, M. "The coordination chemistry of the amidine ligand". *Coord. Chem. Rev.* **1994**, *133*, 219-300.

(44) Holthenrich, D.; Zangrando, E.; Chiarparin, E.; Lippert, B.; Randaccio, L. "Cytosine nucleobase as a tridentate ligand: Metal binding to *N3, N4* and *O2* in the trinuclear complex *cis*-$[Pt(NH_3)_2(mcyt)_2\{Pd(en)\}_2][NO_3]_4 \bullet H_2O$ (mcyt = 1-methylcytosinate, en = ethane-1,2-diamine)". *J. Chem. Soc., Dalton Trans.* **1997**, 4407-4410.

(45) Lippert, B.; Thewalt, U.; Schöllhorn, H.; Goodgame, D. M. L.; Rollins, R. W. "Formation, Crystal Structure, and EPR Spectroscopic Properties of a Heteronuclear (Pt_2, Cu) Mixed Nucleobase (1-Methylcytosine, 1-Methyluracil) Complex : Bis-(m-1-methyluracilato-*N3,O4*)(1-methylcytosine-*N3,O2*)-*cis*-diammineplatinum(II) Copper(II) Tetranitrate-6-Water". *Inorg. Chem.* **1984**, *23*, 2807-2813.

(46) Lippert, B.; Neugebauer, D. "A Heteronuclear (Pt_4, Ag) Complex of 1-Methyluracil and Its Conversion into a Crystalline Platinum Blue". *Inorg. Chem.* **1982**, *21*, 451-452.

(47) Lippert, B.; Schöllhorn, H.; Thewalt, U. "Formation of $[Pt(2.25)]_4$-1-Methyluracil-Blue through Silver(I) Oxidation of $[Pt(2.0)]_2$ and Isolation of a Heteronuclear (Pt_2, Ag_2) Precursor". *Inorg. Chem.* **1987**, *26*, 1736-1741.

(48) Micklitz, W.; Müller, G.; Riede, J.; Lippert, B. "A Novel Type of 1-Methyluracil (Hmeu)-Blue: Trinuclear, Mixed-Metal Complex *cis*-$[(NH_3)_2Pt(meu)_2Pd(meu)_2Pt(NH_3)_2]^{3+}$ ". *J. Chem. Soc., Chem. Commun.* **1987**, 76-77.

(49) Micklitz, W.; Müller, G.; Huber, B.; Riede, J.; Rashwan, F. et al. "Trinuclear, Mixed Pt_2Pd-1-Methyluracil and 1-Methylthymine Blues with + 2.33 Average Metal Oxidation State: Preparation, Crystal Structures, and Solution Studies". *J. Am. Chem. Soc.* **1988**, *110*, 7084-7092.

(50) Gutsche, C. D. "Calixarenes". *Royal Society of Chemistry, Cambridge* **1989**.

(51) Böhmer, V. "Calixarenes, Macrocycles with (Almost) Unlimited Possibilities". *Angew. Chem., Int. Ed. Engl.* **1995**, *34*, 713-745.

(52) Ikeda, A.; Shinkai, S. "Novel Cavity Design Using Calix[n]arene Skeletons: Toward Molecular Recognition and Metal Binding". *Chem. Rev* **1997***, 97*, 1713-1734.

(53) Acho, J. A.; Ren, T.; Yun, J. W.; Lippard, S. J. "Dimolybdenum(II) Calixarene Complexes: Synthesis, Structure, Raman Spectroscopy, and Bonding". *Inorg. Chem.* **1995***, 35*, 5226-5533.

(54) Gianni, L.; Caselli, A.; Solari, E.; Floriani, C.; Chiesi-Villa, A. et al. "Organometallic Reactivity on a Calix[4]arene Oxo Surface. Synthesis and Rearrangement of Zr-C Functionalities Anchored to a Calix[4]arene Moiety". *J. Am. Chem. Soc.* **1997***, 119*, 9198-9210.

(55) Davidson, M. G.; Howard, J. A.; Lamb, S.; Lehmann, C. W. "Synthesis and X-ray structures of tetralithium derivatives of tert-butylcalix[4]arene containing unique Li-O cores based on a square-pyrimidal geometry". *Chem. Commun.* **1997**, 1607-1609.

(56) Hosseini, M. W.; De Cian, A. "Crystal engineering: molecular networks based on inclusion phenomena". *Chem. Commun.* **1998**, 727-733.

(57) Chisholm, M. H.; Folting, K.; Wu, D.-D. "Preparation and characterization of the kinetic and thermodinamic isomers of dinuclear molybdenum and tungsten complexes with metal-metal triple bonds supported by *p-tert*-butylcalix[4]arene anions". *Chem. Commun.* **1998**, 379-380.

(58) Wieser, C.; Dieleman, C. B.; Matt, D. "Calixarene and resorcinarene ligands in transition metal chemistry". *Coord. Chem. Rev.* **1997***, 165*, 93-161.

(59) Ikeda, A.; Shinkai, S. "On the Origin of High Ionophoricity of 1,3-Alternate Calix[4]arenes: p-donor Participation in Complexation of Cations and Evidence for Metal-Tunneling through the Calix[4]arene Cavity". *J. Am. Chem. Soc.* **1994***, 116*, 3102-3110.

(60) Steed, J. W.; Juneja, R. K.; Atwood, J. L. "A Water-Soluble Bear Trap Exhibiting Strong Anion Complexation Properties". *Angew. Chem., Int. Ed. Engl.* **1994***, 33*, 2456-2457.

(61) Staffilani, M.; Hancock, K. S. B.; Steed, J. W.; Holman, T.; Atwood, J. L. et al. "Anion Binding within the Cavity of -Metalated Calixarenes". *J. Am. Chem. Soc.* **1997***, 119*, 6324-6335.

(62) Navarro, J. A. R.; Lippert, B. "Simple 1:1 and 1:2 complexes of metal ions with heterocycles as building blocks for discrete molecular as well as polymeric assemblies". *Coord. Chem. Rev.* **2001***, 222*, 219-250.

(63) Navarro, J. A. R.; Lippert, B. "Molecular architecture with metal ions, nucleobases and other heterocycles". *Coord. Chem. Rev.* **1999***, 185-186*, 653-667.

(64) Barea, E.; Navarro, J. A. R.; Salas, J. M.; Quirós, M.; Willermann, M. et al. "Chiral Pyrimidine Metallacalixarenes: Synthesis, Structure and Host-Guest Chemistry". *Chem. Eur. J.* **2003***, 9*, 4414-4421.

(65) Qin, Z.; Jennings, M. C.; Puddephatt, R. J. "Molecular Triangle of Palladium(II) and Its Anion Binding Properties". *Inorg. Chem.* **2002***, 41*, 3967-3974.

(66) Navarro, J. A. R.; Janik, M. B. L.; Freisinger, E.; Lippert, B. "[(Ethylenediamine)-Pt(uracilate)]$_4$, a metal analogue of calix[4]arene. Coordination and anion host-guest chemistry related to its conformational dynamics". *Inorg. Chem.* **1999***, 38*, 426-432.

(67) Navarro, J. A. R.; Freisinger, E.; Lippert, B. "Self-Assembly of Palladium(II) and Platinum(II) Complexes of 2-Hydroxypyrimidine to Novel Metallacalix[4]arenes. Receptor Properties through Multiple H-Bonding Interactions". *Inorg. Chem.* **2000***, 39*, 2301-2305.

(68) Navarro, J. A. R.; Freisinger, E.; Lippert, B. "[(Ethylendiamine)Pt(uracilate)]$_4$ - A Metal Analogue of Calix[4]arene: Coordination Chemistry of Its *1,3*-Alternate Conformer towards First-Row Trandition-Metal ions". *Eur. J. Inorg. Chem.* **2000**, 147-151.

(69) Navarro, J. A. R.; Salas, J. M. "A palladium metallacalix[4]arene capped with a gadolinium atom". *Chem. Commun.* **2000**, 235-236.

(70) Navarro, J. A. R.; Barea, E.; Galindo, M. A.; Salas, J. M.; Romero, M. A. et al. "Soft functional polynuclear coordination compounds containing pyrimidine bridges". *J. Solid State Chem.* **2005***, 178*, 2436-2451.

(71) Yamanari, K.; Yamamoto, S.; Ito, R.; Kushi, Y.; Fuyuhiro, A. et al. "Cyclic Hexamer with a Cubic Cavity: Crystal Structure of [{Rh(6-Purinethione Ribosido)(Cp*)}$_6$] $(CF_3SO_3)_6$ ". *Angew. Chem., Int. Ed. Engl.* **2001***, 40*, 2268-2271.

(72) Yu, S. Y.; Huang, H.; Liu, H. B.; Chen, Z. N.; Zhang, R. B. et al. "Modular Cavity-Tunable Self-Assembly of Molecular Bowls and Crowns as Structural Analogues of Calix[3]arenes". *Angew. Chem., Int. Ed. Engl.* **2003***, 42*, 686-690.

(73) Galindo, M. A.; Galli, S.; Navarro, J. A. R.; Romero, M. A. "Formation of heterotopic metallacalix[n]arenes (n = 3, 4, 6) containing ethylendiamine-palladium(II) metal fragments and 4,7-phenanthroline and pyrimidinolate bridges. Synthesis, Structure and Host-Guest Chemistry". *Dalton Trans.* **2004**, 2780-2785.

(74) Galindo, M. A.; Navarro, J. A. R.; Romero, M. A.; Quirós, M. "Mononucleotide recognition by cyclic trinuclear palladium(II) complexes containing 4,7-phenanthroline N,N bridges". *Dalton Trans.* **2004**, 1563-1566.

(75) Lehn, J.-M. "Dynamic Combinatorial Chemistry and Virtual Combinatorial Libraries". *Chem. Eur. J.* **1999***, 5*, 2455-2463.

(76) Stulz, E.; Scott, S. M.; Bond, A. D.; Teat, S. J.; Sanders, J. K. M. "Selection and Amplification of Mixed-Metal Porphyrin Cages from Dynamic Combinatorial Libraries". *Chem. Eur. J.* **2003***, 9*, 6039-6048.

(77) Gauthier, S.; Quebatte, L.; Scopelliti, R.; Severin, K. "Combinatorial Synthesis of Bimetallic Complexes with Three Halogeno Bridges". *Chem. Eur. J.* **2004***, 10*, 2811-2821.

(78) Saur, I.; Scopelliti, R.; Severin, K. "Utilization of Self-Sorting Processes To Generate Dynamic Combinatorial Libraries with Network Topologies". *Chem. Eur. J.* **2006***, 12*, 1058-1066.

(79) Brasey, T.; Scopelliti, R.; Severin, K. "Neutral Metallomacrocycles with Four or Ten (PEt_3)Pd(II) Centers". *Inorg. Chem.* **2005***, 44*, 160-162.

(80) Kubota, Y.; Sakamoto, S.; Yamaguchi, K.; Fujita, M. "Guest-Induced Organization of an Optimal Receptorfrom a Dynamic Receptor Library: spectroscopic screening". *Proc. Natl. Acad Sci. U.S.A.* **2002***, 99*, 4854-4856.

(81) Schöllhorn, H.; Thewalt, U.; Lippert, B. "Pt^{II} Coordination trough C(5) of 1-Methyluracil: the first Example of a Pt-Nucleobase Complex containning a Pt-C-bond". *J. Chem. Soc., Chem. Commun.* **1986**, 258-259.

(82) Stang, P. J. "Molecular Architecture: Coordination as the Motif in the Rational Design and Assembly of Discrete Supramolecular Species-Self-Assembly of Metallacyclic Polygons and Polyhedra". *Chem. Eur. J.* **1998***, 4*, 19-27.

(83) Chang, S.-Y.; Jang, H.-Y.; Jeong, K.-S. "Self-Assembly Metallocycles with Two Interactive Binding Domains". *Chem. Eur. J.* **2004***, 10*, 4358-4366.

(84) Brüning, W. "*cis*- und *trans*-(diamin)Platin(II)-Komplexe von Pyrimidin Nukleobasen: Synthese von Bausteinen für Makrocyclische Komplexe sowie Stabilisierung seltener tautomer Formen". In *Dissertation*; Universität Dortmund, Germany, 1997.

(85) Clowney, L.; Jain, S. C.; Srinivasan, A. R.; Westbrook, J.; Olson, W. K. et al. "Geometric Parameters in Nucleic Acids: Nitrogenous Bases". *J. Am. Chem. Soc.* **1996***, 118*, 509-518.

(86) Taylor, R.; Kennard, O. "The molecular structures of nucleosides and nucleotides: Part 1. The influence of protonation on the geometries of nucleic acid constituents". *J. Mol. Structure* **1982***, 78*, 1-28.

(87) Brüning, W.; Ascaso, I.; Freisinger, E.; Sabat, M.; Lippert, B. "Metal-stabilizated rare tautomers of nucleobases. Promotion of rare cytosine tautomer upon complex formation with (dien)M^{2+} (M = Pt, Pd)". *Inorg. Chim. Acta* **2002***, 339*, 400-410.

(88) Brüning, W.; Freisinger, E.; Sabat, M.; Siegel, R. K. O.; Lippert, B. "*N1* and *N3* Linkage Isomers of Neutral and Deprotonated Cytosine with *trans*-[$(CH_3NH_2)_2Pt^{II}$] ". *Chem. Eur. J.* **2002***, 8*, 4681-4692.

(89) Jaworski, S.; Shöllhorn, H.; Eismann, P.; Thewalt, U.; Lippert, B. "Trichloroamine Complexes of Platinum: Preparation, Crystal Structure and Solution Behaviour of Cytosinum trichlorocytosineplatinate(II)". *Inorg. Chem. Acta* **1988***, 153*, 31-38.

(90) Ruf, M.; Weis, K.; Vahrenkamp, H. "Pyrazolylborate-Zinc Complexes of RNA Precursors and Analogues Thereof". *Inorg. Chem.* **1997***, 36*, 2130-2137.

(91) Lippert, B.; Pfab, R.; Neugebauer, D. "The Role of *N1* Coordinated Thymine in 'Platin Thymine Blue' ". *Inorg. Chim. Acta* **1979***, 37*, L495-L497.

(92) Christen, J. J.; Rytting, J. H.; Izatt, R. M. "Thermodynamics of proton dissociation in dilute aqueous solution. VII. pK,.DELTA.H.degree., and DELTA.S.degree. values for proton ionization from several pyrimidines and their nucleosides at 25 degree." *J. Phys. Cem.* **1967***, 71*, 2700-2705.

(93) De Pasquale, R. J. "Uracil. A Perspective". *Ind. Eng. Chem. Prod. Res. Dev.* **1978***, 17*, 278-286.

(94) DeMember, J. R.; Wallace, F. A. "Uracil and its interaction with silver ion in aqueous alkaline media". *J. Am. Chem. Soc.* **1975***, 97*, 6240-6245.

(95) Ganguly, S.; Kundu, K. K. "Protonation/deprotonation energetics of uracil, thymine, and cytosine in water from e.m.f./spectrophotometric measurements". *Can. J. Chem.* **1994***, 72*, 1120-1126.

(96) Micklitz, W.; Riede, J.; Huber, B.; Müller, G.; Lippert, B. "Dinuclear (Pt,Pt) and Heteronuclear (Pt,Pd) Complexes of Uracil Nucleobases with Identical and Mixed Amine (NH_3, en, bpy) Ligands on the Two Metals. Effect of the Heterometal and Amine on the Oxidizability". *Inorg. Chem.* **1988***, 27*, 1979-1986.

(97) Micklitz, W.; Sheldrick, W. S.; Lippert, B. "Mono- and Dinuclear Palladium(II) Complexes of Uracil and Thymine Model Nucleobases and the X-Ray Structure of $[(bpy)Pd(1\text{-}MeT)_2Pd(bpy)](NO_3)_2 \bullet 5.5H_2O$ (*Head-Head*)". *Inorg. Chem.* **1990***, 29*, 211-216.

(98) Trötscher, G.; Micklitz, W.; Schöllhorn, H.; Thewalt, U.; Lippert, B. "*cis*-$\{[(NH_3)_2Pt(1\text{-}MeU)_2Pt(bpy)]_2\}(NO_3)_5 \bullet mHNO_3 \bullet nH_2O$, a Pt(2.25) Blue derived from a Dinuclear, Mixed Amine Complex of 1-Methyluracil. Characterization of the Cation, Analytical Evaluation of Cocrystallized HNO_3, and X-Ray Structure of its Reduced $[Pt(2.0)]_2$ Form". *Inorg. Chem.* **1990***, 29*, 2541-2547.

(99) Abul Haj, M.; Quirós, M.; Salas, J. M. "Solution and solid state coexistence of *head-head* and *head-tail* isomers in dimeric Pd(II) and Pt(II) complexes of the type $[M_2(a\text{-}a)_2(m\text{-}L\text{-}N3,N4)_2]^{2+}$ with a bridging triazolopyrimidine ligand and chelating bidentate diamines". *J. Chem. Soc., Dalton Trans.* **2002**, 4740-4745.

(100) Yu, S. Y.; Huang, H.; Li, S.-H.; Jiao, Q.; Li, Y.-Z. et al. "Solution Self-Assembly, Spontaneous Deprotonation, and Crystal Structures of Bipyrazolate-Bridged Metallamacrocycles with Dimetal Centers". *Inorg. Chem.* **2005***, 44*, 9471-9488.

(101) Krumm, M.; Mutikainen, I.; Lippert, B. "Palladium-1-methylcytosine chemistry: *N3* and *N3,N4* metal binding to 1-methylcytosine and an unexpected *trans-cis* isomerization of two diamminepalladium(II) entities". *Inorg. Chem.* **1991**, *30*, 884-890.

(102) Jeong, K. S.; Kim, S. Y.; Shin, U. S.; Nguyen, t. M. H.; Kogej, M. et al. "Synthesis of Chiral Self-Assembling Rhombs and Their Characterization in Solution, in the Gas Phase, and at the Liquid-Solid Interface". *J. Am. Chem. Soc.* **2005**, *127*, 17672-17685.

(103) Schalley, C. A.; Müller, T.; Linnartz, P.; Witt, M.; Schäfer, M. et al. "Mass Spectrometric Characterization and Gas-Phase Chemistry of Self-Assembling Supramolecular Squares and Triangles". *Chem. Eur. J.* **2002**, *8*, 3538-3551.

(104) Engeser, M.; Rang, A.; Ferrer, M.; Gutiérrez, A.; Schalley, C. A. "Reactivity of Self-Assembled Supramolecular Complexes in the Gas Phase: A Supramolecular Neighbor Group Effect". *Int. J. Mass spectrom., in press.* **2006**.

(105) Pretsch, E.; Bühlmann, P.; Affolter, C. "Strucutre Dertermination of Organic Compounds"; Verlag, S. Ed.: Berlin-Heidelberg-New York, 2000.

(106) Spek, A. L. "PLATON, An Integrated Tool for the Analysis of the Results of a single Crystal Structure Determination". *Acta Crystallogr.* **1990**, *A46*, C34.

(107) Uchida, K.; Toyama, A.; Tamura, Y.; Sugimura, M.; Mitsumuri, F. et al. "Interactions of guanine derivatives with ethylenediamine and diethylenetriamine complexes of palladium(II) in solution: Pd binding sites of the guanine ring and formation of a cyclic adduct, [{Pd(en)(guanine-ring)}$_4$]". *Inorg. Chem.* **1989**, *28*, 2067-2073.

(108) Pienaar, J. J.; Kotowski, M.; Van Eldik, R. "Volume profiles for solvolysis reactions of sterically hindered diethylenetriamine complexes of palladium(II) in aqueous solution". *Inorg. Chem.* **1989**, *28*, 373-375.

(109) Preut, H.; Frommer, G.; Lippert, B. "*cis*-Bis(1-methylcytosine-*N*)(*N,N,N',N'*-tetramethylethylenediamine-*N,N'*)platinum(II) Diperchlorate Monohydrate". *Acta Crystallogr.* **1991**, *C47*, 852-854.

(110) Frommer, G.; Lianza, F.; Albinati, A.; Lippert, B. "Diplatinum and heteronuclear Complexes Derived from (tmeda)Pt(1-MeU)$_2$ (tmeda = *N,N,N',N'*-Tetramethylethylenediamine, 1-MeU = 1-Methyluracilate-*N3*). Steric Effect of the tmeda Ligand on the Orientation of the Second Metal". *Inorg. Chem.* **1992**, *31*, 2434-3439.

(111) Shen, W.-Z.; Gupta, D.; Lippert, B. "Cyclic Trimer versus *Head-Tail* Dimer in Metal-Nucleobase Complexes: Importance of Relative Orientation (*Syn*, *Anti*) of the Metal Entities and Relevance as a Metallaazacrown Compound". *Inorg. Chem.* **2005**, *44*, 8249-8258.

(112) Lippert, B. "Mixed-Ligand Complexes of *cis*-$[Pt(NH_3)_2]^{2+}$ Containing Pyrimidine and Purine Nucleobases". *Biochemie* **1978***, 60*, 1041-1048.

(113) Lippert, B. *"Reaktionen von Cisplatin mit DNA und Modellnukleobasen"*; Verlag Karger,: Basel, 1984.

(114) Lippert, B. "Tris(Nucleobase) Complexes Derived from cis-$Pt(NH_3)_2Cl_2$". *Inorg. Chim. Acta* **1981***, 56*, L23-L24.

(115) Lippert, B. *"Model Nucleobase Complexes of Cisplatin: Differentiation of Metal Binding Sites by Raman Spectroscopy"*; Proc. VIII Intern. Conf. Raman Spectrosc., J. Wiley: Chichester, 1982.

(116) Beyerle, R.; Lippert, B. "Mixed-Nucleobase Complexes *cis*-$Pt(NH_3)_2TX$ with T = 1-Methylthymine Anion and X = 1-Methylcytosine, 9-Ethylguanine, 9-Methyladenine and 9-Methyladenine Cation". *Inorg. Chim. Acta* **1982***, 66*, 141-146.

(117) Schöllhorn, H.; Thewalt, U.; Lippert, B. "X-Ray Structure of a Mono-(1-Methylthyminato) Complex of Cisplatin, Chloro-(1-methyl-thyminato-*N3*)-*cis*-diammineplatinum(II) Monohydrate". *Inorg. Chim. Acta* **1985***, 106*, 177-180.

(118) Faggiani, R.; Lippert, B.; Lock, C. J. L.; Speranzini, R. A. "Model Complexes of Possible Cross-Linking Products of *cis*-$[Pt(NH_3)_2]^{2+}$ with Cytosine and Guanine Bases of DNA: X-ray Structures of three Mixed Ligand Complexes of *cis*-Diammineplatinum(II) with 1-Methylcytosine and Neutral and Anionic 9-Ethylguanine". *Inorg. Chem.* **1982***, 21*, 3216-3225.

(119) Schwarz, F.; Lippert, B.; Iakovidis, A.; Hadjiliadis, N. "Ternary Complexes of *cis*-$(NH_3)_2Pt(II)$ with Model Nucleobases (1-Methylcytosine, 9-Methylguanine) and N and O Bound Amino Acids (gly, ala)". *Inorg. Chim. Acta* **1990***, 168*, 275-281.

(120) Lippert, B.; Raudaschl, G.; Lock, C. J. L.; Pilon, P. "Real Model Compounds for Intrastand Cross-Linking of Two Guanine Bases by Cisplatin: Crystal Structures of cis-Diammine(9-Ethylguanine-*N7*)platinum(II) Dichloride Trihydrate, $[Pt(NH_3)_2(C_7H_9N_5O)_2]Cl_2 \cdot 3H_2O$, and *cis*-Diammine-bis(9-ethylguanine-*N7*)-platinum(II) Sesquichloride Hemibicarbonate Sesquihydrate, $[Pt(NH_3)_2(C_7H_9N_5O)_2]Cl_{1.5}(HCO_3)_{0.5} \cdot 1.5H_2O$". *Inorg. Chim. Acta* **1984***, 93*, 43-50.

(121) Freisinger, E.; Schimanski, A.; Lippert, B. "Thymine-metal ion interactions: relevance for thymine quartet structures". *J. Biol. Inorg. Chem.* **2001***, 6*, 378-389.

(122) Freisinger, E.; Schneider, A.; Drumm, M.; Hegmans, A.; Meier, S. et al. "Exocyclic oxygen atoms of platinated nucleobases as binding sites for alkali metal ions". *J. Chem. Soc., Dalton Trans.* **2000**, 3281-3287.

(123) Zamora, F.; Witkowski, H.; Freisinger, E.; Müller, J.; Thormann, B. et al. "Crystal Structures of protonated form of *trans*-[$Pt(NH_3)_2(mura)_2$] and of a derivative containing three different metal ions, Pt^{2+}, Ag^+, and Na^+ (mura = 1-methyluracilate). Major difference in packing between heteronuclear pyrimidine nucleobase complexes of *cis*- and *trans*-$(NH_3)_2Pt^{II}$ ". *J. Chem. Soc., Dalton Trans.* **1999**, 175-182.

(124) Renn, O.; Lippert, B.; Mutikainen, I. "Simultaneous binding of soft and hard metals to a pyrimidine nucleobase: *trans*-$K_2[PtI_2(1\text{-}MeU)_2]\bullet 6H_2O$, an anionic Pt-1-methyluracil (1-MeU) complex arranged in circles". *Inorg. Chim. Acta* **1994**, *218*, 117-120.

(125) Aukauloo, A.; Ottenwaelder, X.; Ruiz, R.; Journaux, Y.; Pei, Y. et al. "An Na_8 Cluster in the Structure of a Novel Oxamato-Bridged Na^ICu^{II} Three-Dimensional Coordination Polymer". *Eur. J. Inorg. Chem.* **1999**, 209-212.

(126) Sagatys, D. S.; Dahlgren, C.; Smith, G.; Bott, R. C.; White, J. M. "The complex chemistry of N-(phosphonomethyl)glycine (glyphosate): preparation and characterization of the ammonium lithium, sodium (4 polymorphs) and silver(I) complexes". *J. Chem. Soc., Dalton Trans.* **2000**, 3404-3410.

(127) Morgenstern, B.; Sander, J.; Huch, V.; Hegetschweiler, K. "Complexation of a Heptanuclear Poloyoxotantalate Anion with K^+: Formation of a Supramolecular $[K_6\text{-}(m\text{-}OH_2)_6\text{-}(OH_2)_8]^{6+}$ Ring Structure". *Inorg. Chem.* **2001**, *40*, 5307-5310.

(128) Lippert, B. "Rare Iminol Tautomer of 1-Methylthymine through Metal Coordination at *N3*". *Inorg. Chem. Acta* **1981**, *55*, 5-14.

(129) Chen, H.; Ogo, S.; Fish, R. H. "Bioorganometallic Chemistry. The Molecular Recognition of Aromatic and Aliphatic Amino Acids and Substituted Aromatic and Aliphatic Carboxylic Acid Guest with Supramolecular (^{5}-Pentamethylcyclopenta dienyl)rhodium-Nucleobase, Nucleoside, and Nucleotide Cyclic Trimer Host via Non-Covalent - and Hydrophobic Interactions in Water: Steric, Electronic, and Conformational Parameters". *J. Am. Chem. Soc.* **1996**, *118*, 4993-5001.

(130) Piotrowski, H.; Polborn, K.; Hilt, G.; Sverin, K. "A Self-Assembled Metallomacrocyclic Ionophore with High Affinity and Selectvity for Li^+ and Na^+ ". *J. Am. Chem. Soc.* **2001**, *123*, 2699-2700.

(131) Rauterkus, M. J.; Krebs, B. "Fünfkernige Platin(II)-Makrocyclen mit Nukleobasen". *Angew. Chem.* **2004**, *116*, 1321-1324.

(132) Lumry, R.; Smitz, E. L.; Glantz, R. "Kinetics of Carboxypeptidase Action. I. Effect of Various Extrinsic Factors on Kinetic Parameters". *J. Am. Chem. Soc.* **1951**, *73*, 4330-4340.

(133) MESTRELAB RESEARCH, M.: Rúa Xosé Pasín 6-5c, Santiago de Compostela, A Corunia, CP:15706, Spain.

(134) KappaCCD package; Nonius; Delft; The Netherlands, 1997.

(135) Oxford Cryosystems Ltd, B. O. P., Lower Road, Long Hanborough.

(136) Otwinowsky, Z.; Minor, W. "Processing of X-ray diffraction data collected in oscillation mode". *Methods Enzymol.* **1997***, 276*, 307-326.

(137) EvalCCD *Bruker-AXS Inc.*: Madison, Wisconsin, U.S.A., 2002.

(138) Duisenberg, A. J. M.; Kroon-Batenburg, L. M. J.; Schreurs, A. M. M. "An intensity evaluation method: *EVAL*-14". *J. Appl. Cryst.* **2003***, 36*, 220-229.

(139) Sheldrick, G. M. "Phase annealing in *SHELX*-90: direct methods for larger structures". *Acta Crystallogr. Sect. A.* **1990***, A46*, 467-473.

(140) Sheldrick, G. M. *SHELXTL-PLUS (VMS)*; Siemens Analytical X-Ray Instruments, Madison, WI, 1990.

(141) Sheldrick, G. M. *SHELXL-97, Program for Crystal Structure Refinement*; University of Göttingen: Germany, 1993.

(142) *SADABS: Area-Detector Absorption Correction.*; Siemens Industrial Automation, Inc.: Madison, Wisconsin, U.S.A.,1996.

(143) Hall, S. R.; Allen, F. H.; Brown, I. D. "The crystallographic information file (CIF): a new standard archive file for crystallography". *Acta Crystallogr.* **1991***, A47*, 655-685.

(144) Farrugia, L. J. "Windows Programs for the Solution, Refinement and Analysis of Single Crystal X-Ray Diffraction Data". *J. Appl. Cryst.* **1999***, 32*, 837-838.

(145) Farrugia, L. J. "*ORTEP*-3 for Windows- a version of *ORTEP*-III with a Graphical User Interface (GUI)". *J. Appl. Cryst.* **1997***, 30*, 565.

(146) *Persistence of Vision Raytracer (POV-Ray), Version 3.6*; Persistence of Vision Ray-Tracer Pty. Ltd.: Williamstwon, Victoria 3016, Australia, 2005.

(147) Brandenburg, K.; Berndt, M. *"DIAMOND-Visual Crystal Structure Information System*; Crystal Impact: Bonn, Germany, 1997.

(148) Kaufmann, G. B.; Cowan, D. O. "*cis*- and *trans*-Dichlorodiammineplatinum(II)". *Inorg. Synth.* **1963***, 7*, 239-245.

(149) Basolo, F.; Bailar, J. C.; Tarr, B. R. "The Stereochemistry of Complex Inorganic Compounds. X. The stereoisomers of Dichlorobis-(-ethylenediamine)-platinum(IV) Chloride". *J. Am. Chem. Soc.* **1950***, 72*, 2433-2438.

(150) McCormick, B. J.; Jaynes Jr., E. N.; Kaplan, R. I. "Dichloro(ethylenediammine)-palladium(II) and (2,2'-bipyridine)dichloropalladium(II)". *Inorg. Synth.* **1972***, 13*, 216-218.

(151) De Graaf, W.; Boersma, J.; Smeets, J. J. W.; Spek, A. L.; Van Koten, G. "Dimethyl(N,N,N',N'-tetramethylethanediamine)palladium(II) and Dimethyl[1,2-bis(dimethylphosphino)ethane]palladium(II): Syntheses, X-ray Crystal Structures, and Thermolysis, Oxidative-Addition, and Ligand-Exchange Reactions". *Organometallics* **1989***, 8*, 2907-2917.

3 List of Compounds Discussed in this Thesis

(**1a**) * [(en)Pt(UH-*N1*)(CH_2-*N3*)]ClO_4•3H_2O

(**1b**) # [(en)Pt(UH-*N1*)(CH_2-*N3*)]NO_3•3.5H_2O

(**2a**) # [(2,2'-bpy)Pd{(en)Pt(UH-*N1*)(*N3*-CH-*N1*)}$_2$](ClO_4)(NO_3)•4.9H_2O

(**4**) # [{(2,2'-bpy)Pd}$_3${(en)Pt(*N1*-U-*N3,O4*)(*N3*-CH-*N1*)}$_2$](NO_3)$_4$•5H_2O

(**X**) [{(en)Pt(*N1*-U-*N3*)(*N3*-CH-*N1*)}{(2,2'-bpy)Pd}]$_2^{2+}$

(**7**) # [{(2,2'-bpy)Pd}$_4${(en)Pt(*N1*-U-*N3,O4*)(*N3*-HC-*N1,O2*)}$_2$](NO_3)$_6$

(**9**) # [{(2,2'-bpy)Pd}{(en)Pt(*N1*-U-*N3*)(*N3*-HC-*N1*)}]$_4$(NO_3)$_3$(ClO_4)•56.1H_2O

(**Y'**) [{(en)Pt(*N1*-U-*N3*)(*N3*-CH-*N1*)}{(en)Pd}]$_2$(NO_3)$_2$

(**12'**) [{(en)Pt(U-*N1,N3,O2*)(C-*N1,N3,N4*)}$_2${(en)Pd}$_4$]$^{6+}$

(**13'**) # [{(en)Pt(U-*N1,N3,O2,O4*)(C-*N1,N3,N4,O2*)}$_2${(en)Pd}$_6$]
(NO_3)$_5$(ClO_4)$_3$•21.2H_2O

(**14a**) * *cis*-[Pt(UH-*N1*)$_2$(NH_3)$_2$]•2H_2O

(**14b**) # *cis*-Na_2[Pt(U-*N1*)$_2$(NH_3)$_2$]•10H_2O

(**17**) # [{(2,2'-bpy)Pd}$_3${*cis*-[(NH_3)$_2$Pt(*N1*-U-*N3*)(*N1*-U-*N3,O4*)]}$_2$]
(NO_3)$_2$•23.1H_2O

(**24**) [{(2,2'-bpy)Pd}$_4${*cis*-[(NH_3)$_2$Pt(*N1*-U-*N3,O4*)$_2$]}$_2$](NO_3)$_4$•17H_2O

(**24'**) # [{(en)Pd}$_4${*cis*-[(NH_3)$_2$Pt(*N1*-U-*N3,O4*)$_2$]}$_2$](NO_3)$_4$•13.8H_2O

(**28'**) # [{(en)Pd}$_{10}$(U-*N1,N3,O4*)$_2$(U-*N1,N3,O2,O4*)$_6${*cis*-[(NH_3)$_2$Pt]}$_4$]
(NO_3)$_{12}$•30H_2O

X-ray structurall characterized compounds

* Not first prepared in this thesis